2021

FUNCTIONAL CONSEQUENCES OF APOPTOSIS GENE DIVERSIFICATION IN EASTERN OYSTER IMMUNITY

Erin Michele Witkop
University of Rhode Island, erin_roberts@uri.edu

FUNCTIONAL CONSEQUENCES OF APOPTOSIS GENE DIVERSIFICATION IN EASTERN OYSTER IMMUNITY

BY

ERIN MICHELE WITKOP

A DISSERTATION SUBMITTED IN PARTIAL FULFILLMENT OF THE

REQUIREMENTS FOR THE DEGREE OF

DOCTOR OF PHILOSOPHY

IN

BIOLOGICAL AND ENVIRONMENTAL SCIENCES

UNIVERSITY OF RHODE ISLAND

2021

DOCTOR OF PHILOSOPHY DISSERTATION

OF

ERIN MICHELE WITKOP

APPROVED:

Dissertation Committee:

Major Professor Marta Gomez-Chiarri

Rachel Schwartz

Hollie Putnam

Dina Proestou

Gary Wikfors

Brenton DeBoef
DEAN OF THE GRADUATE SCHOOL

UNIVERSITY OF RHODE ISLAND
2021

ABSTRACT

The eastern oyster is an ecologically and economically important filter feeding bivalve mollusc endemic to the east coast of the United States. Outbreaks of disease, such as Dermo disease caused by the parasite *Perkinsus marinus*, threaten natural oyster populations, and oysters have evolved a complex innate immune system containing large, expanded gene families to combat the diverse array of pathogens in their environment. Apoptosis, or programmed cell death, is a critical immune response to Dermo disease involving a series of expanded gene families, including the Inhibitor of Apoptosis (IAP) family of apoptosis regulatory molecules. The goal of this research is to investigate the role of apoptosis in immunity and disease resistance in oysters and characterize the role of IAP diversity in disease response. To address these gaps in knowledge, this dissertation first annotated the full repertoire of apoptosis genes in the eastern oyster, revealing the major apoptosis and regulated cell death pathway proteins in the eastern oyster and providing a detailed resource for future researchers. Second, this dissertation characterized oyster IAP gene family diversification and potential evolutionary mechanisms of expansion, and the role of this diversification in oyster disease response. Research on oyster IAP characterization showed that: 1) oyster IAPs have highly diverse Baculoviral IAP Repeat (BIR) domains and domain architecture; 2) IAPs likely expanded through tandem duplication and retroposition; 3) oysters express unique assemblages of IAPs to diverse disease challenges; and 4) IAP expression is directly correlated with apoptosis pathway response. Third, this dissertation investigated eastern oyster apoptosis mechanisms in response to *P. marinus* challenge. *In vitro P. marinus* challenge and novel use of IAP and caspase inhibitors indicated basal hemocyte apoptosis may be IAP-dependent, apoptosis suppressed by *P.*

marinus may involve caspase-independent pathways, and hemocyte apoptosis suppression following *P. marinus* challenge involves oxidation-reduction, TNFR, and NF-kB pathways. Finally, this dissertation investigated the connection between apoptosis phenotype and resistance to Dermo disease. *In vivo P. marinus* challenge across six selectively bred families revealed families differed in their *P. marinus* resistance in terms of parasite load change over time, apoptotic responses to *P. marinus* significantly differed across families, and apoptotic response at 7 days after challenge was correlated with resistance in the most resistant family. Future research is needed to confirm the role of apoptosis on resistance and the utility of apoptosis as measure of Dermo resistance remains unclear. The relationship between apoptosis gene expression and Dermo resistance should be explored in future research through transcriptome sequencing, differential expression analysis, and Weighted Gene Correlation Network Analysis (WGCNA). Research presented in this dissertation contributes significantly to the study of oyster apoptosis, invertebrate host-parasite interactions, selective breeding for disease resistance, and the role of gene diversification in oyster immune response.

ACKNOWLEDGMENTS

I want to extend my deepest gratitude first to my major professor, Dr. Marta Gomez-Chiarri. It's difficult to enumerate the things she has taught me and how she has shaped me into the researcher I am today. Through her positive attitude, deep excitement for discovery, commitment to mentorship, and unique ability to understand complex connections and distill information, she has helped me build a body of meaningful research, while guiding me to become a more focused, confident, and capable scientist, not only with exciting ideas but actionable plans for how to achieve my goals. Next, I wish to extend my deepest thanks to my committee member, collaborator, and mentor, Dr. Dina Proestou. Through her dedicated and thorough mentorship, she taught me how to clearly focus my research goals, design and execute targeted experiments, and write concisely. By working with her team, particularly Kathryn Markey Lundgren, Mary Sullivan, and Dr. Tal Ben Horin, I have learned critical skills and become a more organized, thorough, and productive scientist. Third, I wish to extend my greatest appreciation to my committee member, mentor, and collaborator Dr. Gary Wikfors. He welcomed me with open arms the first time I met him and asked to try some flow cytometry. Since then, his patient mentorship, constant enthusiasm for discussing flow cytometry plots, curiosity, and passion for science have been a real inspiration to me and led to very interesting discoveries together. I also wish to thank my committee member and mentor Dr. Rachel Schwartz. Taking her classes at URI about coding served as the critical foundation for my research. Without her knowledge, guidance, and technical support I would not have had the skills to do this dissertation. Finally, I would like to thank Hollie Putnam whose valuable advice and

mentorship helped me form ideas at critical times, and whose example of excellence in research inspires me.

I would also like to acknowledge my current and former lab mates Tejashree Modak, Melissa Hoffman, Sam Hughes, Rebecca Stevick, Evelyn Takyi, Jessica Coopersmith, Robbie Hudson, and Jamal Andrews for their friendship, collaboration, support, countless presentation comments, and continuously supplying me with baked goods. I particularly want to thank Rebecca, who sat with me day after day coding at our desks, supplied me with New Yorker jokes and served as a constant friend. I could not have made it through without all your friendship and support.

Finally, I would like to acknowledge my parents Bill and Linda Roberts and my husband Bobby Witkop. To my parents, you have supported me unconditionally at every step in my life and always encouraged me to achieve my dreams. Mom, knowing that you'll be there for me when I call at any time, day or night, to make me laugh, read a paragraph, and give me the strength to keep going means more than you'll ever know. Dad, growing up seeing your life as a Geology professor sparked my deep curiosity for the natural world and showed me that getting a PhD was a possibility. Thank you for your love and support, your humor in every situation, and your enduring positive attitude. To Bobby, thanks for being my teammate in life and my greatest love. You never fail to put a smile on my face, spark my curiosity with a fascinating discussion, and lead me into exciting adventures. Grad school led me to you, and you were my rock throughout the entire process. I truly could not have finished this PhD without your love, support, and constant encouragement. Thank you all.

PREFACE

This dissertation was written in accordance with the manuscript format guidelines established by the Graduate School of the University of Rhode Island. The dissertation includes an introductory chapter, followed by three manuscripts, and is finished with a conclusion chapter.

1. "Apoptosis in Oysters: mechanisms, gene expansion, and the potential functional importance of the Inhibitor of Apoptosis (IAP) gene family in disease response". *Prepared for submission to Journal of Shellfish Research.*
2. "The expanded Inhibitor of Apoptosis gene family in oysters possesses novel domain architectures and may play diverse roles in apoptosis following immune challenge." *Prepared for submission to BMC Genomics.*
3. "*Perkinsus marinus* suppresses *in vitro* eastern oyster apoptosis via IAP-dependent and caspase-independent pathways involving TNFR, NF-kB, and oxidative pathway crosstalk". *Prepared for submission to Developmental and Comparative Immunology.*
4. "Multifamily eastern oyster challenge with *Perkinsus marinus* reveals a correlation between hemocyte apoptosis and parasite resistance". *Prepared for submission to Fish and Shellfish Immunology.*
5. The final chapter summarizes the major findings of this work and their relevance to the field in the context of existing literature.

TABLE OF CONTENTS

LIST OF TABLES

TABLE PAGE

LIST OF FIGURES

FIGURE PAGE

CHAPTER 1: Apoptosis in Oysters: mechanisms, gene expansion, and the potential functional importance of the Inhibitor of Apoptosis (IAP) gene family in disease response

Erin M. Witkop[1], Marta Gomez-Chiarri[1]

[1]University of Rhode Island, Department of Fisheries, Animal and Veterinary Science, Kingston, RI, USA.

Prepared for submission to ***Journal of Shellfish Research***.

Keywords: apoptosis, gene expansion, oyster, Inhibitor of Apoptosis, disease

Introduction to Oyster Immunity

The eastern oyster, *Crassostrea virginica*, is a filter-feeding bivalve mollusc native to the east coast of North America whose range extends from the Gulf of Mexico to Canada (Bersoza Hernández et al., 2018). These sedentary animals form benthic reefs and play critical ecological roles in their estuarine environment, including habitat provision for epibenthic invertebrates and fishes, improvement of local water quality through filtration and concentration of biodeposits, stabilization of benthic habitats, carbon sequestration, and increasing landscape diversity (Grabowski and Peterson, 2007). Oyster aquaculture has emerged as an important industry in the United States and generated a production value of $186 million in 2017 (Ross et al., 2018). Since their peak landings of 27 million bushels a year in the 1890's, eastern oyster natural populations have declined by almost 99% (Mackenzie, 2007). Factors influencing this decline include physical damage to oyster beds (dredging and storms) and outbreaks of diseases such as Dermo and MSX, caused by the parasites *Perkinsus marinus* and *Haplosporidium nelsoni*, respectively (Mackenzie, 2007).

Interest in the study of bivalve immunity has grown significantly in recent decades, driven by the desire to understand basic bivalve immune mechanisms, perform comparative analyses across invertebrates, and the need to produce disease-resistant strains of bivalves for aquaculture (Allam and Raftos, 2015). Unlike vertebrate animals, which possess an adaptive immune system characterized by somatic gene rearrangement of lymphocyte surface antigen receptors, bivalve innate immune systems rely on a complex, multi-faceted innate immune system to fight the array of pathogens in their environment (Boehm and Swann, 2014). Physical barriers, including a hard calcium-carbonate shell and mucus secreted from the mantle tissue, represent the initial physical barriers to pathogens.

Oyster mucus behaves as a physical barrier by trapping bacteria and using the ciliary activity of mantle cells to facilitate its removal. Mucus secretions additionally contain agglutinins, such as lectins (Espinosa et al., 2015), which can bind invading bacteria, enzymes such as lysozyme (Xue et al., 2004) and proteases that can degrade bacteria, and additional pattern recognition receptors (PRRs) such as fibrinogen-related proteins (FREPs) (L. L. Zhang et al., 2012) which can bind invaders targeting them for destruction.

Following contact with physical barriers, invading pathogens interact with the cellular component of oyster immunity mediated by hemocytes (Allam and Raftos, 2015). Hemocytes perform a myriad of critical immune functions and are the first responders to the site of infection. They travel throughout the oyster's body in hemolymph vessels and soft tissues via an open circulatory system and transepithelial migration termed diapedesis (Lau et al., 2018a). Hemocytes display chemotaxis toward products secreted by bacteria (Cheng and Howland, 1979), and following migration to the site of infection, hemocytes can promote encapsulation of large invaders, or granular hemocytes (the phagocytic oyster hemocyte (Wikfors and Alix, 2014)) can phagocytose parasites and bacteria and promote intracellular killing through the release of hydrolytic enzymes and reactive oxygen species (ROS) (Anderson, 1994; Genthner et al., 1999). If intracellular killing of bacteria or parasites is unsuccessful, or sometimes as a direct result of attempts to kill intracellular invaders (ROS release), apoptosis, or type 1 programmed cell death can be triggered (Sokolova, 2009).

Evidence indicates that hemocyte apoptosis may be a general immune response to environmental and disease-related stresses, such as parasites, insecticides, herbicides, and pharmaceuticals (Kiss, 2010). Apoptosis is critical to maintaining normal tissue

homeostasis and cell turnover in molluscs, and high baseline apoptosis levels are observed in circulating hemocytes (5-25%) (Kiss, 2010; Sokolova, 2009). Apoptosis is also a key process during embryogenesis and organogenesis (Lockshin, 2007), neural development, and larval metamorphosis (Gifondorwa et al., 2017). Apoptosis has been studied extensively in vertebrates and model organisms such as *Caenorhabditis elegans* and *Drosophila* melanogaster, and this body of research provides an essential foundation for the study of apoptosis in oysters, including apoptosis mechanisms, apoptosis pathway evolution, and the role of apoptosis in eastern oyster disease response (Romero et al., 2015).

Apoptosis and Cell Death in Model Organisms

Apoptosis is a morphologically distinct process characterized by tightly regulated genetic pathways and key morphological changes (Romero et al., 2015). Early apoptosis hallmarks include cellular shrinkage, DNA segmentation and chromatin condensation. This is followed by expansion of the endoplasmic reticulum, primary lysosome formation, phosphatidylserine (PS) translocation to the outer leaflet of the cellular membrane, and cellular membrane blebbing or budding into apoptotic bodies (Kiss, 2010). Apoptotic bodies are then engulfed by phagocytic hemocytes and digested in a process known as efferocytosis (Elmore, 2007). Unlike necrosis, a non-genetically regulated system of cell death, apoptosis does not lead to DAMP (Death Associated Molecular Patterns) and intracellular cytoplasm release, and therefore does not trigger inflammation (Romero et al., 2015).

There are two major apoptosis pathways, the intrinsic pathway, and the extrinsic pathway (Romero et al., 2015). Though each is triggered by unique stimuli and regulated by specific genes, there is considerable crosstalk between pathways, and both converge on the cysteine-dependent aspartate-directed protease (caspase) family which are critical catalysts of the apoptotic process. The extrinsic, or death-receptor mediated, apoptosis pathway is triggered by extracellular ligand binding by pathogen-associated molecular patterns (PAMPs) to plasma membrane death receptors (including Toll Like Receptors (TLR), Tumor Necrosis Factor Superfamily Receptors (TNFR), and Fas cell surface death receptor (FAS)), or a decrease in binding to extracellular dependence receptors (Galluzzi et al., 2018). Death receptor binding triggers receptor oligomerization and formation of a death-inducing signaling complex (DISC), which can be either "complex I" or "complex II" type.

These complexes involve different proteins depending on the death receptor involved and can lead to different cell death outcomes. Binding to FAS stimulates DISC assembly with Fas-associated death domain (FADD), caspase 8 (CASP8), and c-FLIP, while TNFR1 binding drives formation of a complex with TNFRSF1A associated via DD (TRADD), TNF receptor associated factor 2 (TRAF2), TRAF5, BIRC2/c-IAP1, BIRC3/c-IAP2, Receptor Interacting Protein Kinase 1 (RIPK1), and the Linear Ubiquitin Chain Assembly Complex (LUBAC) (Galluzzi et al., 2018). Formation of these complexes can trigger cell death through activation of caspase 8 (CASP8), followed by activation of executioner caspases 3 and 7 (CASP3, CASP7) and subsequent apoptosis, or trigger survival by stimulating MAPK family members and the NF-kB pathway (Galluzzi et al., 2018). The outcome of extrinsic apoptosis following extracellular ligand binding is

affected by a variety of factors, including crosstalk with the intrinsic apoptosis pathway, assembly of further downstream protein complexes, action of inhibitory proteins such as Inhibitor of Apoptosis Proteins (IAPs) (i.e. X-linked Inhibitor of Apoptosis XIAP), and the degree of death receptor oligomerization (Galluzzi et al., 2018). Dependence receptors, including the DCC netrin 1 receptor (DCC), unc-5 netrin receptors (UNC5A, UNC5B, UNC5C, and UN5D), and the sonic hedgehog receptor patched 1 (PTCH1), typically promote cell survival but can trigger cell death through the extrinsic pathway when availability of dependence receptor ligands drops below a particular threshold (Galluzzi et al., 2018).

The second apoptosis pathway, the intrinsic or mitochondrial pathway, is triggered by intracellular stimuli including reactive oxygen species (ROS), UV radiation, DNA-damage, growth factor withdrawal, and endoplasmic reticulum (ER) stress (Galluzzi et al., 2018). The central morphological feature of this pathway is mitochondrial outer membrane permeabilization (MOMP) which is regulated by members of the BCL2 protein family. BCL2 family members can be either pro-apoptotic or anti-apoptotic. Proteins BCL2 associated X, apoptosis regulator (BAX), BCL2 antagonist/killer 1 (BAK1, best known as BAK) and BCL2 family apoptosis regulator (BOK) are pro-apoptotic and form pores within the outer mitochondrial membrane. Anti-apoptotic BCL2 family members include BCL2, BCL2 like 1 (Bcl2-XL), MCL1, BCL2 family apoptosis regulator (MCL1), BCL2 like 2 (BCL-W), and BCL2 related protein A1 (BCL2A1; BFL-1). Most anti-apoptotic BCL2 family members directly inhibit BAX and BAK. All BCL2 family members are under tight transcriptional and translational regulation and are subject to proteasomal degradation, relocalization, and phosphorylation. Some BCL2 family members are also

involved in ER hemostasis, including BOK, which responds to ER stress and is localized to the ER (Galluzzi et al., 2018).

Following MOMP, apoptogenic proteins, including cytochrome c (cyto c), second mitochondrial activator of caspases (SMAC), and enzymes endonuclease G (EndoG) and Apoptosis Inducing Factor (AIF) are released from the mitochondrial intermembrane space where they are normally sequestered (Galluzzi et al., 2018). SMAC promotes apoptosis by binding and disabling IAP family member XIAP, which physically binds to and inhibits executioner caspases. Cytochrome c forms a complex with pro-caspase 9 (CASP9) and apoptotic peptidase activating factor 1 (APAF1), called the apoptosome. Apoptosome formation and CASP9 activation leads to downstream activation of CASP3 and CASP7, the executioner caspases, which typically leads to the morphological signs of apoptosis (Galluzzi et al., 2018).

Standard methods for measuring apoptosis include electron microscopy, gel electrophoresis, and flow cytometry (Martinez et al., 2010). Scanning electron microscopy allows for visualization of morphological changes, including chromatin condensation and plasma membrane blebbing (Martinez et al., 2010). This technique however can lead to false positives and requires specialized skill to perform. DNA ladder assays with gel electrophoresis can be used to measure the characteristic ladder formation of DNA strand breaks resulting from apoptosis. This technique, however, can only be used for late-stage apoptosis and has low sensitivity. Several protein-based assays are used in conjunction with western blotting to detect caspase activation and cytochrome c release. Finally, optical methods such as flow cytometry and light spectroscopy are used to detect binding of fluorescently labelled probes that indicate apoptosis. Common assays include measurement

of mitochondrial membrane potential (JC-1 assay), chromatin condensation (calcein-AM), caspase activation assays (caspase 3/7 activation), measurement of PS translocation (annexin V staining), and measurement of DNA fragmentation (terminal deoxynucleotidyl transferase dUTP nick end labeling, TUNEL, assay) (Martinez et al., 2010).

Several interesting caveats highlight the complexity of the apoptotic process and the difficultly of using morphological and chemical markers to measure levels of apoptosis. Apoptosis has long been thought irreversible after a "point of no return", typically activation of executioner caspases 3 and 7 and subsequent triggering of morphological changes (Sun et al., 2017). New research, however, reveals that key morphological hallmarks of apoptosis are reversible in some circumstances in a process called anastasis, and cells can recover from cytochrome c release, resorb apoptotic bodies, remove externalized PS, and recover from executioner caspase activation (Galluzzi et al., 2018; Sun et al., 2017; Tang and Tang, 2018). Additionally, caspase enzyme activation does not necessarily indicate apoptosis, and caspases are critical in other cellular processes, including maintenance of tissue integrity, cell differentiation, driving cell proliferation and tissue repair, regulating inflammatory reactions to pathogenic challenges, and inflammasome function (Gorelick-Ashkenazi et al., 2018) (Bell and Megeney, 2017; Feltham et al., 2017; Fogarty and Bergmann, 2017; Galluzzi et al., 2016; Nakajima and Kuranaga, 2017; Solier et al., 2017). These results highlight the importance of careful and nuanced interpretation of morphological results when measuring apoptosis.

Though apoptosis is a critical cellular death pathway, several other non-apoptotic programmed, or regulated cell death (RCD), pathways have been characterized recently in mammals (Galluzzi et al., 2018) (Table 1). Many apoptosis proteins play roles in these

alternative cell death programs, and these cell death modes display some degree of interconnectivity and crosstalk with one another (Galluzzi et al., 2018; Lamb, 2020). Cells can also exhibit molecular and biochemical signatures of several different forms of cell death (Lamb, 2020).

The study of apoptosis and RCD in vertebrates has revealed highly complex and tightly controlled pathways. To fully understand how these pathways evolved, apoptosis has been studied extensively in *C. elegans*, *D. melanogaster*, and marine invertebrates, including the eastern oyster. The study of apoptosis and RCD in invertebrates and oysters has revealed prominent mechanisms of apoptosis pathway diversification and presents exciting avenues for future research.

Apoptosis in Model Invertebrates and Oysters

Investigation of apoptosis pathways in invertebrates initially began with the model organisms *C. elegans* and *D. melanogaster* (Oberst et al., 2009; Romero et al., 2015; Zmasek and Godzik, 2013). *C. elegans* possesses several cell death defective (CED) genes that are homologous with vertebrate apoptosis genes, including CED-9 protein (homologous with Bcl-2), CED-4 (homologous with APAF-1), and CED-3 (homologous with CASP2 and has an executioner caspase function) (Oberst et al., 2009). MOMP and cytochrome c release, however, do not play roles in *C. elegans* apoptosis initiation. *D. melanogaster* contains initiator and executioner caspases similar to mammalian caspases, specifically caspase DRONC is similar to mammalian initiator CASP2 and CASP9, and DRICE is homologous with mammalian CASP3 (Oberst et al., 2009). *D. melanogaster* also possesses two Bcl-2 homologs, Buffy and Debcl, though these do not play critical

roles in fruit fly apoptosis. The major apoptosis regulator in *D. melanogaster* is DIAP1, and it is homologous with mammalian IAPs. DIAP1, similar to XIAP, binds DRONC and can inhibit its activity. DIAP1 is antagonized by Grim, Reaper, and HID which bind to it and induce autoubiquitination. Additionally, activation of caspases and formation of the apoptosome appear to be independent of cytochrome c in *D. melanogaster* (Oberst et al., 2009). Apoptosis pathway simplifications in *D. melanogaster* and *C. elegans* initially suggested the pathway of apoptosis gained increasing complexity as it evolved through time (Zmasek and Godzik, 2013). However, research in additional early diverging and marine invertebrates indicates that the limited number of proteins involved in *C. elegans* and *D. melanogaster* apoptosis is likely the result of secondary simplifications rather than an increase in complexity during vertebrate evolution (Oberst et al., 2009; Zmasek and Godzik, 2013).

The study of apoptosis in molluscs supports the observation that the most recent common ancestor of vertebrates and invertebrates likely contained the major apoptosis machinery known today, and both the major molecules and morphological signs of apoptosis recognized in vertebrates have been identified in molluscs (Kiss, 2010; Li et al., 2017; Romero et al., 2015; Sokolova, 2009). Critical morphological features, including chromatin condensation, DNA fragmentation, phosphatidylserine translocation to the outer leaflet of the cell membrane, cell blebbing, and MOMP have been confirmed in molluscs (Kiss, 2010; Li et al., 2017). Molluscs in general possess the major intrinsic apoptosis pathway members, including cytochrome c, AIF, APAF-1, caspases (CASP2, CASP8, CASP3, CASP7), Bcl-2 family members (Bcl-xL, Bcl-xS, Bcl2, BAX), IAPs, and p53, and the major molecules of the extrinsic pathway, including NF-kB pathway (Rel/NF-kB, AP-

1, IkB, IKK, NEMO) and TNF pathway members (TNF-a, TRAIL, FasL, TRAF, FADD, TTRAP, LITAF) (Kiss, 2010; Li et al., 2017; Romero et al., 2015, 2013; Sokolova, 2009; Vogeler and Carboni, n.d.; Yu et al., 2018). The study of alternative RCD pathways, however, has been very limited in molluscs. Though specific molecules involved in some have been identified, morphological signs of alternative RCD pathways have not been confirmed. Specifically, AIF proteins have been identified in several molluscs, and AIF is known to play roles in parthanatos in model organisms (Galluzzi et al., 2018; Romero et al., 2015), and several necroptosis related proteins have been identified in molluscs, including RIPK3 and PGAM5 (Sokolov et al., 2019), RIPK1 (Gerdol et al., 2018; López-Galindo et al., 2019), TNFAIP3 (Chen et al., 2015; Ertl et al., 2019), TRAF6 and pellino (Lin et al., 2020). Other RCD pathways however remain mostly unexplored in molluscs, presenting an interesting avenue for research.

The molecular mechanisms of apoptosis in the eastern and Pacific oyster have been investigated through transcriptomic, genomic, and phenotypic methods, confirming results presented above for molluscs in general. Whole genome sequencing of the Pacific oyster has allowed for more detailed analysis of apoptosis mechanisms, including recent characterization of the mitochondrial pathway where Bcl-2 homology 3-only subfamily members and APAF-1 protein were found to be absent in *C. gigas* (Li et al., 2017; G. Zhang et al., 2012). Additional comparative and phylogenetic studies of apoptosis-related proteins, including caspases (Vogeler et al., 2021), IAPs (Song et al., 2021), TIR-domain containing proteins (including TLR and MyD88 proteins) (Gerdol et al., 2017), and p53 (Plachetzki et al., 2020), have utilized the *C. gigas* genome and shed light on evolution of these gene families across molluscs. Study of the Pacific oyster genome has also revealed

large scale expansions of immune gene families, some which play key roles in apoptosis (Zhang et al., 2015). This is supported by previous studies of early diverging marine invertebrates, including the starlet sea anemone *Nematostella vectensis*, the hydra *Hydra magnipapillata*, the demosponge *Amphimedon queenslandica*, the Pacific purple sea urchin *Strongylocentrotus purpuratus*, the sea anemone (Amphioxus) *Branchiostoma floridae,* and the quahog (hard clam) *Mercenaria mercenaria*, which revealed many apoptosis regulatory genes were present as large genes families of paralogs (Buckley and Rast, 2012; Song et al., 2021; Zmasek and Godzik, 2013).

Previously, lack of a genome assembly for the eastern oyster has limited the study of apoptosis mechanisms to investigation of particular genes or transcriptomes assembled *de novo* and prevented full characterization of expanded immune gene families involved in apoptosis (Foster et al., 2011; Hughes et al., 2010; Lau et al., 2018b; Sokolova et al., 2004; Sunila and Cooperative, 2017; Sunila and LaBanca, 2003; Wang et al., 2010; Zhang et al., 2014). The genome of the eastern oyster has recently been sequenced (Puritz et al., *in prep*) (Gómez-Chiarri et al., 2015a, 2015b). Availability of both the eastern and Pacific oyster genomes presents an exciting opportunity to explore and compare the overall molecular mechanisms of apoptosis in both oysters, determine apoptosis pathway gene expansion in oysters, and gain insight into the role that gene family expansion and diversification may play in targeting immune responses in the oysters' diverse habitats.

Apoptosis Gene Expansion in Oysters and the IAP Gene Family

Similar to the gene family expansion observed in other marine invertebrates, detailed annotation of the Pacific oyster genome has revealed that accompanying its high level of

genetic polymorphism (one Single Nucleotide Polymorphism (SNP) per 60bp in coding regions (Sauvage et al., 2007)), is great expansion and divergence of multi-gene families with functions related to innate immunity and apoptosis (Zhang et al., 2015). Several of these expanded families are involved in signaling and receptor diversity, including the NOD-like receptor (NLR), TLRs, RIG-I like receptors (RLR), C3 (complement C3), PGRP (peptidoglycan recognition proteins), GNBP (Gram-negative binding protein), CTLDC (C-lectin domain containing protein), FBGDC (fibrinogen-domain-containing proteins), C1qDC (globular head C1q domain containing protein), and MBP (mannose binding protein). *C. gigas* gene expansions also include gene families involved in apoptosis; TLR, MyD88, NF-kB, IRF, TNF, TNFR, TRAF, FADD, Inhibitor of Apoptosis (IAP), CRADD (death domain containing protein CRADD), and AP-1 (activator protein 1) (Zhang et al., 2015). Expansion of these multigene families in *C. gigas* is mainly attributed to multiple tandem duplication events (G. Zhang et al., 2012). Differential usage of members of these expanded gene families has been observed following diverse immune challenges, suggesting that gene expansion in these innate immune families may have allowed for functional divergence, tailoring of immune responses, and a better ability to adapt to a wide range of stressors (G. Zhang et al., 2012).

The IAP gene family in particular was greatly expanded in the *C. gigas* genome, with 48 identified genes, compared with 7 in the sea urchin *S. purpuratus* and 8 in humans (G. Zhang et al., 2012). Whole genome sequencing of the hard clam, *Mercenaria mercenaria*, very recently (concurrent with finalization of this dissertation) (Song et al., 2021) revealed similar IAP family expansion in hard clams. *M. mercenaria* IAP family members have diverse domain structure and display unique expression patterns to environmental stressors

(Song et al., 2021). Functional diversification of the IAP family, whose members play critical roles in apoptosis regulation in model organisms (i.e. BIRC2/cIAP1, BIRC3/cIAP2, and BIRC4/XIAP) may allow for tailored regulation of apoptosis during different immune stressors. Consequently, characterization of these genes in the oysters may help illuminate the role that gene diversification plays in immune response (Estornes and Bertrand, 2015).

In mammals, the IAP, or Baculoviral IAP Repeat Containing (BIRC), protein family includes 8 members, BIRC1/NAIP, BIRC2/cIAP1, BIRC3/cIAP2, BIRC4/XIAP, BIRC5/Survivin, BIRC6/BRUCE, BIRC7/ML-IAP and BIRC8/ILP2 (Estornes and Bertrand, 2015). IAPs possess one to three baculoviral IAP repeat (BIR) domains and can contain unique functional domains, such as a C-terminal Really Interesting New Gene (RING) domain which confer ubiquitin ligase activity, ubiquitin associated domains (UBA) and ubiquitin conjugating domains (UBC) (Eckelman et al., 2006; Estornes and Bertrand, 2015). Protein ubiquitination is critical for regulating protein trafficking, protein degradation, and signal transduction and is catalyzed by the action of Ub-activating enzymes (E1), Ub-conjugating enzymes (E2), and a Ub-ligases (E3) (Zheng and Shabek, 2017). IAPs possess domains that can perform both E2 and E3 functions, making them critical regulators of ubiquitination (Galbán and Duckett, 2010; Kocab and Duckett, 2016; Vasudevan and Don Ryoo, 2015).

Research into specific IAP members has revealed their roles in apoptosis regulation in model organisms. XIAP can inhibit apoptosis through direct physical binding with CASP3, while cIAP1 and cIAP2 can inhibit caspase function through ubiquitination and promotion of proteasomal degradation (Estornes and Bertrand, 2015). cIAP1 and cIAP2 promote both cell death and cell survival by acting as signal transducers following death

receptor binding during extrinsic apoptosis and canonical NF-kB pathway activation (Kocab and Duckett, 2016). cIAP1, cIAP2, and XIAP have also been recognized recently as inflammasome regulators, emphasizing their dual role in both apoptosis and inflammation regulation (Estornes and Bertrand, 2015). BIRC5 negatively regulates apoptosis by binding to SMAC, which typically binds to and inhibits XIAP, resulting in XIAP being able to bind and inhibit CASP9 and CASP3, leading to apoptosis inhibition (Cheung et al., 2020). BIRC5 also negatively regulates AIF, a mitochondria-released enzyme that can trigger apoptosis in the absence of caspase activation (caspase-independent apoptosis). Finally, BIRC8 can protect against intrinsic apoptosis mediated by BAX (Saleem et al., 2013).

Like other apoptosis proteins, IAPs perform functions outside of apoptosis and immunity. The IAPs DIAP1, BIRC7, and XIAP can modulate cell migration (Oberoi-Khanuja et al., 2013, 2012). BIRC6 plays a role in autophagosome-lysosome fusion independent of ubiquitination activity, DNA double strand break repair, and homologous recombination (Ebner et al., 2018; Ge et al., 2015). XIAP, BIRC5, and BIRC6 can influence autophagy regulation (Cheung et al., 2020). BIRC5 also plays a key role in mitosis, where it forms a chromosomal passenger complex (CPC)(Cheung et al., 2020). Large IAP expansions in multiple molluscs, their key roles in apoptosis regulation, and their variable expression during immune challenge make the IAP family particularly attractive to study during eastern oyster disease response, wherein expansion of this gene family may allow for diverse and targeted immune response to disease (Zhang et al., 2015).

Apoptosis and the IAP Gene Family in Oyster Disease Response

Decades of experimentation have explored the role of apoptosis in oyster response to bacterial, viral, and parasitic challenges. These studies inform pathways of apoptosis involved in response to various pathogens and the potential utility of apoptosis as a marker of disease resistance. Several disease challenges have additionally identified IAPs as transcriptionally active following disease challenge, suggesting their role in immunity to disease.

The role of apoptosis in disease response to bacteria has been studied mainly during infection with *Vibri*o strains, the causative agents of Vibriosis (summer mortality), and *Aliiroseovarius crassostreae*, the causative agent of Roseovarius Oyster Disease (ROD, Juvenile Oyster Disease, JOD). Vibriosis can have devastating effects on oyster larvae in hatcheries and on adult oysters, and research has shown that *Vibrio* spp. stimulate ROS production in *C. gigas* (Guo and Ford, 2016; Labreuche et al., 2006b, 2006a; Richards et al., 2015; Samain and McCombie, 2008). Over-stimulation of ROS production may cause host hemocyte toxicity and trigger mitochondrial apoptosis. *C. gigas* challenge with *Vibrio* spp. or lipopolysaccharide (LPS) have also resulted in extrinsic apoptosis pathway activation. *C. gigas* exposure to LPS, *Listeria monocytogenes*, and *V. alginolyticus* induced expression of lipopolysaccharide-induced tumor necrosis factor-alpha factor (LITAF), which regulates TNF-a expression (Yu et al., 2012). Challenge of *C. gigas* with *V. alginolyticus*, *V. aestuarinus*, and LPS stimulated differential expression of four TNF, six TNFR and three TRAF members, as well as various TLR members (Zhang et al., 2015). *V. alginolyticus* challenge stimulated expression of interferon-regulatory factor (IRF) genes, which control transcription of type I interferon which is typically involved in antiviral responses and apoptosis (Mao et al., 2018). Finally, experimental infections

with *V. aestuarianus, V. tasmaniensis* LGP32, and OsHV-1 demonstrated differential expression of IAPs, TNF-ligand, MyD88, TLRs, IkB, and IRF8 (Green et al., 2016). Roseovarius Oyster Disease (ROD) in juvenile eastern oysters is characterized by uneven valve margins, sudden cessation of growth, secretion of successive layers of conchiolin onto inner valves, watery tissues, and a ring of deposits developing around the mantle at advanced stages (Boardman et al., 2008; Maloy et al., 2007). Extracellular products released by *A. crassostreae* are toxic to hemocytes (Gómez-León et al., 2015), and experimental challenge with *A. crassostreae* in resistant and susceptible oysters revealed significant differential expression of multiple members of the IAP and GTPase of the Immune Associated Proteins (GIMAP) proteins, another family of apoptosis regulators, suggesting the important role of these families in immune response (McDowell et al., 2016). These studies overall suggest that IAPs may play important roles in oyster responses to bacterial infection. However, full characterization of the IAP response during bacterial challenge is currently limited because of the absence of detailed IAP family annotation in eastern oysters.

The role of apoptosis in oyster viral challenge has been studied mainly in Pacific oysters since eastern oysters are not currently afflicted by viral diseases of commercial concern. Pacific oyster mortality syndrome (POMS) has a complex etiology and involves primary infection with the virus OsHV-1, leading to an immune-compromised state, followed by secondary infection with pathogenic *Vibrio* bacteria (de Lorgeril et al., 2018). This disease causes mass mortalities of juvenile Pacific oysters, and selective breeding has allowed for the development of Pacific oysters with increased resistance to OsHV-1, revealing a genetic basis for immunity to this disease (Azéma et al., 2017; de Lorgeril et

al., 2018; Dégremont et al., 2015; Samain et al., 2007). A variety of transcriptome experiments has revealed unique responses of apoptosis and inflammatory pathways in oysters following OsHV-1 infection (de Lorgeril et al., 2018; Green et al., 2016, 2015; Segarra et al., 2014; Young et al., 2017). Microarray analysis by Fleury and Huvet (2012) showed *C. gigas* individuals with differential resistance to OsHV-1 significantly differentially expressed AIF, Rho GTPase, Programmed Cell Death Protein 10, and NF-kB (Fleury and Huvet, 2012). In a separate challenge, OsHV-1 resistant oysters expressed antiviral effectors IFI44 and apoptosis transcripts TNF and CASP3, and OsHV-1 susceptible oysters strongly expressed IAP transcripts, suggesting the involvement of this gene family in OsHV-1 response (de Lorgeril et al., 2018). A similar study by Segarra et al. (2014) challenged 16 families with differential susceptibility to OsHV-1 and revealed significant upregulation of MyD88, IFI44, IkB2, and IAP transcripts. This study additionally demonstrated significant correlation between OsHV-1 viral DNA levels and IAP overexpression, and proposed IAP upregulation may be a viral-induced response to increased apoptosis levels stimulated by OsHV-1 (Segarra et al., 2014). Strong induction of IAPs during acute infection with OsHV-1 was also confirmed by Green et al. (2015) and was accompanied by strong expression of the extrinsic TNF pathway. Overall, these studies indicate that concurrent expression of IAPs, TNF, NF-kB and antiviral response proteins may be critical during OsHV-1 response and play important roles in disease resistance. Lack of full characterization of IAPs in *C. gigas*, like *C. virginica*, currently prevents large scale assessment of IAP expression patterns during OsHV-1 challenge and determination of the role IAPs play in OsHV-1 resistance.

Selective breeding for disease resistance has also been applied successfully to Dermo disease in eastern oysters, caused by the parasite *Perkinsus marinus* (Brown et al., 2005; Frank-Lawale et al., 2014; Guo, Ximing ; Ford, Susan ; DeBrosse, 2003; Proestou et al., 2016). First identified in 1951 in the Gulf of Mexico, this alveolate parasite significantly contributes to mortality and morbidity in wild and farmed eastern oyster populations from Texas to Maine (Ford and Smolowitz, 2007; Mackin, 1951; Smolowitz, 2013). *P. marinus* viability is negatively affected by low salinity and low temperature, and the range of dermo disease has expanded northward over time, likely enabled by increased winter temperatures (Burge et al., 2014; Ford and Smolowitz, 2007).

P. marinus infection is caused by contact of oyster hemocytes with the *P. marinus* trophozoite stage in the water column during filter feeding (Smolowitz, 2013). First, the hemocyte cell surface receptor CvGal binds to and recognizes *P. marinus* cell surface PAMPs (Tasumi and Vasta, 2007). Following binding, granular hemocytes engulf the parasite by phagocytosis and attempt digestion in the phagosome, and then the lysosome, deploying ROS and digestive enzymes (Smolowitz, 2013). The parasite itself, however, deploys defenses such as serine proteases and superoxide dismutases (SOD) to counteract digestion by hemocytes to continue their intracellular replication within the hemocyte (Fernández-Robledo et al., 2008; He et al., 2012; Schott et al., 2003; Smolowitz, 2013). Intracellular parasite replication eventually causes hemocyte lysis and release of newly formed trophozoites and inflammation-inducing DAMPs into the extracellular environment (Smolowitz, 2013). Infected hemocytes can also trigger apoptosis in response to intracellular infection which is hypothesized to help slow the spread of *P. marinus* infection (Hughes et al., 2010; Yee et al., 2005). Similar to other well studied intracellular

parasites, including *Toxoplasma gondii* and *Leishmania infantum*, *P. marinus* has been shown to suppress hemocyte apoptosis through mechanisms that are not fully understood but thought to include SOD neutralizing ROS release (Cianciulli et al., 2018; Hughes et al., 2010; Lau et al., 2018b; Lodoen and Lima, 2019).

Differential activation of hemocyte apoptosis has been investigated previously as a contributor to Dermo disease resistance (Goedken et al., 2005). Comparison of apoptotic responses of susceptible *C. virginica* oysters and naturally *P. marinus* resistant *C. gigas* oysters revealed that *C. gigas* oyster hemocytes overcame initial apoptosis suppression by the parasite much faster than *C. virginica* and experienced a significant increase in apoptosis compared to control, suggesting both the timing and strength of apoptotic response may be important in Dermo disease resistance (Davis and Barber, 1999; Goedken et al., 2005; Meyers et al., 1991). Though gene expression following Dermo challenge in resistant and susceptible oysters has been studied (Proestou and Sullivan, 2020), the specific apoptosis pathways affected by *P. marinus* and potential differences in regulation in resistant and susceptible oysters is not fully understood (Hughes et al., 2010; Lau et al., 2018b). Hughes et al. (2010) challenged eastern oyster hemocytes with several *P. marinus* strains *in vitro* and found that highly virulent strains increased apoptosis in initial infection stages, but this was followed by a return to basal levels after 8-24h post infection, likely attributable to apoptosis suppression by the parasite. However, challenge with less virulent strains led to a short hemocyte apoptosis suppression followed by elevated hemocyte apoptosis at later stages, suggesting the ability of hemocytes to overcome *P. marinus* apoptosis suppression at lower virulence levels. Involvement of caspase-dependent apoptosis in response to *P. marinus* was additionally investigated through treatment with

the pan-caspase inhibitor Z-FAD-FMK (Hughes et al., 2010). Z-VAD-fmk treatment did not significantly affect hemocyte apoptosis during *P. marinus* infection, suggesting hemocyte apoptosis during infection may be caspase-independent.

More recently, Lau et al., (2019) assessed apoptosis pathway expression and SOD involvement in apoptosis regulation, and suggested the mitochondrial apoptosis pathway is involved in response to *P. marinus*, and oxidation processes are critical to apoptosis regulation. This work, however, used expression of only a handful of apoptosis-related genes to analyze apoptotic response. Future work should utilize transcriptomics to obtain a broader survey of apoptosis-related genes and use computational analysis such as Weighted Gene Correlation Network Analysis (WGCNA) to correlate observed apoptosis phenotype with apoptosis gene expression. Dermo disease presents an excellent system to assess the effect of apoptosis gene expression on apoptotic response and the potential role of apoptosis in disease resistance. This investigation would improve our understanding of the complex interplay between host genetics, apoptosis phenotype, and parasite resistance and whether markers of apoptosis may be promising candidates to help screen oyster lines for *P. marinus* disease resistance.

Goals of this Dissertation

With this background knowledge in mind, the central theme of this dissertation is to investigate the relationship between apoptosis gene family diversification, apoptosis phenotype, and immune outcomes during disease response. To achieve this, four major connected goals will be addressed.

1) *Determine the full repertoire of apoptosis genes in the eastern oyster*.

This goal is enabled by previous research in molluscs and the Pacific oyster and recent whole genome sequencing of the eastern oyster (Gómez-Chiarri et al., 2015b). This dissertation will use the eastern oyster genome to characterize the molecular components of the apoptotic pathway and perform comparative analysis with *C. gigas*. Without this knowledge, apoptosis mechanisms contributing to eastern oyster disease response cannot be studied. The following specific questions will be addressed:

a) Are the major extrinsic and intrinsic pathway members from model organisms annotated in the eastern oyster genome?
b) Are alternative RCD pathways annotated in the eastern oyster genome?
c) Does the repertoire of apoptosis pathway genes differ between *C. virginica* and *C. gigas*?

2) *Characterize oyster IAP gene family diversification and potential evolutionary mechanisms of expansion, and the role of this diversification in oyster disease response.*

Current evidence indicates the expanded IAP family has diverse architecture and presents complex, orchestrated responses to immune stressors in *C. gigas* and *M. mercenaria* and responds to disease challenge in *C. virginica* (ROD, Dermo, Vibriosis). Recent *C. virginica* whole genome sequencing allows for detailed analysis of the IAP family which has not previously been performed. The importance of this gene family in apoptosis, its demonstrated usage following immune response, and its great genetic expansion in oysters make study of this gene family promising to help understand the role

of gene expansion in the regulation of the apoptotic pathway. This dissertation will specifically address the following questions:

a) How many IAPs are present in the eastern and Pacific oysters and closely related molluscs, and what evolutionary mechanisms contributed to IAP expansion?
b) Do oyster IAPs contain conserved BIR domains and domain architecture, or novel domains and architectures?
c) Is the full diversity of expanded IAP genes expressed during challenge?
d) Is IAP expression across diverse challenges characterized by usage of diverse genes and transcripts or expression of the same IAPs at different levels?

3) *Investigate eastern oyster mechanisms of apoptosis in response to P. marinus challenge.*

Apoptosis is an important immune response to *P. marinus* that has been implicated in Dermo disease resistance. The known connection between eastern oyster apoptosis and *P. marinus* challenge, and the proposed role of apoptosis in Dermo disease resistance, present exciting opportunities to assess relationships between apoptosis genotype, apoptosis phenotype, and disease resistance. To take full advantage of these opportunities, however, mechanisms of apoptosis to *P. marinus* alone must first be better characterized. The following specific questions will be investigated:

a) Is hemocyte apoptosis in response to *P. marinus* caspase-dependent?
b) Does hemocyte apoptosis in response to *P. marinus* involve mitochondrial permeabilization?

c) Are IAPs or IAP-involved pathways (intrinsic apoptosis, TLR and TNFR pathways) involved in the apoptotic response to *P. marinus*?

d) What apoptosis pathways are modulated by *P. marinus* and apoptosis inhibitor challenge, and what potential genes may *P. marinus* express to influence the oyster hemocyte apoptotic response?

e) Is apoptosis gene expression correlated with changes in apoptosis phenotype?

4) *Determine the connection between apoptosis phenotype and disease resistance in Dermo disease.*

With the previous knowledge of eastern oyster apoptosis mechanisms in response to *P. marinus in vitro* gained previously in this dissertation, this final goal will assess the connection between apoptosis phenotype and Dermo disease resistance *in vivo* to determine its potential utility as an additional measure for selective breeding for Dermo resistance, and further explore *in vivo* apoptosis mechanisms in response to *P. marinus*. The following questions will be investigated:

a) Does *P. marinus* resistance differ across the selectively bred eastern oyster families selected with variable survival in the Chesapeake Bay?

b) Does *P. marinus* challenge significantly affect hemocyte apoptosis phenotype and do families differ in their hemocyte apoptotic response?

c) Is family level hemocyte apoptosis phenotype correlated with family level resistance?

d) Is the hemocyte apoptotic response to *P. marinus* caspase-independent *in vivo?*

Knowledge gained in this dissertation contributes significantly to the study of oyster apoptosis, invertebrate host-parasite interactions, selective breeding for disease resistance, and the role of gene diversification in oyster immune response.

References

Allam, B., Raftos, D., 2015. Immune responses to infectious diseases in bivalves. J. Invertebr. Pathol. 131, 121–136. https://doi.org/10.1016/j.jip.2015.05.005

Anderson, R.S., 1994. Hemocyte-derived reactive oxygen intermediate production in four bivalve mollusks. Dev. Comp. Immunol. 18, 89–96. https://doi.org/https://doi.org/10.1016/0145-305X(94)90237-2

Azéma, P., Lamy, J.B., Boudry, P., Renault, T., Travers, M.A., Dégremont, L., 2017. Genetic parameters of resistance to Vibrio aestuarianus, and OsHV-1 infections in the Pacific oyster, Crassostrea gigas, at three different life stages. Genet. Sel. Evol. 49, 1–16. https://doi.org/10.1186/s12711-017-0297-2

Bell, R.A.V., Megeney, L.A., 2017. Evolution of caspase-mediated cell death and differentiation: Twins separated at birth. Cell Death Differ. 24, 1359–1368. https://doi.org/10.1038/cdd.2017.37

Bersoza Hernández, A., Brumbaugh, R.D., Frederick, P., Grizzle, R., Luckenbach, M.W., Peterson, C.H., Angelini, C., 2018. Restoring the eastern oyster: how much progress has been made in 53 years? Front. Ecol. Environ. 16, 463–471. https://doi.org/10.1002/fee.1935

Boardman, C.L., Maloy, A.P., Boettcher, K.J., 2008. Localization of the bacterial agent of juvenile oyster disease (Roseovarius crassostreae) within affected eastern oysters (Crassostrea virginica). J. Invertebr. Pathol. 97, 150–158. https://doi.org/10.1016/j.jip.2007.08.007

Boehm, T., Swann, J.B., 2014. Origin and evolution of adaptive immunity. Annu. Rev. Anim. Biosci. 2, 259–283. https://doi.org/10.1146/annurev-animal-022513-114201

Brown, B.L., Butt, A.J., Meritt, D., Paynter, K.T., 2005. Evaluation of resistance to Dermo in eastern oyster strains tested in Chesapeake Bay. Aquac. Res. 36, 1544–1554. https://doi.org/10.1111/j.1365-2109.2005.01377.x

Buckley, K.M., Rast, J.P., 2012. Dynamic evolution of toll-like receptor multigene families in echinoderms. Front. Immunol. 3. https://doi.org/10.3389/fimmu.2012.00136

Burge, C. a, Mark Eakin, C., Friedman, C.S., Froelich, B., Hershberger, P.K., Hofmann, E.E., Petes, L.E., Prager, K.C., Weil, E., Willis, B.L., Ford, S.E., Harvell, C.D., 2014. Climate change influences on marine infectious diseases: implications for management and society. Ann. Rev. Mar. Sci. 6, 249–77. https://doi.org/10.1146/annurev-marine-010213-135029

Chen, H., Wang, L., Zhou, Z., Hou, Z., Liu, Z., Wang, W., Gao, D., Gao, Q., Wang, M., Song, L., 2015. The comprehensive immunomodulation of NeurimmiRs in haemocytes of oyster Crassostrea gigas after acetylcholine and norepinephrine stimulation. BMC Genomics 16, 1–14. https://doi.org/10.1186/s12864-015-2150-8

Cheng, T.C., Howland, K.H., 1979. Chemotactic attraction between hemocytes of the oyster, Crassostrea virginica, and bacteria. J. Invertebr. Pathol. 33, 204–210. https://doi.org/https://doi.org/10.1016/0022-2011(79)90154-X

Cheung, C.H.A., Chang, Y.C., Lin, T.Y., Cheng, S.M., Leung, E., 2020. Anti-apoptotic proteins in the autophagic world: An update on functions of XIAP, Survivin, and BRUCE. J. Biomed. Sci. 27, 1–10. https://doi.org/10.1186/s12929-020-0627-5

Cianciulli, A., Porro, C., Calvello, R., Trotta, T., Panaro, M.A., 2018. Resistance to apoptosis in Leishmania infantum-infected human macrophages: a critical role for anti-apoptotic Bcl-2 protein and cellular IAP1/2. Clin. Exp. Med. 18, 251–261.

https://doi.org/10.1007/s10238-017-0482-1

Davis, C. V., Barber, B.J., 1999. Growth and survival of selected lines of eastern oysters, Crassostrea virginica (Gmelin 1791) affected by juvenile oyster disease. Aquaculture 178, 253–271. https://doi.org/10.1016/S0044-8486(99)00135-0

de Lorgeril, J., Lucasson, A., Petton, B., Toulza, E., Montagnani, C., Clerissi, C., Vidal-Dupiol, J., Chaparro, C., Galinier, R., Escoubas, J.M., Haffner, P., Dégremont, L., Charrière, G.M., Lafont, M., Delort, A., Vergnes, A., Chiarello, M., Faury, N., Rubio, T., Leroy, M.A., Pérignon, A., Régler, D., Morga, B., Alunno-Bruscia, M., Boudry, P., Le Roux, F., Destoumieux-Garzón, D., Gueguen, Y., Mitta, G., 2018. Immune-suppression by OsHV-1 viral infection causes fatal bacteraemia in Pacific oysters. Nat. Commun. 9. https://doi.org/10.1038/s41467-018-06659-3

Dégremont, L., Nourry, M., Maurouard, E., 2015. Mass selection for survival and resistance to OsHV-1 infection in Crassostrea gigas spat in field conditions: Response to selection after four generations. Aquaculture 446, 111–121. https://doi.org/10.1016/j.aquaculture.2015.04.029

Ebner, P., Poetsch, I., Deszcz, L., Hoffmann, T., Zuber, J., Ikeda, F., 2018. The IAP family member BRUCE regulates autophagosome–lysosome fusion. Nat. Commun. 9, 1–15. https://doi.org/10.1038/s41467-018-02823-x

Eckelman, B.P., Salvesen, G.S., Scott, F.L., 2006. Human inhibitor of apoptosis proteins: Why XIAP is the black sheep of the family. EMBO Rep. 7, 988–994. https://doi.org/10.1038/sj.embor.7400795

Elmore, S., 2007. Apoptosis: A Review of Programmed Cell Death. Toxicol. Pathol. 35, 495–516. https://doi.org/10.1080/01926230701320337

Ertl, N.G., O'Connor, W.A., Elizur, A., 2019. Molecular effects of a variable environment on Sydney rock oysters, Saccostrea glomerata: Thermal and low salinity stress, and their synergistic effect. Mar. Genomics 43, 19–32. https://doi.org/10.1016/j.margen.2018.10.003

Espinosa, E.P., Koller, A., Allam, B., 2015. Proteomic characterization of mucosal secretions in the eastern oyster, Crassostrea virginica. J. Proteomics 132, 63–76. https://doi.org/10.1016/j.jprot.2015.11.018

Estornes, Y., Bertrand, M.J.M., 2015. IAPs, regulators of innate immunity and inflammation. Semin. Cell Dev. Biol. 39, 106–114. https://doi.org/10.1016/j.semcdb.2014.03.035

Feltham, R., Vince, J.E., Lawlor, K.E., 2017. Caspase-8: Not so silently deadly. Clin. Transl. Immunol. 6, 1–13. https://doi.org/10.1038/cti.2016.83

Fernández-Robledo, J.A., Schott, E.J., Vasta, G.R., 2008. Perkinsus marinus superoxide dismutase 2 (PmSOD2) localizes to single-membrane subcellular compartments. Biochem. Biophys. Res. Commun. 375, 215–219. https://doi.org/10.1016/j.bbrc.2008.07.162

Fleury, E., Huvet, A., 2012. Microarray Analysis Highlights Immune Response of Pacific Oysters as a Determinant of Resistance to Summer Mortality. Mar. Biotechnol. 14, 203–217. https://doi.org/10.1007/s10126-011-9403-6

Fogarty, C.E., Bergmann, A., 2017. Killers creating new life: Caspases drive apoptosis-induced proliferation in tissue repair and disease. Cell Death Differ. 24, 1390–1400. https://doi.org/10.1038/cdd.2017.47

Ford, S.E., Smolowitz, Æ.R., 2007. Infection dynamics of an oyster parasite in its newly

expanded range 119–133. https://doi.org/10.1007/s00227-006-0454-6

Foster, B., Grewal, S., Graves, O., Hughes, F.M., Sokolova, I.M., 2011. Fish & Shell fi sh Immunology Copper exposure affects hemocyte apoptosis and Perkinsus marinus infection in eastern oysters Crassostrea virginica (Gmelin). Fish Shellfish Immunol. 31, 341–349. https://doi.org/10.1016/j.fsi.2011.05.024

Frank-Lawale, A., Allen, S.K., Dégremont, L., 2014. Breeding and Domestication of Eastern Oyster (Crassostrea virginica) Lines for Culture in the Mid-Atlantic, Usa: Line Development and Mass Selection for Disease Resistance . J. Shellfish Res. 33, 153–165. https://doi.org/10.2983/035.033.0115

Galbán, S., Duckett, C.S., 2010. XIAP as a ubiquitin ligase in cellular signaling. Cell Death Differ. 17, 54–60. https://doi.org/10.1038/cdd.2009.81

Galluzzi, L., López-Soto, A., Kumar, S., Kroemer, G., 2016. Caspases Connect Cell-Death Signaling to Organismal Homeostasis. Immunity 44, 221–231. https://doi.org/10.1016/j.immuni.2016.01.020

Galluzzi, L., Vitale, I., Aaronson, S.A., Abrams, J.M., Adam, D., Agostinis, P., Alnemri, E.S., Altucci, L., Amelio, I., Andrews, D.W., Annicchiarico-Petruzzelli, M., Antonov, A. V, Arama, E., Baehrecke, E.H., Barlev, N.A., Bazan, N.G., Bernassola, F., Bertrand, M.J.M., Bianchi, K., Blagosklonny, M. V, Blomgren, K., Borner, C., Boya, P., Brenner, C., Campanella, M., Candi, E., Carmona-Gutierrez, D., Cecconi, F., Chan, F.K.-M., Chandel, N.S., Cheng, E.H., Chipuk, J.E., Cidlowski, J.A., Ciechanover, A., Cohen, G.M., Conrad, M., Cubillos-Ruiz, J.R., Czabotar, P.E., D'Angiolella, V., Dawson, T.M., Dawson, V.L., De Laurenzi, V., De Maria, R., Debatin, K.-M., DeBerardinis, R.J., Deshmukh, M., Di Daniele, N., Di Virgilio, F.,

Dixit, V.M., Dixon, S.J., Duckett, C.S., Dynlacht, B.D., El-Deiry, W.S., Elrod, J.W., Fimia, G.M., Fulda, S., García-Sáez, A.J., Garg, A.D., Garrido, C., Gavathiotis, E., Golstein, P., Gottlieb, E., Green, D.R., Greene, L.A., Gronemeyer, H., Gross, A., Hajnoczky, G., Hardwick, J.M., Harris, I.S., Hengartner, M.O., Hetz, C., Ichijo, H., Jäättelä, M., Joseph, B., Jost, P.J., Juin, P.P., Kaiser, W.J., Karin, M., Kaufmann, T., Kepp, O., Kimchi, A., Kitsis, R.N., Klionsky, D.J., Knight, R.A., Kumar, S., Lee, S.W., Lemasters, J.J., Levine, B., Linkermann, A., Lipton, S.A., Lockshin, R.A., López-Otín, C., Lowe, S.W., Luedde, T., Lugli, E., MacFarlane, M., Madeo, F., Malewicz, M., Malorni, W., Manic, G., Marine, J.-C., Martin, S.J., Martinou, J.-C., Medema, J.P., Mehlen, P., Meier, P., Melino, S., Miao, E.A., Molkentin, J.D., Moll, U.M., Muñoz-Pinedo, C., Nagata, S., Nuñez, G., Oberst, A., Oren, M., Overholtzer, M., Pagano, M., Panaretakis, T., Pasparakis, M., Penninger, J.M., Pereira, D.M., Pervaiz, S., Peter, M.E., Piacentini, M., Pinton, P., Prehn, J.H.M., Puthalakath, H., Rabinovich, G.A., Rehm, M., Rizzuto, R., Rodrigues, C.M.P., Rubinsztein, D.C., Rudel, T., Ryan, K.M., Sayan, E., Scorrano, L., Shao, F., Shi, Y., Silke, J., Simon, H.-U., Sistigu, A., Stockwell, B.R., Strasser, A., Szabadkai, G., Tait, S.W.G., Tang, D., Tavernarakis, N., Thorburn, A., Tsujimoto, Y., Turk, B., Vanden Berghe, T., Vandenabeele, P., Vander Heiden, M.G., Villunger, A., Virgin, H.W., Vousden, K.H., Vucic, D., Wagner, E.F., Walczak, H., Wallach, D., Wang, Y., Wells, J.A., Wood, W., Yuan, J., Zakeri, Z., Zhivotovsky, B., Zitvogel, L., Melino, G., Kroemer, G., 2018. Molecular mechanisms of cell death: recommendations of the Nomenclature Committee on Cell Death 2018. Cell Death Differ. 25, 486–541. https://doi.org/10.1038/s41418-017-0012-4

Ge, C., Che, L., Ren, J., Pandita, R.K., Lu, J., Li, K., Pandita, T.K., Du, C., 2015. BRUCE regulates DNA double-strand break response by promoting USP8 deubiquitination of BRIT1. Proc. Natl. Acad. Sci. U. S. A. 112, E1210–E1219. https://doi.org/10.1073/pnas.1418335112

Genthner, F.J., Volety, A.K., Oliver, L.M., Fisher, W.S., 1999. Factors influencing in vitro killing of bacteria by hemocytes of the eastern oyster (Crassostrea virginica). Appl. Environ. Microbiol. 65, 3015–3020.

Gerdol, M., Luo, Y.J., Satoh, N., Pallavicini, A., 2018. Genetic and molecular basis of the immune system in the brachiopod Lingula anatina. Dev. Comp. Immunol. 82, 7–30. https://doi.org/10.1016/j.dci.2017.12.021

Gerdol, M., Venier, P., Edomi, P., Pallavicini, A., 2017. Diversity and evolution of TIR-domain-containing proteins in bivalves and Metazoa: New insights from comparative genomics. Dev. Comp. Immunol. https://doi.org/10.1016/j.dci.2017.01.014

Gifondorwa, D.J., Leise, E.M., Gifondorwa, D.J., Leise, E.M., 2017. Programmed Cell Death in the Apical Ganglion during Larval Metamorphosis of the Marine Mollusc Ilyanassa obsoleta Linked references are available on JSTOR for this article : Programmed Cell Death in the Apical Ganglion During Larval Metamorphosis of the M 210, 109–120.

Goedken, M., Morsey, B., Sunila, I., De Guise, S., 2005. Immunomodulation of Crassostrea gigas and Crassostrea virginica cellular defense mechanism by Perkinsus marinus. J. Shellfish Res. 24, 487–496. https://doi.org/10.2983/0730-8000(2005)24

Gómez-Chiarri, M., Guo, X., Tanguy, A., He, Y., Proestou, D., 2015a. The use of -omic tools in the study of disease processes in marine bivalve mollusks. J. Invertebr. Pathol.

131, 137–154. https://doi.org/10.1016/j.jip.2015.05.007

Gómez-Chiarri, M., Warren, W.C., Guo, X., Proestou, D., 2015b. Developing tools for the study of molluscan immunity: The sequencing of the genome of the eastern oyster, Crassostrea virginica. Fish Shellfish Immunol. 46, 2–4. https://doi.org/10.1016/j.fsi.2015.05.004

Gómez-León, J., Leavitt, D., Gomez-chiarri, M., Gómez-león, J., Villamil, L., Salger, S.A., Sallum, R.H., Remacha-triviño, A., Leavitt, D.F., Gómez-chiarri, M., 2015. Survival of eastern oyster Crassostrea virginica from three lines following experimental challenge with bacterial pathogens . Survival of eastern oysters Crassostrea virginica from three lines following experimental challenge with bacterial pathogens. https://doi.org/10.3354/dao01902

Gorelick-Ashkenazi, A., Weiss, R., Sapozhnikov, L., Florentin, A., Tarayrah-Ibraheim, L., Dweik, D., Yacobi-Sharon, K., Arama, E., 2018. Caspases maintain tissue integrity by an apoptosis-independent inhibition of cell migration and invasion. Nat. Commun. 9. https://doi.org/10.1038/s41467-018-05204-6

Grabowski, J.H., Peterson, C.H., 2007. Restoring oyster reefs to recover ecosystem services. Ecosyst. Eng. plants to protists 4, 281–298.

Green, T.J., Rolland, J.L., Vergnes, A., Raftos, D., Montagnani, C., 2015. OsHV-1 countermeasures to the Pacific oyster's anti-viral response. Fish Shellfish Immunol. 47, 435–443. https://doi.org/10.1016/j.fsi.2015.09.025

Green, T.J., Vergnes, A., Montagnani, C., Lorgeril, J. De, 2016. Distinct immune responses of juvenile and adult oysters (Crassostrea gigas) to viral and bacterial infections. Vet. Res. 1, 1–11. https://doi.org/10.1186/s13567-016-0356-7

Guo, Ximing ; Ford, Susan ; DeBrosse, G., 2003. Breeding and evaluation of eastern oyster strains selected for MSX, Dermo and JOD resistance 22, 2003.

Guo, X., Ford, S.E., 2016. Infectious diseases of marine molluscs and host responses as revealed by genomic tools. Philos. Trans. R. Soc. B Biol. Sci. 371, 20150206. https://doi.org/10.1098/rstb.2015.0206

He, Y., Yu, H., Bao, Z., Zhang, Q., Guo, X., 2012. Mutation in promoter region of a serine protease inhibitor confers Perkinsus marinus resistance in the eastern oyster (Crassostrea virginica). Fish Shellfish Immunol. 33, 411–417. https://doi.org/10.1016/j.fsi.2012.05.028

Hughes, F.M., Foster, B., Grewal, S., Sokolova, I.M., 2010. Apoptosis as a host defense mechanism in Crassostrea virginica and its modulation by Perkinsus marinus. Fish Shellfish Immunol. 29, 247–257. https://doi.org/10.1016/j.fsi.2010.03.003

Kiss, T., 2010. Apoptosis and its functional significance in molluscs. Apoptosis 15, 313–321. https://doi.org/10.1007/s10495-009-0446-3

Kocab, A.J., Duckett, C.S., 2016. Inhibitor of apoptosis proteins as intracellular signaling intermediates. FEBS J. 283, 221–231. https://doi.org/10.1111/febs.13554

Labreuche, Y., Lambert, C., Soudant, P., Boulo, V., Huvet, A., Nicolas, J.L., 2006a. Cellular and molecular hemocyte responses of the Pacific oyster, Crassostrea gigas, following bacterial infection with Vibrio aestuarianus strain 01/32. Microbes Infect. 8, 2715–2724. https://doi.org/10.1016/j.micinf.2006.07.020

Labreuche, Y., Soudant, P., Gonçalves, M., Lambert, C., Nicolas, J.L., 2006b. Effects of extracellular products from the pathogenic Vibrio aestuarianus strain 01/32 on lethality and cellular immune responses of the oyster Crassostrea gigas. Dev. Comp.

Immunol. 30, 367–379. https://doi.org/10.1016/j.dci.2005.05.003

Lamb, H.M., 2020. Double agents of cell death: novel emerging functions of apoptotic regulators. FEBS J. 287, 2647–2663. https://doi.org/10.1111/febs.15308

Lau, Y.T., Gambino, L., Santos, B., Pales Espinosa, E., Allam, B., 2018a. Transepithelial migration of mucosal hemocytes in Crassostrea virginica and potential role in Perkinsus marinus pathogenesis. J. Invertebr. Pathol. 153, 122–129. https://doi.org/10.1016/j.jip.2018.03.004

Lau, Y.T., Santos, B., Barbosa, M., Pales Espinosa, E., Allam, B., 2018b. Regulation of apoptosis-related genes during interactions between oyster hemocytes and the alveolate parasite Perkinsus marinus. Fish Shellfish Immunol. 83, 180–189. https://doi.org/10.1016/j.fsi.2018.09.006

Li, Y., Zhang, L., Qu, T., Tang, X., Li, L., Zhang, G., 2017. Conservation and divergence of mitochondrial apoptosis pathway in the Pacific oyster , Crassostrea gigas 82898701, 1–13. https://doi.org/10.1038/cddis.2017.307

Lin, Y., Mao, F., Zhang, X., Xu, D., He, Z., Li, J., Xiang, Z., Zhang, Y., Yu, Z., 2020. TRAF6 suppresses the apoptosis of hemocytes by activating pellino in Crassostrea hongkongensis. Dev. Comp. Immunol. 103, 103501. https://doi.org/10.1016/j.dci.2019.103501

Lockshin, R.A., 2007. Guest Editor : A . Samali Cell death in health and disease 11, 1214–1224. https://doi.org/10.1111/j.1582-4934.2007.00150.x

Lodoen, M.B., Lima, T.S., 2019. Mechanisms of Human Innate Immune Evasion by Toxoplasma gondii 9, 1–8. https://doi.org/10.3389/fcimb.2019.00103

López-Galindo, L., Juárez, O.E., Larios-Soriano, E., Vecchio, G. Del, Ventura-López, C.,

Lago-Lestón, A., Galindo-Sánchez, C., 2019. Transcriptomic analysis reveals insights on male infertility in octopus maya under chronic thermal stress. Front. Physiol. 9, 1–18. https://doi.org/10.3389/fphys.2018.01920

Mackenzie, C.L., 2007. CAUSES UNDERLYING THE HISTORICAL DECLINE IN EASTERN OYSTER (CRASSOSTREA VIRGINICA GMELIN , 1791) LANDINGS 26, 927–938.

Mackin, J.G., 1951. Histopathology of infection of Crassostrea virginica (Gmelin) by Dermocystidium marinum Mackin, Owen, and Collier. Bull. Mar. Sci. 1, 72–87.

Maloy, A.P., Ford, S.E., Karney, R.C., Boettcher, K.J., 2007. Roseovarius crassostreae, the etiological agent of Juvenile Oyster Disease (now to be known as Roseovarius Oyster Disease) in Crassostrea virginica. Aquaculture 269, 71–83. https://doi.org/10.1016/j.aquaculture.2007.04.008

Mao, F., Lin, Y., Zhou, Y., He, Z., Li, J., Zhang, Y., Yu, Z., 2018. Structural and functional analysis of interferon regulatory factors (IRFs) reveals a novel regulatory model in an invertebrate, Crassostrea gigas. Dev. Comp. Immunol. 89, 14–22. https://doi.org/10.1016/j.dci.2018.07.027

Martinez, M.M., Reif, R.D., Pappas, D., 2010. Detection of apoptosis: A review of conventional and novel techniques. Anal. Methods 2, 996–1004. https://doi.org/10.1039/c0ay00247j

McDowell, I.C., Modak, T.H., Lane, C.E., Gomez-Chiarri, M., 2016. Multi-species protein similarity clustering reveals novel expanded immune gene families in the eastern oyster Crassostrea virginica. Fish Shellfish Immunol. 53, 13–23. https://doi.org/10.1016/j.fsi.2016.03.157

Meyers, J.A., Burreson, E.M., Barber, B.J., Mann, R., 1991. Susceptibility of diploid and triploid oysters, Crassostrea gigas, to Perkinsus marinus. J. Shellfish Res 10, 304.

Nakajima, Y.I., Kuranaga, E., 2017. Caspase-dependent non-apoptotic processes in development. Cell Death Differ. 24, 1422–1430. https://doi.org/10.1038/cdd.2017.36

Oberoi-Khanuja, T.K., Karreman, C., Larisch, S., Rapp, U.R., Rajalingam, K., 2012. Role of melanoma inhibitor of apoptosis (ML-IAP) protein, a member of the baculoviral IAP repeat (BIR) domain family, in the regulation of C-RAF kinase and cell migration. J. Biol. Chem. 287, 28445–28455. https://doi.org/10.1074/jbc.M112.341297

Oberoi-Khanuja, T.K., Murali, A., Rajalingam, K., 2013. IAPs on the move: Role of inhibitors of apoptosis proteins in cell migration. Cell Death Dis. 4. https://doi.org/10.1038/cddis.2013.311

Oberst, A., Bender, C., Green, D.R., 2009. Living with death: The evolution of the mitochondrial pathway of apoptosis in animals 15, 1139–1146. https://doi.org/10.1038/cdd.2008.65.Living

Plachetzki, D.C., Pankey, M.S., MacManes, M.D., Lesser, M.P., Walker, C.W., 2020. The Genome of the Softshell Clam Mya arenaria and the Evolution of Apoptosis. Genome Biol. Evol. 12, 1681–1693. https://doi.org/10.1093/gbe/evaa143

Proestou, D.A., Sullivan, M.E., 2020. Variation in global transcriptomic response to Perkinsus marinus infection among eastern oyster families highlights potential mechanisms of disease resistance. Fish Shellfish Immunol. 96, 141–151. https://doi.org/10.1016/j.fsi.2019.12.001

Proestou, D.A., Vinyard, B.T., Corbett, R.J., Piesz, J., Allen, S.K., Small, J.M., Li, C., Liu,

M., DeBrosse, G., Guo, X., Rawson, P., Gómez-Chiarri, M., 2016. Performance of selectively-bred lines of eastern oyster, Crassostrea virginica, across eastern US estuaries. Aquaculture 464, 17–27. https://doi.org/10.1016/j.aquaculture.2016.06.012

Richards, G.P., Watson, M.A., Needleman, D.S., Church, K.M., Häse, C.C., 2015. Mortalities of Eastern And Pacific oyster larvae caused by the pathogens Vibrio coralliilyticus and Vibrio tubiashii. Appl. Environ. Microbiol. 81, 292–297. https://doi.org/10.1128/AEM.02930-14

Romero, A., Figueras, A., Novoa, B., 2013. Genes of the Mitochondrial Apoptotic Pathway in Mytilus galloprovincialis 8. https://doi.org/10.1371/journal.pone.0061502

Romero, A., Novoa, B., Figueras, A., 2015. The complexity of apoptotic cell death in mollusks: An update. Fish Shellfish Immunol. 46, 79–87. https://doi.org/10.1016/j.fsi.2015.03.038

Ross, W., Timothy Gallaudet, R., Ret, U., Oliver, C., 2018. Fisheries of the United States 2017 Report- NOAA National Marine Fisheries Service.

Saleem, M., Qadir, M.I., Perveen, N., Ahmad, B., Saleem, U., Irshad, T., 2013. Inhibitors of apoptotic proteins: New targets for anticancer therapy. Chem. Biol. Drug Des. 82, 243–251. https://doi.org/10.1111/cbdd.12176

Samain, J.-F., McCombie, H., 2008. Summer mortality of Pacific oyster Crassostrea gigas: the Morest project. Editions Quae.

Samain, J.F., Dégremont, L., Soletchnik, P., Haure, J., Bédier, E., Ropert, M., Moal, J., Huvet, A., Bacca, H., Van Wormhoudt, A., Delaporte, M., Costil, K., Pouvreau, S., Lambert, C., Boulo, V., Soudant, P., Nicolas, J.L., Le Roux, F., Renault, T., Gagnaire, B., Geret, F., Boutet, I., Burgeot, T., Boudry, P., 2007. Genetically based resistance

to summer mortality in the Pacific oyster (Crassostrea gigas) and its relationship with physiological, immunological characteristics and infection processes. Aquaculture 268, 227–243. https://doi.org/10.1016/j.aquaculture.2007.04.044

Sauvage, C., Bierne, N., Lapègue, S., Boudry, P., 2007. Single Nucleotide polymorphisms and their relationship to codon usage bias in the Pacific oyster Crassostrea gigas. Gene 406, 13–22. https://doi.org/10.1016/j.gene.2007.05.011

Schott, E.J., Pecher, W.T., Okafor, F., Vasta, G.R., 2003. The protistan parasite Perkinsus marinus is resistant to selected reactive oxygen species 105, 232–240. https://doi.org/10.1016/j.exppara.2003.12.012

Segarra, A., Mauduit, F., Faury, N., Trancart, S., Dégremont, L., Tourbiez, D., Haffner, P., Barbosa-Solomieu, V., Pépin, J.-F., Travers, M.-A., Renault, T., 2014. Dual transcriptomics of virus-host interactions: comparing two Pacific oyster families presenting contrasted susceptibility to ostreid herpesvirus 1. BMC Genomics 15, 580. https://doi.org/10.1186/1471-2164-15-580

Smolowitz, R., 2013. A Review of Current State of Knowledge Concerning Perkinsus marinus Effects on Crassostrea virginica (Gmelin) (the Eastern Oyster) 50, 404–411. https://doi.org/10.1177/0300985813480806

Sokolov, E.P., Markert, S., Hinzke, T., Hirschfeld, C., Becher, D., Ponsuksili, S., Sokolova, I.M., 2019. Effects of hypoxia-reoxygenation stress on mitochondrial proteome and bioenergetics of the hypoxia-tolerant marine bivalve Crassostrea gigas. J. Proteomics 194, 99–111. https://doi.org/10.1016/j.jprot.2018.12.009

Sokolova, I., 2009. Apoptosis in molluscan immune defense. Invertebr. Surviv. J. 6, 49–58. https://doi.org/10.1242/jcs.00210

Sokolova, I.M., Evans, S., Hughes, F.M., 2004. Cadmium-induced apoptosis in oyster hemocytes involves disturbance of cellular energy balance but no mitochondrial permeability transition 3369–3380. https://doi.org/10.1242/jeb.01152

Solier, S., Fontenay, M., Vainchenker, W., Droin, N., Solary, E., 2017. Non-apoptotic functions of caspases in myeloid cell differentiation. Cell Death Differ. 24, 1337–1347. https://doi.org/10.1038/cdd.2017.19

Song, H., Guo, X., Sun, L., Wang, Qianghui, Han, F., Wang, H., Wray, G.A., Davidson, P., Wang, Qing, Hu, Z., Zhou, C., Yu, Z., Yang, M., 2021. The hard clam genome reveals massive expansion and diversification of inhibitors of apoptosis in Bivalvia 1–20.

Sun, G., Guzman, E., Zhou, H.R., Kosik, K.S., Montell, D.J., 2017. A molecular signature for anastasis, recovery from the brink of apoptotic cell death. bioRxiv 216, 3355–3368. https://doi.org/10.1101/102640

Sunila, I., Cooperative, D., 2017. The effects of temperature and salinity on apoptosis of Crassostrea virginica hemocytes and Perkinsus marinus. https://doi.org/10.2983/0730-8000(2005)24

Sunila, I., LaBanca, J., 2003. Apoptosis in the pathogenesis of infectious diseases of the eastern oyster Crassostrea virginica. Dis. Aquat. Organ. 56, 163–170. https://doi.org/10.3354/dao056163

Tang, H.M., Tang, H.L., 2018. Anastasis: Recovery from the brink of cell death. R. Soc. Open Sci. 5. https://doi.org/10.1098/rsos.180442

Tasumi, S., Vasta, G.R., 2007. A Galectin of Unique Domain Organization from Hemocytes of the Eastern Oyster (Crassostrea virginica) Is a Receptor for the

Protistan Parasite Perkinsus marinus. J. Immunol. 179, 3086–3098. https://doi.org/10.4049/jimmunol.179.5.3086

Vasudevan, D., Don Ryoo, H., 2015. Regulation of Cell Death by IAPs and Their Antagonists, 1st ed, Current Topics in Developmental Biology. Elsevier Inc. https://doi.org/10.1016/bs.ctdb.2015.07.026

Vogeler, S., Carboni, S., n.d. Phylogenetic analysis of the caspase family in bivalves : implications for programmed cell death , immune response and development 1–27.

Vogeler, S., Carboni, S., Li, X., Joyce, A., 2021. Phylogenetic analysis of the caspase family in bivalves: implications for programmed cell death, immune response and development. BMC Genomics 22, 1–17. https://doi.org/10.1186/s12864-021-07380-0

Wang, S., Peatman, E., Liu, H., Bushek, D., Ford, S.E., Kucuktas, H., Quilang, J., Li, P., Wallace, R., Wang, Y., Guo, X., Liu, Z., 2010. Microarray analysis of gene expression in eastern oyster (Crassostrea virginica) reveals a novel combination of antimicrobial and oxidative stress host responses after dermo (Perkinsus marinus) challenge. Fish Shellfish Immunol. 29, 921–929. https://doi.org/10.1016/j.fsi.2010.07.035

Wikfors, G.H., Alix, J.H., 2014. Granular hemocytes are phagocytic, but agranular hemocytes are not, in the Eastern Oyster Crassostrea virginica. Invertebr. Immun. 1, 15–21. https://doi.org/10.2478/invim-2014-0001

Xue, Q.G., Schey, K.L., Volety, A.K., Chu, F.L.E., La Peyre, J.F., 2004. Purification and characterization of lysozyme from plasma of the eastern oyster (Crassostrea virginica). Comp. Biochem. Physiol. - B Biochem. Mol. Biol. 139, 11–25. https://doi.org/10.1016/j.cbpc.2004.05.011

Yee, A., Dungan, C., Hamilton, R., Goedken, M., Guise, S.D.E., Sunila, I., 2005. Apoptosis of the protozoan oyster pathogen Perkinsus marinus in vivo and in vitro in the Chesapeake Bay and the Long Island Sound. J. Shellfish Res. 24, 1035–1042. https://doi.org/10.2983/0730-8000(2005)24[1035:aotpop]2.0.co;2

Young, T., Kesarcodi-Watson, A., Alfaro, A.C., Merien, F., Nguyen, T. V., Mae, H., Le, D. V., Villas-Bôas, S., 2017. Differential expression of novel metabolic and immunological biomarkers in oysters challenged with a virulent strain of OsHV-1. Dev. Comp. Immunol. 73, 229–245. https://doi.org/10.1016/j.dci.2017.03.025

Yu, F., Zhang, Y., Yu, Z., 2012. Characteristics and expression patterns of the lipopolysaccharide-induced TNF-α factor (LITAF) gene family in the Pacific oyster, Crassostrea gigas. Fish Shellfish Immunol. 33, 899–908. https://doi.org/10.1016/j.fsi.2012.07.021

Yu, M., Chen, J., Bao, Y., Li, J., 2018. Genomic analysis of NF-κB signaling pathway reveals its complexity in Crassostrea gigas. Fish Shellfish Immunol. 72, 510–518. https://doi.org/10.1016/j.fsi.2017.11.034

Zhang, G., Fang, X., Guo, X., Li, L., Luo, R., Xu, F., Yang, P., Zhang, L., Wu, F., Chen, Y., Wang, J., Peng, C., Meng, J., Yang, L., Liu, J., Wen, B., Zhang, N., Huang, Z., 2012. The oyster genome reveals stress adaptation and complexity of shell formation. https://doi.org/10.1038/nature11413

Zhang, L., Li, L., Guo, X., Litman, G.W., Dishaw, L.J., Zhang, G., 2015. Massive expansion and functional divergence of innate immune genes in a protostome. Sci. Rep. 5, 8693. https://doi.org/10.1038/srep08693

Zhang, L., Li, L., Zhu, Y., Zhang, G., Guo, X., 2014. Transcriptome Analysis Reveals a

Rich Gene Set Related to Innate Immunity in the Eastern Oyster (Crassostrea virginica). Mar. Biotechnol. 16, 17–33. https://doi.org/10.1007/s10126-013-9526-z

Zhang, L.L., Li, L., Zhang, G.F., 2012. Sequence variability of fibrinogen-related proteins (FREPs) in Crassostrea gigas. Chinese Sci. Bull. 57, 3312–3319. https://doi.org/10.1007/s11434-012-5155-6

Zheng, N., Shabek, N., 2017. Ubiquitin Ligases: Structure, Function, and Regulation. Annu. Rev. Biochem. 86, 129–157. https://doi.org/10.1146/annurev-biochem-060815-014922

Zmasek, C.M., Godzik, A., 2013. Evolution of the animal apoptosis network. Cold Spring Harb. Perspect. Biol. 5. https://doi.org/10.1101/cshperspect.a008649

Tables

Table I. Summary of Major Non-apoptotic Regulated Cell Death Pathways

Cell Death Pathway	Description
Autophagy Dependent Cell Death (ADCD)	RCD pathway that occurs in pathophysiological or developmental settings when the molecular machinery of autophagy contributes to cellular demise (Galluzzi et al., 2018).
Ferroptosis	RCD pathway induced by oxidative disruptions in the intracellular environment, notably severe lipid peroxidation driven by ROS and iron availability, and is controlled by reduced glutathione (GSH)-dependent enzyme glutathione peroxidase 4 (GPX4) (Galluzzi et al., 2018).
Lysosome Dependent Cell Death (LDCD)	RCD pathway triggered by lysosome membrane permeabilization (LMP) in the context of several conditions (aging, inflammation, intracellular pathogens), mediated by lysosomal cathepsins following their release from the lysosome, and sometimes involves MOMP and caspases (Galluzzi et al., 2018).
MPT-driven necrosis	RCD pathway triggered by an overload of intracellular calcium or oxidative stress, relies on the protein cyclophilin D (CYPD), and presents with necrotic morphology (Galluzzi et al., 2018).
Necroptosis	RCD pathway triggered by death-receptor (FAS, TNFR1) or PRR (TLR3, TLR4) binding and critically depends on sequential activation of receptor Interacting Protein Kinase 1 (RIPK3) and mixed lineage kinase domain like pseudokinase (MLKL), and sometimes RIPK1 (Galluzzi et al., 2018).
NETotic cell death	RCD pathway dependent on ROS and involving extrusion of neutrophil extracellular traps (NET) (Galluzzi et al., 2018).
Parthanatos	RCD pathway involved in DNA-damage response to oxidative stress (ROS, RNS) and hypoxia. Hyperactivation of poly (ADP-ribose) polymerase 1 (PARP1) leads to redox and bioenergetic collapse and eventual MOMP, and involves DNA degradation by AIF and macrophage inhibitor factor (MIF) (Galluzzi et al., 2018).
Pyroptosis	RCD pathway in the context of pathogen invasion involving activation of inflammatory caspases, typically CASP1 and CASP3, leading to cleavage and activation of protein members of the gasdermin family which then form pores in the outer plasma membrane of the cell leading to cell death (Galluzzi et al., 2018).

CHAPTER II: The expanded Inhibitor of Apoptosis gene family in oysters possesses novel domain architectures and may play diverse roles in apoptosis following immune challenge

Erin M. Roberts[1], Dina A. Proestou[2], Marta Gomez-Chiarri[1*]

[1]University of Rhode Island, Department of Fisheries, Animal and Veterinary Science, Kingston, RI, USA.

[2]USDA ARS NEA NCWMAC Shellfish Genetics Program, Kingston, RI, USA

*Correspondence:

Marta Gomez-Chiarri

gomezchi@uri.edu

Prepared for submission to ***BMC Genomics***

Keywords: transcriptome, oyster, WGCNA, Inhibitor of Apoptosis Proteins (IAP), DESeq2, gene expansion, apoptosis, immunity

Abstract

Background: Apoptosis plays important roles in a variety of functions, including immunity and response to environmental stress. The Inhibitor of Apoptosis (IAP) gene family of apoptosis regulators is expanded in molluscs, including eastern, *Crassostrea virginica*, and Pacific, *Crassostrea gigas,* oysters. The functional importance of IAP expansion in apoptosis and immunity in oysters remains unknown.

Results: Phylogenetic analysis of IAP genes in 10 molluscs identified lineage specific gene expansion in bivalve species. Greater IAP gene family expansion was observed in *C. virginica* than *C. gigas* (69 vs. 40), resulting mainly from tandem duplications. Functional domain analysis of oyster IAP proteins revealed 3 novel Baculoviral IAP Repeat (BIR) domain types and 14 domain architecture types across gene clusters, 4 of which are not present in model organisms. Phylogenetic analysis of bivalve IAPs suggests a complex history of domain loss and gain. Most IAP genes in oysters (76% of *C. virginica* and 82% of *C. gigas*), representing all domain architecture types, were expressed in response to immune challenge (Ostreid Herpesvirus OsHV-1, bacterial probionts *Phaeobacter inhibens* and *Bacillus pumilus*, several *Vibrio* spp., pathogenic *Aliiroseovarius crassostreae*, and protozoan parasite *Perkinsus marinus*). Patterns of IAP and apoptosis-related differential gene expression differed between the two oyster species, where *C. virginica*, in general, differentially expressed a unique set of IAP genes in each challenge, while *C. gigas* differentially expressed an overlapping set of IAP genes across challenges. Apoptosis gene expression patterns clustered mainly by resistance/susceptibility of the oyster host to immune challenge. WGCNA analysis revealed unique combinations of

transcripts for 1 to 12 IAP domain architecture types, including novel types, were significantly co-expressed in response to immune challenge with transcripts in apoptosis-related pathways.

Conclusions: Unprecedented diversity characterized by novel BIR domains and protein domain architectures was observed in oyster IAPs. Complex patterns of gene expression of novel and conserved IAPs in response to a variety of ecologically-relevant immune challenges, combined with evidence of direct co-expression of IAP genes with apoptosis-related transcripts, suggests IAP expansion facilitates complex and nuanced regulation of apoptosis and other immune responses in oysters.

Introduction

Invertebrates lack the adaptive immune system of vertebrates and instead rely on complex innate immune systems with highly diverse (within and between species) gene families of pattern recognition receptors (PRRs) and effector molecules[1,2]. Whole genome sequencing of several ecologically and economically important bivalve molluscs, including clams, mussels, oysters, and scallops, have revealed large-scale expansion and diversification of several immune gene families, including the PRRs Toll-Like Receptors (TLRs), C1qDC proteins, Fibrinogen-related proteins (FREPs), and members of the Inhibitor of Apoptosis Proteins (IAP) family, also called BIR domain-containing (BIRC) proteins[3–10]. Transcriptomic studies in bivalves indicate expanded immune gene families display highly specific and orchestrated gene expression responses to biotic and abiotic stressors[3,4,6,11–16]. These gene families may have undergone functional diversification, which is hypothesized to enhance the oyster's ability to mount tailored immune responses to the variety of pathogens in their environment[3,4,17].

In oyster *(Crassostrea* and *Ostrea*) species, apoptosis is critical for fighting viral, parasitic, and bacterial infections[18–20]. Apoptosis, or Type 1 programmed cell death, is a highly conserved form of regulated cell death mediated by two major pathways, the death-receptor mediated (extrinsic) pathway, and the mitochondrial (intrinsic) pathway[21]. Apoptosis pathways crosstalk extensively with other immune pathways, including inflammation mediated by Nuclear Factor-κB (NF-κB), autophagy, and alternative forms of cell death like necroptosis and parthanatos[21,22]. In hemocytes, the major immune and phagocytic cell of the oyster, different immune stressors can stimulate or suppress apoptosis in unique ways, leading to varied pathological outcomes[20].

Inhibitor of Apoptosis proteins regulate cell death pathways by directly or indirectly inhibiting caspases, regulating ubiquitin (Ub)-dependent signaling events via E3 ligase activity, and mediating activation of the pro-survival NF-κB pathway[23,24]. Mammals have 8 BIRC members; BIRC1 (NAIP), BIRC2 (cIAP1), BIRC3 (cIAP2), BIRC4 (XIAP), BIRC5 (Survivin), BIRC6 (BRUCE/Apollon), BIRC7 (ML-IAP), and BIRC8 (ILP2)[25], while *Drosophila melanogaster* contains two (DIAP1 and DIAP2)[26]. IAPs are characterized by possession of one to three N-terminal Baculovirus IAP Repeat (BIR) domains, which are classified as Type I or Type II[23]. The unique functions of IAPs are influenced by the number and combinations of Type I and Type II BIR repeats, and by the presence of key additional protein domains. Type II BIRs possess a hydrophobic deep peptide binding groove that binds caspases and IAP antagonists (i.e. Smac/DIABLO) that have N-terminal IAP binding motifs (IBMs). Type I BIRs interact instead with Tumor Necrosis Factor Receptor Associated Factor (TRAF) 1, TRAF2, and transforming growth factor-B activated kinase (TAK1) binding protein (TAB1), involved in promoting cell survival and NF-κB pathway activation[27–29]. IAPs can also possess Really Interesting New Gene (RING), ubiquitin-associated (UBA), ubiquitin-conjugating (UBC), and caspase activation and recruitment (CARD) domains. The RING, UBA, and UBC domains play critical roles in the ubiquitination cascade, where the UBC domain acts as an E2 ubiquitin-conjugating enzyme, the RING domain acts as an E3 ubiquitin ligase, and the UBA domain allows for binding of unique polyubiquitin chains. IAPs therefore also play critical roles in targeting proteins for proteasomal degradation and overall protein turnover[30].

Investigation of the IAP family in mammals has provided key insights into the unique and diverse roles of IAP members in cell death, immune regulation, and critical cellular

processes such as cell migration and replication. BIRC4/XIAP inhibits apoptosis through direct physical binding with caspase 3, while BIRC2 and BIRC3 (cIAP1, cIAP2) can inhibit caspase function through ubiquitination and promotion of proteasomal degradation[25]. BIRC2 and BIRC3 can promote cell death or cell survival through signal transduction of death receptor binding (TNFR) during extrinsic apoptosis and canonical NF-κB pathway activation. BIRC2, BIRC3 and BIRC4 also play roles in inflammasome regulation[24,25,31]. BIRC4, BIRC5, and BIRC6 have been shown to have a regulatory influence on autophagy[32]. BIRC7 and BIRC4 in mammals, as well as DIAP1 in *Drosophila melanogaster,* can modulate cell migration[33,34]. Finally, BIRC6 plays roles in DNA double strand break repair, homologous recombination, and autophagosome-lysosome fusion independent of ubiquitination activity[35,36]. Conservation of these functions in oysters and other bivalves, however, remains unknown.

Expansion of apoptosis pathway gene families, and the IAP family in particular, has been previously noted in molluscs[4,6,12,37]. Transcriptome studies in the Pacific oyster, *Crassostrea gigas,* and the eastern oyster, *C. virginica,* have revealed IAP family members significantly respond to viral challenge with Ostreid Herpesvirus type 1 (OsHV-1, causes mortality in Pacific oysters), bacterial challenge with *Aliiroseovarius crassostreae* (causative agent of Roseovarius or Juvenile Oyster Disease, ROD/JOD, in eastern oysters) and *Vibrio* spp. (causative agent of larval vibriosis in bivalves), and parasitic challenge with the parasite *Perkinsus marinus* (causative agent of Dermo disease in eastern oysters)[12,16,38–42]. However, the role of IAP gene expansion in oyster immune responses remains unknown. Comparison of the usage of this expanded family across a diverse set of immune challenges from economically and ecologically relevant pathogens may provide

insights into the role of IAP gene expansion in oysters' ability to tailor and diversify their immune responses to unique challenges[11]. This study therefore assesses IAP genetic diversity in molluscs, characterizes IAP domain architecture diversity in two oyster species, and utilizes publicly available oyster immune challenge transcriptome data to investigate the role of IAP family diversification in apoptotic and immune responses. This research improves our understanding of the role of gene expansion in invertebrate immune diversity and informs future development of IAP candidate markers associated with apoptosis and disease resistance.

Results

Phylogenetic analysis of expanded IAP gene family in molluscs

Following HMMER analysis and pruning of proteins lacking BIR repeats as identified by Interproscan, 791 IAP transcripts were identified across 10 molluscan genomes. The *C. virginica* reference genome (V3.0, GCA_002022765.4) contained 69 genes and 158 IAP transcripts while the *C. gigas* reference genome (V9.0, GCA_000297895.1) contained 40 genes and 74 IAP transcripts. Pruning this transcript list to remove isoforms with the same amino acid sequence yielded 84 *C. virginica* IAP transcripts and 45 *C. gigas* transcripts. The gastropod *Biomphalaria glabrata* showed the greatest IAP gene expansion, with 88 genes, while cephalopods *Octopus vulgaris* (*sinensis*) and *Octopus bimaculoides* showed the fewest genes, with 10 and 11, respectively (Figure 1a).

A phylogenetic tree of IAP amino acid sequences revealed a complex pattern of species-specific expansions and cross-species conservation of IAP proteins (Figure 1b). In

general, this phylogeny recapitulated evolutionary relationships in molluscs, with *Octopus* spp. as the sister group, separation between bivalve (*C. gigas*, *C. virginica*, and *M. yessoensis*) and non-bivalve molluscs (*B. glabrata*, *E. chlorotica*, *A. californica*, *P. canaliculata*), and IAPs from sister species most clustered together (Figure 1a)[43]. Each species had at least one well-supported (>70 bootstrap support) species-specific protein cluster, and *B. glabrata* had the largest (cluster 1, Figure 1b). Many (41) well supported nodes contained proteins from multiple species, including two conserved protein clusters (clusters 2 and 3) containing sequences from all but one molluscan species. The first cluster (2) contains proteins annotated as BIRC6 (or "hypothetical protein" in *L. gigantea*) from all species except *E. chlorotica*. The second conserved cluster (3) contains proteins annotated as BIRC5 (or "hypothetical protein" in *E. chlorotica* and *L. gigantea*) in all species except *O. bimaculoides*. Clustering of BIRC6 and BIRC5 proteins across molluscan species suggests sequence (and potentially functional) conservation in these two proteins.

Bivalve IAP potential gene expansion mechanisms

C. virginica IAP genes were distributed across 9 of the 10 chromosomes, with the majority located on chromosomes 6 and 7 (Figure 1c). IAP genes on chromosomes 6 and 7 were present in tandem arrays, suggesting tandem duplication as a mechanism of expansion, while genes present on other chromosomes were typically single genes. Retroposition has been previously described as a mechanism of gene duplication in molluscs, with gene duplicates resulting from retroposition showing a lack of introns and a random distribution across genomes[6,44,45]. *L. gigantea* had the largest number of

intronless genes (12), *C. virginica* had the second most (8), *C. gigas* had 3, *B. glabrata* had 2, and *M. yessoensis*, *O. vulgaris*, and *E. chlorotica* had one each (not shown). The 8 intronless *C. virginica* IAP genes were located on chromosomes 5, 7, 8, and 10 (Figure 1c).

The presence of domains suggesting functional retroposition and transposition machinery in IAP gene sequences was investigated in *C. virginica*, *C. gigas*, and *M. yessoensis* (Figure 2). Functional domain analysis of translated gene IAP open reading frames (ORFs) revealed 4 *C. virginica* IAP genes contained domains involved in LTR and non-LTR retroposition, none of them intronless. *M. yessoensis* ORFs across 9 genes also contained retroposition machinery and three possessed DNA transposase machinery (Transposase Tc-1 like domains: IPR002492, IPR027805, IPR038717) (LOC110460644, LOC110452306, LOC110465395). The *C. gigas* genome assembly (V9.0, GCA_000297895.1) only contained one IAP gene with potential retroposition machinery, a reverse transcriptase domain (Figure 2).

Diversity of BIR domain types in oysters

In model organisms, BIR domains are characterized by 15 conserved amino acids forming a central 3-stranded antiparallel β-sheet (β1-3) surrounded by 5 α-helices (α1-5), with four critical residues stabilizing a central zinc atom: Histidine (H77) and three Cysteine residues (C57, C60, C84)[46–48]. Following multiple sequence alignment with all oyster BIR-containing sequences, only 4 of the 15 conserved positions seen in model organisms (G34, C60, H77, C84; considered essential for BIR function in model organisms[47]) were shared across all *C. gigas* and *C. virginica* proteins, revealing considerable diversity in this domain in oysters (Figure 3a). Using amino acids in the α-3 and α-4 helix regions, oyster BIR sequences were classified as conserved Type I (H77, V80

or L80, C84) and conserved Type II (E76 or Q76, H77, W80 or H80, C84)[46,47,49] (Figure 3a, Supplementary Figure 1). BIR repeats were additionally classified as Type I-like, with four Type-I like polymorphisms, if they had a hydrophobic residue at position 80 (I, V or L) and/or a Serine in position 81 (S81 is found in model organism α-3 helices[47]). Type II-like BIR repeats were also identified, and these had an E76 prior to the conserved H77, which is found only in model organism Type II α-3 helices.

BIR sequences containing unique amino acids at key positions not seen in model organisms were classified as novel types (Figure 3a,b). Two potentially functional (*i.e.* Zn-binding) novel BIR domain types were identified. BIR sequences in four *C. virginica* IAP genes were found to have a Glycine substitution at conserved position 80, followed by a substitution of Arginine for Proline at position 82, here called Type X BIR. Though the Arginine substitution is not predicted to alter secondary structure, the Glycine substitution is predicted to lead to a shortening of the α-3 helix (Figure 3b). A second distinct BIR type, here named Type Y, was identified in two *C. virginica* IAP genes and three *C. gigas* IAP genes. Type Y BIRs had a shortened sequence compared to other BIR sequences and appeared to have lost three amino acids, including conserved position 80, leading to a predicted shortened alpha-helix secondary structure. A final BIR variant in *C. gigas* and *C. virginica* was identified by hydrophilic Threonine amino acid substitution at the first coordinating Cysteine residue (C57) of this zinc-binding structural hot spot[46–48]. Though this substitution is not predicted to alter protein secondary structure, loss of this Cysteine may result in decreased ability for these domains to coordinate with Zinc[46–48]; therefore, this domain is referred to as Non-Zinc Binding (NZBIR) here.

Most IAP genes with CDD-identified BIR domains in *C. virginica* contained one BIR domain, while most *C. gigas* genes contained two (Figure 3c). Comparison of domain number across a phylogenetic tree of IAP nucleotide gene sequences suggests a pattern of *C. virginica* BIR domain loss over time compared to *C. gigas* and *M. yessoensis* (Figure 3d). In both *C. virginica* and *C. gigas* conserved Type II repeats were the most common (Figure 3a). IAP genes containing novel BIR types were rare in *C. virginica* and *C. gigas* (from 1 to 3; Figure 3a), were distributed across the phylogenetic tree of IAP gene sequences, and did not group by type, suggesting they may have arisen independently across multiple IAPs (Figure 3d).

Diversity of domain architectures in oyster IAPs

Interproscan analysis of oyster IAP amino acid sequences identified 12 functional domains in addition to the BIR domains described above (Figure 4). Many IAPs contained carboxyl terminus RING-finger domains (cd16713, IPR013083, IPR001841) and death domain (DD) architecture (G3DSA:1.10.533.10). Several proteins in *C. virginica* and *C. gigas* contained UBA (IPR015940), or UBC (IPR016135) domains. BIRC6-like proteins contained the characteristic BIRC6 domain (IPR011333) and a UBC domain (IPR000608), but only contained WD-40 repeat domains (IPR019775, IPR036322) in *C. virginica*. No CARD domains, a subfamily of DD characteristic of model species IAPs, were identified by Interproscan in any studied mollusc IAPs[50].

Phylogenetic analysis of oyster and scallop IAP amino acid sequences revealed 21 protein clusters (>90 bootstrap support) (Figure 4a), with 14 distinct domain architecture types (Figure 4c,d). Of the 21 clusters, 10 clusters included proteins with a domain

architecture resembling model mammalian or *D. melanogaster* domain architectures (referred to as BIRC#-like), while 11 clusters showed novel architectures not found in model organisms (named here BIRC9, BIRC10, BIRC11, and BIRC12; Figure 4d). The BIRC2/3-like (defined here as 2 BIR domains, a DD, and a RING domain, or 2 BIR domains, a DD, a UBA, and a RING domain, assuming a similar function of DD architecture to the CARD domain[50]) and BIRC6-like domain architectures were most common across IAP genes in both oyster species, followed by BIRC11 in *C. virginica* and BIRC12 in *C. gigas* (Supplementary Table 1). Intronless *C. virginica* and *C. gigas* IAP genes (suspected to have arisen from retroposition) were located in protein clusters 17 and 13 and were all BIRC5-like with a single BIR domain (Figure 4a).

The four oyster IAPs that contained the novel NZBIR domain were in cluster 4. Three of these also contained a UBA, DD, and RING domain, most resembling the domain architecture of BIRC2/3 in mammals (though missing one TII domain). Therefore, oyster BIRC2/3-like showed two alternative domain structures: one containing TI-TII-DD-RING domains (clusters 1 and 6), and another that also contains a UBA domain, but in which the TI BIR domain seen in mammals is instead a NZBIR (cluster 4; Figure 4). *C. virginica* Type X sequences were located in cluster 19. Genes containing the novel Type Y BIR domain were not present in a well-supported cluster and were not named. Three sequences with Type Y BIR domains not found in a well-supported cluster also possessed a Type II BIR domain, all possessed a RING domain, and one possessed a RING and DD.

Transcript evaluation indicated that alternative splicing provided an additional source of diversity in domain architectures, with some alternatively spliced transcripts from the same gene having varied functional domains (*e.g.,* cluster 3 LOC111100858, cluster 4

LOC105328049, Figure 4). Comparison of domain architecture diversity across oysters suggests a complex history of domain loss and gain, and the large diversity of IAP domain architectures observed indicates the potential for varied functionality across oyster IAPs that surpasses model organism IAPs.

IAP gene expression in oysters in response to immune challenge

Patterns of IAP expression in response to immune challenge were evaluated through comparative analysis of available transcriptome datasets (SRAs) in public databases (Table 1). Transcriptome experiments revealed that most of the oyster IAP diversity is expressed in response to immune challenge, both in terms of domain architecture and overall IAP gene usage. However, expression patterns differed by oyster species and challenge type, suggesting diversity may have functional relevance in allowing responses to different conditions. Across the four *C. virginica* immune challenge experiments, 53 (77%) of the 69 IAP genes were expressed; 15 significantly differential expressed compared to non-challenged controls (Figure 5), 28 constitutively expressed (*i.e.* not significantly different to controls but expressed in every sample; Supplementary Figure 2), and 10 genes with a mix of differential and constitutive gene expression. In contrast, in the four *C. gigas* immune challenge experiments, 33 (82%) of the 40 genes were expressed, with 20 differentially expressed, 8 constitutively expressed, and 5 genes with a mix of transcripts differentially or constitutively expressed (Figure 5, Supplementary Figure 2).

Differential gene expression of IAPs was seen in all oyster immune challenge experiments, but widely ranged in the number of differentially expressed IAP transcripts per experiment between 5 (CVBAC-B) and 32 (CVBAC-A) in *C. virginica* and 5

(CGBAC-A) and 68 (CGOSHV1-A Susceptible) in *C. gigas* (Supplementary Table 2). Greater gene expression overlap was seen across experiments in *C. gigas* than *C. virginica*, and 87% of differentially expressed genes were shared between *C. gigas* challenge experiments, compared to 48% in *C. virginica*. *C. gigas* also expressed more of the same transcripts across challenges than *C. virginica*, with 67% (CGBAC-B) to 100% (CGBAC-A) of *C. gigas* IAP transcripts shared between experiments, compared to 8% (CVBAC-A) to 20% (CVBAC-B) shared between *C. virginica* challenges (Supplementary Table 2). In both species, expression of alternatively spliced versions of the same gene in different challenges accounted for some transcript expression diversity (4 genes in *C. gigas*, 5 genes in *C. virginica*) (e.g. cluster 3, Figure 5).

Expression patterns of genes with different domain architectures also differed between the two species (Figure 5). Transcripts from all domain architecture types were differentially expressed to immune challenge in at least one oyster species. No strong patterns emerged regarding specific domain structures or domains associated with particular microbe types (*i.e.* parasitic, bacterial, or viral). Each experiment, however, expressed a unique assemblage of IAP domain architectures, ranging from 3 (CVBAC-B) to 10 (CVBAC-A) in *C. virginica* and 3 (CGBAC-A) to 11 (CGOSHV1-A susceptible) in *C. gigas* (Figure 5; Supplementary Table 3). While the DIAP1-like domain architecture was most frequently expressed in *C. virginica* (15 transcripts), the BIRC2/3-like domain architecture was most frequently expressed in *C. gigas* (34 transcripts; Supplementary Table 3). Transcripts containing a UBA domain (cluster 4) were only differentially expressed in response to parasitic challenge in *C. virginica*.

Transcripts containing novel NZBIR (cluster 4), and Type Y (poorly supported group between clusters 2 and 3) domains were only expressed in *C. virginica* challenge experiments (Figure 5). Novel domain architectures were expressed in response to multiple challenge experiments. The BIRC10 domain architecture (cluster 7) was significantly differentially expressed across all experiments except one *C. virginica* bacterial challenge. BIRC9 (clusters 13, 19) was expressed in both bacterial and viral challenges (Supplementary Table 3). BIRC11 and BIRC12 (clusters 5, 8, 12; and clusters 9, 14, 16, 18, 20 respectively) were expressed in bacterial, viral, and parasitic experiments (Figure 5).

Constitutively expressed IAP transcripts in *C. virginica* experiments included representatives from 12 of the 14 domain architectures; all except BIRC5-like and BIRC10 (Supplementary Figure 2; Supplementary Table 3). *C. virginica* and *C. gigas* transcripts from intronless genes were not differentially expressed to any of the immune challenges, though a transcript for one *C. virginica* intronless gene (LOC111132301, BIRC7-like, between cluster 12 and 13) and one *C. gigas* intronless gene (LOC109617982, BIRC11, cluster 12) were constitutively expressed across all experiments (Supplementary Figure 2).

Apoptosis and Regulated Cell Death Pathway Annotation in oysters

To investigate potential relationships between IAP gene expression and apoptotic responses during immune challenge, regulated cell death (RCD) pathway genes and transcripts were identified in *C. gigas* and *C. virginica* annotated reference genomes, revealing 1290 unique RCD-related transcripts in *C. virginica* across 676 gene loci, and 844 unique transcripts in *C. gigas* across 511 gene loci (Supplementary Table 4;

Supplementary Files 1,2). Key molecules in the intrinsic and extrinsic apoptosis pathways, including receptors, signaling molecules, and effectors, were identified in oyster annotations (Figure 6). Components of molecular complexes involved in apoptosis were also identified, including the apoptosome (caspase 9, cytochrome c), the PIDDosome (PIDD1, CRADD, casp2, RIPK1), and DISC complexes (RIPK1, FADD, caspase 8, TRAF2).

A few (76 out of 315; 25%) RCD proteins from the literature were absent in oyster reference annotations, due to either low identity with RefSeq proteins, gene loss in genome assembly and annotation, or true absence in oyster genomes. These included mitochondrial apoptosis pathway proteins (BAD, Bcl-w, Bcl-2, BI-1, BID, BIK, BIM, BMF, Bok, Mcl-1, NOXA, HRK, DEBCL, PUMA, Apaf-1, CHOP), and extrinsic apoptosis pathway ligands, receptors, and adapters (FasL and FasR, DR3 (TNFRSF25), DR4 (TNFRSF10A), DR5 (TNFRSF10B), Apo3L (TNFSF12), c-FLIP, TRADD, RIPK3). Cellular tumor antigen p53, diablo homolog, mitochondrial, and Tumor Necrosis Factor (TNF-α) were only annotated in *C. gigas*.

Several proteins involved in regulated cell death pathways other than apoptosis[21] were also annotated, including necroptosis proteins aurora kinase A (AURKA), E3 ubiquitin-protein ligase CHIP (CHIP), protein phosphatase 1B (PPM1B) tumor necrosis factor alpha-induced protein 3 (TNFAIP3), and receptor-interacting protein kinase 1 (RIPK1). Lysosome-dependent cell death cathepsins (cathepsin Z, B, L, L1, O) were identified, as were critical parthanatos proteins poly [ADP-ribose] polymerase 1 (PARP1), hexokinase 1 (HK1), apoptosis inducing factor (AIF, AIFM1), and macrophage migration inhibitory factor (MIF).

Apoptosis-related gene expression in response to immune challenge

Differential expression of apoptosis-related genes was analyzed for each experiment to determine potential associations between IAP and apoptosis gene expression during immune challenge. The number of apoptosis-related genes differentially expressed in response to immune challenge was much higher in *C. gigas* than *C. virginica* (1632 vs. 440), which could be driven by types of challenge analyzed (*e.g.* no viral challenge was available for *C. virginica*) and/or differences between the two species in the use of apoptosis (Supplementary Table 5).

Total apoptosis-related transcripts differentially expressed in *C. virginica* and *C. gigas* immune challenges ranged between 37 (CVBAC-B) and 1,040 (CGOSHV1-A) (Supplementary Table 5). Clustering immune challenge experiments by log2 fold change (LFC) in apoptosis-related gene expression showed that levels of susceptibility or resistance (achieved by family-based selective breeding within each oyster host; Table 1) to pathogenic challenge (viral challenge in *C. gigas*; bacterial or parasitic challenge in *C. virginica*[13,51,52]) was the strongest factor influencing apoptosis-related gene expression in both host species, with susceptible oysters showing a larger/broader response to challenge than resistant oysters (Figures 7 and 8). In *C. gigas*, CGOSHV1-A susceptible and CGOSHV1-B oysters showed the most unique apoptosis expression patterns, with strong upregulation of transcripts in the extrinsic, TNFR, and interferon (IFN) pathways (TRAF3, IRF1, MyD88, BIRC3, BIRC7, TNFRSF27, IFI44, FAP1, GIMAP4), and strong downregulation of TLR, mitochondrial apoptosis, and p53 pathway transcripts (TLR2, TLR4, TLR6, SARM1, LITAF, CD151) (Figure 7). In *C. virginica*, ROD-susceptible

oysters (CVBAC-C) had the most unique apoptosis gene expression patterns. These differentially expressed transcripts included several coding for proteins in the extrinsic apoptosis pathway, including those shared with the TNFR and TLR pathways (TRAF6, caspase 3, BIRC4/XIAP, RHOT1, MAP3K2, TLR4, CCAR). The *P. marinus* (CVPMA) susceptible 28d oysters also showed downregulation of a large group of apoptosis transcripts involved in apoptosis execution (caspase 7) and the TLR pathway (TLR13, TLR tollo, BIRC3), DNA damage response pathways (PIDD1, CDIP1), and mitochondrial dysfunction related proteases calpains 9, 5, and B (Figure 8).

Characterization of IAP expression directly correlated with apoptosis gene expression

WGCNA was performed to determine whether specific IAP domain architectures were co-expressed with specific apoptosis-related pathways or genes, as determined by connection by a shared edge (Figure 9a,b, Supplementary Table 6,7). In *C. virginica,* IAPs with multiple domain architectures were directly corelated with apoptosis genes in susceptible oysters exposed to *P. marinus* (CVPMA experiment – one IAP gene identified as BIRC12 correlated with a caspase 7-like transcript), and larval oysters exposed to probionts RI and S4 (CVBAC experiment – 5 IAP genes with 4 domain architectures correlated with 52 unique apoptosis-related transcripts; Figure 9a). In *C. gigas*, IAPs with multiple domain architectures were directly correlated with apoptosis-related transcripts in several experiments, and the CGOSHV1-A resistant and CGBAC-B experiments had the highest number of apoptosis-related transcripts correlated with IAP expression (Figure 9a).

At least one transcript from each of the domain types, with the exception of BIRC2/3 – NZBIR, was directly correlated with apoptosis-related genes in both oyster species. Multiple unique IAP domain architecture types across modules were directly correlated with apoptosis-related transcript expression in most experiments (CVBAC-A, CGBAC-B, CGOSHV1-B, CGOSHV-1 A Res.) (Figure 9a). Transcripts from multiple domain architectures were also expressed in the same modules during bacterial and/or viral challenge (Figure 9a), suggesting IAP domain architectures are not specific to particular immune challenge types and that different domain architectures may work together or have complementary functions. For example, in Pacific oysters exposed to OsHV-1[51], BIRC2/3, BIRC11, BIRC9, and BIRC5 showed direct correlation with genes in the extrinsic apoptosis/TLR pathway, inflammation, mitochondrial apoptosis (*e.g.* BAG, BAK, Bcl-xL), antiviral responses (*e.g.* IFIs, IRFs, IL17RD, JAK, STAT, STING), necroptosis (CHIP, PPM1B), ER stress (ATF-4, EIF2K3, CREB3Ls), executioner caspase 7, and DNA damage response caspase 2 (Figure 9c; Supplementary Figure 3). These results demonstrate a complex set of pathways are activated in Pacific oysters in response to viral challenge, and that novel BIRCs may have complementary roles in these pathways (Figure 9c).

Expression of transcripts for the BIRC2/3-like IAP domain architecture was directly correlated with expression of apoptosis-related transcripts in all *C. gigas* experiments except CGBAC-A, suggesting a consistent association of this transcript with apoptosis in this species. Specifically, *C. gigas* BIRC2/3-like transcript XM_020068541.1 (LOC105331304) was consistently associated with TNFRSF27, TNFSF10 (Apo2L), downstream ISGs and IRFs, and the TLR13 pathway (Figure 9d). Expression of this

transcript was also correlated with expression of transcripts for caspases 1 and 6 and TRAF3 (Figure 9d). Association of this transcript with the TNFR and IFN pathways and direct correlation with TRAF3 suggest it may have similar signal adapter functions to mammalian BIRC2/3[24,53].

Finally, potential patterns of IAP domain architecture co-expression with apoptosis pathways or genes was assessed by clustering the direct correlations in each experiment by presence (red) or absence (blue) using a heatmap (Supplementary Figure 3). Similar to what was observed in Figs. 7 and 8, patterns of directly correlated IAP domain architectures and apoptosis pathway transcripts identified in the WGCNA clustered mostly by experiment and not by domain architecture type (Supplementary Table 3).

Discussion

Recent whole genome sequencing of marine invertebrates has revealed large scale expansions of immune gene families, including several related to regulated cell death [3,4,6,8,54–59]. Functional diversification of expanded immune gene repertoires may contribute to the remarkable ability of invertebrates to mount specific responses to immune challenge in the absence of traditional adaptive immunity[3,6,37,58]. Using a comparative genomic and transcriptomic approach, this research: 1) Described great IAP expansion and diversity in oysters, with mechanisms like mutation, tandem duplication, and retroposition leading to novel domains and domain architectures that may allow for unique functionality; 2) Showed that each oyster species expressed unique and variable assemblages of IAP genes and domain architectures in response to immune challenges; 3) Annotated regulated cell death proteins in the genomes of two oyster species, *C. gigas* and *C. virginica*, that had not

been previously recognized; and 4) Revealed direct correlation of diverse oyster IAP assemblages with apoptosis pathways across different immune challenges, with levels of resistance to pathogenic challenge effecting apoptosis-related gene expression in both oyster species. These results suggest a role for the expanded IAP family in regulating complex cell death pathway responses to a variety of immune challenges.

Mechanisms of IAP lineage specific expansion in oysters include tandem duplication and retroposition

As shown in previous research[6], IAP gene expansion differs considerably across molluscs, ranging from 10 genes in *O. sinensis* to 88 in *B. glabrata*, suggesting divergent evolutionary rates and/or selection pressures. Recent investigation of tandemly duplicated IAP genes in the hard clam, *Mercenaria mercenaria,* suggested that IAPs may evolve by purifying selection following duplication[6]. As in *M. mercenaria,* tandem duplication of IAP genes is likely a predominant gene family expansion mechanism in *C. virginica*, (and likely in *C. gigas*) with the majority of IAP genes in *C. virginica* (54 genes, 78% of the IAPs) present in large tandemly duplicated clusters on chromosomes 6 and 7. Tandem duplication as a mechanism of IAP gene family expansion in *C. gigas* has also been noted in the literature[60]. Moreover, tandem duplication as an immune gene expansion mechanism has been noted for other oyster immune gene families, including TNF, MyD88, TLR, Hsp70, and C1qDC[61–65]. The larger repertoire of IAP genes in *C. virginica* compared to *C. gigas* may be due to differences in evolutionary pressure, leading to an increased number of tandem duplications in eastern oysters, and/or potential gene loss in *C. gigas* over time. Further investigation of differences in evolutionary rates and history is necessary to make

a conclusion regarding overall IAP gene family evolution in these two species. The recent availability of chromosome-based assemblies for *C. gigas* will facilitate this analysis (GCA_902806645.1, cgigas_uk_roslin_v1)[66].

Retroposition is another prominent mechanism of gene family expansion[17]. Gene retroposition involves insertion of DNA sequence into a genome in a different location from the parent gene following reverse transcription from mRNA. These genes typically lack introns and other regulatory sequences, though retrogenes are transcribed and functional in some cases[67]. Retroposition as a mechanism of gene expansion has been noted for several immune gene families in molluscs, including the IAP family in *M. mercenaria,* the IL-17 family and fibrinogen-related proteins (FREPs) in *B. glabrata*, and IκB genes in *C. gigas*[44,68,69]. The number of intronless IAP genes (suggesting retroposition) detected in this research varied across targeted species and intronless IAPs comprised a fewer percentage of total IAPs in both *C. gigas* and *C. virginica* than the hard clam *M. mercenaria* (3 in *C. virginica*, 7 in *C. gigas,* and 51 in *M. mercenaria*[6]). Domain analysis of *C. virginica* IAPs revealed several genes with machinery for both LTR and non-LTR type retroposition in translated IAP ORFs, providing further support for past retroposition in this family.

Interestingly, intronless *C. virginica* IAPs lacked retroposition machinery, suggesting they could be retroposed copies from a parent gene that are no longer active retrotransposons, or could be active retrotransposons by relying on machinery from other genes[67]. Intronless IAPs in both *C. virginica* and *M. mercenaria* may retain some functionality, with several *M. mercenaria* IAPs noted to have high expression levels in response to environmental stress[6] and one *C. virginica* IAP constitutively expressed to immune challenge in this research. Overall, this research indicates that tandem duplication

is the predominant mechanism of *C. virginica* IAP expansion but that retroposition may still play an important role.

IAP expansion in oysters allowed for evolution of novel BIR domain sequences and domain architectures

Humans possess 8 known IAPs, while *Drosophila* spp. possess 2[24], and each contains a distinct assemblage of domains which confer unique functions[47]. Interproscan functional analysis revealed IAPs in oysters have greater structural domain architecture diversity than mammals and flies, with 14 total domain architecture types identified, including 8 types with architectures similar to human or fly IAPs and 4 novel types (Figure 4d). The only mammalian IAPs without a similar IAP in oysters were BIRC1 (NAIP) and BIRC8 (ILP2). Domain architecture types in oysters varied in number of BIR repeats, the type of BIR domain (including three novel BIR domain types; X,Y, and NZBIR, see below) and the presence or absence of domains characteristic of IAPs; RING domains, DD instead of CARD, UBA and UBC domains, suggesting a complex history of domain loss and gain over time that may have involved parallel evolution or retention of ancestral forms from a common ancestor[6,70].

Interestingly, BIRC2/3 IAPs, similar to other molluscan IAPs[60], lacked the CARD domain characteristic of mammalian IAPs, possessing instead a DD (BIRC10 and BIRC11 also possessed a DD as well). Despite lacking true CARD domains, the presence of DDs in these oyster IAPs may still allow for mediation of key protein-protein interactions during apoptosis. DD and CARD domains are structurally similar and both mediate protein-protein interactions critical in apoptosis transduction[71]. In mammalian BIRC2/3, the CARD

domain promotes protein stability by preventing RING-domain meditated auto-ubiquitination[72]. During intrinsic apoptosis, a CARD-CARD interaction between Apaf-1 and caspase 9 allows for caspase 9 activation[73]. DD-containing proteins in *D. melanogaster* have also been shown to complex with caspase molecules, and in mammals formation of the PIDDosome during DNA-damage response involves DD-containing proteins PIDD and CRADD complexing with caspase-2[74,75]. WGCNA analysis in this research revealed direct correlation between DD-containing IAPs and caspase expression, suggesting DD-containing oyster IAPs could potentially function similarly to CARD domains. The ability of DD-containing oyster IAPs to directly interact with other apoptosis proteins, such as caspases, should be investigated in the future.

Expansion of novel IAP domain architectures in oysters is also supported by a recent study of *M. mercenaria* IAPs[6]. In the hard clam, 9 distinct architectures were identified and all but two (classified as Type D and E) were also identified in oysters[6]. However, Song et al. (2021) did not consider BIR Type or the presence of UBA or DD domains in clam IAP characterization[6]. Though all types identified in this oyster study were identified in the *M. mercenaria* study, inclusion of these additional domains in the present analysis gave our work the ability to distinguish between expression patterns of novel types and model organism types, such as BIRC10 (TII-DD), which was combined with BIRC5-like proteins (TII) in the *M. mercenaria* G1 type, and BIRC11 (TII-DD-RING or BIR*-DD-RING) which was combined with BIRC7-like (TII-RING) in the *M. mercenaria* C type[6]. The functionality of these novel types, in addition to conserved model organism types, supports the utility of IAP expansion in allowing for functional diversification.

Despite high levels of lineage specific IAP expansion in molluscs, phylogenetic analysis of IAP amino acid sequences revealed that all BIRC5-like and BIRC6-like proteins are highly related between molluscan species, suggesting functional conservation of these sequences over evolutionary time (Figure 1b). Both BIRC5 and BIRC6 play important apoptosis regulatory roles in mammals, but BIRC5 (Survivin) is also essential for cell division[76], while BIRC6 (BRUCE) proteins play critical roles in mitosis, autophagosome/lysosome fusion, DNA double strand break repair and DNA replication[32,36]. Performance of these critical cell cycle and cell division functions may have constrained their sequence evolution and led to low divergence over evolutionary time as compared to other IAP proteins.

BIR domains are the critical functional domain of IAPs and are traditionally classified as Type I or Type II, with Type II BIRs able to physically interact with IAP-binding motif (IBM) containing proteins smac/DIABLO or caspases[47]. Analysis of BIR domain sequences revealed oysters possess both model organism Type I and Type II repeats, as well as divergent types named here Type X, Type Y, and NZBIR (not found in any other organism in the NCBI database, based on *blastp*). Conserved Type II domains, likely able to interact with IBM-containing proteins based on sequence analysis[77], were the most prominent across oyster BIRs (62% of all BIR domains in *C. virginica*, 66% in *C. gigas*). Consistent with this hypothesis, WGCNA analysis indicated direct co-expression of caspases with IAPs possessing Type II repeats (Supplementary Figure 5). Moreover, a previous functional study of an IAP in *C. gigas* (LOC1053280490), classified in this paper as BIRC2/3-like, found its Type II BIR2 repeat was able to mediate interaction with caspase 2[78].

Several oyster IAP genes (BIRC2/3-like and BIRC9, Figure 4d) contained novel BIR types (Types X, Y, and NZBIR) in addition to at least one Type II BIR. Proteins containing novel oyster BIR types were distributed across the IAP phylogenetic tree, suggesting that they may have arisen due to mutations in tandemly duplicated genes independently in *C. virginica* and *C. gigas* (Figure 3d). It is not known if oyster IAPs with these novel domains are functional, either as IAPs or other novel functions, but genes containing each novel BIR domain were significantly differentially expressed in response to immune challenge and co-expressed with apoptosis-related genes in at least one oyster species (more on this in sections below). The presence of at least one Type II BIR in these novel oyster IAPs should preserve their ability to interact with IBMs. The N-terminal BIR Type I repeat in mammalian BIRC2, which is replaced in the novel oyster BIRC2/3-like IAPs by an NZBIR type, is necessary and sufficient for binding to SMAC and TRAF2[79]. Though NZBIR-containing BIRC2/3-like proteins contain a Type II BIR and a UBA domain similar to mammalian BIRC2/3, lack of a third BIR domain and/or alteration of the N-terminal BIR domain may affect this critical function of BIRC2/3 like proteins. While these genes are expressed in *C. virginica,* lack of significant differential expression of NZBIR and Type Y containing IAPs in *C. gigas* suggests these transcripts may respond to other types of environmental or immune challenges in *C. gigas*, or are non-functional. Functional studies should evaluate the potential contributions of these novel BIR domains to IAP function and identify their potential interaction partners.

Eastern and Pacific oysters expressed diverse IAP domain architecture repertoires in response to immune challenge

Overall IAP gene usage in oysters in response to diverse immune challenges (Table 1) was investigated in this research. Most (77% of *C. virginica* and 82% of *C. gigas*) IAP genes were differentially or constitutively expressed in response to one or more challenges, suggesting that most of the expanded IAPs are functional and involved in immunity. It is possible that IAP genes not expressed in these challenges respond to other stressors and/or at life stages not assessed in this study. For example, *M. mercenaria* IAPs were strongly responsive to challenge with aerial exposure, low salinity, high temperature, or low oxygen, revealing IAPs may play important roles in response to both environmental and disease challenge[6].

Interestingly, *C. virginica* largely expressed different gene sets between challenge experiments, while *C. gigas* more often expressed overlapping gene sets to different challenges, suggesting that greater IAP expansion may allow for greater specificity of IAP gene usage in response to different challenges in *C. virginica*. These results should be interpreted with caution, however, since sampled experiments were performed in diverse experimental conditions with oysters at different live stages (from larvae to adults), and with sequencing performed for both oyster pools (larval experiments) and single individuals. Comparative analysis between IAP responses to immune challenge in these two species was also restricted because both are affected by different diseases (consistent with their different geographical distribution[80]), and no transcriptome experiments were currently available at the time of this research in which both species had been concurrently challenged with the same pathogen at the same developmental stage[80]. Finally, natural infection with OsHV-1 in *C. gigas* typically involves co-infection with *Vibrio* spp. which may contribute to strong similarities in IAP and apoptosis pathway responses between

natural OsHV-1 exposure (CGOSHV1-A) and *Vibrio* spp. experiments[51]. Future challenge experiments of both species using the same pathogens and pathogen associated molecular patterns (PAMPs) such as bacterial LPS and the viral response stimulator poly(I:C)[81,82] would allow for better determination of differences in IAP usage between the two species.

Next, analysis of IAP domain architecture expression in oysters revealed expressed IAP genes in both species were from multiple domain architecture types and all domain architecture types, including novel types, were significantly differentially expressed in at least one challenge. None of the domain architecture types appear to be specific to challenge type (parasitic, bacterial, or viral). The domain architecture most frequently differentially expressed in *C. virginica* was the DIAP1-like, while in *C. gigas*, it was the BIRC2/3-like. WGCNA analysis next indicated significant correlation between several domain architectures in each immune challenge, suggesting multiple IAPs with different putative functions may function in the same pathways or participate in different pathways that are co-regulated during immune challenge (Figure 9). However, the expression of unique assemblages of IAP domain architectures in response to the different challenges also suggests that overall IAP activity can be tailored to specific situations. These results support that the expanded IAP genes and domain architecture types in oysters are not merely non-functional artifacts of duplication events and domain loss and gain but allow for critical tailoring of immune responses, which has been previously shown for other expanded gene families such as TLRs and NOD-Like Receptors[83].

IAP expression was directly correlated with apoptosis gene expression suggesting roles in finely regulating apoptosis during immune challenge

Expression of a variety of RCD pathways, including intrinsic and extrinsic apoptosis, parthanatos and necroptosis, differed between challenge type and species. Consistent with known roles of apoptosis in immune response and disease in a variety of organisms, including oysters[84–86], viral challenge in *C. gigas* elicited the strongest apoptotic response, while probiotic challenge in *C. virginica* elicited the weakest apoptotic response. Interestingly, the assemblage of expressed IAP and apoptotic transcripts was affected most strongly by the host's susceptibility to particular challenges, with eastern oysters susceptible to *Aliiroseovarius crassostreae* (CVBAC-C) and Pacific oysters susceptible to viral challenge (CGOSHV1-A) showing the largest changes in gene expression (Figures 7, 8). These results are consistent with previous functional research suggesting a role of apoptosis in disease susceptibility (or resistance) in oysters and other species[18,52,87–91]. Network analysis additionally revealed that viral exposure experiments in *C. gigas*[13,51] showed the highest diversity of IAP domain architecture transcripts, (BIRC2/3-like, BIRC5-like, BIRC6-like, BIRC10, and BIRC11) directly correlated with expression of transcripts in multiple RCD-related pathways (extrinsic and mitochondrial apoptosis, inflammation, antiviral response, necroptosis, and ER stress).

Multiple IAP domain architecture types were directly correlated with apoptosis-related transcripts across experiments, including novel IAP domain architectures (BIRC9, BIRC10, BIRC11, BIRC12), and the combination of expressed IAP domain architecture types differed between each experiment. This result suggests that the importance of IAP expansion in oysters is to allow for expression of multiple IAPs of different potential functional types to fine tune regulation of apoptotic responses to various immune challenges. Expression of an assemblage of IAPs may also provide redundancy and extra

safeguards against aberrant apoptosis. In WGCNA networks, expression of many IAPs was also directly correlated with expression of other IAP domain architecture types, suggesting they may be co-regulated, interact with one another in the same apoptosis pathway, be part of dually activated regulated cell death pathways, or be involved in crosstalk between multiple apoptosis pathways. Indeed, in humans, IAPs have demonstrated the ability to perform in concert and form IAP-IAP complexes, with BIRC5 (survivin) specifically forming a complex with BIRC4 (XIAP)[92]. Moreover, crosstalk between IAPs in mammals has been previously shown to affect IAP levels[92–95].These results together support that rather than individual IAP domain architecture types being associated with single apoptosis pathways or immune challenge types, IAP expansion has allowed for expression of an orchestrated collection of diverse IAPs in order to tailor an apoptosis regulatory response to unique challenges.

Analysis of IAP transcripts directly correlated with apoptosis pathway transcripts across multiple experiments also allowed for identification of a novel *C. gigas* BIRC2/3-like transcript, XM_020068541.1 (LOC105331304) which may have homologous function to BIRC2/3 in mammals. This transcript showed similar domain architecture to mammalian BIRC2/3, though with a DD instead of CARD, and in *C. gigas* was directly correlated with extrinsic pathway partners similar to mammalian BIRC2/3, including TNFR and IFN pathways and direct correlation with TRAF3[24,53]. In mammals, BIRC2/3 proteins are ubiquitin ligases involved in TNFR signaling and activation of the NF-κB pathway[96]. In addition to assessing the ability of this protein and other oyster BIRC2/3-like proteins to perform E3-ubiquitin-ligase activity, future functional studies should assess the potential

for expanded oyster BIRC2/3-like proteins to interact with different members of the expanded oyster TNFR and TRAF families[3].

Oysters contain novel Regulated Cell Death pathway components

To determine the potential role of IAPs in RCD, this research performed an in-depth identification of apoptosis and regulated cell death molecules present in *C. virginica* and *C. gigas*, confirming, updating, and expanding molecules identified in previous studies [6,14,19,20,69,97–101]. It also provided an updated list of RCD-related genes for further work. Lack of annotation of certain oyster apoptosis transcripts present in model organisms should be investigated in-depth using manual annotation methods to determine whether these are truly absent in these oysters or were not annotated due to low sequence identity or limitations in an annotation approach relying on RefSeq assigned annotations. For example, while cellular tumor antigen p53 was not explicitly annotated in the *C. gigas* reference genome utilized, previous studies using manual annotation approaches have identified p53 homologs in *C. gigas* and demonstrated the involvement of *Cg-p53* in mitochondrial apoptosis[97,102]. p53 has also been previously identified in other molluscs, including *Mytilus galloprovincialis,* the soft shell clam *Mya arenaria,* and the blue mussel *Mytilus edulis*[98,103]. Previous manual annotation approaches have also recognized Bcl-2 family homologs in *C. gigas* including *Cg-Bcl2* (not annotated in the reference), *Cg-Bcl-xl* (present in annotation), *Cg-Bak* and *Cg-Bax* (present in annotation), and demonstrated their role in apoptosis regulation in a yeast *Saccharomyces cerevisiae* model[97,99]. Members of the BH3-only Bcl-2 family of proteins, including BIK, BID, BIM, BAD, PUMA, NOXA, and HRK, have yet to be identified in molluscs[97,99].

To our knowledge, this is the most in-depth description of novel regulated cell death pathway molecular components in oysters and this research identified proteins involved in necroptosis, lysosome-dependent cell death, and parthanatos. Molecules involved in parthanatos, including PARP1, and MIF have not been previously discussed in molluscs, while AIF, which is involved in caspase-independent apoptosis, has been previously recognized in several species[99]. Isolated necroptosis pathway components, however, have been previously identified in oysters and molluscs. First, the mitochondrial serine/threonine protein phosphatase PGAM5, which is involved in inflammasome activation and operates downstream of RIPK3 during necroptosis, has been identified in *C. gigas* mitochondria in response to hypoxia and reoxygenation stress[104]. Assessment of the transcriptional response of warm acclimated abalone *Haliotis rufescens* has previously revealed regulation of the necroptotic process[105]. Additionally, in the oyster *Crassostrea hongkongensis*, TRAF6 was found to suppress apoptosis through activation of the necroptosis regulatory protein pellino, which is known to regulate ubiquitination of RIPK1, a key necroptosis enzyme[106]. TNFAIP3 was additionally identified as a potential target for neurotransmitter-responsive miRNAs in *C. gigas* and has been shown to respond to thermal and low salinity stress in the Sydney rock oyster *Saccostrea glomerata*[107,108]. Finally, RIPK1 has been previously recognized in *Lingula anatina*, and in *Octopus maya* under chronic thermal stress[109,110]. These results together support that the necroptosis pathway may be found across molluscs and play diverse roles in environmental stress response.

Conclusion

This research used a genomic and transcriptomic approach as a first step in the characterization of the role of IAP gene expansion in oyster apoptotic response to immune challenge. It also offers an updated and expanded characterization of the apoptotic pathway in oysters and demonstrates the power of a novel, cross-species comparative transcriptomic approach to investigate the potential role of expanded immune gene families in invertebrate immune response. Using this approach, we revealed substantial diversity in the IAP family at the level of genes, BIR domains, and domain architecture that were expressed during immune challenge. Domain variation across IAP domain architectures in molluscs likely resulted from a complex history of domain loss and gain over time.

This research also demonstrated direct correlation of IAP gene expression with expression of apoptosis-related genes. Usage of a different assemblage of IAP genes and domain architecture types in apoptosis pathways across experiments may allow for unique regulation of apoptosis proteins that cannot be understood until further functional work is performed to assess novel BIR domain and domain architecture types. This research suggests that lineage specific expansion in the number of IAP genes in oysters has allowed for the development of novel domain architecture types which may confer uniquely tailored apoptotic responses to immune challenge. Overall, this research represents major steps toward fully characterizing the molecular machinery of apoptosis and regulated-cell death pathways in oysters and understanding the role that diversified and expanded IAPs may play in apoptosis regulation, and provides further evidence that gene expansion is a critical mechanism allowing invertebrates to mount diverse immune responses to disease.

Methods

IAP Gene Family Identification and Phylogenetic Analysis

Annotated molluscan genomes (10) were retrieved from NCBI: the California sea hare *Aplysia californica*, marsh snail *Biomphalaria glabrata*, Pacific oyster *Crassostrea gigas*, eastern oyster *Crassostrea virginica*, eastern emerald elysia *Elysia chlorotica*, owl limpet *Lottia gigantea*, yesso scallop *Mizuhopecten yessoensis*, California two spot octopus *Octopus bimaculoides*, east Asian common octopus *Octopus vulgaris* (*sinensis*), golden apple snail *Pomacea canaliculata* (Supplementary Table 8). Genomes were selected from those available at the time of the analysis based on overall genome completeness and quality.

The program HMMER (V 3.2.1)[111,112] was used to identify IAP protein sequences in the targeted genomes. First, the HMMbuild tool created a hidden markov model (HMM) from a list of model organism BIR sequences compiled based on the curated Pfam (V 32.0) BIR domain model (PF00653). The HMM was compared against the protein annotation for each species with the HMMsearch tool. Putative IAP protein sequences (E-value < 0.001) were further analyzed with Interproscan (V 5.44) to identify functional domains[113]. Those lacking a BIR repeat signature were removed and exact duplicates in protein coding sequence were collapsed with CD-HIT for downstream analysis[114]. Redundant *C. virginica* IAP sequences caused by genome assembly artifacts (haplotigs) (Puritz et al. in prep) were also removed (Supplementary table 9). To do this, alignments of IAP protein sequences were built with MAFFT (V 7.45; auto setting) [49,114] and visualized in Uniprot UGENE[115]. Protein sequences in clusters with > 95% similarity showing lower raw read mapping coverage (< half coverage compared to other proteins in the cluster as identified with CD-

HIT) were suspected as haplotigs and removed from further analysis (Supplementary Table 9). In the RNAseq analysis, read counts from suspected haplotigs were added to the counts for their "parent".

Phylogenetic trees of molluscan or bivalve IAP amino acid sequences were built using RAxML HPC MPI (V 8.2.1)[113,114] with the model PROTGAMMAAUTO, and performing rapid bootstrap analysis and maximum likelihood tree searching using the `autoMRE` bootstrap convergence criterion[116,117]. *Octopus* spp. (*O. bimaculoides*, *O. sinensis*) and scallop (*M. yessoensis*) were used as outgroups for the molluscan and bivalve trees, respectively[58,65]. Phylogenetic trees were generated with ggtree[118] and protein domains were visualized using ggplot `geom_segment` and compiled with cowplot (V 1.0.0, Wilke, Claus). Chromosomal locations of IAP genes in the *C. virginica* genome assembly (GCA_002022765.4) were plotted using RCircos (V 1.2.1)[119]. Intronless genes were identified as genes with a single exon in the annotation "gff3" file for both *C. virginica* and *C. gigas*.

BIR Domain Classification and IAP Protein Functional Analysis

Oyster BIR domains identified by CDD and Interproscan were classified into Type I or Type II domains by aligning the oyster sequences to BIR domain amino acid sequences from well-studied model organisms (*D. melanogaster*, *Homo sapiens*, *Mus musculus, Danio rerio*) using MAFFT (V 7.45; setting `-auto` (BIR domain Multiple Sequence Alignment, Supplementary File 4) and viewed in UGENE for analysis[115]. BIR domain types were identified based on the conserved sequence patterns in the α-3 and α-4 sequence regions. Phylogenetic trees of BIR domains were performed and visualized as described

above. Secondary protein structure prediction of BIR domains was performed using RaptorX with auto settings[120]. Three class secondary structure (H = alpha helix, E = beta sheet, and C = coil), and eight class secondary structure (H = alpha helix, G = five turn helix, I = extended strand in beta ladder, E = isolated beta bridge, T = hydrogen bonded turn, S = bend, L = loop) were determined for each BIR amino acid position[120].

Additional functional domains were identified in mollusc IAP amino acid sequences using Interproscan (V 5.44). IAP sequences from *C. virginica*, *C. gigas*, and *M. yessoensis* were clustered into functional groupings using BIR domain architecture (number and type of BIR domains), the presence of RING finger domains, Death Domains (DD), UBA domains, bootstrapping support in the RAxML tree (> 90%), and presence of proteins in the cluster from both *C. virginica* and *C. gigas*.

Identification of Apoptosis and Regulated Cell Death Genes in *C. virginica* and *C. gigas*

A list of candidate apoptosis and regulated cell death proteins previously identified in selected model organisms and molluscs was gathered via literature search and the Kyoto Encyclopedia of Genes and Genomes (KEGG) reference apoptosis pathway [3,4,8,13,19,20,55,56,121–125]. UniprotKB was used to identify known protein aliases for each protein[126]. Eastern oyster (v3.0, GCA_002022765.4) and Pacific oyster (v 9.0, GCA_000297895.1) reference genome annotations were mined for protein names and aliases in the target list using R (V 3.6.1).

Oyster transcriptomes in response to immune challenge

Apoptosis gene expression was compared across four distinct challenge types (viral, bacterial, parasitic, and probiotic) and 8 transcriptome experiments, containing 199 total raw transcriptomes spanning a variety of conditions (Table 1; Supplementary Table 10). Raw transcriptome data was downloaded between 2016 and 2020 from the NCBI SRA database using the SRA Toolkit (V 2.9.0) [127]. BBTools BBMap (V 37.36) was used to trim adapters, quality trim the left and right sides of reads with Phred quality scores of less than 20, and remove entire reads with an average Phred score of less than 10[128]. Transcriptomes were aligned to their respective NCBI reference genome sequences using HISAT2 (V 2.1.0) with default parameters and without use of a reference annotation to allow for novel transcript discovery[129,130]. HISAT2 output files were sorted and converted into BAM format using SAMtools (V 1.9.0)[131]. Transcripts were assembled and quantified for each experiment separately using their respective reference genome annotations (Supplementary Table 8) using Stringtie (V 2.1.0)[130]. Comparison of transcriptome annotation to the reference for each sample was conducted using gffcompare (V 0.11.5)[130]. Stringtie output was formatted into matrices of transcript count data and uploaded into R Studio (V 3.6.1)[132].

Gene Expression Analysis

Differential transcript expression was calculated for each experiment separately using the package DESeq2 (V 1.24.0)[133]. Models were designed for each experiment to determine the overall effect of immune challenge. Experiments with multiple experimental conditions or timepoints were split so that specific effects in each experimental condition (e.g. time after challenge, host genetics and age) could be measured. In experiments

lacking either controls or replicates for each condition, the effect of condition was corrected in the DESeq model design by pooling similar conditions (Supplementary Table 11).

Transcripts with < 10 read counts were removed from analysis. Log fold change (LFC) in expression between genes within experiments were considered significant when *p*-values adjusted (*Padj*) using the Benjamini–Hochberg to control for the False Discovery rate (FDR) were ≤ 0.05. LFC shrinkage was performed using "apeglm" to improve ranking genes by effect size and enable comparison of LFC between experiments[134]. Transcript counts were log scale transformed and normalized to the library size (*rlog*) for experiments with < 30 samples. The variance stabilizing transformation (*vst)* was used to normalize transcript counts in experiments with > 30 samples[133]. IAP and apoptosis-related transcripts were subset from overall differentially expressed genes using lists of candidate genes identified above.

In order to confirm overall expression for each of the identified oyster IAP genes (*i.e.* to identify potential pseudogenes or genes not expressed at all in the experimental conditions included in this study), constitutive gene expression (transformed read counts) was shown for those genes containing transcripts that showed expression in all experiments but were not significantly differentially expressed in any of experiments included in the DEG analysis. Read counts for each of the genes were transformed using either the *rlog* or *vst* transformations based on sample size (the same way as above during DESeq2 analysis) and were corrected for batch effects using the limma package *'removeBatchEffects'* [135] Transformed read counts were averaged within each individual treatment group for each experiment.

All gene expression figures were generated in ggplot2 (V3.3.2) using "geom_tile" and compiled using cowplot (V1.0.0, Wilke, Claus). LFC heatmaps were generated with ComplexHeatmap (V 2.0.0)[136].

Weighted gene co-expression network analysis (WGCNA)

In order to determine a potential association between IAP gene expression and expression of apoptosis-related genes, weighted gene co-expression of apoptosis genes within each individual experiment was investigated using WGCNA (V 1.68) in R (V 3.6.1)[137]. Expression data was transformed as for the DESeq2 experiment, and batch effect correction was performed the same as in the constitutive expression analysis. Network construction and module identification was performed separately for each experiment. For each network, a "signed hybrid" type network was selected and robust correlation was performed using the bi-weight mid-correlation (corFunc= "bicor")[137]. Soft thresholding powers were set based on fit to scale free topology, or when scale free topology was not satisfied, soft thresholding was selected based on sample size (9 for "signed hybrid" with less than 30 samples). Modules significantly correlated with immune challenge (p-value $\leq$ 0.05) and containing > 1 transcript for both IAP and apoptosis-related genes were analyzed. Direct correlations between apoptosis-related and IAP genes were assessed by isolating nodes where IAPs were directly connected to an apoptosis-related transcript by a shared edge. Presence and absence heatmaps for IAPs and directly correlated apoptosis-related transcripts in each experimental condition were generated with Pheatmap (V 1.0.12)[136]. Upset plots of this data were created using "UpSet" in ComplexHeatmap (V 2.0.0) and figure tables were generated using the gt package (V 0.2.1).

Declarations

Ethics approval and consent to participate:

Not applicable.

Consent for publication:

Not applicable.

Availability of data and materials:

The datasets analyzed during the current study are publicly available on the NCBI SRA (Supplementary Table 10). Mollusc reference annotations utilized are publicly available on NCBI (Supplementary Table 8). Code used to perform analysis and create figures in this publication are publicly available on github (differential expression analysis and WGCNA at https://github.com/erinroberts/apoptosis_data_pipeline; apoptosis pathway and IAP annotation at https://github.com/erinroberts/Apoptosis-Pathway-Annotation-Comparative-Genomics).

Competing interests:

The authors declare they have no competing interests.

Funding:

This work was supported by a USDA NIFA AFRI Pre-Doctoral Fellowship Award# 2019-67011-29553 to EMW, Department of Commerce/NOAA Saltonstall-Kennedy Award

#NA18NMF4270193 to MGC, David R. Nelson, and David C. Rowley, USDA NIFA AFRI Award #2015-67016-22942 to DCR, DRN and MGC, USDA ARS Collaborative Project 58-8030-5-009 to MGC, a USDA NRSP-8 award to MGC and DAP, USDA NIFA RI0019-H020, URI Coastal Institute Grants in Aid,
and the Blount Family Shellfish Restoration Foundation.

Author Contributions:

EMW and MGC conceptualized the project jointly. EMW wrote all analysis code, produced all figures, and wrote the manuscript. MGC contributed to genomic and transcriptomic data analysis and interpretation, figure design, and edited the manuscript. DAP provided data, assisted in interpretation, and edited the manuscript. All authors read and approved the final manuscript.

Acknowledgements:

The authors would like to acknowledge Jon Puritz for his contribution of *C. virginica* genome read coverage data to assist in pruning *C. virginica* reference genome IAP haplotigs (Puritz et al., *in prep*). The authors would also like to acknowledge Matt Hare, Hollie Putnam, and Rachel Schwartz for helpful suggestions to the manuscript.

Abbreviations:

A1=bcl-2-related protein A1, A20=tumor necrosis factor alpha-induced protein 3, AIF/AIFM1=apoptosis-inducing factor 1, mitochondrial, ATF-4=cyclic AMP-dependent transcription factor ATF-4, AURKA=aurora kinase A, BAD=BCL2 associated agonist of cell death, BAG=BAG family molecular chaperone regulator, BAK1=bcl-2 homologous antagonist/killer, BID=BH3-

interacting domain death agonist, BIK=Bcl-2-interacting killer, BIM=Bcl-2-like protein 11, BIR=Baculovirus IAP Repeat , BMF=Bcl-2-modifiying factor, BRUCE=BIR repeat-containing ubiquitin-conjugating enzyme, CARD=caspase activation and recruitment domain , CCAR=cell division cycle and apoptosis regulator protein 1, CD151=CD151 antigen, CDD=conserved domain database, CDIP1=cell death-inducing p53-target protein 1, cdc42=cdc42 homolog, CFU=colony forming units, CHIP=E3 ubiquitin-protein ligase CHIP, CHOP=DNA damage-inducible transcript 3 protein, CRADD=death domain-containing protein CRADD, CREB3L=cyclic AMP-responsive element-binding protein 3-like protein, DD=death domains, DEG=differentially expressed genes, DEBCL= Proapoptotic Bcl-2 homolog DEBCL, DIAP1=death-associated inhibitor of apoptosis 1, DIAP2=death-associated inhibitor of apoptosis 2, DIABLO=diablo homolog, mitochondrial, EIF2K3=eukaryotic translation initiation factor 2-alpha kinase 3, DISC=death-inducing signaling complex, DR=death receptor, ER=endoplasmic reticulum , FADD=fas-associated death domain protein, FAP1=tyrosine-protein phosphatase non-receptor type 13, FDR=false discovery rate, FLIP=FLICE inhibitory protein, FREP=fibrinogen-related protein, FSW=filtered sterile seawater, GADD=growth arrest and DNA damage-inducible protein GADD, GIMAP=GTPase IMAP family member, HK1=hexokinase-1, HRK=Activator of apoptosis harakiri, IAP=inhibitor of apoptosis protein, IFI27=interferon alpha-inducible protein 27, mitochondrial, IFI44=interferon-induced protein 44, IFN=interferon, IL17=interleukin 17-like protein, IL17RD=interleukin-17 receptor D, IRAK4=interleukin-1 receptor-associated kinase 4, IRE1=serine/threonine-protein kinase/endoribonuclease IRE1, IRF=interferon regulatory factor 1, IRF8=interferon regulatory factor 8, JAK2=tyrosine-protein kinase JAK2, LFC=log fold change, LITAF=lipopolysaccharide-induced tumor necrosis factor-alpha factor, LPS=lipopolysaccharide-induced tumor necrosis factor-alpha factor, LTR=long terminal repeat, MAPK=mitogen-activated protein kinase, MIF=macrophage migration inhibitory factor, MyD88=myeloid differentiation primary response protein MyD88, NOXA=phorbol-12-myristate-13-acetate- induced protein 1, NR13=anti-apoptotic protein NR13, ORF=open reading frame, PARP1=poly [ADP-ribose] polymerase 1, PDRG1=p53 and DNA damage-regulated protein 1, PIDD1=leucine-rich repeat and death domain-containing protein 1, PPM1B=protein phosphatase 1B,

PRR=pattern recognition receptor, RCD=regulated cell death, RHOT1=mitochondrial Rho GTPase 1, RING=really interesting new gene, RIPK=receptor-interacting serine/threonine-protein kinase , SARM1=sterile alpha and TIR motif-containing protein 1, SERPINB1=leukocyte elastase inhibitor, STAT=signal transducer and activator of transcription 5A, STING=stimulator of interferon genes protein, TAB1=TGF-beta-activated kinase 1 and MAP3K7-binding protein 1, TAK1=mitogen-activated protein kinase kinase kinase 7, TLR=toll-like receptor , TNF=tumor necrosis factor, TNFAIP=tumor necrosis factor alpha-induced protein, TNFR=tumor necrosis factor receptor, TNFRSF=tumor necrosis factor receptor superfamily member, TRADD=tumor necrosis factor receptor superfamily member 5, TRAF=TNF receptor-associated factor, TRAIL=tumor necrosis factor ligand superfamily member 10, UBA=ubiquitin associated domain, UBC=ubiquitin conjugating domain , XIAP=E3 ubiquitin-protein ligase XIAP.

References

1. Dishaw, L. J. & Litman, G. W. Changing views of the evolution of immunity. *Front. Immunol.* **4**, 2012–2014 (2013).
2. Gerdol, M. et al. Immunity in Molluscs: Recognition and Effector Mechanisms, with a Focus on Bivalvia. in *Advances in Comparative Immunology* 225–341 (2018).
3. Zhang, L. *et al.* Massive expansion and functional divergence of innate immune genes in a protostome. *Sci. Rep.* **5**, 8693 (2015).
4. Zhang, G. *et al.* The oyster genome reveals stress adaptation and complexity of shell formation. (2012). doi:10.1038/nature11413
5. Gómez-Chiarri, M., Guo, X., Tanguy, A., He, Y. & Proestou, D. The use of -omic tools in the study of disease processes in marine bivalve mollusks. *J. Invertebr. Pathol.* **131**, 137–154 (2015).
6. Song, H. *et al.* The hard clam genome reveals massive expansion and diversification of inhibitors of apoptosis in Bivalvia. 1–20 (2021).
7. Gerdol, M. *et al.* The C1q domain containing proteins of the Mediterranean mussel Mytilus galloprovincialis : A widespread and diverse family of immune-related molecules. *Dev. Comp. Immunol.* **35**, 635–643 (2011).
8. Gerdol, M. & Venier, P. An updated molecular basis for mussel immunity. *Fish Shellfish Immunol.* **46**, 17–38 (2015).
9. Zhang, L. L., Li, L. & Zhang, G. F. Sequence variability of fibrinogen-related proteins (FREPs) in Crassostrea gigas. *Chinese Sci. Bull.* **57**, 3312–3319 (2012).
10. Zhu, X. *et al.* IAPs Gene Expansion in the Scallop Patinopecten yessoensis and Their Expression Profiles After Exposure to the Toxic Dinoflagellate. *Front.*

Physiol. **12**, 1–11 (2021).

11. Guo, X. & Ford, S. E. Infectious diseases of marine molluscs and host responses as revealed by genomic tools. *Philos. Trans. R. Soc. B Biol. Sci.* **371**, 20150206 (2016).
12. McDowell, I. C., Modak, T. H., Lane, C. E. & Gomez-Chiarri, M. Multi-species protein similarity clustering reveals novel expanded immune gene families in the eastern oyster Crassostrea virginica. *Fish Shellfish Immunol.* **53**, 13–23 (2016).
13. He, Y. *et al.* Transcriptome analysis reveals strong and complex antiviral response in a mollusc. *Fish Shellfish Immunol.* **46**, 131–144 (2015).
14. Zhang, L., Li, L., Zhu, Y., Zhang, G. & Guo, X. Transcriptome Analysis Reveals a Rich Gene Set Related to Innate Immunity in the Eastern Oyster (Crassostrea virginica). *Mar. Biotechnol.* **16**, 17–33 (2014).
15. Allam, B. & Raftos, D. Immune responses to infectious diseases in bivalves. *J. Invertebr. Pathol.* **131**, 121–136 (2015).
16. Nikapitiya, C. *et al.* Identification of potential general markers of disease resistance in American oysters, *Crassostrea virginica* through gene expression studies. *Fish Shellfish Immunol.* **41**, 27–36 (2014).
17. Eirín-López, J. M., Rebordinos, L., Rooney, A. P. & Rozas, J. The birth-and-death evolution of multigene families revisited. *Repetitive DNA* 170–196 (2012). doi:10.1159/000337119
18. Hughes, F. M., Foster, B., Grewal, S. & Sokolova, I. M. Apoptosis as a host defense mechanism in Crassostrea virginica and its modulation by Perkinsus marinus. *Fish Shellfish Immunol.* **29**, 247–257 (2010).
19. Sokolova, I. Apoptosis in molluscan immune defense. *Invertebr. Surviv. J.* **6**, 49–58

(2009).

20. Kiss, T. Apoptosis and its functional significance in molluscs. *Apoptosis* **15**, 313–321 (2010).

21. Galluzzi, L. *et al.* Molecular mechanisms of cell death: recommendations of the Nomenclature Committee on Cell Death 2018. *Cell Death Differ.* **25**, 486–541 (2018).

22. Tang, D., Kang, R., Berghe, T. Vanden, Vandenabeele, P. & Kroemer, G. The molecular machinery of regulated cell death. *Cell Res.* (2019). doi:10.1038/s41422-019-0164-5

23. Kumar, S., Fairmichael, C., Longley, D. B. & Turkington, R. C. The Multiple Roles of the IAP Super-family in cancer. *Pharmacol. Ther.* **214**, 107610 (2020).

24. Gyrd-Hansen, M. & Meier, P. IAPs: From caspase inhibitors to modulators of NF-κB, inflammation and cancer. *Nat. Rev. Cancer* **10**, 561–574 (2010).

25. Estornes, Y. & Bertrand, M. J. M. IAPs, regulators of innate immunity and inflammation. *Semin. Cell Dev. Biol.* **39**, 106–114 (2015).

26. Vasudevan, D. & Don Ryoo, H. *Regulation of Cell Death by IAPs and Their Antagonists*. *Current Topics in Developmental Biology* **114**, (Elsevier Inc., 2015).

27. Rothe, M., Pan, M. G., Henzel, W. J., Ayres, T. M. & Goeddel, D. V. The TNFR2-TRAF signaling complex contains two novel proteins related to baculoviral inhibitor of apoptosis proteins. *Cell* **83**, 1243–1252 (1995).

28. Uren, A. G., Pakusch, M., Hawkins, C. J., Puls, K. L. & Vaux, D. L. Cloning and expression of apoptosis inhibitory protein homologs that function to inhibit apoptosis and/or bind tumor necrosis factor receptor-associated factors. *Proc. Natl.*

Acad. Sci. U. S. A. **93**, 4974–4978 (1996).

29. Lu, M. *et al.* XIAP Induces NF-κB Activation via the BIR1/TAB1 Interaction and BIR1 Dimerization. *Mol. Cell* **26**, 689–702 (2007).

30. Gyrd-Hansen, M. *et al.* IAPs contain an evolutionarily conserved ubiquitin-binding domain that regulates NF-κB as well as cell survival and oncogenesis. *Nat. Cell Biol.* **10**, 1309–1317 (2008).

31. Kocab, A. J. & Duckett, C. S. Inhibitor of apoptosis proteins as intracellular signaling intermediates. *FEBS J.* **283**, 221–231 (2016).

32. Cheung, C. H. A., Chang, Y. C., Lin, T. Y., Cheng, S. M. & Leung, E. Anti-apoptotic proteins in the autophagic world: An update on functions of XIAP, Survivin, and BRUCE. *J. Biomed. Sci.* **27**, 1–10 (2020).

33. Oberoi-Khanuja, T. K., Murali, A. & Rajalingam, K. IAPs on the move: Role of inhibitors of apoptosis proteins in cell migration. *Cell Death Dis.* **4**, (2013).

34. Oberoi-Khanuja, T. K., Karreman, C., Larisch, S., Rapp, U. R. & Rajalingam, K. Role of melanoma inhibitor of apoptosis (ML-IAP) protein, a member of the baculoviral IAP repeat (BIR) domain family, in the regulation of C-RAF kinase and cell migration. *J. Biol. Chem.* **287**, 28445–28455 (2012).

35. Ebner, P. *et al.* The IAP family member BRUCE regulates autophagosome–lysosome fusion. *Nat. Commun.* **9**, 1–15 (2018).

36. Ge, C. *et al.* BRUCE regulates DNA double-strand break response by promoting USP8 deubiquitination of BRIT1. *Proc. Natl. Acad. Sci. U. S. A.* **112**, E1210–E1219 (2015).

37. Powell, D. *et al.* The genome of the oyster Saccostrea offers insight into the

environmental resilience of bivalves. *DNA Res.* **25**, 655–665 (2018).

38. Mcdowell, I. C. *et al.* Transcriptome of American Oysters , Crassostrea virginica , in Response to Bacterial Challenge : Insights into Potential Mechanisms of Disease Resistance. **9**, (2014).

39. Lorgeril, J. De, Zenagui, R., Rosa, R. D., Piquemal, D. & Bache, E. Whole Transcriptome Profiling of Successful Immune Response to Vibrio Infections in the Oyster Crassostrea gigas by Digital Gene Expression Analysis. **6**, (2011).

40. Rosani, U. *et al.* Dual analysis of host and pathogen transcriptomes in ostreid herpesvirus 1-positive Crassostrea gigas. *Environ. Microbiol.* **17**, 4200–4212 (2015).

41. Green, T. J., Vergnes, A., Montagnani, C. & Lorgeril, J. De. Distinct immune responses of juvenile and adult oysters (Crassostrea gigas) to viral and bacterial infections. *Vet. Res.* **1**, 1–11 (2016).

42. Lau, Y. T., Santos, B., Barbosa, M., Pales Espinosa, E. & Allam, B. Regulation of apoptosis-related genes during interactions between oyster hemocytes and the alveolate parasite Perkinsus marinus. *Fish Shellfish Immunol.* **83**, 180–189 (2018).

43. Wanninger, A. & Wollesen, T. The evolution of molluscs. *Biol. Rev.* **94**, 102–115 (2019).

44. Cao, Y. *et al.* Evolution and function analysis of interleukin-17 gene from Pinctada fucata martensii. *Fish Shellfish Immunol.* **88**, 102–110 (2019).

45. Jiao, Y., Cao, Y., Zheng, Z., Liu, M. & Guo, X. Massive expansion and diversity of nicotinic acetylcholine receptors in lophotrochozoans. *BMC Genomics* **20**, 1–15 (2019).

46. Eckelman, B. P., Drag, M., Snipas, S. J. & Salvesen, G. S. The mechanism of peptide-binding specificity of IAP BIR domains. *Cell Death Differ.* **15**, 920–928 (2008).

47. Cossu, F., Milani, M., Mastrangelo, E. & Lecis, D. Targeting the BIR Domains of Inhibitor of Apoptosis (IAP) Proteins in Cancer Treatment. *Comput. Struct. Biotechnol. J.* **17**, 142–150 (2019).

48. Chen, S. N., Fang, T., Kong, J. Y., Pan, B. Bin & Su, X. C. Third BIR domain of XIAP binds to both Cu(II) and Cu(I) in multiple sites and with diverse affinities characterized at atomic resolution. *Sci. Rep.* **9**, 1–11 (2019).

49. Katoh, K. & Standley, D. M. MAFFT multiple sequence alignment software version 7: Improvements in performance and usability. *Mol. Biol. Evol.* **30**, 772–780 (2013).

50. Park, H. H. *et al.* The death domain superfamily in intracellular signaling of apoptosis and inflammation. *Annu. Rev. Immunol.* **25**, 561–586 (2007).

51. de Lorgeril, J. *et al.* Immune-suppression by OsHV-1 viral infection causes fatal bacteraemia in Pacific oysters. *Nat. Commun.* **9**, (2018).

52. Proestou, D. A. & Sullivan, M. E. Variation in global transcriptomic response to Perkinsus marinus infection among eastern oyster families highlights potential mechanisms of disease resistance. *Fish Shellfish Immunol.* **96**, 141–151 (2020).

53. Häcker, H., Tseng, P. H. & Karin, M. Expanding TRAF function: TRAF3 as a tri-faced immune regulator. *Nat. Rev. Immunol.* **11**, 457–468 (2011).

54. Rosenstiel, P., Philipp, E. E. R., Schreiber, S. & Bosch, T. C. G. Evolution and function of innate immune receptors - Insights from marine invertebrates. *J. Innate Immun.* **1**, 291–300 (2009).

55. Robertson, A. J. *et al.* The genomic underpinnings of apoptosis in Strongylocentrotus purpuratus. *Dev. Biol.* **300**, 321–334 (2006).

56. Buckley, K. M. & Rast, J. P. Dynamic evolution of toll-like receptor multigene families in echinoderms. *Front. Immunol.* **3**, (2012).

57. Huang, S. *et al.* Genomic analysis of the immune gene repertoire of amphioxus reveals extraordinary innate complexity and diversity. *Genome Res.* **18**, 1112–1126 (2008).

58. Lu, L., Loker, E. S., Zhang, S. M., Buddenborg, S. K. & Bu, L. Genome-wide discovery, and computational and transcriptional characterization of an AIG gene family in the freshwater snail Biomphalaria glabrata, a vector for Schistosoma mansoni. *BMC Genomics* **21**, 190 (2020).

59. Vogeler, S., Carboni, S., Li, X. & Joyce, A. Phylogenetic analysis of the caspase family in bivalves: implications for programmed cell death, immune response and development. *BMC Genomics* **22**, 1–17 (2021).

60. Miao, G., Qi, H., Li, L., Que, H. & Zhang, G. Characterization and functional analysis of two inhibitor of apoptosis genes in Zhikong scallop Chlamys farreri. **60**, 1–11 (2016).

61. Gao, D. *et al.* Repertoire and evolution of TNF superfamily in Crassostrea gigas: Implications for expansion and diversification of this superfamily in Mollusca. *Dev. Comp. Immunol.* **51**, 251–260 (2015).

62. Xu, F. *et al.* Expression and function analysis of two naturally truncated MyD88 variants in the Pacific oyster Crassostrea gigas. *Fish Shellfish Immunol.* **45**, 510–516 (2015).

63. Gerdol, M., Greco, S. & Pallavicini, A. Extensive tandem duplication events drive the expansion of the C1q-domain-containing gene family in bivalves. *Mar. Drugs* **17**, 1–13 (2019).

64. Prof, T. *et al.* Chromosome-level analysis of Crassostrea hongkongensis genome reveals extensive duplication of immune-related genes in bivalves. doi:10.1111/1755-0998.13157

65. Jiao, Y., Gu, Z., Luo, S. & Deng, Y. Evolutionary and functional analysis of MyD88 genes in pearl oyster Pinctada fucata martensii. *Fish Shellfish Immunol.* **99**, 322–330 (2020).

66. Peñaloza, C. *et al.* A chromosome-level genome assembly for the Pacific oyster Crassostrea gigas. *Gigascience* **10**, 1–9 (2021).

67. Kaessmann, H., Vinckenbosch, N. & Long, M. RNA-based gene duplication: Mechanistic and evolutionary insights. *Nat. Rev. Genet.* **10**, 19–31 (2009).

68. Zhang, S. M. & Loker, E. S. The FREP gene family in the snail Biomphalaria glabrata: Additional members, and evidence consistent with alternative splicing and FREP retrosequences. *Dev. Comp. Immunol.* **27**, 175–187 (2003).

69. Yu, M., Chen, J., Bao, Y. & Li, J. Genomic analysis of NF-κB signaling pathway reveals its complexity in Crassostrea gigas. *Fish Shellfish Immunol.* **72**, 510–518 (2018).

70. Zmasek, C. M. & Godzik, A. Evolution of the animal apoptosis network. *Cold Spring Harb. Perspect. Biol.* **5**, (2013).

71. Weber, C. H. & Vincenz, C. The death domain superfamily: A tale of two interfaces? *Trends Biochem. Sci.* **26**, 475–481 (2001).

72. Lopez, J. *et al.* CARD-Mediated Autoinhibition of cIAP1's E3 Ligase Activity Suppresses Cell Proliferation and Migration. *Mol. Cell* **42**, 569–583 (2011).

73. Kao, W. P. *et al.* The versatile roles of CARDs in regulating apoptosis, inflammation, and NF-κB signaling. *Apoptosis* **20**, 174–195 (2015).

74. Hu, S. & Yang, X. dFADD, A novel death domain-containing adapter protein for the Drosophila caspase DREDD. *J. Biol. Chem.* **275**, 30761–30764 (2000).

75. Sladky, V., Schuler, F., Fava, L. L. & Villunger, A. The resurrection of the PIDDosome - Emerging roles in the DNA-damage response and centrosome surveillance. *J. Cell Sci.* **130**, 3779–3787 (2017).

76. Wheatley, S. P. & Altieri, D. C. Survivin at a glance. *J. Cell Sci.* **132**, (2019).

77. O'Riordan, M. X. D., Bauler, L. D., Scott, F. L. & Duckett, C. S. Inhibitor of apoptosis proteins in eukaryotic evolution and development: a model of thematic conservation. *Dev. Cell* **15**, 497–508 (2008).

78. Qu, T. *et al.* Characterization of an inhibitor of apoptosis protein in Crassostrea gigas clarifies its role in apoptosis and immune defense. **51**, 74–78 (2015).

79. Samuel, T. *et al.* Distinct BIR domains of cIAP1 mediate binding to and ubiquitination of tumor necrosis factor receptor-associated factor 2 and second mitochondrial activator of caspases. *J. Biol. Chem.* **281**, 1080–1090 (2006).

80. Guo, X. & Ford, S. E. Infectious diseases of marine molluscs and host responses as revealed by genomic tools. *Philos. Trans. R. Soc. Lond. B. Biol. Sci.* **371**, (2016).

81. Green, T. J., Helbig, K., Speck, P. & Raftos, D. A. Primed for success: Oyster parents treated with poly(I:C) produce offspring with enhanced protection against Ostreid herpesvirus type I infection. *Mol. Immunol.* **78**, 113–120 (2016).

82. Green, T. J. & Montagnani, C. Poly I: C induces a protective antiviral immune response in the Pacific oyster (Crassostrea gigas) against subsequent challenge with Ostreid herpesvirus (OsHV-1 μvar). *Fish Shellfish Immunol.* **35**, 382–388 (2013).

83. Zhang, Q., Zmasek, C. M. & Godzik, A. Domain architecture evolution of pattern-recognition receptors. *Immunogenetics* **62**, 263–272 (2010).

84. Barber, G. N. Host defense, viruses and apoptosis. *Cell Death Differ.* **8**, 113–126 (2001).

85. Modak, T. H. & Gomez-Chiarri, M. Contrasting immunomodulatory effects of probiotic and pathogenic bacteria on eastern oyster, crassostrea virginica, larvae. *Vaccines* **8**, 1–23 (2020).

86. Kuebutornye, F. K. A., Abarike, E. D. & Lu, Y. A review on the application of Bacillus as probiotics in aquaculture. *Fish Shellfish Immunol.* **87**, 820–828 (2019).

87. Proestou, D. A., Jr, S. K. A., Corbett, R. J., Horin, T. Ben & Small, J. M. Defining Dermo resistance phenotypes in an eastern oyster breeding population. 2142–2154 (2019). doi:10.1111/are.14095

88. Goedken, M., Morsey, B., Sunila, I. & De Guise, S. Immunomodulation of Crassostrea gigas and Crassostrea virginica cellular defense mechanism by Perkinsus marinus. *J. Shellfish Res.* **24**, 487–496 (2005).

89. Gervais, O. *et al.* Involvement of apoptosis in the dialogue between the parasite Bonamia ostreae and the flat oyster Ostrea edulis. *Fish Shellfish Immunol.* **93**, 958–964 (2019).

90. Segarra, A. *et al.* Dual transcriptomics of virus-host interactions: comparing two Pacific oyster families presenting contrasted susceptibility to ostreid herpesvirus 1.

BMC Genomics **15**, 580 (2014).

91. Mammari, N. *et al.* Toxoplasma gondii Modulates the Host Cell Responses: An Overview of Apoptosis Pathways. *Biomed Res. Int.* **2019**, (2019).

92. Dohi, T. *et al.* An IAP-IAP complex inhibits apoptosis. *J. Biol. Chem.* **279**, 34087–34090 (2004).

93. Conze, D. B. *et al.* Posttranscriptional Downregulation of c-IAP2 by the Ubiquitin Protein Ligase c-IAP1 In Vivo. *Mol. Cell. Biol.* **25**, 3348–3356 (2005).

94. Arora, V. *et al.* Degradation of survivin by the X-linked Inhibitor of Apoptosis (XIAP)-XAF1 complex. *J. Biol. Chem.* **282**, 26202–26209 (2007).

95. Silke, J. *et al.* Determination of cell survival by RING-mediated regulation of inhibitor of apoptosis (IAP) protein abundance. *Proc. Natl. Acad. Sci. U. S. A.* **102**, 16182–16187 (2005).

96. Zhang, J. *et al.* Ubiquitin Ligases cIAP1 and cIAP2 Limit Cell Death to Prevent Inflammation. *Cell Rep.* **27**, 2679-2689.e3 (2019).

97. Li, Y. *et al.* Conservation and divergence of mitochondrial apoptosis pathway in the Pacific oyster , Crassostrea gigas. **82898701**, 1–13 (2017).

98. Romero, A., Figueras, A. & Novoa, B. Genes of the Mitochondrial Apoptotic Pathway in Mytilus galloprovincialis. **8**, (2013).

99. Romero, A., Novoa, B. & Figueras, A. The complexity of apoptotic cell death in mollusks: An update. *Fish Shellfish Immunol.* **46**, 79–87 (2015).

100. Zhang, L., Li, L. & Zhang, G. Gene discovery, comparative analysis and expression profile reveal the complexity of the Crassostrea gigas apoptosis system. *Dev. Comp. Immunol.* **35**, 603–610 (2011).

101. Rosani, U., Varotto, L., Gerdol, M., Pallavicini, A. & Venier, P. IL-17 signaling components in bivalves: Comparative sequence analysis and involvement in the immune responses. *Dev. Comp. Immunol.* **52**, 255–268 (2015).

102. Plachetzki, D. C., Pankey, M. S., MacManes, M. D., Lesser, M. P. & Walker, C. W. The Genome of the Softshell Clam Mya arenaria and the Evolution of Apoptosis. *Genome Biol. Evol.* **12**, 1681–1693 (2020).

103. Walker, C. W. *et al.* Chapter One - p53 Superfamily Proteins in Marine Bivalve Cancer and Stress Biology. in (ed. Lesser, M. B. T.-A. in M. B.) **59**, 1–36 (Academic Press, 2011).

104. Sokolov, E. P. *et al.* Effects of hypoxia-reoxygenation stress on mitochondrial proteome and bioenergetics of the hypoxia-tolerant marine bivalve Crassostrea gigas. *J. Proteomics* **194**, 99–111 (2019).

105. Tripp-Valdez, M. A. *et al.* Growth Performance and Transcriptomic Response of Warm-Acclimated Hybrid Abalone Haliotis rufescens (♀) × H. corrugata (♂). *Mar. Biotechnol.* 62–76 (2020). doi:10.1007/s10126-020-10002-7

106. Lin, Y. *et al.* TRAF6 suppresses the apoptosis of hemocytes by activating pellino in Crassostrea hongkongensis. *Dev. Comp. Immunol.* **103**, 103501 (2020).

107. Chen, H. *et al.* The comprehensive immunomodulation of NeurimmiRs in haemocytes of oyster Crassostrea gigas after acetylcholine and norepinephrine stimulation. *BMC Genomics* **16**, 1–14 (2015).

108. Ertl, N. G., O'Connor, W. A. & Elizur, A. Molecular effects of a variable environment on Sydney rock oysters, Saccostrea glomerata: Thermal and low salinity stress, and their synergistic effect. *Mar. Genomics* **43**, 19–32 (2019).

109. Gerdol, M., Luo, Y. J., Satoh, N. & Pallavicini, A. Genetic and molecular basis of the immune system in the brachiopod Lingula anatina. *Dev. Comp. Immunol.* **82**, 7–30 (2018).

110. López-Galindo, L. *et al.* Transcriptomic analysis reveals insights on male infertility in octopus maya under chronic thermal stress. *Front. Physiol.* **9**, 1–18 (2019).

111. Finn, R. D. *et al.* Pfam: The protein families database. *Nucleic Acids Res.* **42**, 222–230 (2014).

112. Johnson, L. S., Eddy, S. R. & Portugaly, E. Hidden Markov model speed heuristic and iterative HMM search procedure. *BMC Bioinformatics* **11**, 431 (2010).

113. Jones, P. *et al.* InterProScan 5: Genome-scale protein function classification. *Bioinformatics* **30**, 1236–1240 (2014).

114. Fu, L., Niu, B., Zhu, Z., Wu, S. & Li, W. CD-HIT: Accelerated for clustering the next-generation sequencing data. *Bioinformatics* **28**, 3150–3152 (2012).

115. Okonechnikov, K. *et al.* Unipro UGENE: A unified bioinformatics toolkit. *Bioinformatics* **28**, 1166–1167 (2012).

116. Stamatakis, A. RAxML-VI-HPC : maximum likelihood-based phylogenetic analyses with thousands of taxa and mixed models. **22**, 2688–2690 (2006).

117. Stamatakis, A., Hoover, P. & Rougemont, J. A rapid bootstrap algorithm for the RAxML web servers. *Syst. Biol.* **57**, 758–771 (2008).

118. Yu, G. Using ggtree to Visualize Data on Tree-Like Structures. *Curr. Protoc. Bioinforma.* **69**, 1–18 (2020).

119. Zhang, H., Meltzer, P. & Davis, S. RCircos: An R package for Circos 2D track plots. *BMC Bioinformatics* **14**, (2013).

120. Wang, S., Li, W., Liu, S. & Xu, J. RaptorX-Property: a web server for protein structure property prediction. *Nucleic Acids Res.* **44**, W430–W435 (2016).

121. Galluzzi, L., López-Soto, A., Kumar, S. & Kroemer, G. Caspases Connect Cell-Death Signaling to Organismal Homeostasis. *Immunity* **44**, 221–231 (2016).

122. Brault, M. & Oberst, A. Controlled detonation: Evolution of necroptosis in pathogen defense. *Immunol. Cell Biol.* **95**, 131–136 (2017).

123. Kanehisa, M. & Goto, S. KEGG: kyoto encyclopedia of genes and genomes. *Nucleic Acids Res.* **28**, 27–30 (2000).

124. Elmore, S. Apoptosis: A Review of Programmed Cell Death. *Toxicol. Pathol.* **35**, 495–516 (2007).

125. Hibino, T. *et al.* The immune gene repertoire encoded in the purple sea urchin genome. *Dev. Biol.* **300**, 349–365 (2006).

126. Bateman, A. UniProt: A worldwide hub of protein knowledge. *Nucleic Acids Res.* **47**, D506–D515 (2019).

127. SRA Toolkit Development Team. http://ncbi.github.io/sra-tools/. SRA Toolkit.

128. Bushnell, B. BBMap. sourceforge.net/projects/bbmap/.

129. Kim, D., Langmead, B. & Salzberg, S. L. HISAT: a fast spliced aligner with low memory requirements Daehwan. **12**, 357–360 (2016).

130. Pertea, M., Kim, D., Pertea, G. M., Leek, J. T. & Salzberg, S. L. Transcript-level expression analysis of RNA- seq experiments with HISAT , StringTie and Transcript-level expression analysis of RNA-seq experiments with HISAT , StringTie and Ballgown. *Nat. Protoc.* **11**, 1650–1667 (2016).

131. Li, H. *et al.* The Sequence Alignment/Map format and SAMtools. *Bioinformatics*

25, 2078–2079 (2009).

132. Team., Rs. RStudio: Integrated Development for R. http://www.rstudio.com/. (2020).

133. Love, M. I., Huber, W. & Anders, S. Moderated estimation of fold change and dispersion for RNA-seq data with DESeq2. *Genome Biol.* **15**, 1–21 (2014).

134. Zhu, A., Ibrahim, J. G. & Love, M. I. Heavy-tailed prior distributions for sequence count data: removing the noise and preserving large differences. *Bioinformatics* **35**, 2084–2092 (2018).

135. Ritchie, M. E. *et al.* Limma powers differential expression analyses for RNA-sequencing and microarray studies. *Nucleic Acids Res.* **43**, e47 (2015).

136. Gu, Z., Eils, R. & Schlesner, M. Complex heatmaps reveal patterns and correlations in multidimensional genomic data. *Bioinformatics* **32**, 2847–2849 (2016).

137. Langfelder, P. & Horvath, S. WGCNA: An R package for weighted correlation network analysis. *BMC Bioinformatics* **9**, (2008).

Figures and Tables

Figure II-1. IAP expansion across mollusca shows complex species-specific expansion and cross-species conservation.
A) Phylogenetic tree of 10 studied mollusc species genomes produced by OrthoFinder with a heatmap depicting the number of IAP genes in each species. IAPs are most expanded in *B. glabrata*, least expanded in *Octopus* spp., and *C. virginica* IAPs are more expanded than *C. gigas*. B) Phylogenetic tree of the longest isoform IAP transcript sequences across 10 mollusc species produced with RAxML and aligned with MAFFT. Sequences are named with shortened RefSeq product names or gene locus identifiers for those annotated as "uncharacterized protein LOCX". Node shapes indicate bootstrap support (circle = 90-100, upward triangle = 70-89, downward triangle = 50-69) and numbers indicate clusters of interest referred to in text. IAP proteins cluster mainly by species-relationship but present species-specific clusters, with *B. glabrata* having largest (1). BIRC6 (2) and BIRC5 (3) proteins are clustered closely between studied mollusc species, suggesting potential cross-species conservation. C) Ideogram of *C. virginica* genome labelled with chromosome number. Numbers indicate track number (1 = Chromosome length, 2 = Gene density per 1 Mb, 3 = IAP gene location). * = Intronless IAP genes. IAPs are concentrated on chromosomes 6 and 7 in tandemly duplicated arrays and intronless IAPs may be the product of retroposition.

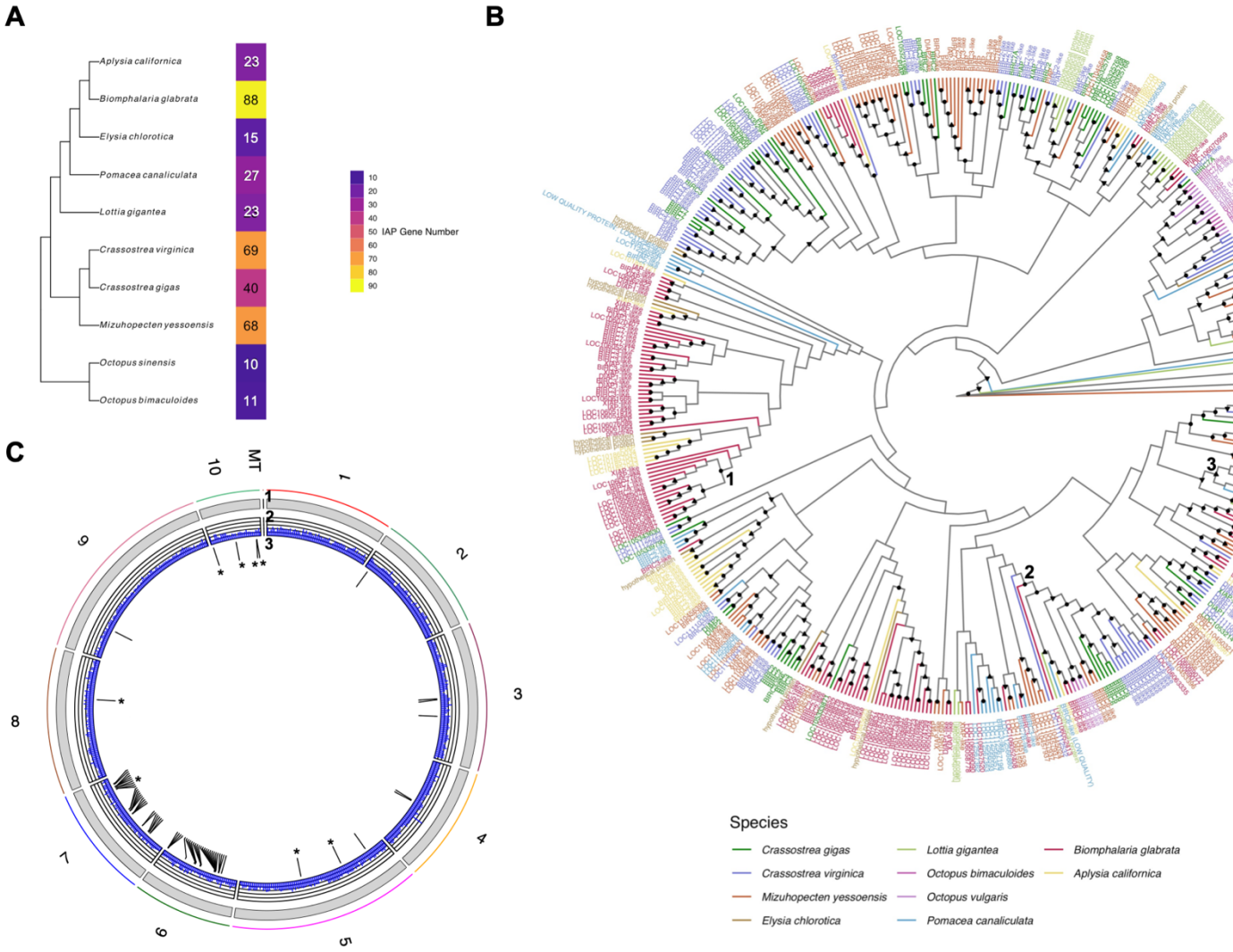
A
Aplysia californica
Biomphalaria glabrata
Elysia chlorotica
Pomacea canaliculata
Lottia gigantea
Crassostrea virginica
Crassostrea gigas
Mizuhopecten yessoensis
Octopus sinensis
Octopus bimaculoides
23
88
15
27
23
69
40
68
10
11
10
20
30
40
50
60
70
80
90
IAP Gene Number
B
1
2
3
Species
Crassostrea gigas
Crassostrea virginica
Mizuhopecten yessoensis
Elysia chlorotica
Lottia gigantea
Octopus bimaculoides
Octopus vulgaris
Pomacea canaliculata
Biomphalaria glabrata
Aplysia californica
C
MT
1
2
3
4
5
6
7
8
9
10

Figure II-2. Oyster and scallop IAP genes possess functional domains related to retroposition.
Functional domains identified in *C. gigas*, *C. virginica*, and *M. yessoensis* IAP gene translated open reading frames (from all IAPs, not only intronless genes) using Interproscan. Full gene sequence lengths are depicted shortened to only the first 1,500 bp, where functional domains were identified. Several IAP genes in *M. yessoensis* and *C. virginica*, and one in *C. gigas*, possess functional domains necessary for active retroposition. This evidence, coupled with presence of intronless IAP genes, suggests retroposition as a potential mechanism of mollusc IAP expansion.

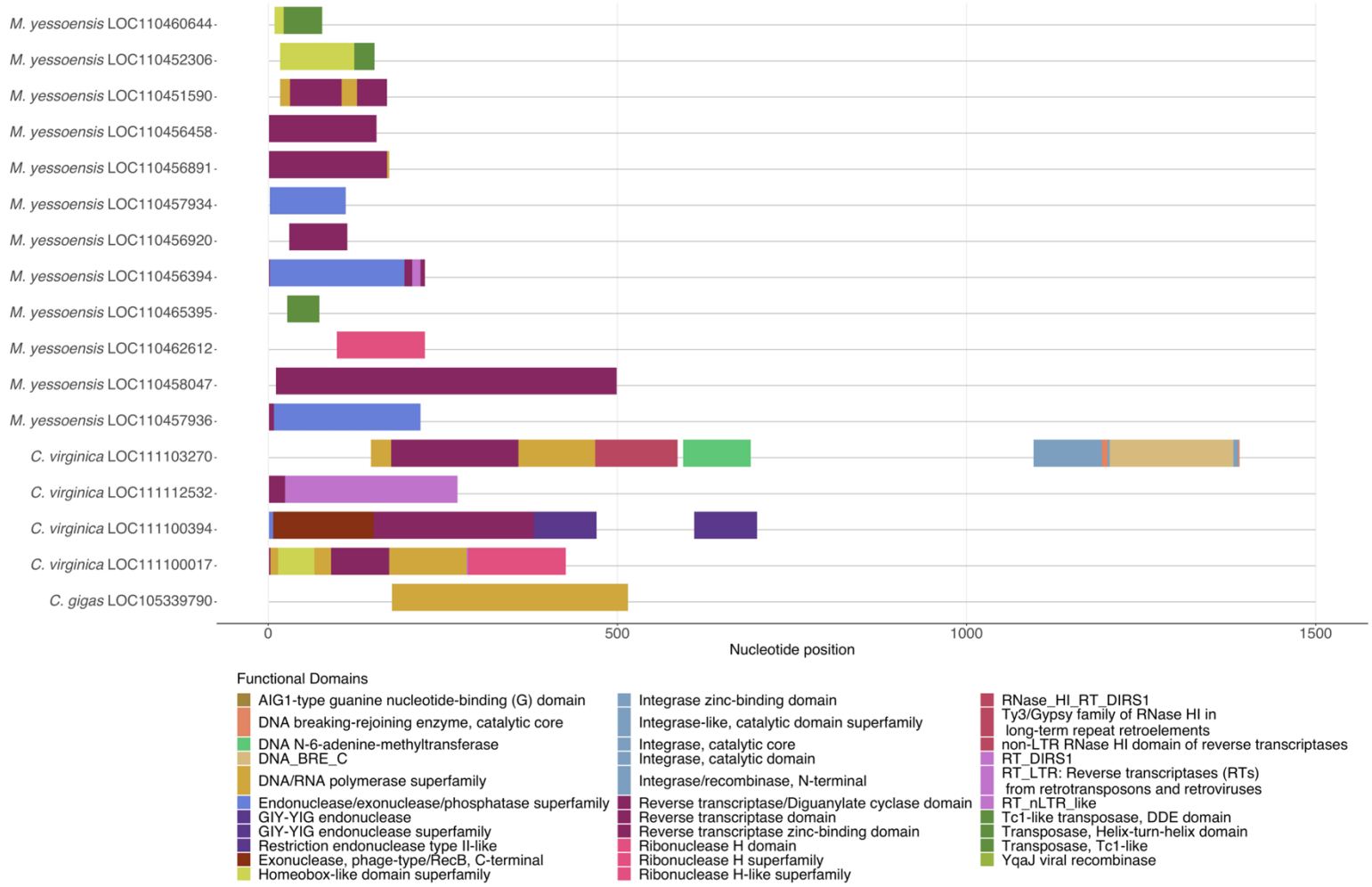
M. yessoensis LOC110460644
M. yessoensis LOC110452306
M. yessoensis LOC110451590
M. yessoensis LOC110456458
M. yessoensis LOC110456891
M. yessoensis LOC110457934
M. yessoensis LOC110456920
M. yessoensis LOC110456394
M. yessoensis LOC110465395
M. yessoensis LOC110462612
M. yessoensis LOC110458047
M. yessoensis LOC110457936
C. virginica LOC111103270
C. virginica LOC111112532
C. virginica LOC111100394
C. virginica LOC111100017
C. gigas LOC105339790
0
500
1000
1500
Nucleotide position
Functional Domains
AIG1-type guanine nucleotide-binding (G) domain
DNA breaking-rejoining enzyme, catalytic core
DNA N-6-adenine-methyltransferase
DNA_BRE_C
DNA/RNA polymerase superfamily
Endonuclease/exonuclease/phosphatase superfamily
GIY-YIG endonuclease
GIY-YIG endonuclease superfamily
Restriction endonuclease type II-like
Exonuclease, phage-type/RecB, C-terminal
Homeobox-like domain superfamily
Integrase zinc-binding domain
Integrase-like, catalytic domain superfamily
Integrase, catalytic core
Integrase, catalytic domain
Integrase/recombinase, N-terminal
Reverse transcriptase/Diguanylate cyclase domain
Reverse transcriptase domain
Reverse transcriptase zinc-binding domain
Ribonuclease H domain
Ribonuclease H superfamily
Ribonuclease H-like superfamily
RNase_HI_RT_DIRS1
Ty3/Gypsy family of RNase HI in long-term repeat retroelements
non-LTR RNase HI domain of reverse transcriptases
RT_DIRS1
RT_LTR: Reverse transcriptases (RTs) from retrotransposons and retroviruses
RT_nLTR_like
Tc1-like transposase, DDE domain
Transposase, Helix-turn-helix domain
Transposase, Tc1-like
YqaJ viral recombinase

Figure II-3. *C. virginica* and *C. gigas* IAPs contain one to three BIR domains with conserved and novel types.
A) Representative BIR amino acid (aa) sequences aligned with MAFFT. Boxes highlight key residues. "Total Genes" indicate the number of oyster IAP genes with each identified BIR domain type, with the most represented highlighted in red. * = Conserved aa positions across all *C. gigas* and *C. virginica* BIR sequences. Zn^{2+} = positions in model organisms involved in Zinc atom stabilization. V = variable aa position used in BIR domain classification. Type II BIRs were the most abundant in *C. gigas* and *C. virginica* and three novel BIR domains, Type X, Type Y, and Type NZBIR were identified. B) Protein secondary structure analysis by RaptorX. Secondary structure predictions were made at the three class (H = alpha helix, E = beta sheet, C = coil) and eight class levels (H = alpha helix, G = five-turn helix, I = extended strand in beta ladder, E = isolated beta bridge, T = hydrogen bonded turn, S = bend, L = loop) for representative BIR type examples. Characteristic regions used in classification are outlined in black. Type X and Type BIRs may have shortened alpha helix structures while Type NZBIR does not have altered secondary structure but loss of Cysteine may prevent Zinc coordination. C) The number of genes in *C. gigas* and *C. virginica* with one, two, or three BIR repeats. [1]Only genes with BIR domains confirmed by CDD were analyzed. One and two BIR repeats were most common studied oysters. D) Phylogenetic tree of IAP gene sequences colored by the number of BIR domains identified by CDD. Intronless genes or genes with novel types are labeled (TY = Type Y, TX = Type X, NZBIR = Non-Zinc Binding, * = Intronless). IAP gene sequence clustering suggests a pattern of domain loss over time and independent gain of novel BIRs.

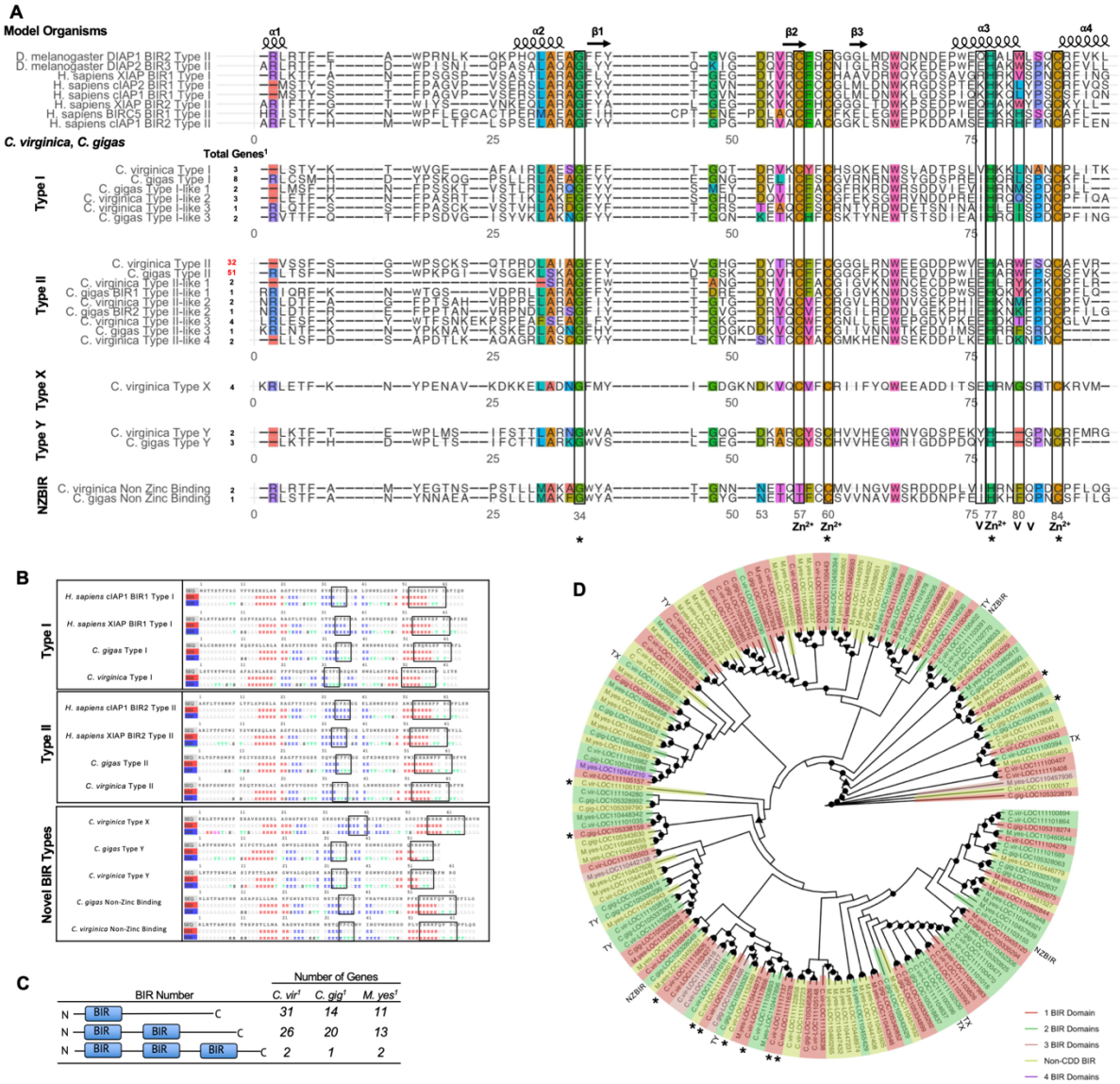
A
Model Organisms
α1
α2
β1
β2
β3
α3
α4
D. melanogaster DIAP1 BIR2 Type II
D. melanogaster DIAP2 BIR3 Type II
H. sapiens XIAP BIR1 Type I
H. sapiens cIAP2 BIR1 Type I
H. sapiens cIAP1 BIR1 Type I
H. sapiens XIAP BIR2 Type II
H. sapiens BIRC5 BIR1 Type II
H. sapiens cIAP1 BIR2 Type II
C. virginica, C. gigas
Total Genes¹
Type I
C. virginica Type I
C. gigas Type I
C. gigas Type I-like 1
C. virginica Type I-like 2
C. virginica Type I-like 3
C. gigas Type I-like 3
Type II
C. virginica Type II
C. gigas Type II
C. virginica Type II-like 1
C. gigas BIR1 Type II-like 1
C. virginica Type II-like 2
C. gigas BIR2 Type II-like 2
C. virginica Type II-like 3
C. gigas Type II-like 3
C. virginica Type II-like 4
Type X
C. virginica Type X
Type Y
C. virginica Type Y
C. gigas Type Y
NZBIR
C. virginica Non Zinc Binding
C. gigas Non Zinc Binding
Zn²⁺
B
Type I
H. sapiens cIAP1 BIR1 Type I
H. sapiens XIAP BIR1 Type I
C. gigas Type I
C. virginica Type I
Type II
H. sapiens cIAP1 BIR2 Type II
H. sapiens XIAP BIR2 Type II
C. gigas Type II
C. virginica Type II
Novel BIR Types
C. virginica Type X
C. gigas Type Y
C. virginica Type Y
C. gigas Non-Zinc Binding
C. virginica Non-Zinc Binding
C
BIR Number
Number of Genes
C. vir¹
C. gig¹
M. yes¹
N
BIR
C
31 14 11
26 20 13
2 1 2
D
TY
NZBIR
TX
1 BIR Domain
2 BIR Domains
3 BIR Domains
Non-CDD BIR
4 BIR Domains

Figure II-4. Oyster IAPs possess model organism and multiple novel domain architectures.
A) Phylogenetic tree of IAP proteins labelled by their gene ID in *C. gigas* (green), *C. virginica* (blue), and *M. yessoensis* (orange). A square node tip indicates collapsed *M. yessoensis* proteins for improved visualization. Node shapes indicate bootstrap support (circle = 90-100, upward triangle = 70-89, downward triangle = 50-69). When multiple transcripts from the same gene cluster together, all but one are labelled with a "---". IAPs grouped into 21 well supported clusters. B) Functional domain architecture of each transcript isoform plotted by amino acid position with domains labeled by color. Asterisk indicates transcripts where IAP repeats were only identified by Interproscan and not CDD. Shaded boxes surround each well supported protein cluster. C). Domain architecture type (TI = Type I BIR, TII = Type II BIR, UBA = UBA domain, RING = RING domain, DD = Death domain, BIR* = BIR domain identified by Interproscan and not CDD). Clusters where architecture is conserved between all proteins are labelled in bold. Clusters were classified into 14 domain architecture types, 4 of which are not found in model organisms. D) Table of domain architecture types in *D. melanogaster* and mammals, and similar domain architectures and clusters identified in oysters (top panel) and novel domain architectures and clusters found in oysters not identified in model organisms (bottom panel). Novel IAP domain architectures are here named BIRC9, BIRC10, BIRC11, and BIRC12.

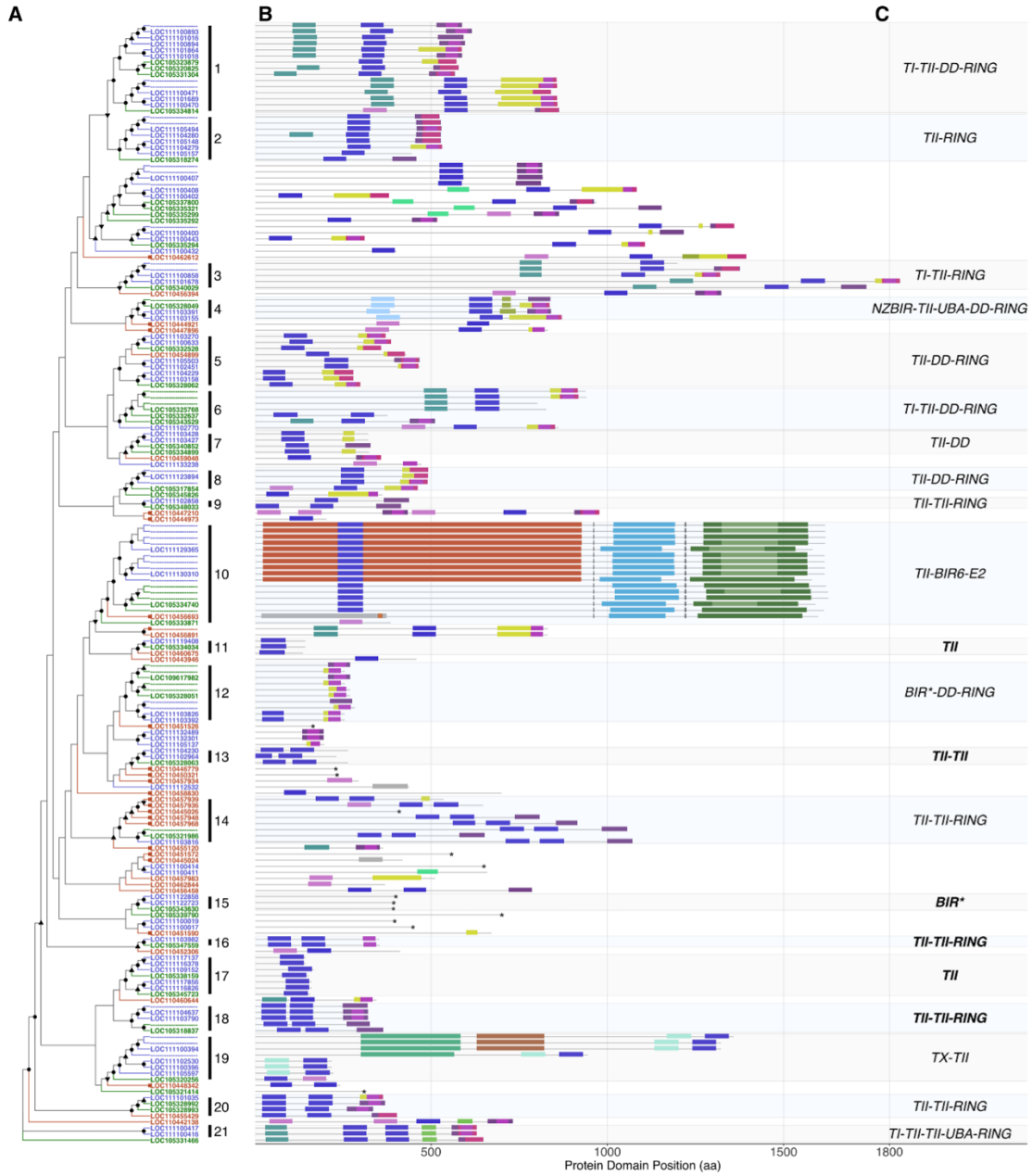

D

Organism	Protein Name (Alias)	Domain Architecture	Similar Domain Architecture	Clusters	*C. vir.* IAP Genes	*C. gig.* IAP Genes
D. melanogaster	DIAP1	BIR BIR RING	TI-TII-RING	3	2	1
	DIAP2	BIR BIR BIR UBA RING	TI-TII-TII-UBA-RING	21	2	1
Mammals	BIRC1 (NAIP)	BIR BIR BIR NACHT // LRR	none	none	0	0
	BIRC2 (cIAP1)	BIR BIR BIR UBA CARD RING	TI-TII-DD-RING, NZBIR-TII-UBA-DD-RING	1, 4, 6	11	7
	BIRC3 (cIAP2)	BIR BIR BIR UBA CARD RING	TI-TII-DD-RING, NZBIR-TII-UBA-DD-RING	1, 4, 6	11	7
	BIRC4 (XIAP)	BIR BIR BIR UBA RING	TI-TII-TII-UBA-RING	21	2	1
	BIRC5 (Survivin)	BIR	TII, BIR*	11, 15, 17	8	4
	BIRC6 (BRUCE)	BIR // UBC	TII-BIR6-E2	10	2	1
	BIRC7 (ML-IAP)	BIR RING	TII-RING	2	5	1
	BIRC8 (ILP2)	BIR UBA RING	none	none	0	0
Crassostrea spp.	*BIRC9*	BIR BIR	TX-TII, TII-TII	13, 19	6	2
	BIRC10	BIR DD	TII-DD	7	2	2
	BIRC11	BIR DD RING	TII-DD-RING, BIR*-DD-RING	5, 8, 12	8	5
	BIRC12	BIR BIR RING	TII-TII-RING	9, 14, 16, 18, 20	6	6

Figure II-5. *C. gigas* and *C. virginica* differential gene expression reveal complex patterns of IAP domain architecture and gene usage across immune challenges.
A) Phylogenetic tree of IAP amino acid sequences labelled by their gene name in *C. gigas* (green), *C. virginica* (blue), and *M. yessoensis* (orange). A square node tip indicates collapsed *M. yessoensis* proteins for the purpose of plotting. Node shapes indicate bootstrap support (circle = 90-100, upward triangle = 70-89, downward triangle = 50-69). Vertical bars indicate well-supported protein clusters (Figure 4). Transcripts with the same amino acid sequence were collapsed by RAxML when producing the tree. Multiple Proteins from the same gene are named once on the lowest node and then represented by dashes ("----"). B,C) Heatmap of log2 fold change expression of significantly differentially expressed *C. virginica* (B) and *C. gigas* (C) IAPs in each experiment plotted for each transcript parallel to its corresponding position on the phylogenetic tree. Shaded boxes surround each well supported protein cluster. Most of the identified IAP diversity was significantly differentially expressed in some experiment in each species, though the number of differentially expressed IAP transcripts ranged from 5 (CVBAC-B, CGBAC-A) to 68 (CGOSHV1-A Susceptible). *C. virginica* expressed more unique genes and transcripts in each experiment than *C. gigas* which expressed more overlapping sets. All domain architectures, including novel architectures, were significantly differentially expressed in at least one oyster and experiments expressed unique assemblages of multiple IAP domain architectures.

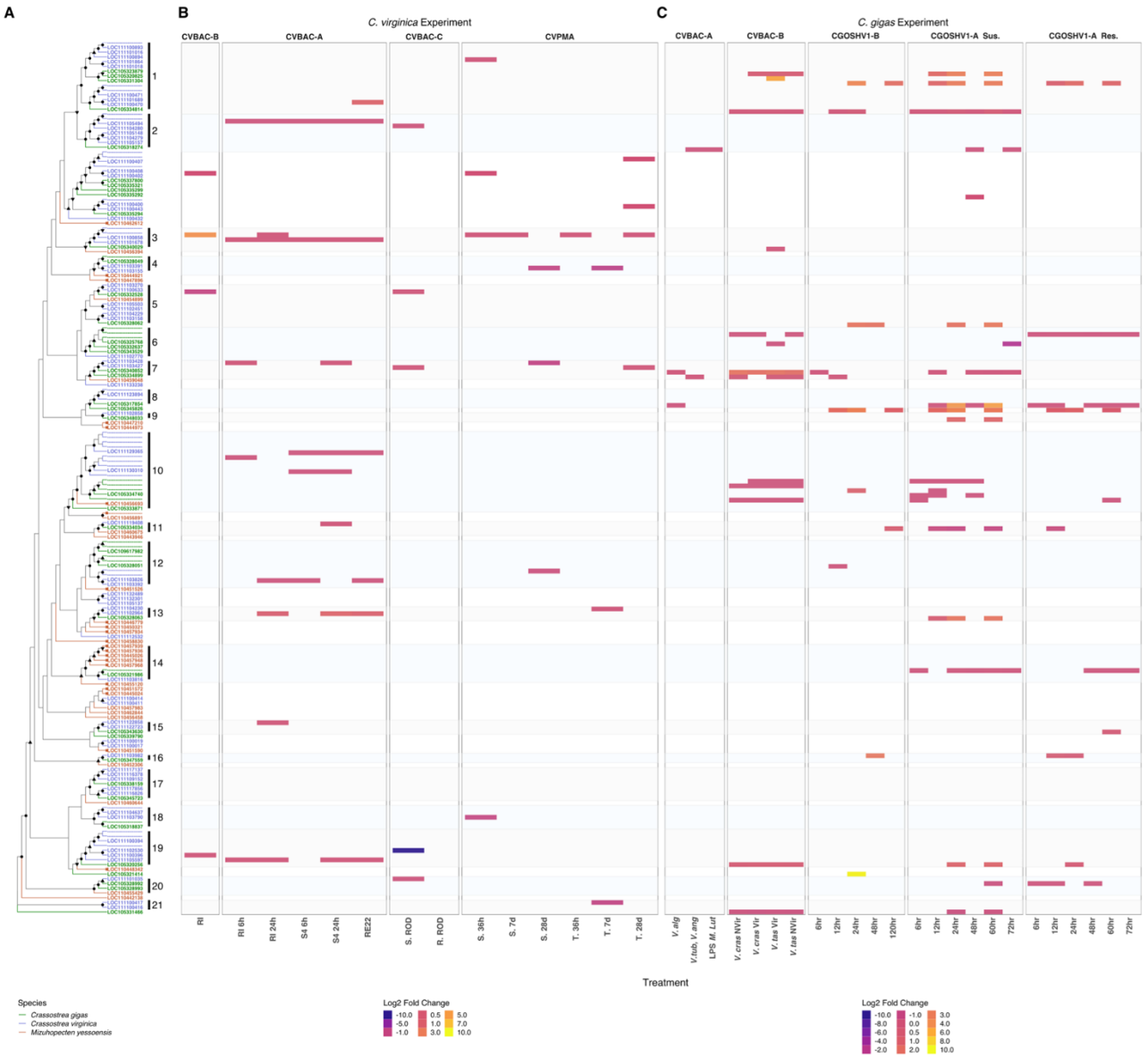
A
B
C
C. virginica Experiment
C. gigas Experiment
CVBAC-B
CVBAC-A
CVBAC-C
CVPMA
CVBAC-A
CVBAC-B
CGOSHV1-B
CGOSHV1-A Sus.
CGOSHV1-A Res.
RI
RI 6h
RI 24h
S4 6h
S4 24h
RE22
S. ROD
R. ROD
S. 36h
S. 7d
S. 28d
T. 36h
T. 7d
T. 28d
V. alg
V.tub, V. ang
LPS M. Lut
V. cras NVir
V. cras Vir
V. tas Vir
V. tas NVir
6hr
12hr
24hr
48hr
120hr
6hr
12hr
24hr
48hr
60hr
72hr
6hr
12hr
24hr
48hr
60hr
72hr
Treatment
Species
Crassostrea gigas
Crassostrea virginica
Mizuhopecten yessoensis
Log2 Fold Change
-10.0
-5.0
-1.0
0.5
1.0
3.0
5.0
7.0
10.0
Log2 Fold Change
-10.0
-8.0
-6.0
-4.0
-2.0
-1.0
0.0
0.5
1.0
2.0
3.0
4.0
6.0
8.0
10.0

Figure II-6. *C. virginica* and *C. gigas* annotated genomes possess major intrinsic and extrinsic apoptosis pathway proteins.
Annotated apoptosis-related proteins identified in oyster reference annotations. Proteins present in the *C. gigas* annotated genome and not in the *C. virginica* annotated genome are colored in gray and outlined with a bold black border. Proteins only in *C. virginica* are in grey. Potential multi-protein complexes are boxed with a dashed black line. Multiple (about 25%) model organism apoptosis and RCD proteins identified in the literature were not found in oyster annotated reference genomes, either due to errors in annotation or true absence in oysters. Molecules from the novel cell death pathways necroptosis, parthanatos, and lysosome dependent cell death were also identified.

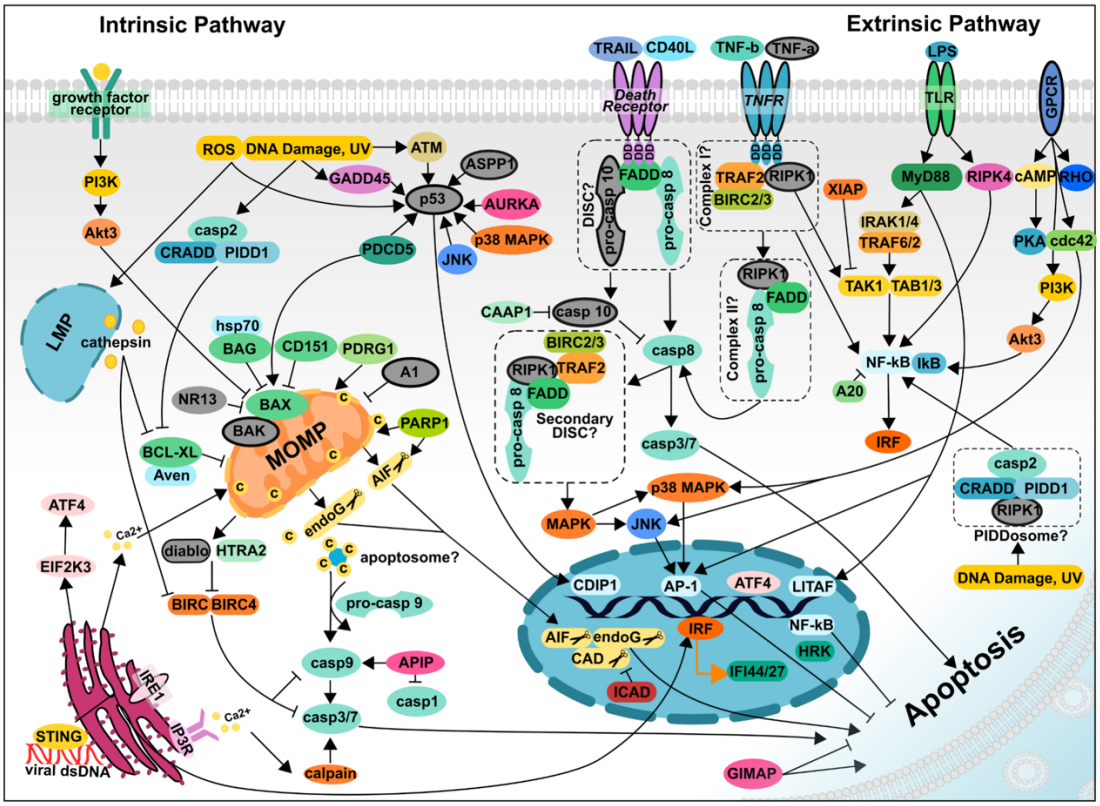

Figure II-7. The apoptosis pathway was more differentially expressed in *C. gigas* than *C. virginica* and expression clustered by susceptibility or resistance to viral challenge. Heatmap of significantly differentially expressed apoptosis pathway transcripts with LFC > 1 in *C. gigas* experimental groups. Plot colored by LFC and generated by ComplexHeatmap. Experimental treatment groups are along the X-axis and grouped by similarity of apoptosis transcript LFC. Apoptosis transcript IDs followed by their product name assigned by RefSeq are along the y-axis. Total differentially expressed apoptosis-related transcripts were almost quadrupled in *C. gigas* compared to *C. virginica*, potentially due to challenges studied. CGOSHV1-A susceptible and CGOSHV1-B experiments showed the most unique apoptosis expression and strong extrinsic apoptosis pathway upregulation.

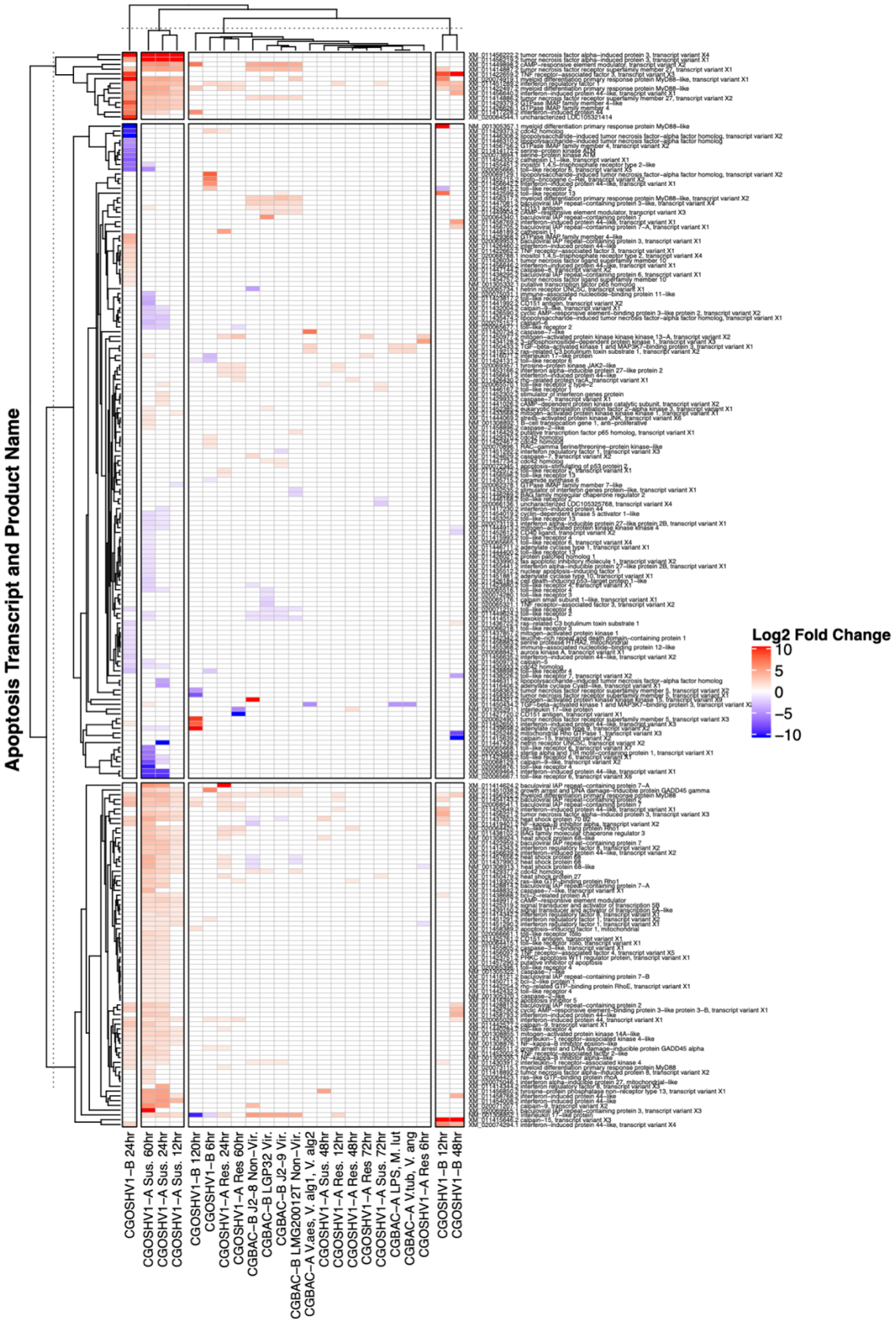
Apoptosis Transcript and Product Name
Log2 Fold Change
10
5
0
−5
−10
CGOSHV1−B 24hr
CGOSHV1−A Sus. 60hr
CGOSHV1−A Sus. 24hr
CGOSHV1−A Sus. 12hr
CGOSHV1−B 12hr
CGOSHV1−B 6hr
CGOSHV1−A Res. 24hr
CGOSHV1−A Res 60hr
CGBAC−B J2−8 Non−Vir.
CGBAC−B LGP32 Vir.
CGBAC−B J2−9 Vir.
CGBAC−B LMG20012T Non−Vir.
CGBAC−A Vaes, V. alg1, V. alg2
CGOSHV1−A Sus. 48hr
CGOSHV1−A Res. 12hr
CGOSHV1−A Res. 48hr
CGOSHV1−A Res 72hr
CGOSHV1−A Sus. 72hr
CGBAC−A LPS, M. lut
CGBAC−A V.tub, V. ang
CGOSHV1−A Res 6hr
CGOSHV1−B 12hr
CGOSHV1−B 48hr

Figure II-8. Apoptosis pathway differential expression in *C. virginica* clustered by susceptibility or resistance to bacterial or parasitic challenge.
Heatmap of significantly differentially expressed apoptosis pathway transcripts with LFC > 1 in *C. virginica* experimental groups. Plot colored by LFC and generated by ComplexHeatmap. Experimental treatment groups are along the X-axis and grouped by similarity of apoptosis transcript LFC. Apoptosis transcript IDs followed by their product name assigned by RefSeq are along the y-axis. CVBAC-C displayed the most unique apoptosis pathway expression comprised mainly of extrinsic pathway transcripts. CVPMA 28d susceptible oysters also displayed strong downregulation of transcripts involved in apoptosis execution, the TLR pathway, DNA damage response, and mitochondrial dysfunction related proteins.

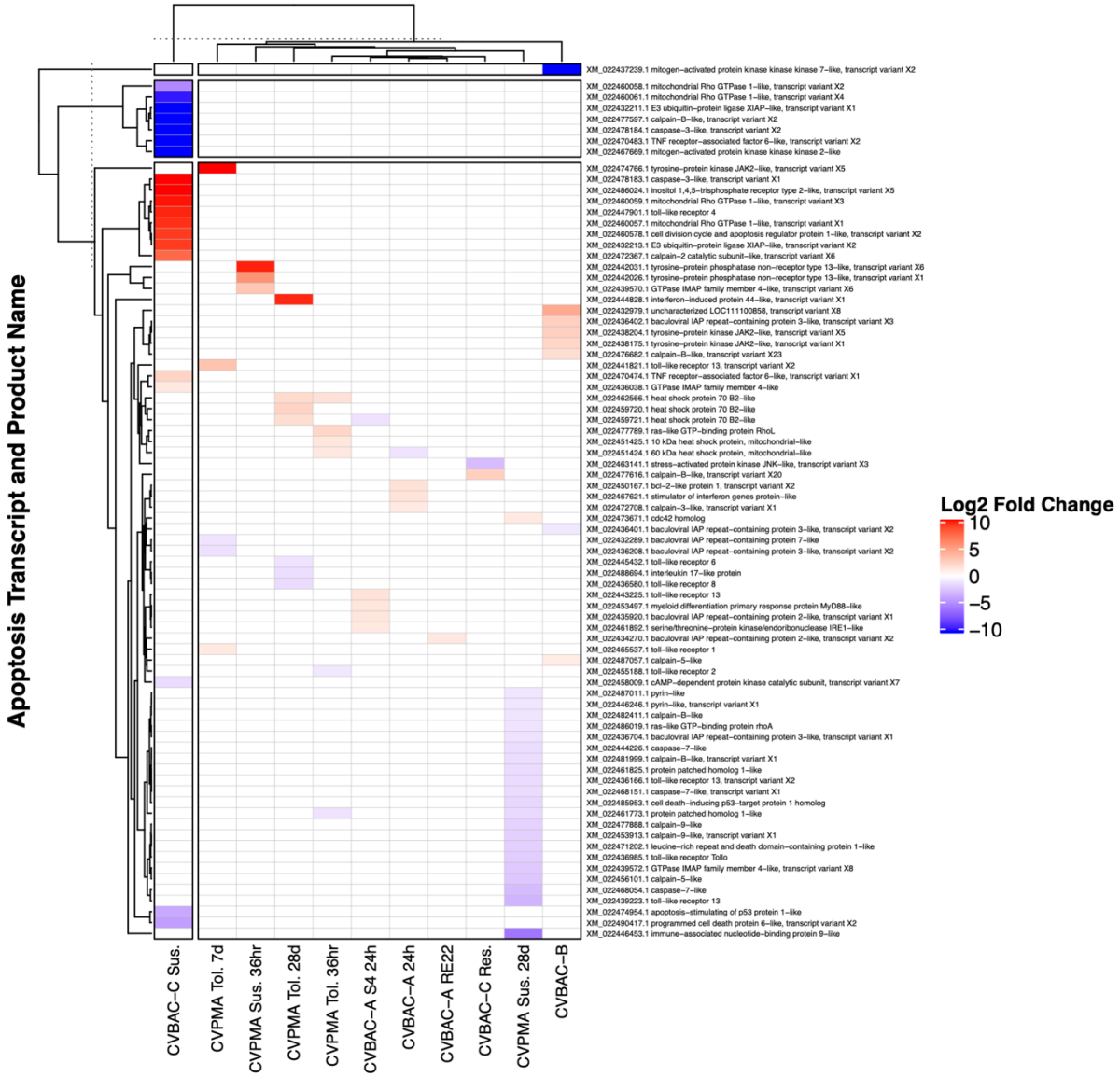

Figure II-9. Expression of IAPs with multiple domain architectures was directly correlated with apoptosis-related transcript expression and not specific to challenge type in *C. gigas* and *C. virginica*.

A) Table presenting the number of IAP genes, unique apoptosis transcripts, and domain structures directly correlated in each WGCNA experiment, with darker shading representing higher number. Multiple domain architectures of different type were directly correlated with apoptosis-related transcripts and were not unique to particular challenge types. This indicates IAPs may be co-regulated with or work with the apoptosis pathway and expression of unique assemblages of IAPs with different potential functions may be important for apoptosis pathway regulation. B) Apoptosis-related transcripts directly correlated with BIRC2/3-like, BIRC5-like, BIRC9, BIRC11 IAPs in the CGOSHV1-B resistant WGCNA significant modules. C) *C. gigas* transcript XM_020068541.1 (LOC105331304) potentially homologous with mammalian BIRC2/3 shown in a pathway diagram with directly correlated extrinsic apoptosis transcripts from CGOSHV1-B and CGOSHV1-A Resistant experiment WGCNA modules. Purple transcripts were directly correlated in both viral experiments, while those in orange were only directly correlated with this BIRC2/3-like transcript in the CGOSHV1-A Resistant experiment. BIRCs are outlined in black and molecules outlined in gray were not identified in modules but are important pathway members in model organisms.

A

Experiment	Unique** IAP Genes	Unique** Apoptosis Transcripts	Total IAP Domain Architectures	IAP Domain Architecture Types
CVBAC-A RI/S4	5	52	4	DIAP1, BIRC10, BIRC12, BIRC11
CVPMA Sus.	1	1	1	BIRC12
CGBAC-A LPS, M. lut	1	14	1	BIRC11
CGBAC-B Non-virulent Vibrio spp.	10	160	6	BIRC2/3-like, BIRC4-like, BIRC7, BIRC9, BIRC10, BIRC11
CGOSHV1-B	6	50	5	BIRC2/3-like, BIRC5-like, BIRC6-like, BIRC10, BIRC11
CGOSHV1-A Res.	7	121	4	BIRC2/3-like, BIRC5-like, BIRC9, BIRC11
CGOSHV1-A Sus.	1	69	1	BIRC2/3-like

** = *Unique = only counted once if identified across several experiment modules.*

B

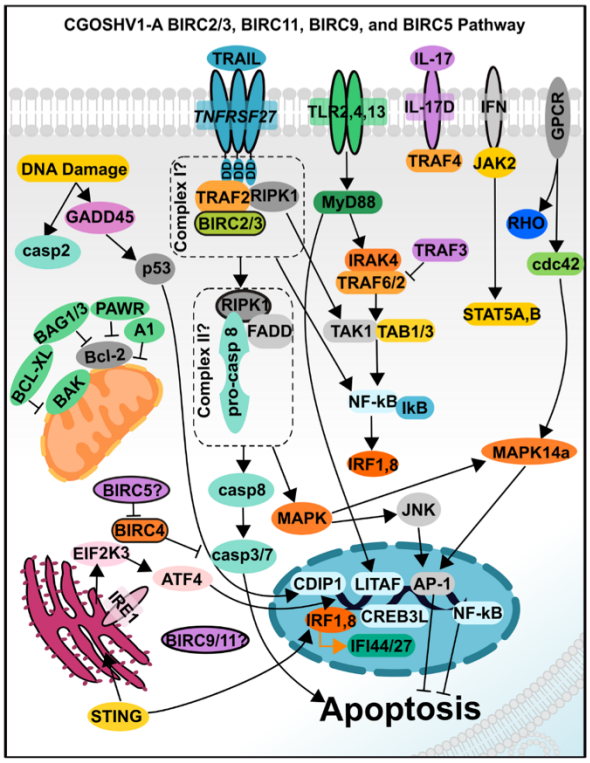

C

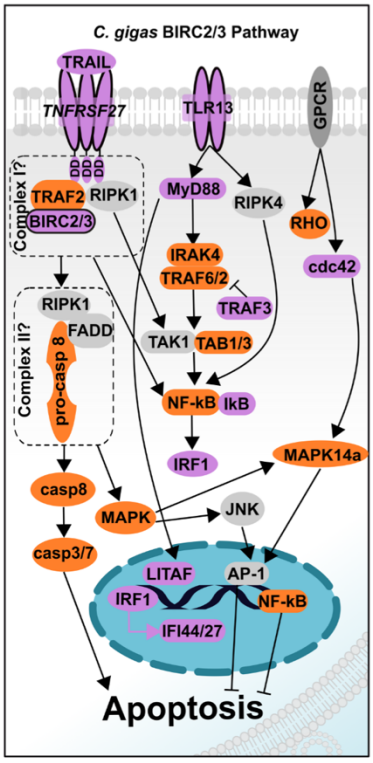

Table II. Summary of immune challenge transcriptome experiments analyzed.

Experiment ID	Host Life Stage	Challenge Method	Host Genetics	Challenge Type	Challenge Species	Sample Collection Post-Challenge	Citation
CVBAC-A Probiotic/Vibrio RE22	larvae	hatchery(probiotic)/lab(RE22)	not evaluated	probiotic bacteria	*Phaeobacter inhibens* S4 and *Bacillus pumilus* RI06-95, or pathogen *Vibrio coralliilyticus* RE22	6 h (RE22, RI, S4) or 24 h (S4, RI)	Modak, T. H. & Gomez-Chiarri, M. Contrasting immunomodulatory effects of probiotic and pathogenic bacteria on eastern oyster, crassostrea virginica, larvae. Vaccines 8, 1–23 (2020).
CVBAC-B	larvae	hatchery	not evaluated	probiotic bacteria	*Phaeobacter inhibens* S4 and *Bacillus pumilus* RI06-95	5 d, 12 d, 16 d	Modak, T. H. & Gomez-Chiarri, M. Contrasting immunomodulatory effects of probiotic and pathogenic bacteria on eastern oyster, crassostrea virginica, larvae. Vaccines 8, 1–23 (2020).
CVBAC-C	juvenile	lab	susceptible and resistant selectively bred lines	pathogenic bacteria	*Aliiroseovarius crassostreae* (Roseovarius, or Juvenile Oyster Disease)	1 d,5 d,15 d, 30 d	Mcdowell, I. C. et al. Transcriptome of American Oysters , Crassostrea virginica , in Response to Bacterial Challenge : Insights into Potential Mechanisms of Disease Resistance. 9, (2014).
CVPMA	adult	lab	susceptible and tolerant selectively bred lines	intracellular parasite	*Perkinsus marinus*	36 h, 7 d, 28 d	Proestou, D. A. & Sullivan, M. E. Variation in global transcriptomic response to Perkinsus marinus infection among eastern oyster families highlights potential mechanisms of disease resistance. Fish Shellfish

							Immunol. 96, 141–151 (2020).
CGBAC-A	adult	lab	not evaluated	pathogenic bacteria	*V. anguillarum*, *V. tubiashii*, *V. aestuarianus*, V. alginolyticus-1, V. alginolyticus-2, Micrococcus luteus), LPS (Sigma-Aldrich, USA) or sterile PBS (control sample)	12 h	Zhang, L. et al. Massive expansion and functional divergence of innate immune genes in a protostome. Sci. Rep. 5, 8693 (2015).
CGBAC-B	spat	lab	not evaluated	pathogenic/ non-pathogenic bacteria	(intracellular V. tasmaniensis (LGP32) virulent V. crassostreae (J2-9), and nonvirulent intracellular V. tasmaniensis (LMG20012T), or non-virulent V. crassostreae (J2-8) or sterile seawater)	8 h	Rubio, T. et al. Species-specific mechanisms of cytotoxicity toward immune cells determine the successful outcome of Vibrio infections. 116, (2019).
CGOSHV1-A Res., CGOSHV1-A Sus.	juvenile	natural	two biparental families with highly contrasted resistance phenotypes, susceptible and resistant	viral	OsHV-1	0 h, 6 h, 12 h, 24 h, 48 h, 60 h, 72 h	de Lorgeril, J. et al. Immune-suppression by OsHV-1 viral infection causes fatal bacteraemia in Pacific oysters. Nat. Commun. 9, (2018).

CGOSHV1-B	juvenile	lab	susceptible	viral	OsHV-1	0 h, 6 h, 12 h, 24 h, 48 h, 120 h	He, Y. et al. Transcriptome analysis reveals strong and complex antiviral response in a mollusc. Fish Shellfish Immunol. 46, 131–144 (2015).

Supplementary Material

Supplementary Figure 1. Phylogenetic tree and multiple sequence alignment of BIR-repeat domains across *C. virginica*, *C. gigas*, and *M. yessoensis* reveal conserved and novel BIR domain types. A) BIR protein sequence domain clustering by RAxML following by MAFFT multiple sequence alignment. Nodes are colored by their BIR classification type. Sequences are labeled with their protein NCBI Accession, the sequential order of that BIR in the parent protein (i.e. BIR2 = second BIR domain from the N-terminus) and the parent gene locus. Sequences from model organisms are also labeled for their known BIR types (T1, T2). Node shapes indicate bootstrap support (circle = 90-100, upward triangle = 70-89, downward triangle = 50-69). B) Genus and species names for mollusc and model organism species aligned; *C. virginica*, *C. gigas*, *M. yessoensis*, sequences from *D. melanogaster*, *Homo sapiens*, *Mus musculus, Danio rerio* were used as outgroup sequences; C) Multiple sequence alignment of BIR domain sequences in the order of the RAxML tree, visualized in R using ggmsa.

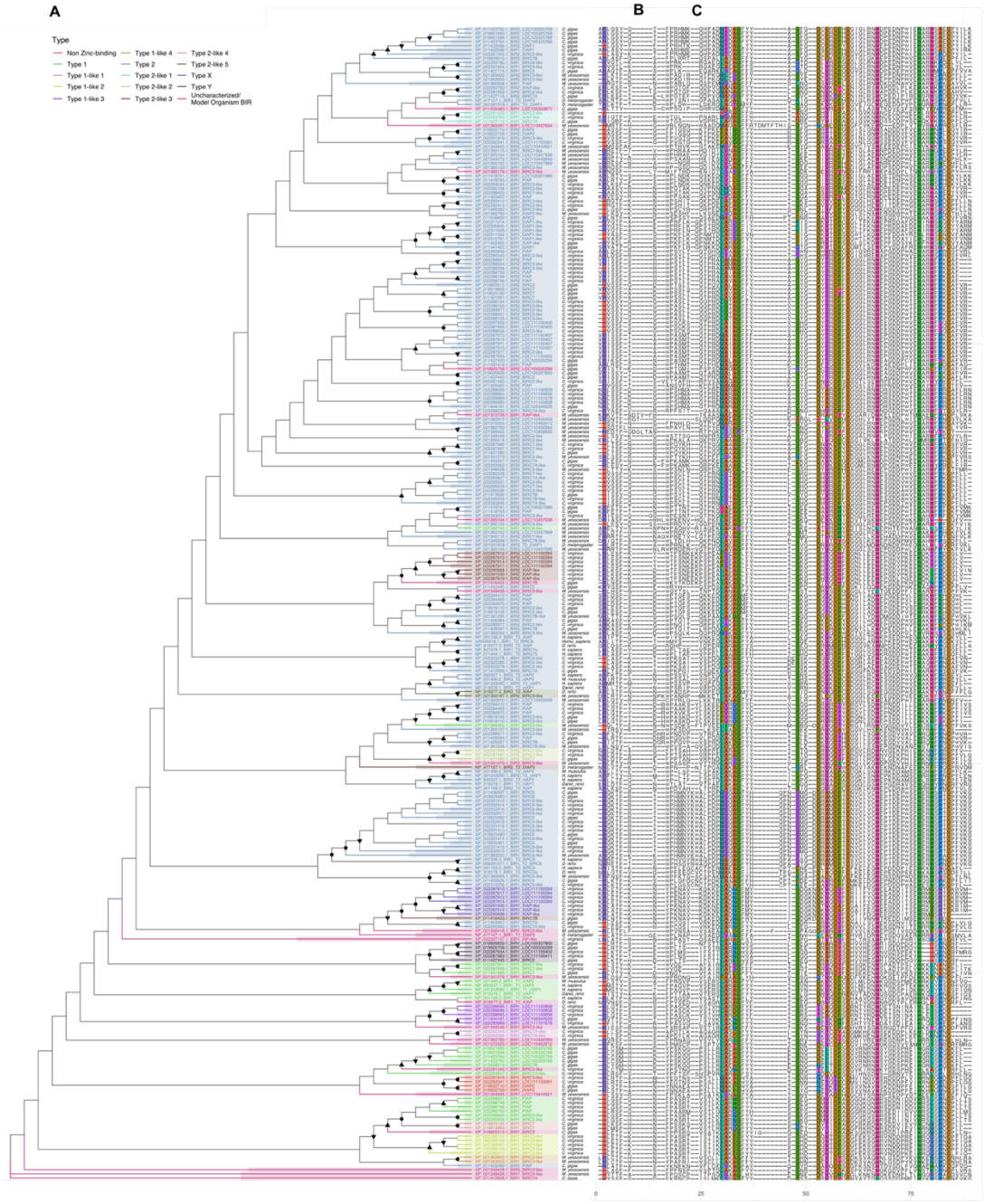
A
B
C
Type
Non Zinc-binding
Type 1
Type 1-like 1
Type 1-like 2
Type 1-like 3
Type 1-like 4
Type 2
Type 2-like 1
Type 2-like 2
Type 2-like 3
Type 2-like 4
Type 2-like 5
Type X
Type Y
Uncharacterized/
Model Organism BIR
0
25
50
75

Supplementary Figure 2: More IAP genes and domain architectures are constitutively expressed in *C. virginica* than *C. gigas*. A) Phylogenetic tree of IAP amino acid sequences labelled by their gene name in *C. gigas* (green), *C. virginica* (blue), and *M. yessoensis* (orange). A square node tip indicates collapsed *M. yessoensis* proteins for the purpose of plotting. Node shapes indicate bootstrap support (circle = 90-100, upward triangle = 70-89, downward triangle = 50-69). Vertical bars indicate well-supported protein clusters previously designated in Figure 4. Transcripts with the same amino acid sequence were collapsed by RAxML when producing the tree. Multiple Proteins from the same gene are named once on the lowest node and then represented by dashes ("----"). B) Heatmap of rlog or vst transformed read counts, averaged across individual treatment groups, of constitutively expressed *C. virginica* IAPs in each experiment plotted for each transcript parallel to its corresponding position on the phylogenetic tree. Shaded boxes surround each well supported protein cluster. C) Heatmap of rlog or vst transformed read counts, averaged across individual treatment groups, of constitutively expressed *C. gigas* IAPs in each experiment plotted for each transcript parallel to its corresponding position on the phylogenetic tree. Shaded boxes surround each well supported protein cluster.


A
B
C
C. virginica Experiment
C. gigas Experiment
CVBAC-B
CVBAC-A
CVBAC-C
CVPMA
CVBAC-A
CVBAC-B
CGOSHV1-B
CGOSHV1-A Sus.
CGOSHV1-A Res.
Con
RI
RI 6h
RI 24h
S4 6h
S4 24h
RE22
S. Con
S. ROD
R. Con
R. ROD
S. Con. 36h
S. Con. 7d
S. Con 28d
S. Pm 36h
S. Pm 7d
S. Pm 28d
T. Con 36h
T. Con 7d
T. Con 28d
T. Pm 36h
T. Pm 7d
T. Pm 28d
V. alg
V.tub, V. ang
LPS, M. Lut
V. cras NVir
V. cras Vir
V. tas Vir
V. tas NVir
0h Con
6h Con
6h OsHv-1
12h Con
12h OsHv-1
24h Con
24h OsHv-1
48h Con
48h OsHv-1
120h Con
120h OsHv-1
6h OsHv-1
12h OsHv-1
24h OsHv-1
48h OsHv-1
60h OsHv-1
72h OsHv-1
Treatment
Species
Crassostrea gigas
Crassostrea virginica
Mizuhopecten yessoensis
Average Read Count
Average Read Count

Supplementary Figure 3: Direct correlations between IAP transcripts and apoptosis-related transcripts across significant WGCNA modules in *C. gigas* and *C. virginica* show little clustering by IAP domain architecture type. The y-axis shows an IAP transcript, named for its domain architecture, tightly correlated with apoptosis transcripts (x-axis). Apoptosis transcripts are colored by presence (red) and absence (blue).

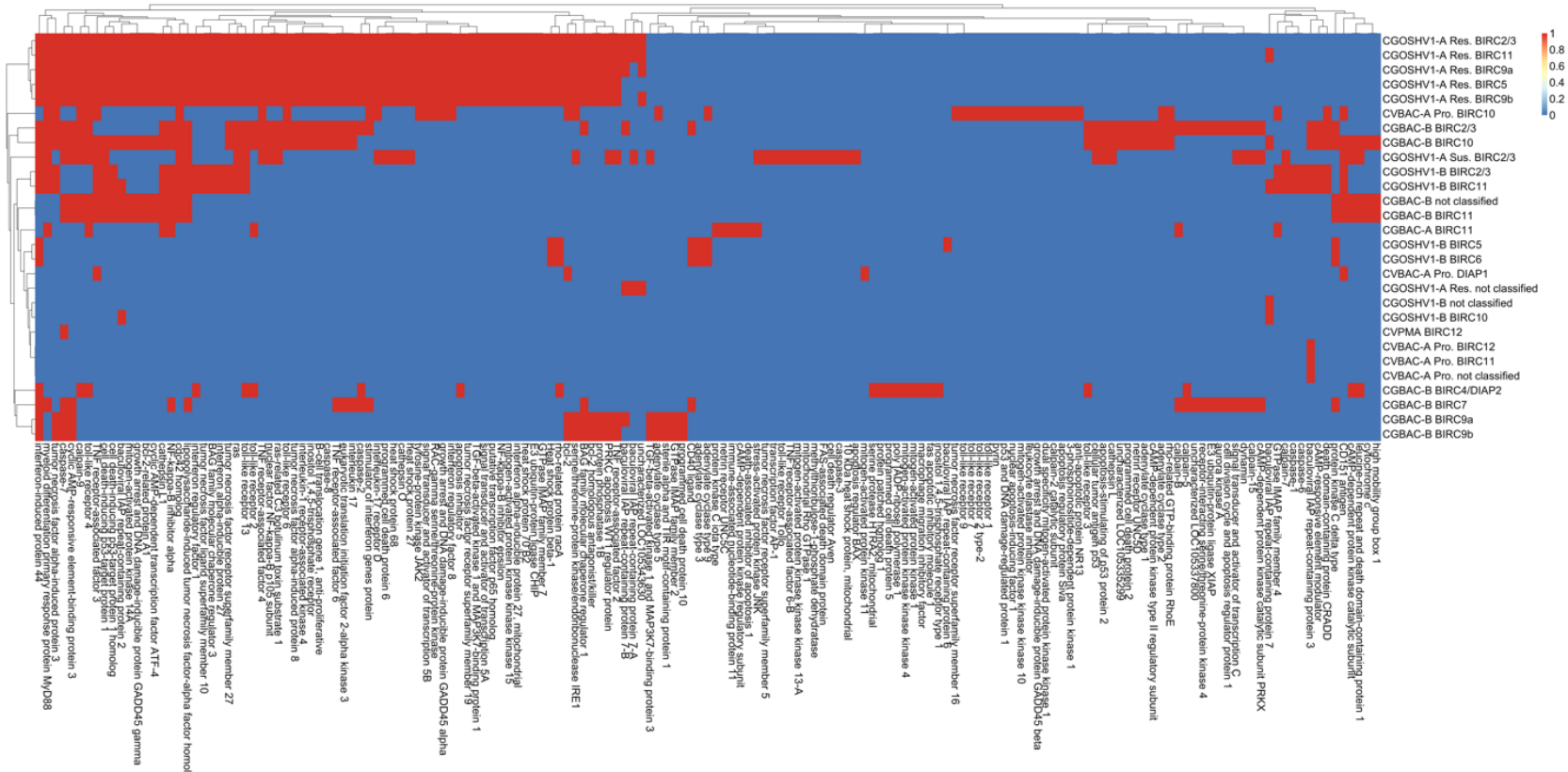

Supplementary Table 1: Number of genes and transcripts with each domain architecture type in *C. virginica* (Cv) *and C. gigas* (Cg) reference annotations. * = IAP Domain Identified by Interproscan and not CDD search.

Name	Domain Architecture	Number of Cv Transcripts	Number of Cv Genes	Number of Cg Transcripts	Number of Cg Genes
DIAP1-like	TI-TII-RING	8	2	1	1
DIAP2-like/XIAP-like	TI-TII-TII-UBA-RING	2	2	1	1
BIRC2/3-like	TI-TII-DD-RING	32	9	11	6
BIRC2/3-like	NZBIR-TII-UBA-DD-RING	3	2	3	1
BIRC5-like	BIR*	2	2	1	1
BIRC5-like	TII	6	6	3	3
BIRC6-like	TII-BIR6-E2	10	2	6	1
BIRC7-like	TII-RING	10	5	1	1
BIRC9	TII-TII	4	2	1	1
BIRC9	TX-TII	13	4	1	1
BIRC10	TII-DD	3	2	7	2
BIRC11	BIR*-DD-RING	4	2	6	2
BIRC11	TII-DD-RING	11	6	3	3
BIRC12	TII-TII-RING	12	6	15	6
NA	Non-Domain Grouped	38	17	14	10

Supplementary Table 2: IAP Gene and Transcript Differential Expression Across Experiments.

Experiment	Total Distinct* Transcripts	Transcripts Uniquely** Expressed	Percent Uniquely** Expressed Transcripts	Percent Shared Transcripts	Total Distinct* Genes	Genes Uniquely** Expressed	Percent Uniquely** Expressed Genes	Percent Genes Shared
CVBAC-B	5	4	80	20	4	1	25	75
CVBAC-A	32	12	92	8	31	8	73	27
CVBAC-C	7	6	86	14	5	2	40	60
CVPMA	16	12	80	20	16	8	67	33
CGBAC-A	5	0	0	100	5	0	0	100
CGBAC-B	42	5	33	67	32	2	20	80
CGOSHV1-B	17	3	23	77	16	2	18	82
CGOSHV1-A Susceptible	68	7	28	72	51	3	17	83
CGOSHV1-A Resistant	30	2	18	82	30	1	9	91

**Distinct refers to unique "XM" ID in that experiment. Duplicates not counted.*

***Uniquely refers to those only expressed in that experiment and not expressed in any other.*

Supplementary Table 3: Domain Architecture Groupings of Significantly Differentially Expressed and Constitutively Expressed IAP Transcripts in *C. virginica* (Cv) *and C. gigas* (Cg). DEG = significantly differentially expressed genes, CE = constitutively expressed genes. * = IAP Domain Identified by Interproscan and not CDD search.

Type	Count Category	DIAP1-like (TI-TII-RING)	DIAP2-like/XIAP-like (TI-TII-TII-UBA-BIR)	BIRC2/3-like (NZBIR-TII-UBA-DD-RING)	BIRC2/3-like (TI-TII-DD-RING)	BIRC5-like (BIR*)	BIRC5-like (TII)	BIRC6-like (TII-BIR6-E2)	BIRC7-like (TII-RING)	BIRC9 (TII-TII)	BIRC9 (TX-TII)	BIRC10 (TII-DD)	BIRC11 (BIR*-DD-RING)	BIRC11 (TII-DD-RING)	BIRC12 (TII-TII-RING)	Non-Domain Grouped
DEG	Cv Total Transcripts Per Type	15	1	4	3	2	2	8	14	4	10	10	7	0	2	12
DEG	Cv Percent of Total	16	1	4	3	2	2	9	15	4	11	11	7	0	2	13
DEG	Cg Total Transcripts Per Type	1	6	0	34	2	5	30	4	3	7	24	1	15	22	23
DEG	Cg Percent of Total	1	4	0	21	1	3	19	2	2	4	15	1	9	14	14
DEG	CVBAC-B*	1	0	0	0	0	0	0	0	0	1	0	0	0	0	3
DEG	CVBAC-A*	6	0	0	1	1	1	6	5	3	4	2	3	0	0	0

DEG	CVBAC-C*	0	0	0	0	0	0	0	2	0	2	1	0	0	1	1
DEG	CVPMA*	4	1	2	1	0	0	0	0	1	0	2	1	0	1	3
DEG	CGBAC-A*	0	0	0	0	0	0	0	2	0	0	2	0	1	0	0
DEG	CGBAC-B*	1	4	0	10	0	0	11	0	0	4	8	0	0	0	4
DEG	CGOSHV1-B*	0	0	0	4	0	1	1	0	0	0	2	1	2	1	5
DEG	CGOSHV1-A Susceptible*	0	2	0	11	0	3	9	2	3	2	12	0	6	8	10
DEG	CGOSHV1-A Resistant*	0	0	0	9	1	1	1	0	0	1	0	0	6	8	3
CE	Cv Total Transcripts Per Type	1	1	1	6	1	0	4	4	1	2	0	2	3	5	9
CE	Cv Percent of Total	3	3	3	15	3	0	10	10	3	5	0	5	8	13	23
CE	Cg Total Transcripts Per Type	0	0	1	1	0	1	0	0	0	0	1	5	1	3	3
CE	Cg Percent of Total	0	0	6	6	0	6	0	0	0	0	6	31	6	19	19

** = Distinct transcripts. Refers to unique "XM" ID in that experiment. Duplicates not counted.*

Supplementary Table 4: Apoptosis and regulated cell death products identified in *C. gigas* and *C. virginica* reference annotations.

Abbreviation	***C. gigas* Gene LOC**	***C. virginica* Gene LOC**	**Product Name**	**General RCD Pathway**	**Apoptosis-Related Sub Pathway**	**Select Alternate Protein Names**
HSP10	LOC105348624	LOC111113293	10 kDa heat shock protein, mitochondrial	apoptosis, intrinsic pathway	Bcl2 pathway, execution	10 kDa chaperonin
PDK1	LOC105331792	LOC111119108	3-phosphoinositide-dependent protein kinase 1	apoptosis, extrinsic pathway	NFkB pathway	PDPK1
HSP60	LOC105348623	LOC111113292	60 kDa heat shock protein, mitochondrial	apoptosis, intrinsic pathway	Bcl2 pathway	60 kDa chaperonin, Chaperonin 60, Heat shock protein 60, HuCHA60, Mitochondrial matrix protein P1, P60 lymphocyte protein
CyaB	LOC105318154	NA	adenylate cyclase CyaB	apoptosis, intrinsic pathway	Bcl2 pathway	Adenylyl cyclase, ATP pyrophosphate-lyase
ADCY1	LOC105340585	NA	adenylate cyclase type 1	apoptosis, intrinsic and extrinsic pathways	GPCR signaling pathway, calcium signaling	Adenylate cyclase type I, Adenylyl cyclase 1,
ADCY10	LOC105344201	LOC111129720	adenylate cyclase type 10	apoptosis, intrinsic pathway	Bcl2 pathway	AH-related protein, Adenylate cyclase homolog, Germ cell soluble adenylyl cyclase, Testicular soluble adenylyl cyclase
ADCY2	LOC105336030	LOC111134509	adenylate cyclase type 2	apoptosis, extrinsic pathway	GPCR signaling pathway	ATP pyrophosphate-lyase 2, Adenylate cyclase type II, Adenylyl cyclase 2
ADCY3	LOC105328828	NA	adenylate cyclase type 3	apoptosis, extrinsic pathway	GPCR signaling pathway	ATP pyrophosphate-lyase 3, Adenylate cyclase type III, Adenylate cyclase, olfactive type, Adenylyl cyclase 3
ADCY5	LOC105346394	LOC111132182	adenylate cyclase type 5	apoptosis, intrinsic and extrinsic pathway	GPCR signaling pathway, calcium signaling	ATP pyrophosphate-lyase 5, Adenylate cyclase type V, Adenylyl cyclase 5
ADCY9	LOC105335675	LOC111123748	adenylate cyclase type 9	apoptosis, extrinsic pathway	GPCR signaling pathway	ATP pyrophosphate-lyase 9, Adenylate cyclase type IX, Adenylyl cyclase 9
ACB	NA	LOC111116379	adenylate cyclase, terminal-differentiation specific	apoptosis, non-specific pathway	pathway unclear	ATP pyrophosphate-lyase, Adenylyl cyclase
NR13	NA	LOC111131320	anti-apoptotic protein NR13	apoptosis, intrinsic pathway	Bcl2 pathway	Apoptosis regulator Nr-13

API5	LOC105319023	LOC111132033	apoptosis inhibitor 5	apoptosis, intrinsic and extrinsic pathways	execution	Antiapoptosis clone 11 protein (AAC-11), Cell migration-inducing gene 8 protein, Fibroblast growth factor 2-interacting factor
BAX	LOC105326257	LOC111103080	apoptosis regulator BAX	apoptosis, intrinsic pathway	Bcl2 pathway	Bcl-2-like protein 4
Siva1	LOC105340131	LOC111128140	apoptosis regulatory protein Siva	apoptosis, intrinsic pathway	Bcl2 pathway, NFkB pathway	CD27-binding protein
AIF	LOC105348828	LOC111123103	apoptosis-inducing factor 1, mitochondrial	apoptosis intrinsic pathway, parthanatos, apoptosis execution	execution, parthanatos	Programmed Cell Death Protein 8, AIFM1
ASPP1	NA	LOC111128974	apoptosis-stimulating of p53 protein 1	apoptosis, intrinsic pathway	p53 pathway	Protein phosphatase 1 regulatory subunit 13B
ASPP2	LOC105340616	NA	apoptosis-stimulating of p53 protein 2	apoptosis, intrinsic pathway	p53 pathway	Bcl2-binding protein(Bbp), Renal carcinoma antigen NY-REN-51, Tumor suppressor p53-binding protein 2, 53BP2, p53-binding protein 2, p53BP2
ACIN1	LOC105337759	LOC111134707	apoptotic chromatin condensation inducer in the nucleus	apoptosis, intrinsic and extrinsic pathways	Bcl2 pathway, execution	Apoptotic chromatin condensation inducer in the nucleus
AURKA	LOC105332077	LOC111137330	aurora kinase A	apoptosis, intrinsic pathway, necroptosis	p53, necroptosis	Aurora 2, Aurora family kinase 1, Aurora/IPL1-related kinase 1, ARK-1, Aurora-related kinase 1, Ipl1- and aurora-related kinase 1, Serine/threonine-protein kinase 6, Serine/threonine-protein kinase Ayk1, Serine/threonine-protein kinase aurora-A
BTG1	Btg1	NA	B-cell translocation gene 1, anti-proliferative	apoptosis, pathway unclear	pathway unclear	Protein BTG1
BIRC2	LOC105328051	LOC111123894	baculoviral IAP repeat-containing protein 2	apoptosis, intrinsic and extrinsic pathways	TNFR pathway, NFkB pathway, execution, Bcl2-pathway, TLR pathway	Cellular inhibitor of apoptosis 1 (C-IAP1), IAP homolog B, Inhibitor of apoptosis protein 2 (hIAP-2), RING finger protein 48, RING-type E3 ubiquitin transferase BIRC2, TNFR2-TRAF-signaling complex protein 2
BIRC3	LOC105334814	LOC111101864	baculoviral IAP repeat-containing protein 3	apoptosis, intrinsic and extrinsic pathways	TNFR pathway, NFkB pathway, TLR pathway, execution	Apoptosis inhibitor 2 (API2, Cellular inhibitor of apoptosis 2 (C-IAP2), IAP homolog C, Inhibitor of apoptosis protein 1 (hIAP-1), RING finger protein 49,

						RING-type E3 ubiquitin transferase BIRC3, TNFR2-TRAF-signaling complex protein 1
BIRC5	LOC105334034	LOC111119408	baculoviral IAP repeat-containing protein 5	apoptosis, intrinsic pathway	execution	Apoptosis inhibitor 4, Apoptosis inhibitor survivin
BIRC6	LOC105334740	LOC111129365	baculoviral IAP repeat-containing protein 6	apoptosis, intrinsic pathway	Bcl2 pathway, execution	BIR repeat-containing ubiquitin-conjugating enzyme, RING-type E3 ubiquitin transferase BIRC6, Ubiquitin-conjugating BIR domain enzyme apollon, BRUCE
BIRC7	LOC105331304	LOC111136287	baculoviral IAP repeat-containing protein 7	apoptosis, intrinsic pathway	Bcl2 pathway, TNFR pathway, execution	Kidney inhibitor of apoptosis protein (KIAP), Livin, Melanoma inhibitor of apoptosis protein (ML-IAP), RING finger protein 50, RING-type E3 ubiquitin transferase BIRC7
BIRC7A	LOC105347559	LOC111100432	baculoviral IAP repeat-containing protein 7-A	apoptosis, intrinsic pathway	execution	E3 ubiquitin-protein ligase EIAP-A, RING-type E3 ubiquitin transferase EIAP-A, XIAP homolog XLX
BIRC7B	LOC105328993	LOC111105137	baculoviral IAP repeat-containing protein 7-B	apoptosis, intrinsic pathway	execution	E3 ubiquitin-protein ligase EIAP-B, Embryonic/Egg IAP-B, EIAP/XLX-B, RING-type E3 ubiquitin transferase EIAP-B
BIRC8	NA	LOC111103158	baculoviral IAP repeat-containing protein 8	apoptosis, intrinsic pathway	Bcl2 pathway	Inhibitor of apoptosis-like protein 2, IAP-like protein 2, ILP-2
BAG1	LOC105334567	LOC111127391	BAG family molecular chaperone regulator 1	apoptosis, intrinsic pathway	Bcl2 pathway	BCL2 associated athanogene 1
BAG2	LOC105340315	LOC111122068	BAG family molecular chaperone regulator 2	apoptosis, intrinsic pathway	Bcl2 pathway	Bcl-2-associated athanogene 2
BAG3	LOC105334580	LOC111103765	BAG family molecular chaperone regulator 3	apoptosis, intrinsic pathway	Bcl2 pathway	Bcl-2-associated athanogene 3, Bcl-2-binding protein Bis
BAK1	LOC105336915	NA	bcl-2 homologous antagonist/killer	apoptosis, intrinsic pathway	Bcl2 pathway	Apoptosis regulator BAK, Bcl-2-like protein 7 (Bcl2-L-7)
Bcl-XL/XS	LOC105343381	LOC111112596	bcl-2-like protein 1	apoptosis, intrinsic pathway	Bcl2 pathway	Apoptosis regulator Bcl-X, BCL2 Like 1, BCL-XL/S
A1	LOC105335025	NA	bcl-2-related protein A1	apoptosis, intrinsic pathway	Bcl2 pathway	A1-A, Hemopoietic-specific early response protein, Protein BFL-1

CAPNS1	LOC109617095	LOC111121215	calpain small subunit 1	apoptosis, intrinsic pathway	calcium signaling	Calcium-activated neutral proteinase small subunit, Calcium-dependent protease small subunit, Calpain regulatory subunit, CAPN4
CAPNS2	LOC105333798	NA	calpain small subunit 2	apoptosis, intrinsic pathway	calcium signaling	Calcium-dependent protease small subunit 2
CAPN1	LOC105335223	LOC111115102	calpain-1 catalytic subunit	apoptosis, intrinsic pathway	Bcl2 pathway, execution, parthanatos	Calcium-activated neutral proteinase 1, Calpain mu-type, Calpain-1 large subunit, Cell proliferation-inducing gene 30 protein, Micromolar-calpain, muCANP
CAPN15	LOC105318471	LOC111125070	calpain-15	apoptosis, intrinsic pathway	calcium signaling	Small optic lobes homolog
CAPN2	NA	LOC111127234	calpain-2 catalytic subunit	apoptosis, intrinsic pathway	Bcl2 pathway, execution	80 kDa M-calpain subunit, Calcium-activated neutral proteinase 2, Calpain M-type, Calpain-2 large subunit, Millimolar-calpain
CAPN3	NA	LOC111099881	calpain-3	apoptosis, intrinsic pathway	calcium signaling	Calcium-activated neutral proteinase 3, Calpain L3, Calpain p94, Muscle-specific calcium-activated neutral protease 3, New calpain 1
CAPN5	LOC105337433	LOC111126401	calpain-5	apoptosis, intrinsic pathway	calcium signaling	Calpain htra-3, New calpain 3, nCL-3
CAPN6	LOC105345615	NA	calpain-6	apoptosis, intrinsic pathway	calcium signaling	Calpain-like protease X-linked, Calpamodulin
CAPN7	LOC105334505	LOC111110907	calpain-7	apoptosis, intrinsic pathway	calcium signaling	PalB homolog
CAPN8	LOC105331075	LOC111127849	calpain-8	apoptosis, intrinsic pathway	calcium signaling	New calpain 2, Stomach-specific M-type calpain
CAPN9	LOC105330366	LOC111124603	calpain-9	apoptosis, intrinsic pathway	calcium signaling	Digestive tract-specific calpain, New calpain 4, Protein CG36
CALPA	LOC105323377	LOC111121599	calpain-A	apoptosis, intrinsic pathway	calcium signaling	Calcium-activated neutral proteinase A
CALPB	LOC105337008	LOC111130040	calpain-B	apoptosis, intrinsic pathway	calcium signaling	Calcium-activated neutral proteinase B
CAPND	LOC105339007	NA	calpain-D	apoptosis, intrinsic pathway	calcium signaling	Calcium-activated neutral proteinase D, Small optic lobes protein
PKA-C	LOC105336635	LOC111118497	cAMP-dependent protein kinase catalytic subunit	apoptosis, intrinsic and extrinsic pathway	Bcl2 pathway, GPCR signaling	PKA-C
PRKX	LOC105346669	LOC111135327	cAMP-dependent protein kinase catalytic subunit PRKX	apoptosis, intrinsic and extrinsic pathway	Bcl2 pathway, GPCR signaling	Protein kinase X, Serine/threonine-protein kinase PRKX, Protein kinase PKX1

PRKR	LOC105330415	LOC111119982	cAMP-dependent protein kinase regulatory subunit	apoptosis, intrinsic and extrinsic pathway	Bcl2 pathway, GPCR signaling	Protein kinase A, regulatory subunit
PRKAR2	LOC105342800	LOC111135307	cAMP-dependent protein kinase type II regulatory subunit	apoptosis, intrinsic and extrinsic pathway	Bcl2 pathway, GPCR signaling	none
CREM	LOC105342857	LOC111111886	cAMP-responsive element modulator	apoptosis, intrinsic and extrinsic pathway	Bcl2 pathway, GPCR signaling	Inducible cAMP early repressor
CAAP1	LOC105335105	LOC111122401	caspase activity and apoptosis inhibitor 1	apoptosis, intrinsic pathway	execution, TNFR pathway	Conserved anti-apoptotic protein, CAAP
Dronc	LOC105322339	NA	caspase Dronc	apoptosis, execution	execution	NEDD2-like caspase
casp1	LOC105346966	LOC111136318	caspase-1	pyroptosis	pyroptosis, inflammation	Interleukin-1 beta convertase (IL-1BC), Interleukin-1 beta-converting enzyme (ICE), IL-1 beta-converting enzyme
casp10	NA	LOC111106182	caspase-10	apoptosis, execution, extrinsic, intrinsic pathway	execution, TNFR pathway, NFkB pathway	Apoptotic protease Mch-4, FAS-associated death domain protein interleukin-1B-converting enzyme 2, FLICE2, ICE-like apoptotic protease 4
casp2	LOC105340308	LOC111120235	caspase-2	apoptosis, instrinsic and extrinsic pathway	Bcl2 pathway, p53 pathway	Neural precursor cell expressed developmentally down-regulated protein 2 (NEDD-2), Protease ICH-1
casp3	LOC105346972	LOC111118290	caspase-3	apoptosis, execution	execution	Apopain, Cysteine protease CPP32 (CPP-32), Protein Yama, SREBP cleavage activity 1 (SCA-1)
casp6	LOC105348272	LOC111099155	caspase-6	apoptosis, execution	execution	Apoptotic protease Mch-2
casp7	LOC109617035	LOC111124839	caspase-7	apoptosis, execution	execution	Apoptotic protease Mch-3, CMH-1, ICE-like apoptotic protease 3 (ICE-LAP3)
casp8	LOC105340890	LOC111125491	caspase-8	apoptosis, extrinsic pathway	TNFR pathway, TNFR pathway	Apoptotic protease Mch-5, FADD-homologous ICE/ced-3-like protease, FADD-like ICE (FLICE), ICE-like apoptotic protease 5
casp9	LOC105332032	LOC111133186	caspase-9	apoptosis, intrinsic pathway	Bcl2 pathway	Apoptotic protease Mch-6, Apoptotic protease-activating factor 3 (APAF-3), ICE-like apoptotic protease 6 (ICE-LAP6)
CTSB	LOC105328916	LOC111111564	cathepsin B	lysosome-dependent cell death	lysosome-dependent cell death, Bcl2 pathway	APP secretase (APPS), Cathepsin B1

CTSL	LOC105331753	LOC111138065	cathepsin L	lysosome-dependent cell death	lysosome-dependent cell death, Bcl2 pathway	Cysteine proteinase 1
CTSL1	LOC105330701	LOC111122564	cathepsin L1	lysosome-dependent cell death	lysosome-dependent cell death, Bcl2 pathway	Major excreted protein (MEP)
CTSO	LOC105335927	LOC111123154	cathepsin O	lysosome-dependent cell death	lysosome-dependent cell death, Bcl2 pathway	none
CTSZ	LOC105327153	NA	cathepsin Z	lysosome-dependent cell death	lysosome-dependent cell death, Bcl2 pathway	Cathepsin X
CD151	LOC105325952	LOC111115832	CD151 antigen	apoptosis, instrinsic pathway	Bcl2 pathway	GP27, Membrane glycoprotein SFA-1, Platelet-endothelial tetraspan antigen 3 (PETA-3), Tetraspanin-24, CD antigen CD151
CD40LG	LOC105344743	LOC111099523	CD40 ligand	apoptosis, extrinsic pathway	TNFR pathway	T-cell antigen Gp39, TNF-related activation protein (TRAP), Tumor necrosis factor ligand superfamily member 5 (TNFSF5), CD antigen CD154
cdc42	LOC105325966	LOC111130934	cdc42 homolog	apoptosis, extrinsic pathway	GPCR signaling pathway	Cell division control protein 42 homolog
Aven	LOC105338032	LOC111127766	cell death regulator Aven	apoptosis, instrinsic pathway	Bcl2 pathway	Aven
CDIP1	LOC105326260	LOC111118102	cell death-inducing p53-target protein 1	apoptosis, extrinsic pathway	p53 pathway	Cell death inCGOSHV1-Aved p53-target, Cell death-inducing protein, LITAF-like protein, Lipopolysaccharide-induced tumor necrosis factor-alpha-like protein, Transmembrane protein I1
CDIP1	LOC105340329	LOC111127658	cell death-inducing p53-target protein 1 homolog	apoptosis, extrinsic pathway	p53 pathway	Cell death inCGOSHV1-Aved p53-target, Cell death-inducing protein, LITAF-like protein, Lipopolysaccharide-induced tumor necrosis factor-alpha-like protein, Transmembrane protein I1
CCAR	LOC105335754	LOC111119776	cell division cycle and apoptosis regulator protein 1	apoptosis, intrinsic and extrinsic pathway	p53 pathway, TNFR pathway	Cell cycle and apoptosis regulatory protein 1 (CARP-1), Death inducer with SAP domain
p53	LOC105340434	NA	cellular tumor antigen p53	apoptosis, instrinsic pathway	p53 pathway	Antigen NY-CO-13, Phosphoprotein p53, Tumor suppressor p53

CERS2	LOC105335972	LOC111114186	ceramide synthase 2	apoptosis, instrinsic and extrinsic pathway	Bcl2 pathway, TNFR pathway	LAG1 longevity assurance homolog 2, Sphingosine N-acyltransferase CERS2, EC 2.3.1.24, Translocating chain-associating membrane protein homolog 3, TRAM homolog 3
CERS5	NA	LOC111111442	ceramide synthase 5	apoptosis, instrinsic and extrinsic pathway	Bcl2 pathway, TNFR pathway	LAG1 longevity assurance homolog 5, Sphingosine N-acyltransferase CERS5
CERS6	LOC105332957	NA	ceramide synthase 6	apoptosis, instrinsic and extrinsic pathway	Bcl2 pathway, TNFR pathway	LAG1 longevity assurance homolog 6
ATF-4	LOC105336468	LOC111130043	cyclic AMP-dependent transcription factor ATF-4	apoptosis, instrinsic pathway	ER stress	Activating transcription factor 4, Cyclic AMP-responsive element-binding protein 2, DNA-binding protein TAXREB67
CREB3L1	LOC105336068	LOC111103513	cyclic AMP-responsive element-binding protein 3-like protein 1	apoptosis, extrinsic pathway	ER stress, GPCR signaling	Old astrocyte specifically-induced substance, OASIS
CREB3L2	LOC105326506	NA	cyclic AMP-responsive element-binding protein 3-like protein 2	apoptosis, extrinsic pathway	ER stress, GPCR signaling	cAMP-responsive element-binding protein 3-like protein 2
CREB3L3	NA	LOC111128897	cyclic AMP-responsive element-binding protein 3-like protein 3	apoptosis, extrinsic pathway	ER stress, GPCR signaling	cAMP-responsive element-binding protein 3-like protein 3
CREB3L3B	LOC105326649	LOC111129050	cyclic AMP-responsive element-binding protein 3-like protein 3-B	apoptosis, extrinsic pathway	ER stress, GPCR signaling	cAMP-responsive element-binding protein 3-like protein 3-B
p35	LOC105345740	LOC111115094	cyclin-dependent kinase 5 activator 1	apoptosis, intrinsic pathway	Bcl2 pathway	P35 protein, Early 35 kDa protein, Cyclin-dependent kinase 5 regulatory subunit 1, TPKII regulatory subunit
cyto-c	LOC105344150	LOC111112645	cytochrome c	apoptosis, intrinsic pathway	Bcl2 pathway	Cytochrome c1, heme protein, mitochondrial

DAXX	LOC105322965	NA	death domain-associated protein 6	apoptosis, intrinsic and extrinsic pathway	p53 pathway, TNFR pathway	ETS1-associated protein 1, Fas death domain-associated protein
CRADD	LOC105327431	LOC111109418	death domain-containing protein CRADD	apoptosis, instrinsic and extrinsic pathway	p53 pathway, NFkB pathway	Caspase and RIP adapter with death domain, RIP-associated protein with a death domain
DIAP1	LOC105332637	LOC111109152	death-associated inhibitor of apoptosis 1	apoptosis, intrinsic pathway	execution	Apoptosis 1 inhibitor, E3 ubiquitin-protein ligase th, Inhibitor of apoptosis 1, Protein thread, RING-type E3 ubiquitin transferase Diap1
DIAP2	LOC105328049	LOC111100802	death-associated inhibitor of apoptosis 2	apoptosis, intrinsic pathway	execution	Apoptosis 2 inhibitor, IAP homolog A, IAP-like protein, ILP, dILP, Inhibitor of apoptosis 2
Diablo	LOC105319883	NA	diablo homolog, mitochondrial	apoptosis, intrinsic pathway	Bcl2 pathway	Direct IAP-binding protein with low pI, Second mitochondria-derived activator of caspase, Smac
ICAD	LOC105326479	LOC111136682	DNA fragmentation factor subunit alpha	apoptosis, execution	execution	DNA fragmentation factor 45 kDa subunit (DFF-45), Inhibitor of CAD (ICAD)
CAD	LOC105341521	LOC111137968	DNA fragmentation factor subunit beta	apoptosis, execution	execution	Caspase-activated deoxyribonuclease, CAD, Caspase-activated Dnase, Caspase-activated nuclease, CPAN, DNA fragmentation factor 40 kDa subunit, DFF-40
MAP2K1	LOC105339480	LOC111128693	dual specificity mitogen-activated protein kinase kinase 1	NETosis	NETosis	MAP2K1, MAP kinase kinase 1, MAPKK 1, MKK1, ERK activator kinase 1, MAPK/ERK kinase 1, MEK 1
OPA1	LOC105325345	LOC111136008	dynamin-like 120 kDa protein, mitochondrial	apoptosis, intrinsic pathway	Bcl2 pathway	mitochondrial dynamin like GTPase
CHIP	LOC105334775	LOC111122139	E3 ubiquitin-protein ligase CHIP	necroptosis	necroptosis	Antigen NY-CO-7, CLL-associated antigen KW-8, Carboxy terminus of Hsp70-interacting protein, RING-type E3 ubiquitin transferase CHIP, STIP1 homology and U box-containing protein 1
XIAP	LOC105332528	LOC111100396	E3 ubiquitin-protein ligase XIAP	apoptosis, intrinsic and extrinsic pathway, execution	Bcl2 pathway, execution, NFkB signaling, TNFR pathway	Baculoviral IAP repeat-containing protein 4, IAP-like protein, ILP, hILP, Inhibitor of apoptosis protein 3, IAP-3, hIAP-3, hIAP3, RING-type E3 ubiquitin transferase XIAP, X-linked inhibitor of apoptosis protein, X-linked IAP
EndoG	LOC105324886	LOC111126118	endonuclease G, mitochondrial	apoptosis, intrinsic pathway, apoptosis execution	execution	none

EIF2AK3	LOC105337070	LOC111135701	eukaryotic translation initiation factor 2-alpha kinase 3	apoptosis, instrinsic pathway	ER stress	PRKR-like endoplasmic reticulum kinase, Pancreatic eIF2-alpha kinase
FAIM1	LOC105331684	LOC111135797	fas apoptotic inhibitory molecule 1	apoptosis, extrinsic pathway	TNFR pathway	none
FADD	LOC105346692	LOC111118231	FAS-associated death domain protein	apoptosis, extrinsic pathway	TNFR pathway, TNFR pathway	FAS-associating death domain-containing protein, Growth-inhibiting gene 3 protein, Mediator of receptor induced toxicity, Protein FADD
FADD	LOC105323317	NA	fas-associated death domain protein	apoptosis, extrinsic pathway	TNFR pathway, TNFR pathway	FAS-associating death domain-containing protein, Growth-inhibiting gene 3 protein, Mediator of receptor induced toxicity, Protein FADD
DDIT-1	LOC105340465	LOC111121109	growth arrest and DNA damage-inducible protein GADD45 alpha	apoptosis, intrinsic pathway	p53 pathway	DNA damage-inducible transcript 1 protein
GADD45B	NA	LOC111118444	growth arrest and DNA damage-inducible protein GADD45 beta	apoptosis, intrinsic pathway	p53 pathway	Myeloid differentiation primary response protein MyD118, Negative growth regulatory protein MyD118
DDIT-2	LOC105340466	NA	growth arrest and DNA damage-inducible protein GADD45 gamma	apoptosis, intrinsic pathway	p53 pathway	Cytokine-responsive protein CR6, DNA damage-inducible transcript 2 protein
GIMAP2	LOC105348675	NA	GTPase IMAP family member 2	apoptosis, intrinsic pathway	pathway unclear	Immunity-associated protein 2, hIMAP2
GIMAP4	LOC105328473	LOC111119582	GTPase IMAP family member 4	apoptosis, intrinsic pathway	pathway unclear	Immunity-associated nucleotide 1 protein, IAN-1, Immunity-associated protein 4
GIMAP7	LOC105331782	LOC111106989	GTPase IMAP family member 7	apoptosis, intrinsic pathway	pathway unclear	Immunity-associated nucleotide 7 protein, IAN-7
GIMAP8	LOC105318994	LOC111120314	GTPase IMAP family member 8	apoptosis, intrinsic pathway	pathway unclear	Immune-associated nucleotide-binding protein 9, IAN-9, Protein IanT
HSP27	LOC105343216	LOC111137387	heat shock protein 27	apoptosis, intrinsic pathway	chaperone, Bcl2 pathway, TNFR pathway	28 kDa heat shock protein, Estrogen-regulated 24 kDa protein, Heat shock 27 kDa protein, HSP 27, Stress-responsive protein 27, SRP27, HSPB1
HSP30C	NA	LOC111125908	heat shock protein 30C	apoptosis, intrinsic pathway	chaperone	none
HSP68	LOC105334510	LOC111121333	heat shock protein 68	apoptosis, intrinsic pathway	chaperone	none

HSP70B2	LOC105334234	LOC111119512	heat shock protein 70 B2	apoptosis, intrinsic pathway	chaperone	none
HSP75	LOC105321567	LOC111123621	heat shock protein 75 kDa, mitochondrial	apoptosis, intrinsic pathway	chaperone	TNFR-associated protein 1, Tumor necrosis factor type 1 receptor-associated protein, TRAP-1
HSP83	LOC105345989	LOC111129671	heat shock protein 83	apoptosis, intrinsic pathway	chaperone	HSP82
HSPB1	LOC105331471	NA	Heat shock protein beta-1	apoptosis, intrinsic pathway	chaperone, Bcl2 pathway, TNFR pathway	28 kDa heat shock protein, Estrogen-regulated 24 kDa protein, Heat shock 27 kDa protein, HSP 27, Stress-responsive protein 27, SRP27
HSP90B	NA	LOC111129841	heat shock protein HSP 90-beta	apoptosis, intrinsic and extrinsic pathway, necroptosis	chaperone, necroptosis, TGF-beta pathway, Bcl2-pathway	Heat shock 84 kDa, HSP 84, HSP84
HSP16.2	NA	LOC111118166	heat shock protein Hsp-16.2	apoptosis, intrinsic pathway	chaperone	none
HK1	LOC105317783	LOC111099882	hexokinase-1	parthanatos	parthanatos, inflammation	Brain form hexokinase, Hexokinase type I, HK I, Hexokinase-A
HMGB1	Hmgb1	NA	high mobility group box 1	apoptosis, intrinsic and extrinsic pathway	inflammation, TLR pathway, chaperone	High mobility group protein 1, HMG-1
IAN11	LOC105347560	NA	immune-associated nucleotide-binding protein 11	apoptosis, intrinsic pathway	pathway unclear	IAN11
IAN12	LOC105346672	LOC111103088	immune-associated nucleotide-binding protein 12	apoptosis, intrinsic pathway	pathway unclear	IAN12
IAN13	NA	LOC111115187	immune-associated nucleotide-binding protein 13	apoptosis, intrinsic pathway	pathway unclear	IAN13
IAN8	NA	LOC111107223	immune-associated nucleotide-binding protein 8	apoptosis, intrinsic pathway	pathway unclear	IAN8, AIG1

IAN9	LOC105339767	LOC111110097	immune-associated nucleotide-binding protein 9	apoptosis, intrinsic pathway	pathway unclear	IAN9, GIMAP8
IAP	NA	LOC111133238	inhibitor of apoptosis protein	apoptosis, intrinsic pathway	pathway unclear	IAP
IP3R1	LOC105325881	LOC111106119	inositol 1,4,5-trisphosphate receptor type 1	apoptosis, extrinsic pathway	calcium signaling	IP3 receptor isoform 1, IP3R 1, InsP3R1, Inositol 1,4,5-trisphosphate-binding protein P400, Protein PCD-6, Purkinje cell protein 1, Type 1 inositol 1,4,5-trisphosphate receptor, Type 1 InsP3 receptor
IP3R2	LOC105331933	LOC111138392	inositol 1,4,5-trisphosphate receptor type 2	apoptosis, extrinsic pathway	calcium signaling	IP3 receptor isoform 2, IP3R 2, InsP3R2, Inositol 1,4,5-trisphosphate type V receptor, Type 2 inositol 1,4,5-trisphosphate receptor, Type 2 InsP3 receptor
IP3R3	NA	LOC111132623	inositol 1,4,5-trisphosphate receptor type 3	apoptosis, extrinsic pathway	calcium signaling	IP3 receptor isoform 3, IP3R 3, InsP3R3, Type 3 inositol 1,4,5-trisphosphate receptor, Type 3 InsP3 receptor
iPLA	LOC105327218	NA	inositol 1,4,5-trisphosphate receptor-like protein A	apoptosis, extrinsic pathway	calcium signaling	none
IFI27L2	LOC105345119	NA	interferon alpha-inducible protein 27-like protein 2	apoptosis, intrinsic pathway	IFN pathway	Interferon-stimulated gene 12b protein, ISG12(b), ISG12B, ,Protein TLH29, pIFI27-like protein
Ifi27l2b	LOC109620516	LOC111112746	interferon alpha-inducible protein 27-like protein 2B	apoptosis, intrinsic pathway	IFN pathway	Interferon-stimulated gene 12 protein B2
IFI27	LOC105347592	NA	interferon alpha-inducible protein 27, mitochondrial	apoptosis, intrinsic pathway	IFN pathway	Interferon alpha-induced 11.5 kDa protein, Interferon-stimulated gene 12a protein, ISG12(a), ISG12A
IRF1	LOC105343805	LOC111118091	interferon regulatory factor 1	apoptosis, extrinsic pathway	IFN pathway	None
IRF2BP2	LOC105319831	LOC111129225	interferon regulatory factor 2-binding protein	apoptosis, extrinsic pathway	IFN pathway	None
IRF8	LOC105317636	LOC111136943	interferon regulatory factor 8	apoptosis, extrinsic pathway	IFN pathway	Interferon consensus sequence-binding protein (H-ICSBP, ICSBP)

IFI44	LOC109619467	LOC111134552	interferon-induced protein 44	apoptosis, extrinsic pathway	IFN pathway	Microtubule-associated protein 44, p44
IL17	LOC105318790	LOC111119445	interleukin 17-like protein	apoptosis, extrinsic pathway	inflammation	None
IRAK1BP1	LOC105344940	LOC111104074	interleukin-1 receptor-associated kinase 1-binding protein 1	apoptosis, extrinsic pathway	inflammation	None
IRAK4	LOC105334452	LOC111136488	interleukin-1 receptor-associated kinase 4	apoptosis, extrinsic pathway	inflammation	None
IL17RD	LOC105340255	LOC111107347	interleukin-17 receptor D	apoptosis, extrinsic pathway	inflammation	IL17Rhom, Sef homolog
PIDD1/LRDD	LOC105337567	LOC111126510	leucine-rich repeat and death domain-containing protein 1	apoptosis, intrinsic pathway	p53 pathway, NFkB pathway, Bcl2 pathway	p53-induced death domain-containing protein 1
SERPINB1	LOC105343764	LOC111105842	leukocyte elastase inhibitor	apoptosis, extrinsic pathway	inflammation	Monocyte/neutrophil elastase inhibitor
LITAF	NA	LOC111121311	lipopolysaccharide-induced tumor necrosis factor-alpha factor	apoptosis, extrinsic pathway	TNFR pathway, TLR pathway	LPS-induced TNF-alpha factor homolog, Estrogen-enhanced transcript protein, mEET, LITAF-like protein, (NEDD4 WW domain-binding protein 3
LITAF	LOC105332776	LOC111099109	lipopolysaccharide-induced tumor necrosis factor-alpha factor homolog	apoptosis, extrinsic pathway	TNFR pathway, TLR pathway	LPS-induced TNF-alpha factor homolog, Estrogen-enhanced transcript protein, mEET, LITAF-like protein, (NEDD4 WW domain-binding protein 3
LTA	NA	LOC111135889	lymphotoxin-alpha	apoptosis, extrinsic pathway	TNFR pathway	Tumor necrosis factor beta, Tumor necrosis factor ligand superfamily member 1
MIF	LOC105343631	LOC111133619	macrophage migration inhibitory factor	parthanatos	parthanatos	Glycosylation-inhibiting factor, GIF, L-dopachrome isomerase, L-dopachrome tautomerase
MIF	LOC105319375	LOC111133621	macrophage migration inhibitory factor homolog	parthanatos	parthanatos	Glycosylation-inhibiting factor, GIF, L-dopachrome isomerase, L-dopachrome tautomerase

MADD	LOC105348971	LOC111108068	MAP kinase-activating death domain protein	apoptosis, extrinsic pathway	TNFR pathway	Differentially expressed in normal and neoplastic cells, Insulinoma glucagonoma clone 20, Rab3 GDP/GTP exchange factor
APIP	LOC105342692	LOC111100699	methylthioribulose-1-phosphate dehydratase	apoptosis, intrinsic pathway, pyroptosis	pyroptosis, inflammation, Bcl2 pathway	APAF-1 interacting protein
RHOT1	LOC105325608	LOC111119655	mitochondrial Rho GTPase 1	apoptosis, extrinsic pathway	GPCR signaling pathway	Rac-GTP-binding protein-like protein, Ras homolog gene family member T1
MAPK1	LOC105334418	LOC111135362	mitogen-activated protein kinase 1	apoptosis, intrinsic and extrinsic pathway	Bcl2 pathway, execution	MAP Kinase 1, Extracellular signal-regulated kinase 2, ERK-2, MAP kinase isoform p42, p42-MAPK. Mitogen-activated protein kinase 2, MAP kinase 2, MAPK 2
MAPK11	NA	LOC111112844	mitogen-activated protein kinase 11	apoptosis, intrinsic and extrinsic pathway	p53 pathway, Bcl2 pathway, TNFR pathway, GPCR signaling pathway	p38 mitogen-activated protein kinase 11, p38-B
MAPK14A	LOC105347124	LOC111108651	mitogen-activated protein kinase 14A	apoptosis, intrinsic and extrinsic pathway	p53 pathway, Bcl2 pathway, TNFR pathway, GPCR signaling pathway	MAP kinase 14A, Mitogen-activated protein kinase p38a, MAP kinase p38a, zp38a
MEKK1	LOC105331404	LOC111119906	mitogen-activated protein kinase kinase kinase 1	apoptosis, intrinsic and extrinsic pathway	p53 pathway, Bcl2 pathway, NFkB pathway, TNFR pathway	MAP3K1, MAPK/ERK kinase kinase 1, MEK kinase 1, MEKK 1
MAP3K10	LOC105317550	LOC111129307	mitogen-activated protein kinase kinase kinase 10	apoptosis, intrinsic and extrinsic pathway	p53 pathway, Bcl2 pathway, NFkB pathway, TNFR pathway	MAP kinase p49 3F12, Stress-activated protein kinase 1b, Stress-activated protein kinase JNK, c-Jun N-terminal kinase 3
MAP3K13	NA	LOC111124479	mitogen-activated protein kinase kinase kinase 13	apoptosis, intrinsic and extrinsic pathway	p53 pathway, Bcl2 pathway, NFkB pathway, TNFR pathway	Mitogen-activated protein kinase p38 delta, MAP kinase p38 delta, Stress-activated protein kinase 4
MAP3K13a	LOC105343569	NA	mitogen-activated protein kinase kinase kinase 13-A	apoptosis, intrinsic and extrinsic pathway	p53 pathway, Bcl2 pathway, NFkB pathway, TNFR pathway	None
MAP3K15	LOC105338968	NA	mitogen-activated protein kinase kinase kinase 15	apoptosis, intrinsic and extrinsic pathway	p53 pathway, Bcl2 pathway,	Apoptosis signal-regulating kinase 3, MAPK/ERK kinase kinase 15, MEK kinase 15, MEKK15

					NFkB pathway, TNFR pathway	
MAPK3K2	LOC105335847	LOC111124631	mitogen-activated protein kinase kinase kinase 2	apoptosis, intrinsic and extrinsic pathway	p53 pathway, Bcl2 pathway, NFkB pathway, TNFR pathway	MAPK/ERK kinase kinase 2, MEK kinase 2, MEKK 2
MAP3K20	NA	LOC111114895	mitogen-activated protein kinase kinase kinase 20	apoptosis, intrinsic and extrinsic pathway	p53 pathway, Bcl2 pathway, NFkB pathway, TNFR pathway	Human cervical cancer suppressor gene 4 protein, Leucine zipper- and sterile alpha motif-containing kinase, MLK-like mitogen-activated protein triple kinase, Mitogen-activated protein kinase kinase kinase MLT, Mixed lineage kinase-related kinase, MLK-related kinase, MRK, Sterile alpha motif- and leucine zipper-containing kinase AZK
MAP3K4	LOC105334041	LOC111102022	mitogen-activated protein kinase kinase kinase 4	apoptosis, intrinsic and extrinsic pathway	p53 pathway, Bcl2 pathway, NFkB pathway, TNFR pathway	HPK/GCK-like kinase HGK, MAPK/ERK kinase kinase kinase 4, MEK kinase kinase 4, MEKKK 4, Nck-interacting kinase
TAK1	LOC105332318	LOC111103778	mitogen-activated protein kinase kinase kinase 7	apoptosis, intrinsic and extrinsic pathway, necroptosis	p53 pathway, Bcl2 pathway, NFkB pathway, TNFR pathway, necroptosis, TLR pathway, TGF-beta pathway	MAP3K7, Transforming growth factor-beta-activated kinase 1, TGF-beta-activated kinase 1
TAB3	NA	LOC111103484	mitogen-activated protein kinase kinase kinase 7-interacting protein 3 homolog	apoptosis, intrinsic and extrinsic pathway	p53 pathway, Bcl2 pathway, NFkB pathway, TNFR pathway, necroptosis, TLR pathway, TGF-beta pathway	TGF-beta-activated kinase 1 and MAP3K7-binding protein 3, NF-kappa-B-activating protein 1, TAK1-binding protein 3
ANP1	LOC109617748	NA	mitogen-activated protein kinase kinase kinase ANP1	apoptosis, intrinsic and extrinsic pathway	p53 pathway, Bcl2 pathway, NFkB pathway, TNFR pathway	Arabidopsis NPK1-related kinase 1
MAPK20	LOC105335956	NA	mitogen-activated protein kinase kinase kinase MLT	apoptosis, intrinsic and extrinsic pathway	p53 pathway, Bcl2 pathway, NFkB pathway, TNFR pathway	(See above, mitogen-activated protein kinase kinase kinase 20)

MYD88	LOC105337632	LOC111114939	myeloid differentiation primary response protein MyD88	apoptosis, intrinsic and extrinsic pathway	TLR pathway, NFkB pathway	MYD88 innate immune signal transduction adaptor
DCC	NA	LOC111127517	netrin receptor DCC	dependence receptor pathway	dependence receptor pathway	Colorectal cancer suppressor, Immunoglobulin superfamily DCC subclass member 1, Tumor suppressor protein DCC
UNC5B	NA	LOC111131792	netrin receptor UNC5B-b	dependence receptor pathway	dependence receptor pathway	Protein unc-5 homolog 2, Protein unc-5 homolog B
UNC5C	LOC105341106	LOC111118753	netrin receptor UNC5C	dependence receptor pathway	dependence receptor pathway	Protein unc-5 homolog 3, Protein unc-5 homolog C
UNC5D	LOC109620298	NA	netrin receptor UNC5D	dependence receptor pathway	dependence receptor pathway	Protein unc-5 homolog 4, Protein unc-5 homolog D
IKBA	LOC105319273	LOC111131219	NF-kappa-B inhibitor alpha	apoptosis, extrinsic pathway	NFkB pathway	I-kappa-B-alpha, IkB-alpha, IkappaBalpha, Major histocompatibility complex enhancer-binding protein MAD3
IKBE	LOC105318255	LOC111101116	NF-kappa-B inhibitor epsilon	apoptosis, extrinsic pathway	NFkB pathway	I-kappa-B-epsilon, IkB-E, IkB-epsilon, IkappaBepsilon
NAIF1	LOC105327890	LOC111122449	nuclear apoptosis-inducing factor 1	apoptosis, intrinsic pathway	pathway unclear	None
NFkB2	NA	LOC111126322	nuclear factor NF-kappa-B p100 subunit	apoptosis, extrinsic pathway	NFkB pathway	DNA-binding factor KBF2, Lymphocyte translocation chromosome 10 protein, (Nuclear factor of kappa light polypeptide gene enhancer in B-cells 2) (Oncogene Lyt-10, Lyt10
NFkB1	LOC105325572	LOC111121590	nuclear factor NF-kappa-B p105 subunit	apoptosis, extrinsic pathway	NFkB pathway	DNA-binding factor KBF1, EBP-1, NF-kappa-B1 p84/NF-kappa-B1 p98, Nuclear factor of kappa light polypeptide gene enhancer in B-cells
PDRG1	LOC105317392	LOC111119526	p53 and DNA damage-regulated protein 1	apoptosis, intrinsic pathway	p53 pathway	none
PIK3C3	LOC105334736	LOC111129370	phosphatidylinositol 3-kinase catalytic subunit type 3	apoptosis, intrinsic and extrinsic pathways	GPCR signaling pathway, p53 pathway, growth factor receptor pathway	Phosphatidylinositol 3-kinase p100 subunit, Phosphoinositide-3-kinase class 3, hVps34
PIK3R1	NA	LOC111118072	phosphatidylinositol 3-kinase regulatory subunit alpha	apoptosis, intrinsic and extrinsic pathways	GPCR signaling pathway, ER stress, growth factor receptor pathway	Phosphatidylinositol 3-kinase 85 kDa regulatory subunit alpha

PARP1	LOC105323392	LOC111131837	poly [ADP-ribose] polymerase 1	parthanatos	parthanatos, execution	ADP-ribosyltransferase diphtheria toxin-like 1, DNA ADP-ribosyltransferase PARP1, NAD(+) ADP-ribosyltransferase 1, Poly[ADP-ribose] synthase 1, Protein poly-ADP-ribosyltransferase PARP1
PAWR	LOC105324629	LOC111104168	PRKC apoptosis WT1 regulator protein	apoptosis, intrinsic pathway	TNFR pathway, Bcl2 pathway	Prostate apoptosis response 4 protein, Par-4
PDCD10	LOC105319535	LOC111135606	programmed cell death protein 10	apoptosis, intrinsic pathway	MAPK pathway	Cerebral cavernous malformations 3 protein, TF-1 cell apoptosis-related protein 15
PDCD2	LOC105328904	LOC111122416	programmed cell death protein 2	apoptosis, intrinsic pathway	pathway unclear	Zinc finger MYND domain-containing protein 7, Zinc finger protein Rp-8
PDCD4	LOC105325372	LOC111135600	programmed cell death protein 4	apoptosis, intrinsic pathway	MAPK pathway	Death up-regulated gene protein
PDCD5	LOC105325744	LOC111133889	programmed cell death protein 5	apoptosis, intrinsic pathway	p53 pathway, Bcl2 pathway	TF-1 cell apoptosis-related protein 19, Protein TFAR19
PDCD6	LOC105334025	LOC111121630	programmed cell death protein 6	apoptosis, intrinsic pathway	execution, Calcium signaling	Apoptosis-linked gene 2 protein homolog, ALG-2
PDCD7	LOC105333100	LOC111130466	programmed cell death protein 7	apoptosis, intrinsic pathway	pathway unclear	ES18
BTG1	NA	LOC111106649	protein BTG1	apoptosis, intrinsic pathway	pathway unclear	Anti-proliferative factor, B-cell translocation gene 1 protein, Protein BTG1
PRKCD	LOC105333888	LOC111107462	protein kinase C delta type	apoptosis, intrinsic and extrinsic pathways	p53 pathway, ER stress, TNFR pathway, Bcl2 pathway, NFkB pathway	Tyrosine-protein kinase PRKCD, nPKC-delta
PRKC1	LOC105334479	LOC111134328	protein kinase C iota type	apoptosis, intrinsic and extrinsic pathways	NFkB pathway, Bcl2 pathway	Atypical protein kinase C-lambda/iota, PRKC-lambda/iota, aPKC-lambda/iota, nPKC-iota
PTCH1	LOC105326154	LOC111120833	protein patched homolog 1	dependence receptor pathway	dependence receptor pathway	None
PPM1B	LOC105339254	LOC111129147	protein phosphatase 1B	necroptosis	necroptosis	Protein phosphatase 2C isoform beta, PP2C-beta
REL	LOC105346928	NA	proto-oncogene c-Rel	apoptosis, extrinsic pathway	NFkB pathway	Reticuloendotheliosis oncogene
PIAP	LOC105328992	LOC111132301	putative inhibitor of apoptosis	apoptosis, intrinsic pathway	pathway unclear	none
RELA	LOC105319044	LOC111130067	putative transcription	apoptosis, extrinsic pathway	NFkB pathway	Nuclear factor NF-kappa-B p65 subunit, Nuclear factor of kappa light polypeptide gene enhancer in B-cells 3

			factor p65 homolog			
pyrin	LOC105338982	LOC111120624	pyrin	apoptosis, extrinsic pathway	inflammation	Marenostrin
AKT3	LOC105336892	LOC111130266	RAC-gamma serine/threonine-protein kinase	apoptosis, intrinsic pathway	GPCR signaling pathway, growth factor receptor pathway	Protein kinase Akt-3, Protein kinase B gamma, PKB gamma, RAC-PK-gamma, STK-2
RHO	LOC105342781	LOC111134629	ras-like GTP-binding protein RHO	apoptosis, intrinsic and extrinsic pathways	GPCR signaling pathway	none
RHO1	LOC105342783	NA	ras-like GTP-binding protein Rho1	apoptosis, intrinsic and extrinsic pathways	GPCR signaling pathway	none
RHOA	LOC105321104	LOC111135719	ras-like GTP-binding protein rhoA	apoptosis, intrinsic and extrinsic pathways	GPCR signaling pathway	Ras homolog family member A
RHOL	NA	LOC111130624	ras-like GTP-binding protein RhoL	apoptosis, intrinsic and extrinsic pathways	GPCR signaling pathway	none
RAC1	LOC105333654	LOC111118435	ras-related C3 botulinum toxin substrate 1	apoptosis, intrinsic and extrinsic pathways	GPCR signaling pathway	Cell migration-inducing gene 5 protein, Ras-like protein TC25, p21-Rac1
RIPK1	NA	LOC111134641	receptor-interacting serine/threonine-protein kinase 1	apoptosis extrinsic pathway, necroptosis	necroptosis, TNFR signaling, TLR signaling	Cell death protein RIP, Receptor-interacting protein 1, RIP-1
RIPK4	LOC109619138	LOC111133968	receptor-interacting serine/threonine-protein kinase 4	apoptosis, extrinsic pathway	TLR pathway, NFkB pathway	Ankyrin repeat domain-containing protein 3, PKC-delta-interacting protein kinase
RHOE	LOC105337521	LOC111114558	rho-related GTP-binding protein RhoE	apoptosis, intrinsic and extrinsic pathways	GPCR signaling pathway	Protein MemB, Rho family GTPase 3, Rho-related GTP-binding protein Rho8, Rnd3
RACA	LOC105326415	LOC111103466	rho-related protein racA	apoptosis, intrinsic and extrinsic pathways	GPCR signaling pathway	none
HTRA2	LOC105347711	LOC111133695	serine protease HTRA2, mitochondrial	apoptosis, intrinsic pathway	execution, Bcl2 pathway	High temperature requirement protein A2, Omi stress-regulated endoprotease

ATM	LOC105344838	LOC111135770	serine-protein kinase ATM	apoptosis, intrinsic pathway	DNA damage response	Ataxia telangiectasia mutated
IRE1	LOC105321014	LOC111120876	serine/threonine-protein kinase/endoribonuclease IRE1	apoptosis, extrinsic pathway	ER stress	Endoplasmic reticulum-to-nucleus signaling 1-2, Inositol-requiring protein 1-2, AtIRE1-2, Serine/threonine-protein kinase/endoribonuclease IRE1-2
STAT5A	LOC105335326	LOC111125906	signal transducer and activator of transcription 5A	apoptosis, extrinsic pathway	IFN pathway	None
STAT5B	LOC105325656	LOC111128718	signal transducer and activator of transcription 5B	apoptosis, extrinsic pathway	IFN pathway	None
STATC	LOC105335704	NA	signal transducer and activator of transcription C	apoptosis, extrinsic pathway	IFN pathway	STAT5 homolog C
HSPM	NA	LOC111102062	small heat shock protein hspM	apoptosis, intrinsic pathway	chaperone	none
SARM1	LOC105337295	LOC111134691	sterile alpha and TIR motif-containing protein 1	apoptosis, extrinsic pathway	TLR pathway, NFkB pathway	NAD(+) hydrolase SARM1, NADase SARM1, hSARM1, Sterile alpha and Armadillo repeat protein, Sterile alpha and TIR motif-containing protein 1
STING	LOC105330678	LOC111124607	stimulator of interferon genes protein	apoptosis, extrinsic pathway	IFN pathway	TMEM173
JNK1	LOC105338795	LOC111121739	stress-activated protein kinase JNK	apoptosis, intrinsic and extrinsic pathways	p53 pathway, TNFR pathway, GPCR pathway, Bcl2 pathway	Mitogen-activated protein kinase 8, MAP kinase 8
TAB1	LOC105348086	LOC111118003	TGF-beta-activated kinase 1 and MAP3K7-binding protein 1	apoptosis, extrinsic pathway	TGF-beta pathway, TLR pathway, NFkB pathway	Mitogen-activated protein kinase kinase kinase 7-interacting protein 1, TGF-beta-activated kinase 1-binding protein 1
TAB3	LOC105343186	NA	TGF-beta-activated kinase 1 and MAP3K7-binding protein 3	apoptosis, extrinsic pathway	TGF-beta pathway, TLR pathway, NFkB pathway	TGF-beta-activated kinase 1 and MAP3K7-binding protein 3, NF-kappa-B-activating protein 1, TAK1-binding protein 3
TRAF2	LOC105332371	LOC111123728	TNF receptor-associated factor 2	apoptosis, extrinsic pathway	TNFR pathway, TLR pathway, NFkB pathway	E3 ubiquitin-protein ligase TRAF2, RING-type E3 ubiquitin transferase TRAF2, Tumor necrosis factor type 2 receptor-associated protein 3

TRAF3	LOC105327202	LOC111130375	TNF receptor-associated factor 3	apoptosis, extrinsic pathway	TNFR pathway, TLR pathway, NFkB pathway	CAP-1, CD40 receptor-associated factor 1, CRAF1, CD40-binding protein, CD40BP, LMP1-associated protein 1, LAP1, RING-type E3 ubiquitin transferase TRAF3
TRAF4	LOC105347139	LOC111135695	TNF receptor-associated factor 4	apoptosis, extrinsic pathway	TNFR pathway, TLR pathway, NFkB pathway	Cysteine-rich domain associated with RING and Traf domains protein 1, Metastatic lymph node gene 62 protein, MLN 62, RING finger protein 83
TRAF5	NA	LOC111131697	TNF receptor-associated factor 5	apoptosis, extrinsic pathway	TNFR pathway, TLR pathway, NFkB pathway	RING finger protein 84
TRAF6	LOC105348659	LOC111126076	TNF receptor-associated factor 6	apoptosis, extrinsic pathway	TNFR pathway, TLR pathway, NFkB pathway	E3 ubiquitin-protein ligase TRAF6, Interleukin-1 signal transducer, RING finger protein 85) (RING-type E3 ubiquitin transferase TRAF6)
TRAF6B	LOC105346921	NA	TNF receptor-associated factor 6-B	apoptosis, extrinsic pathway	TNFR pathway, TLR pathway, NFkB pathway	E3 ubiquitin-protein ligase TRAF6, RING-type E3 ubiquitin transferase TRAF6-B
TLR1	LOC105324641	LOC111123291	toll-like receptor 1	apoptosis, extrinsic pathway	TLR pathway, NFkB pathway	Toll/interleukin-1 receptor-like protein, TIL, CD antigen CD281
TLR10	NA	LOC111106502	toll-like receptor 10	apoptosis, extrinsic pathway	TLR pathway, NFkB pathway	CD antigen CD290
TLR13	LOC105334474	LOC111108047	toll-like receptor 13	apoptosis, extrinsic pathway	TLR pathway, NFkB pathway	none
TLR2	LOC105330702	LOC111109580	toll-like receptor 2	apoptosis, extrinsic pathway	TLR pathway, NFkB pathway	Toll/interleukin-1 receptor-like protein 4, CD antigen CD282
TLR2-1	NA	LOC111110584	toll-like receptor 2 type-1	apoptosis, extrinsic pathway	TLR pathway, NFkB pathway	none
TLR2-2	LOC109618244	LOC111118613	toll-like receptor 2 type-2	apoptosis, extrinsic pathway	TLR pathway, NFkB pathway	none
TLR3	LOC109618462	LOC111126105	toll-like receptor 3	apoptosis, extrinsic pathway	TLR pathway, NFkB pathway	CD antigen CD283
TLR4	LOC105318740	LOC111128415	toll-like receptor 4	apoptosis, extrinsic pathway	TLR pathway, NFkB pathway	hToll, CD antigen CD284
TLR6	LOC105344170	LOC111118728	toll-like receptor 6	apoptosis, extrinsic pathway	TLR pathway, NFkB pathway	CD antigen CD286
TLR7	LOC105334681	LOC111132464	toll-like receptor 7	apoptosis, extrinsic pathway	TLR pathway, NFkB pathway	none
TLR8	LOC105325978	LOC111103362	toll-like receptor 8	apoptosis, extrinsic pathway	TLR pathway, NFkB pathway	CD antigen CD288
TLR9	NA	LOC111114412	toll-like receptor 9	apoptosis, extrinsic pathway	TLR pathway, NFkB pathway	CD antigen CD289

Tollo	LOC105326951	LOC111103601	toll-like receptor Tollo	apoptosis, extrinsic pathway	TLR pathway, NFkB pathway	Tollo Tl-8, Toll-8, CG6890
TP53BP1	NA	LOC111131374	TP53-binding protein 1	apoptosis, instrinsic pathway	p53 pathway	p53-binding protein 1
c-Jun	LOC105341654	LOC111120138	transcription factor AP-1	apoptosis, instrinsic and extrinsic pathway	NFkB pathway, TNFR pathway, TLR pathway, GPCR signaling	Activator protein 1, AP1, Proto-oncogene c-Jun, V-jun avian sarcoma virus 17 oncogene homolog, p39
Myc-a	LOC105337948	LOC111121429	transcriptional regulator Myc-A	apoptosis, extrinsic pathway	growth factor receptor pathway	c-Myc-A, zc-Myc
TNF	LOC105344501	NA	tumor necrosis factor	apoptosis, extrinsic pathway	TNFR pathway	Cachectin, TNF-alpha, Tumor necrosis factor ligand superfamily member 2, TNF-a
A20	LOC105347244	LOC111134417	tumor necrosis factor alpha-induced protein 3	apoptosis, extrinsic pathway, necroptosis	necroptosis, TNFR pathway, TLR pathway, NFkB pathway	A20, OTU domain-containing protein 7C, Putative DNA-binding protein A20, Zinc finger protein A20
TNFAIP8	LOC105320815	LOC111129502	tumor necrosis factor alpha-induced protein 8	apoptosis, extrinsic pathway	TNFR pathway	Head and neck tumor and metastasis-related protein, MDC-3.13, NF-kappa-B-inducible DED-containing protein, NDED, SCC-S2, TNF-induced protein GG2-1
TRAIL	LOC105326166	LOC111133004	tumor necrosis factor ligand superfamily member 10	apoptosis, extrinsic pathway	TNFR pathway	TNF-related apoptosis inducing ligand, Tumor necrosis factor ligand superfamily member 10, Protein TRAIL, CD antigen CD253, TNFSF10, Apo2L
TNFRSF16	LOC105346085	LOC111125492	tumor necrosis factor receptor superfamily member 16	apoptosis, extrinsic pathway	TNFR pathway	Gp80-LNGFR, Low affinity neurotrophin receptor p75NTR, Low-affinity nerve growth factor receptor, NGF receptor, p75 ICD, CD antigen CD271
TNFRSF19	LOC105338387	NA	tumor necrosis factor receptor superfamily member 19	apoptosis, extrinsic pathway	TNFR pathway	TRADE, Toxicity and JNK inducer
TNFRSF1A	NA	LOC111106184	tumor necrosis factor receptor superfamily member 1A	apoptosis, extrinsic pathway	TNFR pathway	Tumor necrosis factor receptor 1, TNF-R1, Tumor necrosis factor receptor type I, TNF-RI, TNFR-I, p55, p60, CD antigen CD120a
TNFRSF27	LOC105335155	NA	tumor necrosis factor receptor superfamily member 27	apoptosis, extrinsic pathway	TNFR pathway	X-linked ectodysplasin-A2 receptor, EDA-A2 receptor
TNFRSF5	LOC105348770	LOC111135959	tumor necrosis factor receptor	apoptosis, extrinsic pathway	TNFR pathway	B-cell surface antigen CD40, Bp50, CD40L receptor, CDw40, CD antigen CD40

			superfamily member 5			
JAK2	LOC105333485	LOC111128838	tyrosine-protein kinase JAK2	apoptosis, extrinsic pathway	IFN pathway	Janus Kinase 2
FAP1	LOC105347683	LOC111118576	tyrosine-protein phosphatase non-receptor type 13	apoptosis, extrinsic pathway	IFN pathway, TNFR pathway	Fas-associated protein-tyrosine phosphatase 1, Protein-tyrosine phosphatase 1E, Protein-tyrosine phosphatase PTPL1
*IAP**	LOC105321414	NA	uncharacterized LOC105321414	apoptosis, intrinsic pathway	putative IAP	putative IAP
*IAP**	LOC105325768	NA	uncharacterized LOC105325768	apoptosis, intrinsic pathway	putative IAP	putative IAP
*IAP**	LOC105333871	NA	uncharacterized LOC105333871	apoptosis, intrinsic pathway	putative IAP	putative IAP
*IAP**	LOC105335294	NA	uncharacterized LOC105335294	apoptosis, intrinsic pathway	putative IAP	putative IAP
*IAP**	LOC105335299	NA	uncharacterized LOC105335299	apoptosis, intrinsic pathway	putative IAP	putative IAP
*IAP**	LOC105337800	NA	uncharacterized LOC105337800	apoptosis, intrinsic pathway	putative IAP	putative IAP
*IAP**	LOC105339790	NA	uncharacterized LOC105339790	apoptosis, intrinsic pathway	putative IAP	putative IAP
*IAP**	LOC105340029	NA	uncharacterized LOC105340029	apoptosis, intrinsic pathway	putative IAP	putative IAP
*IAP**	LOC105343630	NA	uncharacterized LOC105343630	apoptosis, intrinsic pathway	putative IAP	putative IAP
*IAP**	NA	LOC111100017	uncharacterized LOC111100017	apoptosis, intrinsic pathway	putative IAP	putative IAP
*IAP**	NA	LOC111100019	uncharacterized LOC111100019	apoptosis, intrinsic pathway	putative IAP	putative IAP
*IAP**	NA	LOC111100394	uncharacterized LOC111100394	apoptosis, intrinsic pathway	putative IAP	putative IAP
*IAP**	NA	LOC111100400	uncharacterized LOC111100400	apoptosis, intrinsic pathway	putative IAP	putative IAP
*IAP**	NA	LOC111100402	uncharacterized LOC111100402	apoptosis, intrinsic pathway	putative IAP	putative IAP
*IAP**	NA	LOC111100407	uncharacterized LOC111100407	apoptosis, intrinsic pathway	putative IAP	putative IAP
*IAP**	NA	LOC111100411	uncharacterized LOC111100411	apoptosis, intrinsic pathway	putative IAP	putative IAP

*IAP**	NA	LOC111100414	uncharacterized LOC111100414	apoptosis, intrinsic pathway	putative IAP	putative IAP
*IAP**	NA	LOC111100858	uncharacterized LOC111100858	apoptosis, intrinsic pathway	putative IAP	putative IAP
*IAP**	NA	LOC111101678	uncharacterized LOC111101678	apoptosis, intrinsic pathway	putative IAP	putative IAP
*IAP**	NA	LOC111103391	uncharacterized LOC111103391	apoptosis, intrinsic pathway	putative IAP	putative IAP
*IAP**	NA	LOC111112532	uncharacterized LOC111112532	apoptosis, intrinsic pathway	putative IAP	putative IAP
*IAP**	NA	LOC111122723	uncharacterized LOC111122723	apoptosis, intrinsic pathway	putative IAP	putative IAP
*IAP**	NA	LOC111122858	uncharacterized LOC111122858	apoptosis, intrinsic pathway	putative IAP	putative IAP

**Genes putatively identified as IAPs in this research*

Supplementary Table 5: *C. virginica* and *C. gigas* Immune Challenge Apoptosis Differential Expression.

Experiment	Challenge Group	Total Significant DEGs	Apoptosis DEGS	Percent Apoptosis DEGs
CVBAC-B	RI	1762	37	2
CVBAC-A Probiotic/Vibrio RE22	RI 6h	1795	31	2
	RI 24h	2569	57	2
	S4 6h	2424	52	2
	S4 24h	3683	64	2
	RE22	2005	38	2
CVBAC-C	ROD Susceptible	2020	46	2
	ROD Resistant	68	5	7
CVPMA	Susceptible 36h	617	15	2
	Susceptible 7d	378	4	1
	Susceptible 28d	2642	38	1
	Tolerant 36h	747	17	2
	Tolerant 7d	989	16	2
	Tolerant 28d	437	20	5
CGBAC-A	*V. aes.*, *V. alg.1*, *V. alg.2*	1322	26	2
	V. tub., *V. ang.*	882	18	2

	LPS, *M. lut.*	833	20	2
CGBAC-B	J2-8 Non-Virulent	3532	81	2
	J2-9 Virulent	3719	90	2
	LGP32 Virulent	3783	92	2
	LMG20012T Non-Virulent	3571	81	2
CGOSHV1-B	6h	783	28	4
	12h	936	34	4
	24h	2895	75	3
	48h	836	26	3
	120h	991	21	2
CGOSHV1-A Susceptible	Susceptible 6h	1445	36	2
	Susceptible 12h	3435	110	3
	Susceptible 24h	8298	201	2
	Susceptible 48h	1778	43	2
	Susceptible 60h	10425	235	2
	Susceptible 72h	2991	63	2
CGOSHV1-A Resistant	Resistant 6h	1644	31	2
	Resistant 12h	2691	69	3
	Resistant 24h	3775	101	3
	Resistant 48h	1593	31	2
	Resistant 60h	3403	77	2
	Resistant 72h	2309	43	2

Supplementary Table 6: *C. virginica* and *C. gigas* Immune Challenge Apoptosis Co-Expression.

Experiment	Significant modules with Apoptosis transcripts	Total Apoptosis-related transcripts	Total Apoptosis-related Genes	Total IAP Transcripts Across Significant Modules	Total IAP Genes Across Significant Modules	Percent of total IAP Genes	Total IAP Domain Structure Types
CVBAC-B	3	53	45	4	4	6	3
CVBAC-A - RI	10	192	174	26	26	38	12
CVBAC-A - S4	10	128	117	20	20	29	10
CVBAC-A - Vibrio RE22	2	100	96	14	13	19	7
CVBAC-C - Susceptible	*	*	*	*	*	*	*
CVBAC-C - Resistant	1	8	8	2	2	3	1
CVPMA - Susceptible	2	5	5	2	2	3	1
CVPMA - Tolerant	4	74	72	8	8	12	7
CGBAC-A - LPS, M. lut	10	109	104	17	17	25	8
CGBAC-A - Vibrio spp.	3	23	23	5	5	7	3

CGBAC-B - Non-virulent Vibrio spp.	7	210	179	17	16	23	9
CGBAC-B - Virulent Vibrio spp.	8	219	188	18	17	25	9
CGOSHV1-B	5	160	153	15	15	22	9
CGOSHV1-A Susceptible	2	95	84	3	3	4	3
CGOSHV1-A Resistant	2	131	123	9	9	13	8

** = No significant modules*

Supplementary Table 7: Domain Architectures of IAP Transcripts Significantly Co-expressed with Immune Challenge. * = IAP Domain Identified by Interproscan and not CDD search.

Name	Domain Architecture	CVBAC-B	CVBAC-A-RI	CVBAC-A - S4	CVBAC-A - RE22	CVBAC-C - Resistant	CVPMA Susceptible	CVPMA Tolerant	CGBAC-A - LPS, M. lut	CGBAC-A - Vibrio spp.	CGBAC-B - Non-virulent Vibrio spp.	CGBAC-B - Virulent Vibrio spp.	CGOSHV1-B	CGOSHV1-A Susceptible	CGOSHV1-A Resistant
DIAP1-like	TI-TII-RING	0	1	1	1	0	0	1	0	0	0	0	0	0	0
DIAP2-like/XIAP-like	TI-TII-TII-UBA-RING	0	1	0	0	0	0	1	0	0	1	1	0	0	0
BIRC2/3-like	TI-TII-DD-RING	1	2	0	3	0	0	2	5	2	2	2	2	1	1
BIRC2/3-like	NZBIR-TII-UBA-DD-RING	0	0	0	0	0	0	0	1	0	0	0	1	0	0
BIRC5-like	BIR*	1	0	2	1	0	0	1	0	0	0	0	1	0	1
BIRC5-like	TII	0	0	0	0	0	0	0	1	0	0	0	0	0	0
BIRC6-like	TII-BIR6-E2	0	3	1	0	0	0	0	1	0	0	0	1	1	0
BIRC7-like	TII-RING	0	1	1	0	0	0	1	0	0	1	1	1	0	0
BIRC9	TII-TII	0	1	0	2	0	0	0	0	0	1	1	0	0	1
BIRC9	TX-TII	0	2	3	3	0	0	0	0	0	1	1	1	0	1
BIRC10	TII-DD	0	2	3	0	0	0	0	1	0	4	4	2	0	0
BIRC11	BIR*-DD-RING	0	1	2	1	0	0	0	0	0	2	2	0	0	1
BIRC11	TII-DD-RING	0	1	3	0	0	0	1	2	0	2	2	2	0	2
BIRC12	TII-TII-RING	0	5	2	0	0	2	0	2	1	0	0	0	0	1
NA	Non-Domain Grouped	2	6	2	3	2	0	1	4	2	3	4	4	1	1

Supplementary Table 8: Molluscan Genome Metadata.

Organism Name	**Common Name**	**Phylum**	**Assembly**	**Level**	**Size(Mb)**	**GC%**	**WGS**	**Scaffolds**	**CDS**	**Release Date**
Aplysia californica	california sea hare (sea slug)	Mollusca	GCA_000002075.2	Scaffold	927.31	41.9999	AASC03	4332	27608	2006-08-17T00:00:00Z
Biomphalaria glabrata	marsh snail	Mollusca	GCA_000457365.1	Scaffold	916.388	36.1998	APKA01	331401	36675	2013-08-09T00:00:00Z
Crassostrea gigas	Pacific oyster	Mollusca	GCA_000297895.1	Scaffold	557.736	35.3	AFTI01	7659	46753	2012-09-17T00:00:00Z
Crassostrea virginica	eastern oyster	Mollusca	GCA_002022765.4	Chromosome	684.741	34.8191	MWPT03	11	60213	2017-03-07T00:00:00Z
Elysia chlorotica	eastern emerald elysia	Mollusca	GCA_003991915.1	Scaffold	557.48	36.5	RQTK01	9989	23871	2019-01-04T00:00:00Z
Lottia gigantea	owl limpet	Mollusca	GCA_000327385.1	Scaffold	359.506	36	AMQO01	4469	23822	2012-12-20T00:00:00Z
Mizuhopecten yessoensis	japanese scallop	Mollusca	GCA_002113885.1	Scaffold	987.589	37.6001	NEDP02	82659	41567	2017-04-27T00:00:00Z
Octopus bimaculoides	california two spot octopus	Mollusca	GCA_001194135.1	Scaffold	2338.19	37.8	LGKD01	151674	23994	2015-07-31T00:00:00Z
Octopus vulgaris (sinensis)	east asian common octopus	Mollusca	GCA_006345805.1	Chromosome	2719.15	36.3702	VCDQ01	13516	25656	2019-06-14T00:00:00Z
Pomacea canaliculata	golden apple snail	Mollusca	GCA_003073045.1	Chromosome	440.16	40.6223	PZQS01	24	40391	2018-04-26T00:00:00Z

Supplementary Table 9: *C. virginica* IAP Haplotig Identification.

Species	**Haplotig Gene**	**Haplotig Protein Accession**	**Haplotig Mean Coverage**	**Gene Haplotig Collapsed Into**	**Protein Haplotig Collapsed Into**	**Coverage of Protein Haplotig Collapsed Into**
C. virginica	LOC111114013	XP_022308010.1	103.34	LOC111132489	XP_022336007.1	890.4
C. virginica	LOC111103682	XP_022292821.1	103.1	LOC111132301	XP_022335805.1	383.9
C. virginica	LOC111132589	XP_022336127.1	223.2	LOC111132301	XP_022335805.1	383.9
C. virginica	LOC111102106	XP_022290466.1	148.7	LOC111132301	XP_022335805.1	383.9
C. virginica	LOC111114070	XP_022308067.1	113.5	LOC111132301	XP_022335805.1	383.9
C. virginica	LOC111111659	XP_022304464.1	85	LOC111116826	XP_022311552.1	373.4

Supplementary Table 10: *C. virginica* and *C. gigas* Transcriptome Experiment Metadata.

EXPERIMENT	RUN	ASSAY TYPE	BIOPROJECT	BIOSAMPLE
CVBAC-A	SRR10982739	RNA-Seq	PRJNA603627	SAMN13938801
CVBAC-A	SRR10982729	RNA-Seq	PRJNA603627	SAMN13938795
CVBAC-A	SRR10982743	RNA-Seq	PRJNA603627	SAMN13938789
CVBAC-A	SRR10982736	RNA-Seq	PRJNA603627	SAMN13938804
CVBAC-A	SRR10982726	RNA-Seq	PRJNA603627	SAMN13938798
CVBAC-A	SRR10982732	RNA-Seq	PRJNA603627	SAMN13938792
CVBAC-A	SRR10982734	RNA-Seq	PRJNA603627	SAMN13938806
CVBAC-A	SRR10982737	RNA-Seq	PRJNA603627	SAMN13938803
CVBAC-A	SRR10982740	RNA-Seq	PRJNA603627	SAMN13938800
CVBAC-A	SRR10982727	RNA-Seq	PRJNA603627	SAMN13938797
CVBAC-A	SRR10982730	RNA-Seq	PRJNA603627	SAMN13938794
CVBAC-A	SRR10982733	RNA-Seq	PRJNA603627	SAMN13938791
CVBAC-A	SRR10982735	RNA-Seq	PRJNA603627	SAMN13938805
CVBAC-A	SRR10982738	RNA-Seq	PRJNA603627	SAMN13938802
CVBAC-A	SRR10982741	RNA-Seq	PRJNA603627	SAMN13938799
CVBAC-A	SRR10982728	RNA-Seq	PRJNA603627	SAMN13938796
CVBAC-A	SRR10982731	RNA-Seq	PRJNA603627	SAMN13938793
CVBAC-A	SRR10982742	RNA-Seq	PRJNA603627	SAMN13938790
CVBAC-B	SRR5357618	RNA-Seq	PRJNA376014	SAMN06617317
CVBAC-B	SRR5357623	RNA-Seq	PRJNA376014	SAMN06617325
CVBAC-B	SRR5357617	RNA-Seq	PRJNA376014	SAMN06617320
CVBAC-B	SRR5357619	RNA-Seq	PRJNA376014	SAMN06617322
CVBAC-B	SRR5357622	RNA-Seq	PRJNA376014	SAMN06617319
CVBAC-B	SRR5357626	RNA-Seq	PRJNA376014	SAMN06617323
CVBAC-C	SRR1298387	RNA-Seq	PRJNA248114	SAMN02797586
CVBAC-C	SRR1298417	RNA-Seq	PRJNA248114	SAMN02797576
CVBAC-C	SRR1298421	RNA-Seq	PRJNA248114	SAMN02797578
CVBAC-C	SRR1298693	RNA-Seq	PRJNA248114	SAMN02797579
CVBAC-C	SRR1298698	RNA-Seq	PRJNA248114	SAMN02797581
CVBAC-C	SRR1298701	RNA-Seq	PRJNA248114	SAMN02797582
CVBAC-C	SRR1298703	RNA-Seq	PRJNA248114	SAMN02797583
CVBAC-C	SRR1298704	RNA-Seq	PRJNA248114	SAMN02797584
CVBAC-C	SRR1298708	RNA-Seq	PRJNA248114	SAMN02797585
CVBAC-C	SRR1298710	RNA-Seq	PRJNA248114	SAMN02797577
CVBAC-C	SRR1298711	RNA-Seq	PRJNA248114	SAMN02797580
CVBAC-C	SRR1293904	RNA-Seq	PRJNA248114	SAMN02786835
CVPMA	SRR10482816	RNA-Seq	PRJNA590205	SAMN13321312

CVPMA	SRR10482817	RNA-Seq	PRJNA590205	SAMN13321311
CVPMA	SRR10482818	RNA-Seq	PRJNA590205	SAMN13321310
CVPMA	SRR10482819	RNA-Seq	PRJNA590205	SAMN13321309
CVPMA	SRR10482820	RNA-Seq	PRJNA590205	SAMN13321308
CVPMA	SRR10482821	RNA-Seq	PRJNA590205	SAMN13321307
CVPMA	SRR10482822	RNA-Seq	PRJNA590205	SAMN13321271
CVPMA	SRR10482823	RNA-Seq	PRJNA590205	SAMN13321306
CVPMA	SRR10482824	RNA-Seq	PRJNA590205	SAMN13321305
CVPMA	SRR10482825	RNA-Seq	PRJNA590205	SAMN13321304
CVPMA	SRR10482826	RNA-Seq	PRJNA590205	SAMN13321303
CVPMA	SRR10482827	RNA-Seq	PRJNA590205	SAMN13321302
CVPMA	SRR10482828	RNA-Seq	PRJNA590205	SAMN13321301
CVPMA	SRR10482829	RNA-Seq	PRJNA590205	SAMN13321300
CVPMA	SRR10482830	RNA-Seq	PRJNA590205	SAMN13321299
CVPMA	SRR10482831	RNA-Seq	PRJNA590205	SAMN13321298
CVPMA	SRR10482832	RNA-Seq	PRJNA590205	SAMN13321297
CVPMA	SRR10482833	RNA-Seq	PRJNA590205	SAMN13321270
CVPMA	SRR10482834	RNA-Seq	PRJNA590205	SAMN13321296
CVPMA	SRR10482835	RNA-Seq	PRJNA590205	SAMN13321295
CVPMA	SRR10482836	RNA-Seq	PRJNA590205	SAMN13321276
CVPMA	SRR10482837	RNA-Seq	PRJNA590205	SAMN13321275
CVPMA	SRR10482838	RNA-Seq	PRJNA590205	SAMN13321274
CVPMA	SRR10482839	RNA-Seq	PRJNA590205	SAMN13321328
CVPMA	SRR10482840	RNA-Seq	PRJNA590205	SAMN13321327
CVPMA	SRR10482841	RNA-Seq	PRJNA590205	SAMN13321273
CVPMA	SRR10482842	RNA-Seq	PRJNA590205	SAMN13321326
CVPMA	SRR10482843	RNA-Seq	PRJNA590205	SAMN13321325
CVPMA	SRR10482844	RNA-Seq	PRJNA590205	SAMN13321280
CVPMA	SRR10482845	RNA-Seq	PRJNA590205	SAMN13321323
CVPMA	SRR10482846	RNA-Seq	PRJNA590205	SAMN13321322
CVPMA	SRR10482847	RNA-Seq	PRJNA590205	SAMN13321321
CVPMA	SRR10482848	RNA-Seq	PRJNA590205	SAMN13321320
CVPMA	SRR10482849	RNA-Seq	PRJNA590205	SAMN13321319
CVPMA	SRR10482850	RNA-Seq	PRJNA590205	SAMN13321318
CVPMA	SRR10482851	RNA-Seq	PRJNA590205	SAMN13321317
CVPMA	SRR10482852	RNA-Seq	PRJNA590205	SAMN13321272
CVPMA	SRR10482853	RNA-Seq	PRJNA590205	SAMN13321316
CVPMA	SRR10482854	RNA-Seq	PRJNA590205	SAMN13321315
CVPMA	SRR10482855	RNA-Seq	PRJNA590205	SAMN13321314
CVPMA	SRR10482856	RNA-Seq	PRJNA590205	SAMN13321313

CVPMA	SRR10482857	RNA-Seq	PRJNA590205	SAMN13321294
CVPMA	SRR10482858	RNA-Seq	PRJNA590205	SAMN13321293
CVPMA	SRR10482859	RNA-Seq	PRJNA590205	SAMN13321292
CVPMA	SRR10482860	RNA-Seq	PRJNA590205	SAMN13321291
CVPMA	SRR10482861	RNA-Seq	PRJNA590205	SAMN13321290
CVPMA	SRR10482862	RNA-Seq	PRJNA590205	SAMN13321289
CVPMA	SRR10482863	RNA-Seq	PRJNA590205	SAMN13321288
CVPMA	SRR10482864	RNA-Seq	PRJNA590205	SAMN13321287
CVPMA	SRR10482865	RNA-Seq	PRJNA590205	SAMN13321269
CVPMA	SRR10482866	RNA-Seq	PRJNA590205	SAMN13321286
CVPMA	SRR10482867	RNA-Seq	PRJNA590205	SAMN13321285
CVPMA	SRR10482868	RNA-Seq	PRJNA590205	SAMN13321284
CVPMA	SRR10482869	RNA-Seq	PRJNA590205	SAMN13321283
CVPMA	SRR10482870	RNA-Seq	PRJNA590205	SAMN13321282
CVPMA	SRR10482871	RNA-Seq	PRJNA590205	SAMN13321281
CVPMA	SRR10482872	RNA-Seq	PRJNA590205	SAMN13321324
CVPMA	SRR10482873	RNA-Seq	PRJNA590205	SAMN13321279
CVPMA	SRR10482874	RNA-Seq	PRJNA590205	SAMN13321278
CVPMA	SRR10482875	RNA-Seq	PRJNA590205	SAMN13321277
CVPMA	SRR10482876	RNA-Seq	PRJNA590205	SAMN13321268
CVPMA	SRR10482877	RNA-Seq	PRJNA590205	SAMN13321267
CGBAC-A	SRR796589	RNA-Seq	PRJNA194084	SAMN01986149
CGBAC-A	SRR796591	RNA-Seq	PRJNA194084	SAMN01986150
CGBAC-A	SRR796592	RNA-Seq	PRJNA194084	SAMN01986151
CGBAC-A	SRR796593	RNA-Seq	PRJNA194084	SAMN01986152
CGBAC-A	SRR796594	RNA-Seq	PRJNA194084	SAMN01986153
CGBAC-A	SRR796595	RNA-Seq	PRJNA194084	SAMN01986154
CGBAC-A	SRR796596	RNA-Seq	PRJNA194084	SAMN01986155
CGBAC-A	SRR796597	RNA-Seq	PRJNA194084	SAMN01986156
CGBAC-A	SRR796598	RNA-Seq	PRJNA194084	SAMN01986157
CGBAC-B	SRR8551077	RNA-Seq	PRJNA515169	SAMN10762892
CGBAC-B	SRR8551079	RNA-Seq	PRJNA515169	SAMN10762900
CGBAC-B	SRR8551080	RNA-Seq	PRJNA515169	SAMN10762907
CGBAC-B	SRR8551081	RNA-Seq	PRJNA515169	SAMN10762908
CGBAC-B	SRR8551084	RNA-Seq	PRJNA515169	SAMN10762903
CGBAC-B	SRR8551086	RNA-Seq	PRJNA515169	SAMN10762901
CGBAC-B	SRR8551088	RNA-Seq	PRJNA515169	SAMN10762897
CGBAC-B	SRR8551076	RNA-Seq	PRJNA515169	SAMN10762891
CGBAC-B	SRR8551078	RNA-Seq	PRJNA515169	SAMN10762899
CGBAC-B	SRR8551082	RNA-Seq	PRJNA515169	SAMN10762905

CGBAC-B	SRR8551083	RNA-Seq	PRJNA515169	SAMN10762906
CGBAC-B	SRR8551085	RNA-Seq	PRJNA515169	SAMN10762904
CGBAC-B	SRR8551087	RNA-Seq	PRJNA515169	SAMN10762902
CGBAC-B	SRR8551089	RNA-Seq	PRJNA515169	SAMN10762898
CGBAC-B	SRR8551090	RNA-Seq	PRJNA515169	SAMN10762895
CGBAC-B	SRR8551091	RNA-Seq	PRJNA515169	SAMN10762896
CGBAC-B	SRR8551092	RNA-Seq	PRJNA515169	SAMN10762893
CGBAC-B	SRR8551093	RNA-Seq	PRJNA515169	SAMN10762894
CGOSHV1-B	SRR2002822	RNA-Seq	PRJNA282703	SAMN03575960
CGOSHV1-B	SRR2002845	RNA-Seq	PRJNA282703	SAMN03575961
CGOSHV1-B	SRR2002864	RNA-Seq	PRJNA282703	SAMN03575962
CGOSHV1-B	SRR2002935	RNA-Seq	PRJNA282703	SAMN03575962
CGOSHV1-B	SRR2002936	RNA-Seq	PRJNA282703	SAMN03575963
CGOSHV1-B	SRR2002938	RNA-Seq	PRJNA282703	SAMN03575963
CGOSHV1-B	SRR2002941	RNA-Seq	PRJNA282703	SAMN03575964
CGOSHV1-B	SRR2002943	RNA-Seq	PRJNA282703	SAMN03575965
CGOSHV1-B	SRR2002945	RNA-Seq	PRJNA282703	SAMN03575965
CGOSHV1-B	SRR2002948	RNA-Seq	PRJNA282703	SAMN03575966
CGOSHV1-B	SRR2002950	RNA-Seq	PRJNA282703	SAMN03575967
CGOSHV1-B	SRR2002952	RNA-Seq	PRJNA282703	SAMN03575967
CGOSHV1-B	SRR2002954	RNA-Seq	PRJNA282703	SAMN03575968
CGOSHV1-B	SRR2002957	RNA-Seq	PRJNA282703	SAMN03575969
CGOSHV1-B	SRR2002959	RNA-Seq	PRJNA282703	SAMN03575970
CGOSHV1-B	SRR2002961	RNA-Seq	PRJNA282703	SAMN03575970
CGOSHV1-B	SRR2002821	RNA-Seq	PRJNA282703	SAMN03575960
CGOSHV1-B	SRR2002823	RNA-Seq	PRJNA282703	SAMN03575960
CGOSHV1-B	SRR2002846	RNA-Seq	PRJNA282703	SAMN03575961
CGOSHV1-B	SRR2002934	RNA-Seq	PRJNA282703	SAMN03575962
CGOSHV1-B	SRR2002940	RNA-Seq	PRJNA282703	SAMN03575964
CGOSHV1-B	SRR2002942	RNA-Seq	PRJNA282703	SAMN03575964
CGOSHV1-B	SRR2002944	RNA-Seq	PRJNA282703	SAMN03575965
CGOSHV1-B	SRR2002947	RNA-Seq	PRJNA282703	SAMN03575966
CGOSHV1-B	SRR2002949	RNA-Seq	PRJNA282703	SAMN03575966
CGOSHV1-B	SRR2002951	RNA-Seq	PRJNA282703	SAMN03575967
CGOSHV1-B	SRR2002953	RNA-Seq	PRJNA282703	SAMN03575968
CGOSHV1-B	SRR2002955	RNA-Seq	PRJNA282703	SAMN03575968
CGOSHV1-B	SRR2002956	RNA-Seq	PRJNA282703	SAMN03575969
CGOSHV1-B	SRR2002958	RNA-Seq	PRJNA282703	SAMN03575969
CGOSHV1-B	SRR2002962	RNA-Seq	PRJNA282703	SAMN03575970
CGOSHV1-B	SRR2002844	RNA-Seq	PRJNA282703	SAMN03575961

CGOSHV1-A	SRR6679052	RNA-Seq	PRJNA423079	SAMN08382971
CGOSHV1-A	SRR6679053	RNA-Seq	PRJNA423079	SAMN08382970
CGOSHV1-A	SRR6679054	RNA-Seq	PRJNA423079	SAMN08382967
CGOSHV1-A	SRR6679055	RNA-Seq	PRJNA423079	SAMN08382966
CGOSHV1-A	SRR6679056	RNA-Seq	PRJNA423079	SAMN08382969
CGOSHV1-A	SRR6679057	RNA-Seq	PRJNA423079	SAMN08382968
CGOSHV1-A	SRR6679058	RNA-Seq	PRJNA423079	SAMN08382963
CGOSHV1-A	SRR6679059	RNA-Seq	PRJNA423079	SAMN08382962
CGOSHV1-A	SRR6679060	RNA-Seq	PRJNA423079	SAMN08382965
CGOSHV1-A	SRR6679061	RNA-Seq	PRJNA423079	SAMN08382964
CGOSHV1-A	SRR6679062	RNA-Seq	PRJNA423079	SAMN08382949
CGOSHV1-A	SRR6679063	RNA-Seq	PRJNA423079	SAMN08382948
CGOSHV1-A	SRR6679064	RNA-Seq	PRJNA423079	SAMN08382947
CGOSHV1-A	SRR6679065	RNA-Seq	PRJNA423079	SAMN08382946
CGOSHV1-A	SRR6679066	RNA-Seq	PRJNA423079	SAMN08382945
CGOSHV1-A	SRR6679068	RNA-Seq	PRJNA423079	SAMN08382943
CGOSHV1-A	SRR6679069	RNA-Seq	PRJNA423079	SAMN08382942
CGOSHV1-A	SRR6679070	RNA-Seq	PRJNA423079	SAMN08382951
CGOSHV1-A	SRR6679071	RNA-Seq	PRJNA423079	SAMN08382950
CGOSHV1-A	SRR6679072	RNA-Seq	PRJNA423079	SAMN08382937
CGOSHV1-A	SRR6679073	RNA-Seq	PRJNA423079	SAMN08382936
CGOSHV1-A	SRR6679075	RNA-Seq	PRJNA423079	SAMN08382938
CGOSHV1-A	SRR6679076	RNA-Seq	PRJNA423079	SAMN08382933
CGOSHV1-A	SRR6679077	RNA-Seq	PRJNA423079	SAMN08382932
CGOSHV1-A	SRR6679078	RNA-Seq	PRJNA423079	SAMN08382935
CGOSHV1-A	SRR6679079	RNA-Seq	PRJNA423079	SAMN08382934
CGOSHV1-A	SRR6679080	RNA-Seq	PRJNA423079	SAMN08382941
CGOSHV1-A	SRR6679081	RNA-Seq	PRJNA423079	SAMN08382940
CGOSHV1-A	SRR6679082	RNA-Seq	PRJNA423079	SAMN08382972
CGOSHV1-A	SRR6679083	RNA-Seq	PRJNA423079	SAMN08382973
CGOSHV1-A	SRR6679084	RNA-Seq	PRJNA423079	SAMN08382960
CGOSHV1-A	SRR6679085	RNA-Seq	PRJNA423079	SAMN08382961
CGOSHV1-A	SRR6679086	RNA-Seq	PRJNA423079	SAMN08382958
CGOSHV1-A	SRR6679087	RNA-Seq	PRJNA423079	SAMN08382959
CGOSHV1-A	SRR6679088	RNA-Seq	PRJNA423079	SAMN08382956
CGOSHV1-A	SRR6679089	RNA-Seq	PRJNA423079	SAMN08382957
CGOSHV1-A	SRR6679090	RNA-Seq	PRJNA423079	SAMN08382954
CGOSHV1-A	SRR6679091	RNA-Seq	PRJNA423079	SAMN08382955
CGOSHV1-A	SRR6679092	RNA-Seq	PRJNA423079	SAMN08382952
CGOSHV1-A	SRR6679093	RNA-Seq	PRJNA423079	SAMN08382953

CGOSHV1-A	SRR6679074	RNA-Seq	PRJNA423079	SAMN08382939
CGOSHV1-A	SRR6679067	RNA-Seq	PRJNA423079	SAMN08382944

Supplementary Table 11: *C. virginica* and *C. gigas* Transcriptome Experiment DESeq2 Analysis Data.

Experiment ID	**Run**	**Condition**	**Family**	**Experiment**	**Sample**	**Time**	**Tech Rep**	***Species***	**DESeq2 Formula**	**Analysis Description**
CVBAC-A	SRR10982739	Control_no_treatment	Pro_RE22	Pro_RE22	C_K_0	10d	Rep1	*C. virginica*	~`Time + Condition`	CVBAC-A transcriptomes from three different larval sources were compared to untreated control and corrected for the effect of time using the model ~`Time + Condition`
CVBAC-A	SRR10982729	Control_no_treatment	Pro_RE22	Pro_RE22	C_M_0	6d	Rep1	*C. virginica*	~`Time + Condition`	CVBAC-A transcriptomes from three different larval sources were compared to untreated control and corrected for the effect of time using the model ~`Time + Condition`
CVBAC-A	SRR10982743	Control_no_treatment	Pro_RE22	Pro_RE22	C_V_0	7d	Rep1	*C. virginica*	~`Time + Condition`	CVBAC-A transcriptomes from three different larval sources were compared to untreated control and corrected for the effect of time using the model ~`Time + Condition`
CVBAC-A	SRR10982734	Bacillus_pumilus_RI06_95_exposure_24h	Pro_RE22	Pro_RE22	RI_K_24	10d	Rep1	*C. virginica*	~`Time + Condition`	CVBAC-A transcriptomes from three different larval sources were compared to untreated control and corrected for the effect of time using the model ~`Time + Condition`
CVBAC-A	SRR10982740	Bacillus_pumilus_RI06_95_exposure_24h	Pro_RE22	Pro_RE22	RI_M_24	6d	Rep1	*C. virginica*	~`Time + Condition`	CVBAC-A transcriptomes from three different larval sources were compared to untreated control and corrected for the effect of time using the model ~`Time + Condition`
CVBAC-A	SRR10982730	Bacillus_pumilus_RI06_95_exposure_24h	Pro_RE22	Pro_RE22	RI_V_24	7d	Rep1	*C. virginica*	~`Time + Condition`	CVBAC-A transcriptomes from three different larval sources were compared to untreated control and corrected for the effect of time using the model ~`Time + Condition`
CVBAC-A	SRR10982737	Bacillus_pumilus_RI06_95_exposure_6h	Pro_RE22	Pro_RE22	RI_K_6	10d	Rep1	*C. virginica*	~`Time + Condition`	CVBAC-A transcriptomes from three different larval sources were compared to untreated control and corrected for the effect of time using the model ~`Time + Condition`
CVBAC-A	SRR10982727	Bacillus_pumilus_RI06_95_exposure_6h	Pro_RE22	Pro_RE22	RI_M_6	6d	Rep1	*C. virginica*	~`Time + Condition`	CVBAC-A transcriptomes from three different larval sources were compared to untreated control and corrected for the effect of time using the model ~`Time + Condition`
CVBAC-A	SRR10982733	Bacillus_pumilus_RI06_95_exposure_6h	Pro_RE22	Pro_RE22	RI_V_6	7d	Rep1	*C. virginica*	~`Time + Condition`	CVBAC-A transcriptomes from three different larval sources were compared to untreated control and corrected for the effect of time using the model ~`Time + Condition`
CVBAC-A	SRR10982735	Phaeobacter_inhibens_S4_exposure_24h	Pro_RE22	Pro_RE22	S4_K_24	10d	Rep1	*C. virginica*	~`Time + Condition`	CVBAC-A transcriptomes from three different larval sources were compared to untreated control and corrected for the effect of time using the model ~`Time + Condition`
CVBAC-A	SRR10982741	Phaeobacter_inhibens_S4_exposure_24h	Pro_RE22	Pro_RE22	S4_M_24	6d	Rep1	*C. virginica*	~`Time + Condition`	CVBAC-A transcriptomes from three different larval sources were compared to untreated control and corrected for the effect of time using the model ~`Time + Condition`
CVBAC-A	SRR10982731	Phaeobacter_inhibens_S4_exposure_24h	Pro_RE22	Pro_RE22	S4_V_24	7d	Rep1	*C. virginica*	~`Time + Condition`	CVBAC-A transcriptomes from three different larval sources were compared to untreated control and corrected for the effect of time using the model ~`Time + Condition`
CVBAC-A	SRR10982738	Phaeobacter_inhibens_S4_exposure_6h	Pro_RE22	Pro_RE22	S4_K_6	10d	Rep1	*C. virginica*	~`Time + Condition`	CVBAC-A transcriptomes from three different larval sources were compared to untreated control and corrected for the effect of time using the model ~`Time + Condition`
CVBAC-A	SRR10982728	Phaeobacter_inhibens_S4_exposure_6h	Pro_RE22	Pro_RE22	S4_M_6	6d	Rep1	*C. virginica*	~`Time + Condition`	CVBAC-A transcriptomes from three different larval sources were compared to untreated control and corrected for the effect of time using the model ~`Time + Condition`

CVBAC-A	SRR10982742	Phaeobacter_inhibens_S4_exposure_6h	Pro_RE22	Pro_RE22	S4_V_6	7d	Rep1	*C. virginica*	~`Time + Condition`	CVBAC-A transcriptomes from three different larval sources were compared to untreated control and corrected for the effect of time using the model ~`Time + Condition`
CVBAC-A	SRR10982736	Vibrio_coralliilyticus_RE22_exposure_6h	Pro_RE22	Pro_RE22	RE_K_6	10d	Rep1	*C. virginica*	~`Time + Condition`	CVBAC-A transcriptomes from three different larval sources were compared to untreated control and corrected for the effect of time using the model ~`Time + Condition`
CVBAC-A	SRR10982726	Vibrio_coralliilyticus_RE22_exposure_6h	Pro_RE22	Pro_RE22	RE_M_6	6d	Rep1	*C. virginica*	~`Time + Condition`	CVBAC-A transcriptomes from three different larval sources were compared to untreated control and corrected for the effect of time using the model ~`Time + Condition`
CVBAC-A	SRR10982732	Vibrio_coralliilyticus_RE22_exposure_6h	Pro_RE22	Pro_RE22	RE_V_6	7d	Rep1	*C. virginica*	~`Time + Condition`	CVBAC-A transcriptomes from three different larval sources were compared to untreated control and corrected for the effect of time using the model ~`Time + Condition`
CVBAC-B	SRR5357618	Bacillus_pumilus_RI0695	Probiotic	Probiotic	Bacillus_pumilus_RI0695_16 d	16d	Rep1	*C. virginica*	`~Time + Condition`	CVBAC-B transcriptomes were compared to untreated control using the model `~Time + Condition`. The effect of time was controlled for in the model due to lack of replicates.
CVBAC-B	SRR5357623	Untreated_control	Probiotic	Probiotic	Untreated_control_5 d	5d	Rep1	*C. virginica*	`~Time + Condition`	CVBAC-B transcriptomes were compared to untreated control using the model `~Time + Condition`. The effect of time was controlled for in the model due to lack of replicates.
CVBAC-B	SRR5357617	Untreated_control	Probiotic	Probiotic	Untreated_control_16 d	16d	Rep1	*C. virginica*	`~Time + Condition`	CVBAC-B transcriptomes were compared to untreated control using the model `~Time + Condition`. The effect of time was controlled for in the model due to lack of replicates.
CVBAC-B	SRR5357619	Bacillus_pumilus_RI0695	Probiotic	Probiotic	Bacillus_pumilus_RI0695_5 d	5d	Rep1	*C. virginica*	`~Time + Condition`	CVBAC-B transcriptomes were compared to untreated control using the model `~Time + Condition`. The effect of time was controlled for in the model due to lack of replicates.
CVBAC-B	SRR5357622	Untreated_control	Probiotic	Probiotic	Untreated_control_12 d	12d	Rep1	*C. virginica*	`~Time + Condition`	CVBAC-B transcriptomes were compared to untreated control using the model `~Time + Condition`. The effect of time was controlled for in the model due to lack of replicates.
CVBAC-B	SRR5357626	Bacillus_pumilus_RI0695	Probiotic	Probiotic	Bacillus_pumilus_RI0695_12 d	12d	Rep1	*C. virginica*	`~Time + Condition`	CVBAC-B transcriptomes were compared to untreated control using the model `~Time + Condition`. The effect of time was controlled for in the model due to lack of replicates.
CVBAC-C	SRR1293904	Control_Resistant	GX	ROD	CGX_1day	1d	Rep1	*C. virginica*	`~Time + Condition`	CVBAC-C transcriptomes from the resistant family were compared to control and corrected for the effect of time using the model `~Time + Condition`. Transcriptomes from the susceptible family were the assessed by comparing early timepoint (1 d, 5 d) to late timepoints (15 d, 30 d) using the formula `~Condition` due to mortality in control samples.
CVBAC-C	SRR1298417	Control_Resistant	GX	ROD	CGX_5d	5d	Rep1	*C. virginica*	`~Time + Condition`	CVBAC-C transcriptomes from the resistant family were compared to control and corrected for the effect of time using the model `~Time + Condition`. Transcriptomes from the susceptible family were the assessed by comparing early timepoint (1 d, 5 d) to late timepoints (15 d, 30 d) using the formula `~Condition` due to mortality in control samples.
CVBAC-C	SRR1298710	Control_Resistant	GX	ROD	CGX_15d	15d	Rep1	*C. virginica*	`~Time + Condition`	CVBAC-C transcriptomes from the resistant family were compared to control and corrected for the effect of time using the model `~Time + Condition`. Transcriptomes from the susceptible family were the assessed by comparing early timepoint (1 d, 5 d) to late timepoints (15 d, 30 d) using the formula `~Condition` due to mortality in control samples.

CVBAC-C	SRR1298421	Control_Resistant	GX	ROD	CGX_30d	30d	Rep1	*C. virginica*	`~Time + Condition`	CVBAC-C transcriptomes from the resistant family were compared to control and corrected for the effect of time using the model `~Time + Condition`. Transcriptomes from the susceptible family were the assessed by comparing early timepoint (1 d, 5 d) to late timepoints (15 d, 30 d) using the formula `~Condition` due to mortality in control samples.
CVBAC-C	SRR1298703	Early_Susceptible	F3L	ROD	F3L_1d	1d	Rep1	*C. virginica*	`~Condition`	CVBAC-C transcriptomes from the resistant family were compared to control and corrected for the effect of time using the model `~Time + Condition`. Transcriptomes from the susceptible family were the assessed by comparing early timepoint (1 d, 5 d) to late timepoints (15 d, 30 d) using the formula `~Condition` due to mortality in control samples.
CVBAC-C	SRR1298704	Early_Susceptible	F3L	ROD	F3L_5d	5d	Rep1	*C. virginica*	`~Condition`	CVBAC-C transcriptomes from the resistant family were compared to control and corrected for the effect of time using the model `~Time + Condition`. Transcriptomes from the susceptible family were the assessed by comparing early timepoint (1 d, 5 d) to late timepoints (15 d, 30 d) using the formula `~Condition` due to mortality in control samples.
CVBAC-C	SRR1298708	Late_Susceptible	F3L	ROD	F3L_15d	15d	Rep1	*C. virginica*	`~Condition`	CVBAC-C transcriptomes from the resistant family were compared to control and corrected for the effect of time using the model `~Time + Condition`. Transcriptomes from the susceptible family were the assessed by comparing early timepoint (1 d, 5 d) to late timepoints (15 d, 30 d) using the formula `~Condition` due to mortality in control samples.
CVBAC-C	SRR1298387	Late_Susceptible	F3L	ROD	F3L_30d	30d	Rep1	*C. virginica*	`~Condition`	CVBAC-C transcriptomes from the resistant family were compared to control and corrected for the effect of time using the model `~Time + Condition`. Transcriptomes from the susceptible family were the assessed by comparing early timepoint (1 d, 5 d) to late timepoints (15 d, 30 d) using the formula `~Condition` due to mortality in control samples.
CVBAC-C	SRR1298693	Resistant_Challenge	GX	ROD	GX_01d	1d	Rep1	*C. virginica*	`~Time + Condition`	CVBAC-C transcriptomes from the resistant family were compared to control and corrected for the effect of time using the model `~Time + Condition`. Transcriptomes from the susceptible family were the assessed by comparing early timepoint (1 d, 5 d) to late timepoints (15 d, 30 d) using the formula `~Condition` due to mortality in control samples.
CVBAC-C	SRR1298711	Resistant_Challenge	GX	ROD	GX_5d	5d	Rep1	*C. virginica*	`~Time + Condition`	CVBAC-C transcriptomes from the resistant family were compared to control and corrected for the effect of time using the model `~Time + Condition`. Transcriptomes from the susceptible family were the assessed by comparing early timepoint (1 d, 5 d) to late timepoints (15 d, 30 d) using the formula `~Condition` due to mortality in control samples.
CVBAC-C	SRR1298698	Resistant_Challenge	GX	ROD	GX_15d	15d	Rep1	*C. virginica*	`~Time + Condition`	CVBAC-C transcriptomes from the resistant family were compared to control and corrected for the effect of time using the model `~Time + Condition`. Transcriptomes from the susceptible family were the assessed by comparing early timepoint (1 d, 5 d) to late timepoints (15 d, 30 d) using the formula `~Condition` due to mortality in control samples.

CVBAC-C	SRR1298701	Resistant_Challenge	GX	ROD	GX_30d	30d	Rep1	*C. virginica*	`~Time + Condition`	CVBAC-C transcriptomes from the resistant family were compared to control and corrected for the effect of time using the model `~Time + Condition`. Transcriptomes from the susceptible family were the assessed by comparing early timepoint (1 d, 5 d) to late timepoints (15 d, 30 d) using the formula `~Condition` due to mortality in control samples.
CVPMA	DP47_GGCTAC_TechRep1	Control	DA	Dermo	DA135_28d_Control	28d	Rep1	*C. virginica*	`~Lib_prep_date + Condition`	CVPMA transcriptomes were separated by timepoint and family, technical replicates merged using collapseReplicates() in DESeq2, corrected for batch effects due to library prep date and compared to their own timepoint control with the model `~Lib_prep_date + Condition`
CVPMA	DP47_GGCTAC_TechRep2	Control	DA	Dermo	DA135_28d_Control	28d	Rep2	*C. virginica*	`~Lib_prep_date + Condition`	CVPMA transcriptomes were separated by timepoint and family, technical replicates merged using collapseReplicates() in DESeq2, corrected for batch effects due to library prep date and compared to their own timepoint control with the model `~Lib_prep_date + Condition`
CVPMA	DP48_TAGCTT_TechRep1	Control	DA	Dermo	DA137_28d_Control	28d	Rep1	*C. virginica*	`~Lib_prep_date + Condition`	CVPMA transcriptomes were separated by timepoint and family, technical replicates merged using collapseReplicates() in DESeq2, corrected for batch effects due to library prep date and compared to their own timepoint control with the model `~Lib_prep_date + Condition`
CVPMA	DP48_TAGCTT_TechRep2	Control	DA	Dermo	DA137_28d_Control	28d	Rep2	*C. virginica*	`~Lib_prep_date + Condition`	CVPMA transcriptomes were separated by timepoint and family, technical replicates merged using collapseReplicates() in DESeq2, corrected for batch effects due to library prep date and compared to their own timepoint control with the model `~Lib_prep_date + Condition`
CVPMA	DP53_TAGCTT_TechRep1	Control	DA	Dermo	DA149_28d_Control	28d	Rep1	*C. virginica*	`~Lib_prep_date + Condition`	CVPMA transcriptomes were separated by timepoint and family, technical replicates merged using collapseReplicates() in DESeq2, corrected for batch effects due to library prep date and compared to their own timepoint control with the model `~Lib_prep_date + Condition`
CVPMA	DP53_TAGCTT_TechRep2	Control	DA	Dermo	DA149_28d_Control	28d	Rep2	*C. virginica*	`~Lib_prep_date + Condition`	CVPMA transcriptomes were separated by timepoint and family, technical replicates merged using collapseReplicates() in DESeq2, corrected for batch effects due to library prep date and compared to their own timepoint control with the model `~Lib_prep_date + Condition`
CVPMA	DCS2015_P9_DA155_AGTTCC	Control	DA	Dermo	DA155_28d_Control	28d	Rep1	*C. virginica*	`~Lib_prep_date + Condition`	CVPMA transcriptomes were separated by timepoint and family, technical replicates merged using collapseReplicates() in DESeq2, corrected for batch effects due to library prep date and compared to their own timepoint control with the model `~Lib_prep_date + Condition`
CVPMA	DCS2015_P10_DA157_TGACCA	Control	DA	Dermo	DA157_28d_Control	28d	Rep1	*C. virginica*	`~Lib_prep_date + Condition`	CVPMA transcriptomes were separated by timepoint and family, technical replicates merged using collapseReplicates() in DESeq2, corrected for batch effects due to library prep date and compared to their own timepoint control with the model `~Lib_prep_date + Condition`
CVPMA	DCS2015_P11_D	Control	DA	Dermo	DA174_28d_Control	28d	Rep1	*C. virginica*	`~Lib_prep_date + Condition`	CVPMA transcriptomes were separated by timepoint and family, technical replicates merged using collapseReplicates() in DESeq2, corrected for batch effects due to library prep date and compared to

	A174_AGTTCC									their own timepoint control with the model `~Lib_prep_date + Condition`
CVPMA	DP21_ATCACG_TechRep1	Injected	DA	Dermo	DA17_28d_Injected	28d	Rep1	*C. virginica*	`~Lib_prep_date + Condition`	CVPMA transcriptomes were separated by timepoint and family, technical replicates merged using collapseReplicates() in DESeq2, corrected for batch effects due to library prep date and compared to their own timepoint control with the model `~Lib_prep_date + Condition`
CVPMA	DP21_ATCACG_TechRep2	Injected	DA	Dermo	DA17_28d_Injected	28d	Rep2	*C. virginica*	`~Lib_prep_date + Condition`	CVPMA transcriptomes were separated by timepoint and family, technical replicates merged using collapseReplicates() in DESeq2, corrected for batch effects due to library prep date and compared to their own timepoint control with the model `~Lib_prep_date + Condition`
CVPMA	DP24_ATCACG_TechRep1	Injected	DA	Dermo	DA25_28d_Injected	28d	Rep1	*C. virginica*	`~Lib_prep_date + Condition`	CVPMA transcriptomes were separated by timepoint and family, technical replicates merged using collapseReplicates() in DESeq2, corrected for batch effects due to library prep date and compared to their own timepoint control with the model `~Lib_prep_date + Condition`
CVPMA	DP24_ATCACG_TechRep2	Injected	DA	Dermo	DA25_28d_Injected	28d	Rep2	*C. virginica*	`~Lib_prep_date + Condition`	CVPMA transcriptomes were separated by timepoint and family, technical replicates merged using collapseReplicates() in DESeq2, corrected for batch effects due to library prep date and compared to their own timepoint control with the model `~Lib_prep_date + Condition`
CVPMA	DP28_ATCACG_TechRep1	Injected	DA	Dermo	DA37_28d_Injected	28d	Rep1	*C. virginica*	`~Lib_prep_date + Condition`	CVPMA transcriptomes were separated by timepoint and family, technical replicates merged using collapseReplicates() in DESeq2, corrected for batch effects due to library prep date and compared to their own timepoint control with the model `~Lib_prep_date + Condition`
CVPMA	DP28_ATCACG_TechRep2	Injected	DA	Dermo	DA37_28d_Injected	28d	Rep2	*C. virginica*	`~Lib_prep_date + Condition`	CVPMA transcriptomes were separated by timepoint and family, technical replicates merged using collapseReplicates() in DESeq2, corrected for batch effects due to library prep date and compared to their own timepoint control with the model `~Lib_prep_date + Condition`
CVPMA	DCS2015_P9_DA49_TGACCA	Injected	DA	Dermo	DA49_28d_Injected	28d	Rep1	*C. virginica*	`~Lib_prep_date + Condition`	CVPMA transcriptomes were separated by timepoint and family, technical replicates merged using collapseReplicates() in DESeq2, corrected for batch effects due to library prep date and compared to their own timepoint control with the model `~Lib_prep_date + Condition`
CVPMA	DCS2015_P11_DA60_TGACCA	Injected	DA	Dermo	DA60_28d_Injected	28d	Rep1	*C. virginica*	`~Lib_prep_date + Condition`	CVPMA transcriptomes were separated by timepoint and family, technical replicates merged using collapseReplicates() in DESeq2, corrected for batch effects due to library prep date and compared to their own timepoint control with the model `~Lib_prep_date + Condition`
CVPMA	DP45_TAGCTT_TechRep1	Control	DA	Dermo	DA129_36h_Control	36h	Rep1	*C. virginica*	`~Lib_prep_date + Condition`	CVPMA transcriptomes were separated by timepoint and family, technical replicates merged using collapseReplicates() in DESeq2, corrected for batch effects due to library prep date and compared to their own timepoint control with the model `~Lib_prep_date + Condition`

CVPMA	DP45_TAGCTT_TechRep2	Control	DA	Dermo	DA129_36h_Control	36h	Rep2	*C. virginica*	`~Lib_prep_date + Condition`	CVPMA transcriptomes were separated by timepoint and family, technical replicates merged using collapseReplicates() in DESeq2, corrected for batch effects due to library prep date and compared to their own timepoint control with the model `~Lib_prep_date + Condition`
CVPMA	DP51_GGCTAC_TechRep1	Control	DA	Dermo	DA143_36h_Control	36h	Rep1	*C. virginica*	`~Lib_prep_date + Condition`	CVPMA transcriptomes were separated by timepoint and family, technical replicates merged using collapseReplicates() in DESeq2, corrected for batch effects due to library prep date and compared to their own timepoint control with the model `~Lib_prep_date + Condition`
CVPMA	DP51_GGCTAC_TechRep2	Control	DA	Dermo	DA143_36h_Control	36h	Rep2	*C. virginica*	`~Lib_prep_date + Condition`	CVPMA transcriptomes were separated by timepoint and family, technical replicates merged using collapseReplicates() in DESeq2, corrected for batch effects due to library prep date and compared to their own timepoint control with the model `~Lib_prep_date + Condition`
CVPMA	DP54_ACTGAT_TechRep1	Control	DA	Dermo	DA152_36h_Control	36h	Rep1	*C. virginica*	`~Lib_prep_date + Condition`	CVPMA transcriptomes were separated by timepoint and family, technical replicates merged using collapseReplicates() in DESeq2, corrected for batch effects due to library prep date and compared to their own timepoint control with the model `~Lib_prep_date + Condition`
CVPMA	DP54_ACTGAT_TechRep2	Control	DA	Dermo	DA152_36h_Control	36h	Rep2	*C. virginica*	`~Lib_prep_date + Condition`	CVPMA transcriptomes were separated by timepoint and family, technical replicates merged using collapseReplicates() in DESeq2, corrected for batch effects due to library prep date and compared to their own timepoint control with the model `~Lib_prep_date + Condition`
CVPMA	DCS2015_P10_DA176_CGATGT	Control	DA	Dermo	DA176_36h_Control	36h	Rep1	*C. virginica*	`~Lib_prep_date + Condition`	CVPMA transcriptomes were separated by timepoint and family, technical replicates merged using collapseReplicates() in DESeq2, corrected for batch effects due to library prep date and compared to their own timepoint control with the model `~Lib_prep_date + Condition`
CVPMA	DCS2015_P12_DA180_AGTCAA	Control	DA	Dermo	DA180_36h_Control	36h	Rep1	*C. virginica*	`~Lib_prep_date + Condition`	CVPMA transcriptomes were separated by timepoint and family, technical replicates merged using collapseReplicates() in DESeq2, corrected for batch effects due to library prep date and compared to their own timepoint control with the model `~Lib_prep_date + Condition`
CVPMA	DP23_TTAGGC_TechRep1	Injected	DA	Dermo	DA21_36h_Injected	36h	Rep1	*C. virginica*	`~Lib_prep_date + Condition`	CVPMA transcriptomes were separated by timepoint and family, technical replicates merged using collapseReplicates() in DESeq2, corrected for batch effects due to library prep date and compared to their own timepoint control with the model `~Lib_prep_date + Condition`
CVPMA	DP23_TTAGGC_TechRep2	Injected	DA	Dermo	DA21_36h_Injected	36h	Rep2	*C. virginica*	`~Lib_prep_date + Condition`	CVPMA transcriptomes were separated by timepoint and family, technical replicates merged using collapseReplicates() in DESeq2, corrected for batch effects due to library prep date and compared to their own timepoint control with the model `~Lib_prep_date + Condition`
CVPMA	DP30_GTGGCC_TechRep1	Injected	DA	Dermo	DA43_36h_Injected	36h	Rep1	*C. virginica*	`~Lib_prep_date + Condition`	CVPMA transcriptomes were separated by timepoint and family, technical replicates merged using collapseReplicates() in DESeq2, corrected for batch effects due to library prep date and compared to

										their own timepoint control with the model `~Lib_prep_date + Condition`
CVPMA	DP30_GTGGCC_TechRep2	Injected	DA	Dermo	DA43_36h_Injected	36h	Rep2	*C. virginica*	`~Lib_prep_date + Condition`	CVPMA transcriptomes were separated by timepoint and family, technical replicates merged using collapseReplicates() in DESeq2, corrected for batch effects due to library prep date and compared to their own timepoint control with the model `~Lib_prep_date + Condition`
CVPMA	DCS2015_P9_DA56_CGATGT	Injected	DA	Dermo	DA56_36h_Injected	36h	Rep1	*C. virginica*	`~Lib_prep_date + Condition`	CVPMA transcriptomes were separated by timepoint and family, technical replicates merged using collapseReplicates() in DESeq2, corrected for batch effects due to library prep date and compared to their own timepoint control with the model `~Lib_prep_date + Condition`
CVPMA	DCS2015_P11_DA59_CGATGT	Injected	DA	Dermo	DA59_36h_Injected	36h	Rep1	*C. virginica*	`~Lib_prep_date + Condition`	CVPMA transcriptomes were separated by timepoint and family, technical replicates merged using collapseReplicates() in DESeq2, corrected for batch effects due to library prep date and compared to their own timepoint control with the model `~Lib_prep_date + Condition`
CVPMA	DCS2015_P12_DA69_CGATGT	Injected	DA	Dermo	DA69_36h_Injected	36h	Rep1	*C. virginica*	`~Lib_prep_date + Condition`	CVPMA transcriptomes were separated by timepoint and family, technical replicates merged using collapseReplicates() in DESeq2, corrected for batch effects due to library prep date and compared to their own timepoint control with the model `~Lib_prep_date + Condition`
CVPMA	DP49_ATTCCT_TechRep1	Control	DA	Dermo	DA139_7d_Control	7d	Rep1	*C. virginica*	`~Lib_prep_date + Condition`	CVPMA transcriptomes were separated by timepoint and family, technical replicates merged using collapseReplicates() in DESeq2, corrected for batch effects due to library prep date and compared to their own timepoint control with the model `~Lib_prep_date + Condition`
CVPMA	DP49_ATTCCT_TechRep2	Control	DA	Dermo	DA139_7d_Control	7d	Rep2	*C. virginica*	`~Lib_prep_date + Condition`	CVPMA transcriptomes were separated by timepoint and family, technical replicates merged using collapseReplicates() in DESeq2, corrected for batch effects due to library prep date and compared to their own timepoint control with the model `~Lib_prep_date + Condition`
CVPMA	DP52_ATTCCT_TechRep1	Control	DA	Dermo	DA147_7d_Control	7d	Rep1	*C. virginica*	`~Lib_prep_date + Condition`	CVPMA transcriptomes were separated by timepoint and family, technical replicates merged using collapseReplicates() in DESeq2, corrected for batch effects due to library prep date and compared to their own timepoint control with the model `~Lib_prep_date + Condition`
CVPMA	DP52_ATTCCT_TechRep2	Control	DA	Dermo	DA147_7d_Control	7d	Rep2	*C. virginica*	`~Lib_prep_date + Condition`	CVPMA transcriptomes were separated by timepoint and family, technical replicates merged using collapseReplicates() in DESeq2, corrected for batch effects due to library prep date and compared to their own timepoint control with the model `~Lib_prep_date + Condition`
CVPMA	DP55_GGCTAC_TechRep1	Control	DA	Dermo	DA153_7d_Control	7d	Rep1	*C. virginica*	`~Lib_prep_date + Condition`	CVPMA transcriptomes were separated by timepoint and family, technical replicates merged using collapseReplicates() in DESeq2, corrected for batch effects due to library prep date and compared to their own timepoint control with the model `~Lib_prep_date + Condition`

CVPMA	DP55_GGCTAC_TechRep2	Control	DA	Dermo	DA153_7d_Control	7d	Rep2	*C. virginica*	`~Lib_prep_date + Condition`	CVPMA transcriptomes were separated by timepoint and family, technical replicates merged using collapseReplicates() in DESeq2, corrected for batch effects due to library prep date and compared to their own timepoint control with the model `~Lib_prep_date + Condition`
CVPMA	DCS2015_P9_DA159_AGTCAA	Control	DA	Dermo	DA159_7d_Control	7d	Rep1	*C. virginica*	`~Lib_prep_date + Condition`	CVPMA transcriptomes were separated by timepoint and family, technical replicates merged using collapseReplicates() in DESeq2, corrected for batch effects due to library prep date and compared to their own timepoint control with the model `~Lib_prep_date + Condition`
CVPMA	DCS2015_P11_DA170_AGTCAA	Control	DA	Dermo	DA170_7d_Control	7d	Rep1	*C. virginica*	`~Lib_prep_date + Condition`	CVPMA transcriptomes were separated by timepoint and family, technical replicates merged using collapseReplicates() in DESeq2, corrected for batch effects due to library prep date and compared to their own timepoint control with the model `~Lib_prep_date + Condition`
CVPMA	DCS2015_P12_DA179_AGTTCC	Control	DA	Dermo	DA179_7d_Control	7d	Rep1	*C. virginica*	`~Lib_prep_date + Condition`	CVPMA transcriptomes were separated by timepoint and family, technical replicates merged using collapseReplicates() in DESeq2, corrected for batch effects due to library prep date and compared to their own timepoint control with the model `~Lib_prep_date + Condition`
CVPMA	DP25_GTTTCG_TechRep1	Injected	DA	Dermo	DA28_7d_Injected	7d	Rep1	*C. virginica*	`~Lib_prep_date + Condition`	CVPMA transcriptomes were separated by timepoint and family, technical replicates merged using collapseReplicates() in DESeq2, corrected for batch effects due to library prep date and compared to their own timepoint control with the model `~Lib_prep_date + Condition`
CVPMA	DP25_GTTTCG_TechRep2	Injected	DA	Dermo	DA28_7d_Injected	7d	Rep2	*C. virginica*	`~Lib_prep_date + Condition`	CVPMA transcriptomes were separated by timepoint and family, technical replicates merged using collapseReplicates() in DESeq2, corrected for batch effects due to library prep date and compared to their own timepoint control with the model `~Lib_prep_date + Condition`
CVPMA	DP29_GTTTCG_TechRep1	Injected	DA	Dermo	DA41_7d_Injected	7d	Rep1	*C. virginica*	`~Lib_prep_date + Condition`	CVPMA transcriptomes were separated by timepoint and family, technical replicates merged using collapseReplicates() in DESeq2, corrected for batch effects due to library prep date and compared to their own timepoint control with the model `~Lib_prep_date + Condition`
CVPMA	DP29_GTTTCG_TechRep2	Injected	DA	Dermo	DA41_7d_Injected	7d	Rep2	*C. virginica*	`~Lib_prep_date + Condition`	CVPMA transcriptomes were separated by timepoint and family, technical replicates merged using collapseReplicates() in DESeq2, corrected for batch effects due to library prep date and compared to their own timepoint control with the model `~Lib_prep_date + Condition`
CVPMA	DP31_TTAGGC_TechRep1	Injected	DA	Dermo	DA51_7d_Injected	7d	Rep1	*C. virginica*	`~Lib_prep_date + Condition`	CVPMA transcriptomes were separated by timepoint and family, technical replicates merged using collapseReplicates() in DESeq2, corrected for batch effects due to library prep date and compared to their own timepoint control with the model `~Lib_prep_date + Condition`
CVPMA	DP31_TTAGGC_TechRep2	Injected	DA	Dermo	DA51_7d_Injected	7d	Rep2	*C. virginica*	`~Lib_prep_date + Condition`	CVPMA transcriptomes were separated by timepoint and family, technical replicates merged using collapseReplicates() in DESeq2, corrected for batch effects due to library prep date and compared to

										their own timepoint control with the model `~Lib_prep_date + Condition`
CVPMA	DCS2015_P10_DA53_AGTCAA	Injected	DA	Dermo	DA53_7d_Injected	7d	Rep1	*C. virginica*	`~Lib_prep_date + Condition`	CVPMA transcriptomes were separated by timepoint and family, technical replicates merged using collapseReplicates() in DESeq2, corrected for batch effects due to library prep date and compared to their own timepoint control with the model `~Lib_prep_date + Condition`
CVPMA	DCS2015_P12_DA62_TGACCA	Injected	DA	Dermo	DA62_7d_Injected	7d	Rep1	*C. virginica*	`~Lib_prep_date + Condition`	CVPMA transcriptomes were separated by timepoint and family, technical replicates merged using collapseReplicates() in DESeq2, corrected for batch effects due to library prep date and compared to their own timepoint control with the model `~Lib_prep_date + Condition`
CVPMA	DP82_GTCCGC_TechRep1	Control	LB	Dermo	LB131_28d_Control	28d	Rep1	*C. virginica*	`~Lib_prep_date + Condition`	CVPMA transcriptomes were separated by timepoint and family, technical replicates merged using collapseReplicates() in DESeq2, corrected for batch effects due to library prep date and compared to their own timepoint control with the model `~Lib_prep_date + Condition`
CVPMA	DP82_GTCCGC_TechRep2	Control	LB	Dermo	LB131_28d_Control	28d	Rep2	*C. virginica*	`~Lib_prep_date + Condition`	CVPMA transcriptomes were separated by timepoint and family, technical replicates merged using collapseReplicates() in DESeq2, corrected for batch effects due to library prep date and compared to their own timepoint control with the model `~Lib_prep_date + Condition`
CVPMA	DP85_CAGATC_TechRep1	Control	LB	Dermo	LB140_28d_Control	28d	Rep1	*C. virginica*	`~Lib_prep_date + Condition`	CVPMA transcriptomes were separated by timepoint and family, technical replicates merged using collapseReplicates() in DESeq2, corrected for batch effects due to library prep date and compared to their own timepoint control with the model `~Lib_prep_date + Condition`
CVPMA	DP85_CAGATC_TechRep2	Control	LB	Dermo	LB140_28d_Control	28d	Rep2	*C. virginica*	`~Lib_prep_date + Condition`	CVPMA transcriptomes were separated by timepoint and family, technical replicates merged using collapseReplicates() in DESeq2, corrected for batch effects due to library prep date and compared to their own timepoint control with the model `~Lib_prep_date + Condition`
CVPMA	DP88_CAGATC_TechRep1	Control	LB	Dermo	LB149_28d_Control	28d	Rep1	*C. virginica*	`~Lib_prep_date + Condition`	CVPMA transcriptomes were separated by timepoint and family, technical replicates merged using collapseReplicates() in DESeq2, corrected for batch effects due to library prep date and compared to their own timepoint control with the model `~Lib_prep_date + Condition`
CVPMA	DP88_CAGATC_TechRep2	Control	LB	Dermo	LB149_28d_Control	28d	Rep2	*C. virginica*	`~Lib_prep_date + Condition`	CVPMA transcriptomes were separated by timepoint and family, technical replicates merged using collapseReplicates() in DESeq2, corrected for batch effects due to library prep date and compared to their own timepoint control with the model `~Lib_prep_date + Condition`
CVPMA	DCS2015_P9_LB168_CCGTCC	Control	LB	Dermo	LB168_28d_Control	28d	Rep1	*C. virginica*	`~Lib_prep_date + Condition`	CVPMA transcriptomes were separated by timepoint and family, technical replicates merged using collapseReplicates() in DESeq2, corrected for batch effects due to library prep date and compared to their own timepoint control with the model `~Lib_prep_date + Condition`

CVPMA	DCS2015_P11_LB177_ATGTCA	Control	LB	Dermo	LB177_28d_Control	28d	Rep1	*C. virginica*	`~Lib_prep_date + Condition`	CVPMA transcriptomes were separated by timepoint and family, technical replicates merged using collapseReplicates() in DESeq2, corrected for batch effects due to library prep date and compared to their own timepoint control with the model `~Lib_prep_date + Condition`
CVPMA	DP57_CGATGT_TechRep1	Injected	LB	Dermo	LB19_28d_Injected	28d	Rep1	*C. virginica*	`~Lib_prep_date + Condition`	CVPMA transcriptomes were separated by timepoint and family, technical replicates merged using collapseReplicates() in DESeq2, corrected for batch effects due to library prep date and compared to their own timepoint control with the model `~Lib_prep_date + Condition`
CVPMA	DP57_CGATGT_TechRep2	Injected	LB	Dermo	LB19_28d_Injected	28d	Rep2	*C. virginica*	`~Lib_prep_date + Condition`	CVPMA transcriptomes were separated by timepoint and family, technical replicates merged using collapseReplicates() in DESeq2, corrected for batch effects due to library prep date and compared to their own timepoint control with the model `~Lib_prep_date + Condition`
CVPMA	DP62_AGTCAA_TechRep1	Injected	LB	Dermo	LB32_28d_Injected	28d	Rep1	*C. virginica*	`~Lib_prep_date + Condition`	CVPMA transcriptomes were separated by timepoint and family, technical replicates merged using collapseReplicates() in DESeq2, corrected for batch effects due to library prep date and compared to their own timepoint control with the model `~Lib_prep_date + Condition`
CVPMA	DP62_AGTCAA_TechRep2	Injected	LB	Dermo	LB32_28d_Injected	28d	Rep2	*C. virginica*	`~Lib_prep_date + Condition`	CVPMA transcriptomes were separated by timepoint and family, technical replicates merged using collapseReplicates() in DESeq2, corrected for batch effects due to library prep date and compared to their own timepoint control with the model `~Lib_prep_date + Condition`
CVPMA	DP68_AGTTCC_TechRep1	Injected	LB	Dermo	LB51_28d_Injected	28d	Rep1	*C. virginica*	`~Lib_prep_date + Condition`	CVPMA transcriptomes were separated by timepoint and family, technical replicates merged using collapseReplicates() in DESeq2, corrected for batch effects due to library prep date and compared to their own timepoint control with the model `~Lib_prep_date + Condition`
CVPMA	DP68_AGTTCC_TechRep2	Injected	LB	Dermo	LB51_28d_Injected	28d	Rep2	*C. virginica*	`~Lib_prep_date + Condition`	CVPMA transcriptomes were separated by timepoint and family, technical replicates merged using collapseReplicates() in DESeq2, corrected for batch effects due to library prep date and compared to their own timepoint control with the model `~Lib_prep_date + Condition`
CVPMA	DCS2015_P10_LB64_ATGTCA	Injected	LB	Dermo	LB64_28d_Injected	28d	Rep1	*C. virginica*	`~Lib_prep_date + Condition`	CVPMA transcriptomes were separated by timepoint and family, technical replicates merged using collapseReplicates() in DESeq2, corrected for batch effects due to library prep date and compared to their own timepoint control with the model `~Lib_prep_date + Condition`
CVPMA	DCS2015_P11_LB70_ACAGTG	Injected	LB	Dermo	LB70_28d_Injected	28d	Rep1	*C. virginica*	`~Lib_prep_date + Condition`	CVPMA transcriptomes were separated by timepoint and family, technical replicates merged using collapseReplicates() in DESeq2, corrected for batch effects due to library prep date and compared to their own timepoint control with the model `~Lib_prep_date + Condition`
CVPMA	DP84_GTGAAA_TechRep1	Control	LB	Dermo	LB136_36h_Control	36h	Rep1	*C. virginica*	`~Lib_prep_date + Condition`	CVPMA transcriptomes were separated by timepoint and family, technical replicates merged using collapseReplicates() in DESeq2, corrected for batch effects due to library prep date and compared to

										their own timepoint control with the model `~Lib_prep_date + Condition`
CVPMA	DP84_GTGAAA_TechRep2	Control	LB	Dermo	LB136_36h_Control	36h	Rep2	*C. virginica*	`~Lib_prep_date + Condition`	CVPMA transcriptomes were separated by timepoint and family, technical replicates merged using collapseReplicates() in DESeq2, corrected for batch effects due to library prep date and compared to their own timepoint control with the model `~Lib_prep_date + Condition`
CVPMA	DP86_GTCCGC_TechRep1	Control	LB	Dermo	LB143_36h_Control	36h	Rep1	*C. virginica*	`~Lib_prep_date + Condition`	CVPMA transcriptomes were separated by timepoint and family, technical replicates merged using collapseReplicates() in DESeq2, corrected for batch effects due to library prep date and compared to their own timepoint control with the model `~Lib_prep_date + Condition`
CVPMA	DP86_GTCCGC_TechRep2	Control	LB	Dermo	LB143_36h_Control	36h	Rep2	*C. virginica*	`~Lib_prep_date + Condition`	CVPMA transcriptomes were separated by timepoint and family, technical replicates merged using collapseReplicates() in DESeq2, corrected for batch effects due to library prep date and compared to their own timepoint control with the model `~Lib_prep_date + Condition`
CVPMA	DP91_CTTGTA_TechRep1	Control	LB	Dermo	LB156_36h_Control	36h	Rep1	*C. virginica*	`~Lib_prep_date + Condition`	CVPMA transcriptomes were separated by timepoint and family, technical replicates merged using collapseReplicates() in DESeq2, corrected for batch effects due to library prep date and compared to their own timepoint control with the model `~Lib_prep_date + Condition`
CVPMA	DP91_CTTGTA_TechRep2	Control	LB	Dermo	LB156_36h_Control	36h	Rep2	*C. virginica*	`~Lib_prep_date + Condition`	CVPMA transcriptomes were separated by timepoint and family, technical replicates merged using collapseReplicates() in DESeq2, corrected for batch effects due to library prep date and compared to their own timepoint control with the model `~Lib_prep_date + Condition`
CVPMA	DCS2015_P9_LB173_ATGTCA	Control	LB	Dermo	LB173_36h_Control	36h	Rep1	*C. virginica*	`~Lib_prep_date + Condition`	CVPMA transcriptomes were separated by timepoint and family, technical replicates merged using collapseReplicates() in DESeq2, corrected for batch effects due to library prep date and compared to their own timepoint control with the model `~Lib_prep_date + Condition`
CVPMA	DCS2015_P12_LB179_ACAGTG	Control	LB	Dermo	LB179_36h_Control	36h	Rep1	*C. virginica*	`~Lib_prep_date + Condition`	CVPMA transcriptomes were separated by timepoint and family, technical replicates merged using collapseReplicates() in DESeq2, corrected for batch effects due to library prep date and compared to their own timepoint control with the model `~Lib_prep_date + Condition`
CVPMA	DP58_AGTCAA_TechRep1	Injected	LB	Dermo	LB20_36h_Injected	36h	Rep1	*C. virginica*	`~Lib_prep_date + Condition`	CVPMA transcriptomes were separated by timepoint and family, technical replicates merged using collapseReplicates() in DESeq2, corrected for batch effects due to library prep date and compared to their own timepoint control with the model `~Lib_prep_date + Condition`
CVPMA	DP58_AGTCAA_TechRep2	Injected	LB	Dermo	LB20_36h_Injected	36h	Rep2	*C. virginica*	`~Lib_prep_date + Condition`	CVPMA transcriptomes were separated by timepoint and family, technical replicates merged using collapseReplicates() in DESeq2, corrected for batch effects due to library prep date and compared to their own timepoint control with the model `~Lib_prep_date + Condition`

CVPMA	DP63_TGACCA_TechRep1	Injected	LB	Dermo	LB36_36h_Injected	36h	Rep1	*C. virginica*	`~Lib_prep_date + Condition`	CVPMA transcriptomes were separated by timepoint and family, technical replicates merged using collapseReplicates() in DESeq2, corrected for batch effects due to library prep date and compared to their own timepoint control with the model `~Lib_prep_date + Condition`
CVPMA	DP63_TGACCA_TechRep2	Injected	LB	Dermo	LB36_36h_Injected	36h	Rep2	*C. virginica*	`~Lib_prep_date + Condition`	CVPMA transcriptomes were separated by timepoint and family, technical replicates merged using collapseReplicates() in DESeq2, corrected for batch effects due to library prep date and compared to their own timepoint control with the model `~Lib_prep_date + Condition`
CVPMA	DP67_TGACCA_TechRep1	Injected	LB	Dermo	LB43_36h_Injected	36h	Rep1	*C. virginica*	`~Lib_prep_date + Condition`	CVPMA transcriptomes were separated by timepoint and family, technical replicates merged using collapseReplicates() in DESeq2, corrected for batch effects due to library prep date and compared to their own timepoint control with the model `~Lib_prep_date + Condition`
CVPMA	DP67_TGACCA_TechRep2	Injected	LB	Dermo	LB43_36h_Injected	36h	Rep2	*C. virginica*	`~Lib_prep_date + Condition`	CVPMA transcriptomes were separated by timepoint and family, technical replicates merged using collapseReplicates() in DESeq2, corrected for batch effects due to library prep date and compared to their own timepoint control with the model `~Lib_prep_date + Condition`
CVPMA	DCS2015_P9_LB46_ACAGTG	Injected	LB	Dermo	LB46_36h_Injected	36h	Rep1	*C. virginica*	`~Lib_prep_date + Condition`	CVPMA transcriptomes were separated by timepoint and family, technical replicates merged using collapseReplicates() in DESeq2, corrected for batch effects due to library prep date and compared to their own timepoint control with the model `~Lib_prep_date + Condition`
CVPMA	DCS2015_P10_LB69_AGTTCC	Injected	LB	Dermo	LB69_36h_Injected	36h	Rep1	*C. virginica*	`~Lib_prep_date + Condition`	CVPMA transcriptomes were separated by timepoint and family, technical replicates merged using collapseReplicates() in DESeq2, corrected for batch effects due to library prep date and compared to their own timepoint control with the model `~Lib_prep_date + Condition`
CVPMA	DP81_CAGATC_TechRep1	Control	LB	Dermo	LB129_7d_Control	7d	Rep1	*C. virginica*	`~Lib_prep_date + Condition`	CVPMA transcriptomes were separated by timepoint and family, technical replicates merged using collapseReplicates() in DESeq2, corrected for batch effects due to library prep date and compared to their own timepoint control with the model `~Lib_prep_date + Condition`
CVPMA	DP81_CAGATC_TechRep2	Control	LB	Dermo	LB129_7d_Control	7d	Rep2	*C. virginica*	`~Lib_prep_date + Condition`	CVPMA transcriptomes were separated by timepoint and family, technical replicates merged using collapseReplicates() in DESeq2, corrected for batch effects due to library prep date and compared to their own timepoint control with the model `~Lib_prep_date + Condition`
CVPMA	DP89_GTGAAA_TechRep1	Control	LB	Dermo	LB154_7d_Control	7d	Rep1	*C. virginica*	`~Lib_prep_date + Condition`	CVPMA transcriptomes were separated by timepoint and family, technical replicates merged using collapseReplicates() in DESeq2, corrected for batch effects due to library prep date and compared to their own timepoint control with the model `~Lib_prep_date + Condition`
CVPMA	DP89_GTGAAA_TechRep2	Control	LB	Dermo	LB154_7d_Control	7d	Rep2	*C. virginica*	`~Lib_prep_date + Condition`	CVPMA transcriptomes were separated by timepoint and family, technical replicates merged using collapseReplicates() in DESeq2, corrected for batch effects due to library prep date and compared to

										their own timepoint control with the model `~Lib_prep_date + Condition`
CVPMA	DP92_GTGAAA_TechRep1	Control	LB	Dermo	LB160_7d_Control	7d	Rep1	*C. virginica*	`~Lib_prep_date + Condition`	CVPMA transcriptomes were separated by timepoint and family, technical replicates merged using collapseReplicates() in DESeq2, corrected for batch effects due to library prep date and compared to their own timepoint control with the model `~Lib_prep_date + Condition`
CVPMA	DP92_GTGAAA_TechRep2	Control	LB	Dermo	LB160_7d_Control	7d	Rep2	*C. virginica*	`~Lib_prep_date + Condition`	CVPMA transcriptomes were separated by timepoint and family, technical replicates merged using collapseReplicates() in DESeq2, corrected for batch effects due to library prep date and compared to their own timepoint control with the model `~Lib_prep_date + Condition`
CVPMA	DCS2015_P10_LB165_ACAGTG	Control	LB	Dermo	LB165_7d_Control	7d	Rep1	*C. virginica*	`~Lib_prep_date + Condition`	CVPMA transcriptomes were separated by timepoint and family, technical replicates merged using collapseReplicates() in DESeq2, corrected for batch effects due to library prep date and compared to their own timepoint control with the model `~Lib_prep_date + Condition`
CVPMA	DCS2015_P12_LB180_GCCAAT	Control	LB	Dermo	LB180_7d_Control	7d	Rep1	*C. virginica*	`~Lib_prep_date + Condition`	CVPMA transcriptomes were separated by timepoint and family, technical replicates merged using collapseReplicates() in DESeq2, corrected for batch effects due to library prep date and compared to their own timepoint control with the model `~Lib_prep_date + Condition`
CVPMA	DP59_TGACCA_TechRep1	Injected	LB	Dermo	LB21_7d_Injected	7d	Rep1	*C. virginica*	`~Lib_prep_date + Condition`	CVPMA transcriptomes were separated by timepoint and family, technical replicates merged using collapseReplicates() in DESeq2, corrected for batch effects due to library prep date and compared to their own timepoint control with the model `~Lib_prep_date + Condition`
CVPMA	DP59_TGACCA_TechRep2	Injected	LB	Dermo	LB21_7d_Injected	7d	Rep2	*C. virginica*	`~Lib_prep_date + Condition`	CVPMA transcriptomes were separated by timepoint and family, technical replicates merged using collapseReplicates() in DESeq2, corrected for batch effects due to library prep date and compared to their own timepoint control with the model `~Lib_prep_date + Condition`
CVPMA	DP61_CGATGT_TechRep1	Injected	LB	Dermo	LB26_7d_Injected	7d	Rep1	*C. virginica*	`~Lib_prep_date + Condition`	CVPMA transcriptomes were separated by timepoint and family, technical replicates merged using collapseReplicates() in DESeq2, corrected for batch effects due to library prep date and compared to their own timepoint control with the model `~Lib_prep_date + Condition`
CVPMA	DP61_CGATGT_TechRep2	Injected	LB	Dermo	LB26_7d_Injected	7d	Rep2	*C. virginica*	`~Lib_prep_date + Condition`	CVPMA transcriptomes were separated by timepoint and family, technical replicates merged using collapseReplicates() in DESeq2, corrected for batch effects due to library prep date and compared to their own timepoint control with the model `~Lib_prep_date + Condition`
CVPMA	DP65_CGATGT_TechRep1	Injected	LB	Dermo	LB39_7d_Injected	7d	Rep1	*C. virginica*	`~Lib_prep_date + Condition`	CVPMA transcriptomes were separated by timepoint and family, technical replicates merged using collapseReplicates() in DESeq2, corrected for batch effects due to library prep date and compared to their own timepoint control with the model `~Lib_prep_date + Condition`

CVPMA	DP65_CGATGT_TechRep2	Injected	LB	Dermo	LB39_7d_Injected	7d	Rep2	*C. virginica*	`~Lib_prep_date + Condition`	CVPMA transcriptomes were separated by timepoint and family, technical replicates merged using collapseReplicates() in DESeq2, corrected for batch effects due to library prep date and compared to their own timepoint control with the model `~Lib_prep_date + Condition`
CVPMA	DCS2015_P9_LB62_GCCAAT	Injected	LB	Dermo	LB62_7d_Injected	7d	Rep1	*C. virginica*	`~Lib_prep_date + Condition`	CVPMA transcriptomes were separated by timepoint and family, technical replicates merged using collapseReplicates() in DESeq2, corrected for batch effects due to library prep date and compared to their own timepoint control with the model `~Lib_prep_date + Condition`
CVPMA	DCS2015_P12_LB67_ATGTCA	Injected	LB	Dermo	LB67_7d_Injected	7d	Rep1	*C. virginica*	`~Lib_prep_date + Condition`	CVPMA transcriptomes were separated by timepoint and family, technical replicates merged using collapseReplicates() in DESeq2, corrected for batch effects due to library prep date and compared to their own timepoint control with the model `~Lib_prep_date + Condition`
CGBAC-A	SRR796589	control	Zhang	Zhang	Control_No_injection	0h	Rep1	*C. gigas*	'~Time + Condition'	CGBAC-A transcriptomes had only one replicate per condition. Samples were therefore placed into four groups based on clustering during PCA analysis of rlog transformed counts using DESeq2 (V 1.24.0): Group 1 = PBS and control non-injected oysters, Group 2 = non-pathogenic Vibrio spp. (V. alginolyticus 1, V. alginolyticus 2, V. aestuarianus), Group 3 = pathogenic Vibrio spp. (V. tubiashii, and V. anguillarum) and Group 4 = LPS and M. luteus
CGBAC-A	SRR796591	control	Zhang	Zhang	PBS_12h	12h	Rep1	*C. gigas*	'~Time + Condition'	CGBAC-A transcriptomes had only one replicate per condition. Samples were therefore placed into four groups based on clustering during PCA analysis of rlog transformed counts using DESeq2 (V 1.24.0): Group 1 = PBS and control non-injected oysters, Group 2 = non-pathogenic Vibrio spp. (V. alginolyticus 1, V. alginolyticus 2, V. aestuarianus), Group 3 = pathogenic Vibrio spp. (V. tubiashii, and V. anguillarum) and Group 4 = LPS and M. luteus
CGBAC-A	SRR796592	LPS_M_lut	Zhang	Zhang	LPS_12h	12h	Rep1	*C. gigas*	'~Time + Condition'	CGBAC-A transcriptomes had only one replicate per condition. Samples were therefore placed into four groups based on clustering during PCA analysis of rlog transformed counts using DESeq2 (V 1.24.0): Group 1 = PBS and control non-injected oysters, Group 2 = non-pathogenic Vibrio spp. (V. alginolyticus 1, V. alginolyticus 2, V. aestuarianus), Group 3 = pathogenic Vibrio spp. (V. tubiashii, and V. anguillarum) and Group 4 = LPS and M. luteus
CGBAC-A	SRR796593	V_aes_V_alg1_V_alg2	Zhang	Zhang	V_aes_12h	12h	Rep1	*C. gigas*	'~Time + Condition'	CGBAC-A transcriptomes had only one replicate per condition. Samples were therefore placed into four groups based on clustering during PCA analysis of rlog transformed counts using DESeq2 (V 1.24.0): Group 1 = PBS and control non-injected oysters, Group 2 = non-pathogenic Vibrio spp. (V. alginolyticus 1, V. alginolyticus 2, V. aestuarianus), Group 3 = pathogenic Vibrio spp. (V. tubiashii, and V. anguillarum) and Group 4 = LPS and M. luteus
CGBAC-A	SRR796594	V_tub_V_ang	Zhang	Zhang	V_ang_12h	12h	Rep1	*C. gigas*	'~Time + Condition'	CGBAC-A transcriptomes had only one replicate per condition. Samples were therefore placed into four groups based on clustering during PCA analysis of rlog transformed counts using DESeq2 (V 1.24.0): Group 1 = PBS and control non-injected oysters, Group 2 = non-pathogenic Vibrio spp. (V. alginolyticus 1, V. alginolyticus 2, V.

										aestuarianus), Group 3 = pathogenic Vibrio spp. (V. tubiashii, and V. anguillarum) and Group 4 = LPS and M. luteus
CGBAC-A	SRR796595	V_aes_V_alg1_V_alg2	Zhang	Zhang	V_alg_1_12h	12h	Rep1	*C. gigas*	'~Time + Condition'	CGBAC-A transcriptomes had only one replicate per condition. Samples were therefore placed into four groups based on clustering during PCA analysis of rlog transformed counts using DESeq2 (V 1.24.0): Group 1 = PBS and control non-injected oysters, Group 2 = non-pathogenic Vibrio spp. (V. alginolyticus 1, V. alginolyticus 2, V. aestuarianus), Group 3 = pathogenic Vibrio spp. (V. tubiashii, and V. anguillarum) and Group 4 = LPS and M. luteus
CGBAC-A	SRR796596	V_aes_V_alg1_V_alg2	Zhang	Zhang	V_alg_2_12h	12h	Rep1	*C. gigas*	'~Time + Condition'	CGBAC-A transcriptomes had only one replicate per condition. Samples were therefore placed into four groups based on clustering during PCA analysis of rlog transformed counts using DESeq2 (V 1.24.0): Group 1 = PBS and control non-injected oysters, Group 2 = non-pathogenic Vibrio spp. (V. alginolyticus 1, V. alginolyticus 2, V. aestuarianus), Group 3 = pathogenic Vibrio spp. (V. tubiashii, and V. anguillarum) and Group 4 = LPS and M. luteus
CGBAC-A	SRR796597	V_tub_V_ang	Zhang	Zhang	V_tub_12h	12h	Rep1	*C. gigas*	'~Time + Condition'	CGBAC-A transcriptomes had only one replicate per condition. Samples were therefore placed into four groups based on clustering during PCA analysis of rlog transformed counts using DESeq2 (V 1.24.0): Group 1 = PBS and control non-injected oysters, Group 2 = non-pathogenic Vibrio spp. (V. alginolyticus 1, V. alginolyticus 2, V. aestuarianus), Group 3 = pathogenic Vibrio spp. (V. tubiashii, and V. anguillarum) and Group 4 = LPS and M. luteus
CGBAC-A	SRR796598	LPS_M_lut	Zhang	Zhang	M_lut_12h	12h	Rep1	*C. gigas*	'~Time + Condition'	CGBAC-A transcriptomes had only one replicate per condition. Samples were therefore placed into four groups based on clustering during PCA analysis of rlog transformed counts using DESeq2 (V 1.24.0): Group 1 = PBS and control non-injected oysters, Group 2 = non-pathogenic Vibrio spp. (V. alginolyticus 1, V. alginolyticus 2, V. aestuarianus), Group 3 = pathogenic Vibrio spp. (V. tubiashii, and V. anguillarum) and Group 4 = LPS and M. luteus
CGBAC-B	SRR8551090	Control_anesthesis	Rubio	Rubio	Control_anesthesis_replicate2	NA	Rep1	*C. gigas*	'~Condition'	CGBAC-B transcriptomes were each compared to the control untreated sample using the design '~Condition'
CGBAC-B	SRR8551091	Control_anesthesis	Rubio	Rubio	Control_anesthesis_replicate3	NA	Rep1	*C. gigas*	'~Condition'	CGBAC-B transcriptomes were each compared to the control untreated sample using the design '~Condition'
CGBAC-B	SRR8551093	Control_anesthesis	Rubio	Rubio	Control_anesthesis_replicate1	NA	Rep1	*C. gigas*	'~Condition'	CGBAC-B transcriptomes were each compared to the control untreated sample using the design '~Condition'
CGBAC-B	SRR8551076	Control_untreated	Rubio	Rubio	Control_untreated_replicate1	NA	Rep1	*C. gigas*	'~Condition'	CGBAC-B transcriptomes were each compared to the control untreated sample using the design '~Condition'
CGBAC-B	SRR8551077	Control_untreated	Rubio	Rubio	Control_untreated_replicate2	NA	Rep1	*C. gigas*	'~Condition'	CGBAC-B transcriptomes were each compared to the control untreated sample using the design '~Condition'
CGBAC-B	SRR8551092	Control_untreated	Rubio	Rubio	Control_untreated_replicate3	NA	Rep1	*C. gigas*	'~Condition'	CGBAC-B transcriptomes were each compared to the control untreated sample using the design '~Condition'

CGBAC-B	SRR8551078	Vcrass_J2_8	Rubio	Rubio	Vcrass_J2_8_replicate3	NA	Rep1	*C. gigas*	'~Condition'	CGBAC-B transcriptomes were each compared to the control untreated sample using the design '~Condition'
CGBAC-B	SRR8551088	Vcrass_J2_8	Rubio	Rubio	Vcrass_J2_8_replicate1	NA	Rep1	*C. gigas*	'~Condition'	CGBAC-B transcriptomes were each compared to the control untreated sample using the design '~Condition'
CGBAC-B	SRR8551089	Vcrass_J2_8	Rubio	Rubio	Vcrass_J2_8_replicate2	NA	Rep1	*C. gigas*	'~Condition'	CGBAC-B transcriptomes were each compared to the control untreated sample using the design '~Condition'
CGBAC-B	SRR8551079	Vcrass_J2_9	Rubio	Rubio	Vcrass_J2_9_replicate1	NA	Rep1	*C. gigas*	'~Condition'	CGBAC-B transcriptomes were each compared to the control untreated sample using the design '~Condition'
CGBAC-B	SRR8551086	Vcrass_J2_9	Rubio	Rubio	Vcrass_J2_9_replicate2	NA	Rep1	*C. gigas*	'~Condition'	CGBAC-B transcriptomes were each compared to the control untreated sample using the design '~Condition'
CGBAC-B	SRR8551087	Vcrass_J2_9	Rubio	Rubio	Vcrass_J2_9_replicate3	NA	Rep1	*C. gigas*	'~Condition'	CGBAC-B transcriptomes were each compared to the control untreated sample using the design '~Condition'
CGBAC-B	SRR8551080	Vtasma_LGP32	Rubio	Rubio	Vtasma_LGP32_replicate2	NA	Rep1	*C. gigas*	'~Condition'	CGBAC-B transcriptomes were each compared to the control untreated sample using the design '~Condition'
CGBAC-B	SRR8551081	Vtasma_LGP32	Rubio	Rubio	Vtasma_LGP32_replicate3	NA	Rep1	*C. gigas*	'~Condition'	CGBAC-B transcriptomes were each compared to the control untreated sample using the design '~Condition'
CGBAC-B	SRR8551083	Vtasma_LGP32	Rubio	Rubio	Vtasma_LGP32_replicate1	NA	Rep1	*C. gigas*	'~Condition'	CGBAC-B transcriptomes were each compared to the control untreated sample using the design '~Condition'
CGBAC-B	SRR8551082	Vtasma_LMG20012T	Rubio	Rubio	Vtasma_LMG20012T_replicate3	NA	Rep1	*C. gigas*	'~Condition'	CGBAC-B transcriptomes were each compared to the control untreated sample using the design '~Condition'
CGBAC-B	SRR8551084	Vtasma_LMG20012T	Rubio	Rubio	Vtasma_LMG20012T_replicate1	NA	Rep1	*C. gigas*	'~Condition'	CGBAC-B transcriptomes were each compared to the control untreated sample using the design '~Condition'
CGBAC-B	SRR8551085	Vtasma_LMG20012T	Rubio	Rubio	Vtasma_LMG20012T_replicate2	NA	Rep1	*C. gigas*	'~Condition'	CGBAC-B transcriptomes were each compared to the control untreated sample using the design '~Condition'
CGOSHV1-A	SRR6679052	AF11_Susceptible	AF11_Susceptible	deLorgeril	AF11_T72_R1_RNAseq	72h	Rep1	*C. gigas*	`~Time`	CGOSHV1-A transcriptomic data was split up first by family, and then modeled with `~Time`, comparing each time point in each family separately to time 0 h
CGOSHV1-A	SRR6679053	AF11_Susceptible	AF11_Susceptible	deLorgeril	AF11_T60_R3_RNAseq	60h	Rep1	*C. gigas*	`~Time`	CGOSHV1-A transcriptomic data was split up first by family, and then modeled with `~Time`, comparing each time point in each family separately to time 0 h
CGOSHV1-A	SRR6679054	AF11_Susceptible	AF11_Susceptible	deLorgeril	AF11_T48_R3_RNAseq	48h	Rep1	*C. gigas*	`~Time`	CGOSHV1-A transcriptomic data was split up first by family, and then modeled with `~Time`, comparing each time point in each family separately to time 0 h

CGOSHV1-A	SRR6679055	AF11_Susceptible	AF11_Susceptible	deLorgeril	AF11_T48_R2_RNAseq	48h	Rep1	*C. gigas*	`~Time`	CGOSHV1-A transcriptomic data was split up first by family, and then modeled with `~Time`, comparing each time point in each family separately to time 0 h
CGOSHV1-A	SRR6679056	AF11_Susceptible	AF11_Susceptible	deLorgeril	AF11_T60_R2_RNAseq	60h	Rep1	*C. gigas*	`~Time`	CGOSHV1-A transcriptomic data was split up first by family, and then modeled with `~Time`, comparing each time point in each family separately to time 0 h
CGOSHV1-A	SRR6679057	AF11_Susceptible	AF11_Susceptible	deLorgeril	AF11_T60_R1_RNAseq	60h	Rep1	*C. gigas*	`~Time`	CGOSHV1-A transcriptomic data was split up first by family, and then modeled with `~Time`, comparing each time point in each family separately to time 0 h
CGOSHV1-A	SRR6679058	AF11_Susceptible	AF11_Susceptible	deLorgeril	AF11_T24_R2_RNAseq	24h	Rep1	*C. gigas*	`~Time`	CGOSHV1-A transcriptomic data was split up first by family, and then modeled with `~Time`, comparing each time point in each family separately to time 0 h
CGOSHV1-A	SRR6679059	AF11_Susceptible	AF11_Susceptible	deLorgeril	AF11_T24_R1_RNAseq	24h	Rep1	*C. gigas*	`~Time`	CGOSHV1-A transcriptomic data was split up first by family, and then modeled with `~Time`, comparing each time point in each family separately to time 0 h
CGOSHV1-A	SRR6679060	AF11_Susceptible	AF11_Susceptible	deLorgeril	AF11_T48_R1_RNAseq	48h	Rep1	*C. gigas*	`~Time`	CGOSHV1-A transcriptomic data was split up first by family, and then modeled with `~Time`, comparing each time point in each family separately to time 0 h
CGOSHV1-A	SRR6679061	AF11_Susceptible	AF11_Susceptible	deLorgeril	AF11_T24_R3_RNAseq	24h	Rep1	*C. gigas*	`~Time`	CGOSHV1-A transcriptomic data was split up first by family, and then modeled with `~Time`, comparing each time point in each family separately to time 0 h
CGOSHV1-A	SRR6679082	AF11_Susceptible	AF11_Susceptible	deLorgeril	AF11_T72_R2_RNAseq	72h	Rep1	*C. gigas*	`~Time`	CGOSHV1-A transcriptomic data was split up first by family, and then modeled with `~Time`, comparing each time point in each family separately to time 0 h
CGOSHV1-A	SRR6679083	AF11_Susceptible	AF11_Susceptible	deLorgeril	AF11_T72_R3_RNAseq	72h	Rep1	*C. gigas*	`~Time`	CGOSHV1-A transcriptomic data was split up first by family, and then modeled with `~Time`, comparing each time point in each family separately to time 0 h
CGOSHV1-A	SRR6679084	AF11_Susceptible	AF11_Susceptible	deLorgeril	AF11_T12_R2_RNAseq	12h	Rep1	*C. gigas*	`~Time`	CGOSHV1-A transcriptomic data was split up first by family, and then modeled with `~Time`, comparing each time point in each family separately to time 0 h
CGOSHV1-A	SRR6679085	AF11_Susceptible	AF11_Susceptible	deLorgeril	AF11_T12_R3_RNAseq	12h	Rep1	*C. gigas*	`~Time`	CGOSHV1-A transcriptomic data was split up first by family, and then modeled with `~Time`, comparing each time point in each family separately to time 0 h
CGOSHV1-A	SRR6679086	AF11_Susceptible	AF11_Susceptible	deLorgeril	AF11_T6_R3_RNAseq	6h	Rep1	*C. gigas*	`~Time`	CGOSHV1-A transcriptomic data was split up first by family, and then modeled with `~Time`, comparing each time point in each family separately to time 0 h
CGOSHV1-A	SRR6679087	AF11_Susceptible	AF11_Susceptible	deLorgeril	AF11_T12_R1_RNAseq	12h	Rep1	*C. gigas*	`~Time`	CGOSHV1-A transcriptomic data was split up first by family, and then modeled with `~Time`, comparing each time point in each family separately to time 0 h
CGOSHV1-A	SRR6679088	AF11_Susceptible	AF11_Susceptible	deLorgeril	AF11_T6_R1_RNAseq	6h	Rep1	*C. gigas*	`~Time`	CGOSHV1-A transcriptomic data was split up first by family, and then modeled with `~Time`, comparing each time point in each family separately to time 0 h
CGOSHV1-A	SRR6679089	AF11_Susceptible	AF11_Susceptible	deLorgeril	AF11_T6_R2_RNAseq	6h	Rep1	*C. gigas*	`~Time`	CGOSHV1-A transcriptomic data was split up first by family, and then modeled with `~Time`, comparing each time point in each family separately to time 0 h
CGOSHV1-A	SRR6679090	AF11_Susceptible_control	AF11_Susceptible	deLorgeril	AF11_T0_R2_RNAseq	0h	Rep1	*C. gigas*	`~Time`	CGOSHV1-A transcriptomic data was split up first by family, and then modeled with `~Time`, comparing each time point in each family separately to time 0 h

CGOSHV1-A	SRR6679091	AF11_Susceptible_control	AF11_Susceptible	deLorgeril	AF11_T0_R3_RNAseq	0h	Rep1	*C. gigas*	`~Time`	CGOSHV1-A transcriptomic data was split up first by family, and then modeled with `~Time`, comparing each time point in each family separately to time 0 h
CGOSHV1-A	SRR6679093	AF11_Susceptible_control	AF11_Susceptible	deLorgeril	AF11_T0_R1_RNAseq	0h	Rep1	*C. gigas*	`~Time`	CGOSHV1-A transcriptomic data was split up first by family, and then modeled with `~Time`, comparing each time point in each family separately to time 0 h
CGOSHV1-A	SRR6679062	AF21_Resistant	AF21_Resistant	deLorgeril	AF21_T60_R3_RNAseq	60h	Rep1	*C. gigas*	`~Time`	CGOSHV1-A transcriptomic data was split up first by family, and then modeled with `~Time`, comparing each time point in each family separately to time 0 h
CGOSHV1-A	SRR6679063	AF21_Resistant	AF21_Resistant	deLorgeril	AF21_T60_R2_RNAseq	60h	Rep1	*C. gigas*	`~Time`	CGOSHV1-A transcriptomic data was split up first by family, and then modeled with `~Time`, comparing each time point in each family separately to time 0 h
CGOSHV1-A	SRR6679064	AF21_Resistant	AF21_Resistant	deLorgeril	AF21_T60_R1_RNAseq	60h	Rep1	*C. gigas*	`~Time`	CGOSHV1-A transcriptomic data was split up first by family, and then modeled with `~Time`, comparing each time point in each family separately to time 0 h
CGOSHV1-A	SRR6679065	AF21_Resistant	AF21_Resistant	deLorgeril	AF21_T48_R3_RNAseq	48h	Rep1	*C. gigas*	`~Time`	CGOSHV1-A transcriptomic data was split up first by family, and then modeled with `~Time`, comparing each time point in each family separately to time 0 h
CGOSHV1-A	SRR6679066	AF21_Resistant	AF21_Resistant	deLorgeril	AF21_T48_R2_RNAseq	48h	Rep1	*C. gigas*	`~Time`	CGOSHV1-A transcriptomic data was split up first by family, and then modeled with `~Time`, comparing each time point in each family separately to time 0 h
CGOSHV1-A	SRR6679068	AF21_Resistant	AF21_Resistant	deLorgeril	AF21_T24_R3_RNAseq	24h	Rep1	*C. gigas*	`~Time`	CGOSHV1-A transcriptomic data was split up first by family, and then modeled with `~Time`, comparing each time point in each family separately to time 0 h
CGOSHV1-A	SRR6679069	AF21_Resistant	AF21_Resistant	deLorgeril	AF21_T24_R2_RNAseq	24h	Rep1	*C. gigas*	`~Time`	CGOSHV1-A transcriptomic data was split up first by family, and then modeled with `~Time`, comparing each time point in each family separately to time 0 h
CGOSHV1-A	SRR6679070	AF21_Resistant	AF21_Resistant	deLorgeril	AF21_T72_R2_RNAseq	72h	Rep1	*C. gigas*	`~Time`	CGOSHV1-A transcriptomic data was split up first by family, and then modeled with `~Time`, comparing each time point in each family separately to time 0 h
CGOSHV1-A	SRR6679071	AF21_Resistant	AF21_Resistant	deLorgeril	AF21_T72_R1_RNAseq	72h	Rep1	*C. gigas*	`~Time`	CGOSHV1-A transcriptomic data was split up first by family, and then modeled with `~Time`, comparing each time point in each family separately to time 0 h
CGOSHV1-A	SRR6679072	AF21_Resistant	AF21_Resistant	deLorgeril	AF21_T6_R3_RNAseq	6h	Rep1	*C. gigas*	`~Time`	CGOSHV1-A transcriptomic data was split up first by family, and then modeled with `~Time`, comparing each time point in each family separately to time 0 h
CGOSHV1-A	SRR6679073	AF21_Resistant	AF21_Resistant	deLorgeril	AF21_T6_R2_RNAseq	6h	Rep1	*C. gigas*	`~Time`	CGOSHV1-A transcriptomic data was split up first by family, and then modeled with `~Time`, comparing each time point in each family separately to time 0 h
CGOSHV1-A	SRR6679075	AF21_Resistant	AF21_Resistant	deLorgeril	AF21_T12_R1_RNAseq	12h	Rep1	*C. gigas*	`~Time`	CGOSHV1-A transcriptomic data was split up first by family, and then modeled with `~Time`, comparing each time point in each family separately to time 0 h
CGOSHV1-A	SRR6679076	AF21_Resistant_control	AF21_Resistant	deLorgeril	AF21_T0_R2_RNAseq	0h	Rep1	*C. gigas*	`~Time`	CGOSHV1-A transcriptomic data was split up first by family, and then modeled with `~Time`, comparing each time point in each family separately to time 0 h
CGOSHV1-A	SRR6679077	AF21_Resistant_control	AF21_Resistant	deLorgeril	AF21_T0_R1_RNAseq	0h	Rep1	*C. gigas*	`~Time`	CGOSHV1-A transcriptomic data was split up first by family, and then modeled with `~Time`, comparing each time point in each family separately to time 0 h

CGOSHV1-A	SRR6679078	AF21_Resistant	AF21_Resistant	deLorgeril	AF21_T6_R1_RNAseq	6h	Rep1	*C. gigas*	`~Time`	CGOSHV1-A transcriptomic data was split up first by family, and then modeled with `~Time`, comparing each time point in each family separately to time 0 h
CGOSHV1-A	SRR6679079	AF21_Resistant_control	AF21_Resistant	deLorgeril	AF21_T0_R3_RNAseq	0h	Rep1	*C. gigas*	`~Time`	CGOSHV1-A transcriptomic data was split up first by family, and then modeled with `~Time`, comparing each time point in each family separately to time 0 h
CGOSHV1-A	SRR6679080	AF21_Resistant	AF21_Resistant	deLorgeril	AF21_T24_R1_RNAseq	24h	Rep1	*C. gigas*	`~Time`	CGOSHV1-A transcriptomic data was split up first by family, and then modeled with `~Time`, comparing each time point in each family separately to time 0 h
CGOSHV1-A	SRR6679081	AF21_Resistant	AF21_Resistant	deLorgeril	AF21_T12_R3_RNAseq	12h	Rep1	*C. gigas*	`~Time`	CGOSHV1-A transcriptomic data was split up first by family, and then modeled with `~Time`, comparing each time point in each family separately to time 0 h
CGOSHV1-A	SRR6679092	AF21_Resistant	AF21_Resistant	deLorgeril	AF21_T72_R3_RNAseq	72h	Rep1	*C. gigas*	`~Time`	CGOSHV1-A transcriptomic data was split up first by family, and then modeled with `~Time`, comparing each time point in each family separately to time 0 h
CGOSHV1-A	SRR6679074	AF21_Resistant	AF21_Resistant	deLorgeril	AF21_T12_R2_RNAseq	12h	Rep1	*C. gigas*	`~Time`	CGOSHV1-A transcriptomic data was split up first by family, and then modeled with `~Time`, comparing each time point in each family separately to time 0 h
CGOSHV1-A	SRR6679067	AF21_Resistant	AF21_Resistant	deLorgeril	AF21_T48_R1_RNAseq	48h	Rep1	*C. gigas*	`~Time`	CGOSHV1-A transcriptomic data was split up first by family, and then modeled with `~Time`, comparing each time point in each family separately to time 0 h
CGOSHV1-B	SRR2002821	Time0	He	He	Time0_1	0h	Rep1	*C. gigas*	`~Condition`	CGOSHV1-B transcriptomes were separated for each time point and compared to their timepoint control with the model `~Condition`
CGOSHV1-B	SRR2002822	Time0	He	He	Time0_2	0h	Rep1	*C. gigas*	`~Condition`	CGOSHV1-B transcriptomes were separated for each time point and compared to their timepoint control with the model `~Condition`
CGOSHV1-B	SRR2002823	Time0	He	He	Time0_3	0h	Rep1	*C. gigas*	`~Condition`	CGOSHV1-B transcriptomes were separated for each time point and compared to their timepoint control with the model `~Condition`
CGOSHV1-B	SRR2002844	control	He	He	6h_control_1	6h	Rep1	*C. gigas*	`~Condition`	CGOSHV1-B transcriptomes were separated for each time point and compared to their timepoint control with the model `~Condition`
CGOSHV1-B	SRR2002845	control	He	He	6h_control_2	6h	Rep1	*C. gigas*	`~Condition`	CGOSHV1-B transcriptomes were separated for each time point and compared to their timepoint control with the model `~Condition`
CGOSHV1-B	SRR2002846	control	He	He	6h_control_3	6h	Rep1	*C. gigas*	`~Condition`	CGOSHV1-B transcriptomes were separated for each time point and compared to their timepoint control with the model `~Condition`
CGOSHV1-B	SRR2002864	OsHV1	He	He	6h_OsHV_1_1	6h	Rep1	*C. gigas*	`~Condition`	CGOSHV1-B transcriptomes were separated for each time point and compared to their timepoint control with the model `~Condition`
CGOSHV1-B	SRR2002934	OsHV1	He	He	6h_OsHV_1_2	6h	Rep1	*C. gigas*	`~Condition`	CGOSHV1-B transcriptomes were separated for each time point and compared to their timepoint control with the model `~Condition`
CGOSHV1-B	SRR2002935	OsHV1	He	He	6h_OsHV_1_3	6h	Rep1	*C. gigas*	`~Condition`	CGOSHV1-B transcriptomes were separated for each time point and compared to their timepoint control with the model `~Condition`
CGOSHV1-B	SRR2002936	control	He	He	12h_control_1	12h	Rep1	*C. gigas*	`~Condition`	CGOSHV1-B transcriptomes were separated for each time point and compared to their timepoint control with the model `~Condition`
CGOSHV1-B	SRR2002938	control	He	He	12h_control_2	12h	Rep1	*C. gigas*	`~Condition`	CGOSHV1-B transcriptomes were separated for each time point and compared to their timepoint control with the model `~Condition`
CGOSHV1-B	SRR2002940	OsHV1	He	He	12h_OsHV_1_1	12h	Rep1	*C. gigas*	`~Condition`	CGOSHV1-B transcriptomes were separated for each time point and compared to their timepoint control with the model `~Condition`
CGOSHV1-B	SRR2002941	OsHV1	He	He	12h_OsHV_1_2	12h	Rep1	*C. gigas*	`~Condition`	CGOSHV1-B transcriptomes were separated for each time point and compared to their timepoint control with the model `~Condition`

CGOSHV1-B	SRR2002942	OsHV1	He	He	12h_OsHV_1_3	12h	Rep1	*C. gigas*	`~Condition`	CGOSHV1-B transcriptomes were separated for each time point and compared to their timepoint control with the model `~Condition`
CGOSHV1-B	SRR2002943	control	He	He	24h_control_1	24hr	Rep1	*C. gigas*	`~Condition`	CGOSHV1-B transcriptomes were separated for each time point and compared to their timepoint control with the model `~Condition`
CGOSHV1-B	SRR2002944	control	He	He	24h_control_2	24hr	Rep1	*C. gigas*	`~Condition`	CGOSHV1-B transcriptomes were separated for each time point and compared to their timepoint control with the model `~Condition`
CGOSHV1-B	SRR2002945	control	He	He	24h_control_3	24hr	Rep1	*C. gigas*	`~Condition`	CGOSHV1-B transcriptomes were separated for each time point and compared to their timepoint control with the model `~Condition`
CGOSHV1-B	SRR2002947	OsHV1	He	He	24h_OsHV_1_1	24hr	Rep1	*C. gigas*	`~Condition`	CGOSHV1-B transcriptomes were separated for each time point and compared to their timepoint control with the model `~Condition`
CGOSHV1-B	SRR2002948	OsHV1	He	He	24h_OsHV_1_2	24hr	Rep1	*C. gigas*	`~Condition`	CGOSHV1-B transcriptomes were separated for each time point and compared to their timepoint control with the model `~Condition`
CGOSHV1-B	SRR2002949	OsHV1	He	He	24h_OsHV_1_3	24hr	Rep1	*C. gigas*	`~Condition`	CGOSHV1-B transcriptomes were separated for each time point and compared to their timepoint control with the model `~Condition`
CGOSHV1-B	SRR2002950	control	He	He	48h_control_1	48h	Rep1	*C. gigas*	`~Condition`	CGOSHV1-B transcriptomes were separated for each time point and compared to their timepoint control with the model `~Condition`
CGOSHV1-B	SRR2002951	control	He	He	48h_control_2	48h	Rep1	*C. gigas*	`~Condition`	CGOSHV1-B transcriptomes were separated for each time point and compared to their timepoint control with the model `~Condition`
CGOSHV1-B	SRR2002952	control	He	He	48h_control_3	48h	Rep1	*C. gigas*	`~Condition`	CGOSHV1-B transcriptomes were separated for each time point and compared to their timepoint control with the model `~Condition`
CGOSHV1-B	SRR2002953	OsHV1	He	He	48h_OsHV_1_1	48h	Rep1	*C. gigas*	`~Condition`	CGOSHV1-B transcriptomes were separated for each time point and compared to their timepoint control with the model `~Condition`
CGOSHV1-B	SRR2002954	OsHV1	He	He	48h_OsHV_1_2	48h	Rep1	*C. gigas*	`~Condition`	CGOSHV1-B transcriptomes were separated for each time point and compared to their timepoint control with the model `~Condition`
CGOSHV1-B	SRR2002955	OsHV1	He	He	48h_OsHV_1_3	48h	Rep1	*C. gigas*	`~Condition`	CGOSHV1-B transcriptomes were separated for each time point and compared to their timepoint control with the model `~Condition`
CGOSHV1-B	SRR2002956	control	He	He	120h_control_1	120h	Rep1	*C. gigas*	`~Condition`	CGOSHV1-B transcriptomes were separated for each time point and compared to their timepoint control with the model `~Condition`
CGOSHV1-B	SRR2002957	control	He	He	120h_control_2	120h	Rep1	*C. gigas*	`~Condition`	CGOSHV1-B transcriptomes were separated for each time point and compared to their timepoint control with the model `~Condition`
CGOSHV1-B	SRR2002958	control	He	He	120h_control_3	120h	Rep1	*C. gigas*	`~Condition`	CGOSHV1-B transcriptomes were separated for each time point and compared to their timepoint control with the model `~Condition`
CGOSHV1-B	SRR2002959	OsHV1	He	He	120h_OsHV_1_1	120h	Rep1	*C. gigas*	`~Condition`	CGOSHV1-B transcriptomes were separated for each time point and compared to their timepoint control with the model `~Condition`
CGOSHV1-B	SRR2002961	OsHV1	He	He	120h_OsHV_1_2	120h	Rep1	*C. gigas*	`~Condition`	CGOSHV1-B transcriptomes were separated for each time point and compared to their timepoint control with the model `~Condition`
CGOSHV1-B	SRR2002962	OsHV1	He	He	120h_OsHV_1_3	120h	Rep1	*C. gigas*	`~Condition`	CGOSHV1-B transcriptomes were separated for each time point and compared to their timepoint control with the model `~Condition`

Supplementary File 1: *C. virginica* apoptosis genes, transcripts, and proteins. Text file containing GFF3 information about all identified apoptosis transcripts, genes, and proteins in the *C. virginica* reference genome annotation. Access file here https://drive.google.com/drive/folders/1FM0h-5cKhCcMFqPJP9ID0R-icqN7R-UE?usp=sharing.

Supplementary File 2: *C. gigas* apoptosis genes, transcripts, and proteins. Text file containing GFF3 information about all identified apoptosis transcripts, genes, and proteins in the *C. gigas* reference genome annotation. Access file here https://drive.google.com/drive/folders/1FM0h-5cKhCcMFqPJP9ID0R-icqN7R-UE?usp=sharing.

Supplementary File 3: Mollusc IAP Protein Multiple Sequence Alignment. FASTA file containing multiple sequence alignment of the full IAP amino acid sequences from all studied molluscs produced by MAFFT.Access file here https://drive.google.com/drive/folders/1FM0h-5cKhCcMFqPJP9ID0R-icqN7R-UE?usp=sharing.

Supplementary File 4: BIR domain Multiple Sequence Alignment. FASTA file containing Multiple Sequence alignment by MAFFT of individual BIR amino acid sequences from each protein. Sequences are named by their protein accession (XP), followed by which BIR domain the sequence was from (reading from 5' to 3'), then ending with the gene accession (LOC). Species names for each are given in Supplementary Figure 1b. Access file here https://drive.google.com/drive/folders/1FM0h-5cKhCcMFqPJP9ID0R-icqN7R-UE?usp=sharing.

CHAPTER III: *Perkinsus marinus* suppresses *in vitro* eastern oyster apoptosis via IAP-dependent and caspase-independent pathways involving TNFR, NF-kB, and oxidative pathway crosstalk

Erin M. Witkop[1], Gary H. Wikfors[2], Dina A. Proestou[3], Kathryn Markey Lundgren[3], Mary Sullivan[3], Marta Gomez-Chiarri[1]

[1]University of Rhode Island, Department of Fisheries, Animal and Veterinary Science, 120 Flagg Rd. Kingston, RI, USA

[2]NOAA Northeast Fisheries Science Center Milford Laboratory, 212 Rogers Ave. Milford, CT, USA

[3]USDA ARS NEA NCWMAC Shellfish Genetics Program, 120 Flagg Rd. Kingston, RI, USA

Correspondence:

Marta Gomez-Chiarri

gomezchi@uri.edu

Prepared for submission to ***Developmental and Comparative Immunology*.**

Keywords: apoptosis, mitochondria, oyster, differential expression, IAP, WGCNA, Dermo

Highlights

- Basal hemocyte apoptosis in oysters may be IAP-dependent
- *P. marinus* suppression of apoptosis may involve caspase-independent pathways
- *P. marinus* suppressed apoptosis downstream of mitochondrial permeabilization involving an IAP-associated pathway
- Hemocyte apoptosis suppression involved oxidation-reduction, TNFR, NF-kB pathways
- *P. marinus* enzymes potentially involved in apoptosis suppression were identified

Abstract

Perkinsus marinus is an intracellular parasite that causes Dermo disease in eastern oysters, *Crassostrea virginica*. Apoptosis of *P. marinus*-infected hemocytes, the major oyster immune cell, is a key host immune strategy to limit parasite replication. *P. marinus* can suppress apoptosis to prolong its own survival; however, these mechanisms of suppression are poorly understood. This study investigated hemocyte apoptosis and hemocyte and parasite gene expression after a 1 hr *in vitro* challenge with *P. marinus* in the presence or absence of caspase inhibitor Z-VAD-FMK or Inhibitor of Apoptosis protein (IAP) inhibitor GDC-0152. Exposure of hemocytes to the parasite *P. marinus* led to significant inhibition of granular hemocyte apoptosis. Preincubation of hemocytes with a pan-caspase inhibitor prior to *P. marinus* challenge had no significant effect on *P. marinus*-induced apoptosis suppression or mitochondrial permeabilization. Preincubation of hemocytes with an IAP inhibitor prior to *P. marinus* challenge led to a significant reduction of apoptosis of granular hemocytes engulfing the parasite, but no significant change in

mitochondrial permeabilization as compared to *P. marinus* alone. These results suggest that apoptosis suppression by the parasite may involve caspase-independent mechanisms, affects an IAP-involved pathway, and likely occurs downstream of mitochondrial membrane permeabilization. Differential gene expression analysis indicated the hemocyte response to *P. marinus* involves a combination of oxidation-reduction processes and the TNFR and NF-kB pathways. WGCNA analysis of *P. marinus* expression in response to hemocyte exposure revealed correlated expression of proteases, kinases and hydrolases that could contribute to *P. marinus* enzymatic interference with a hemocyte IAP-involved pathway, such as the NF-kB, TNFR, and/or caspase-independent apoptosis pathways. This functional study of hemocyte apoptosis mechanisms and concurrent *P. marinus* expression provides molecular targets for future evaluation of the role of apoptosis on disease resistance in oysters.

Introduction

Emergence and widespread expansion of Dermo disease, caused by the alveolate parasite *Perkinsus marinus*, has contributed to severe declines of the eastern oyster, *Crassostrea virginica* along the Gulf of Mexico and the eastern coast of the United States (Smolowitz, 2013). Infective *P. marinus* trophozoites are ingested by oysters during filter-feeding at mucosal interfaces, recognized by oyster lectins such as CvGal1 and CvGal2, and engulfed by granular hemocytes, the main phagocytic immune cell in oysters (Allam et al., 2013; Lau et al., 2018a; Smolowitz, 2013; Vasta et al., 2020; Wikfors and Alix, 2014). Once inside the granular hemocyte, an array of complex host responses are induced, including release of cytotoxic enzymes, reactive oxygen species (ROS), and serine protease inhibitors by hemocytes (He et al., 2012; La Peyre et al., 2010; Lau et al., 2018b; Sullivan and Proestou, 2021). The parasite can defend itself from the oyster immune response by releasing serine proteases, such as perkinsin, or ROS-neutralizing enzymes, such as superoxide dismutase (SOD) (Faisal et al., 1999; Fernández-Robledo et al., 2008; Lau et al., 2018b). In oysters susceptible to Dermo disease, *P. marinus* is able to overcome, subvert, or suppress host hemocyte defenses, particularly the respiratory burst and apoptosis (a form of regulated cell death) pathways, and replicate intracellularly, leading to hemocyte lysis and release of new parasitic bodies (Alavi et al., 2009; Smolowitz, 2013). The immune pathways affected by *P. marinus* infection, and the mechanisms involved in parasite avoidance of oyster immunity, however, remain incompletely described. Understanding these pathways will enhance our knowledge of host-parasite interactions in the eastern oyster and mechanisms of apoptosis during oyster disease response and provide targets for disease management.

Previous research has shown that apoptosis of eastern oyster hemocytes is a key immune response to *P. marinus*, and increased hemocyte apoptosis following *P. marinus* infection may contribute to oyster resistance to infection by limiting parasite propagation (Michael Goedken et al., 2005; Hughes et al., 2010). Apoptosis is a critical immune pathway in bivalve molluscs and other organisms, aiding in maintenance of cellular homeostasis and contributing to defense responses against pathogens and parasites by, for example, preventing pathogen intracellular replication (Romero et al., 2015). Major pathways of regulated cell death, including apoptosis, are conserved in oysters and apoptosis involves two separate but linked pathways (Gerdol, 2018; Kiss, 2010; Romero et al., 2015). The intrinsic, or mitochondrial, pathway of apoptosis is stimulated by intrinsic damage and is characterized by mitochondrial outer membrane permeabilization (MOMP). In contrast, the extrinsic, or death receptor-mediated, pathway of apoptosis is triggered by extrinsic binding of ligands to pattern recognition receptors and does not typically involve MOMP. Both pathways converge on the action of a family of cysteine-aspartic proteases, collectively termed caspases, which cleave apoptosis substrates and eventually lead to apoptosis execution (Galluzzi et al., 2016). Caspase-independent apoptosis pathways exist, however, and have been identified in bivalves (Romero et al., 2015). Caspase-independent apoptosis pathways often involve the release of enzymes from the mitochondria, such as Apoptosis Inducing Factor (AIF) and endonuclease G (endoG) which translocate to the nucleus and trigger the final steps of apoptosis (Romero et al., 2015).

One important family of apoptosis pathway regulators is the Inhibitor of Apoptosis (IAP), or Baculoviral IAP Repeat-Containing (BIRC) gene family (Estornes and Bertrand, 2015). IAPs are involved in both pathways of apoptosis, and in mammals IAPs assist in

extrinsic pathway initiation by complexing with TNFR, TRAF2, and RIPK1 following extracellular ligand binding, and can interfere with mitochondrial apoptosis by inhibiting caspase 9 and executioner caspase 3/7 (Estornes and Bertrand, 2015). In oysters, the IAP gene family is highly expanded, presenting diverse domain architectures not observed in humans and other model organisms (Witkop et al., in preparation, Chapter II). Diverse assemblages of IAPs are also expressed across different immune challenges, including challenge with *P. marinus,* and are tightly associated with apoptosis pathway expression, suggesting IAPs may help tailor regulation of apoptosis to particular pathogenic challenges (Witkop et al., in preparation, Chapter II).

The parasite *P. marinus* can suppress oyster hemocyte apoptosis likely as a mechanism to prolong its own survival and allow for intracellular replication, although factors such as *P. marinus* strain, salinity, time post-infection, and oyster Dermo resistance status make apoptosis suppression nuanced and variable (Michael Goedken et al., 2005; Micheal Goedken et al., 2005; Hughes et al., 2010; Lau et al., 2018b; Yee et al., 2005). The exact molecular mechanisms of apoptosis suppression by *P. marinus* in eastern oyster apoptosis are unknown. Suppression or modulation of host apoptosis is a common strategy among intracellular parasites, as shown in other host-pathogen systems. The intracellular parasite *Toxoplasma gondii*, for example, has evolved complex strategies to evade or suppress host apoptosis, including prevention of cytochrome c release from the mitochondria, inhibition of caspase enzymes, and activation of the Nuclear Factor-Kappa B (NF-kB) pathway involving complexes of TRAFs and BIRC2/3 (cIAP1/cIAP2) to promote host cell survival and allow for parasite intracellular replication (Lodoen and Lima, 2019; Sangaré et al., 2019). *T. gondii* additionally affects apoptosis regulatory proteins, and triggers

upregulation of antiapoptotic Bcl-2 family proteins and IAPs (Mammari et al., 2019). Current knowledge of *P. marinus*-oyster interactions, combined with our understanding of host-parasite interactions in *T. gondii* and other intracellular parasite systems, informs hypotheses regarding *P. marinus* mechanisms of apoptosis suppression in eastern oyster hemocytes.

To further investigate the mechanisms of apoptosis involved in oyster granular hemocyte response to *P. marinus*, as well as examine the role of IAPs in *P. marinus* infection, this study performed *in vitro* hemocyte assays coupling flow cytometry and dual transcriptomics of *C. virginica* and *P. marinus*. Specifically, this research assessed the role of caspases, mitochondrial membrane permeabilization, and IAPs in hemocyte *P. marinus* response after pretreatment of oyster hemocytes with the IAP inhibitor GDC-0152 and the pan-caspase inhibitor Z-VAD-FMK (Ekert et al., 1999; Flygare et al., 2012) through combined assessment of the cellular apoptotic phenotype and differential gene expression. Understanding the involvement of caspases and IAPs will shed light on mechanisms *P. marinus* employs to modulate hemocyte apoptosis. By identifying apoptosis pathways affected by *P. marinus* and potential *P. marinus* apoptosis-modulatory enzymes for future investigation, this research advances our understanding of the role of apoptosis in host-parasite interactions in the eastern oyster.

Materials and Methods

Oyster source and maintenance

Eastern oysters were obtained from the family-based breeding program at the Aquaculture Genetics and Breeding Technology Center (ABC) at the Virginia Institute of

Marine Science (VIMS). Oyster juveniles (<one year old) from 22 selectively-bred families with varying levels of survival in the Chesapeake Bay were delivered to the USDA ARS Shellfish Genetics Laboratory, Kingston, RI, in early June 2020 and subjected to a state-required disinfection protocol. Oyster maintenance and parasite challenge protocols have been previously described in detail (Proestou et al., 2019). Briefly, oysters were maintained in a 750-L, recirculating, aerated aquarium system running 1-µm filtered, UV-sterilized seawater following filtration. Oysters were acclimated to experimental conditions of 25°C and 25 ppt over a period of two weeks and fed daily with Shellfish Diet 1800® instant algae (Reed Mariculture) throughout the experiment. Temperature was maintained at 25°C using tank heaters when necessary and kept at ambient salinity (25-30 ppt) until hemocyte extraction.

Perkinsus marinus **culture**

Perkinsus marinus from ATCC® strain 50509, 'DBNJ', (American Type Culture Collection) was cultured as previously described (Bushek et al., 1994). This strain, originally isolated from diseased oysters from Delaware Bay, is comparable in virulence to *P. marinus* strains present in the Chesapeake Bay (Bushek and Allen, 1996). Cultures were used during the more virulent log phase growth stage (Ford et al., 2002). Parasite cell preparation for challenge was performed according to previous protocols (Proestou and Sullivan, 2020). Briefly, *P. marinus* cells were concentrated in 50-mL falcon tubes by centrifugation at 1,500 g for 5 min at 4°C and washed using 0.45-µm filtered, sterile seawater at 28 PSU (FSW) three times. Cells were counted using neutral red staining with

a hemacytometer and light microscope, and cell concentration was adjusted to the desired stock concentration for treatment.

Hemolymph isolation and preparation

To assess general *in vitro* mechanisms of apoptotic response to *P. marinus* independent of the disease resistance level of each of the oyster families used, and to have enough hemocytes to perform multiple assays and treatments in parallel, three biological replicate pools were prepared using hemolymph extracted from a mix of randomly selected oysters from the 22 families (total of 48 mL in each pool, n=12-15 oysters per hemocyte pool per bleeder, 1-3 oysters per family). Prior to hemolymph collection, oysters were scrubbed and cleaned using a freshwater rinse, wiped with 70% ethanol, and notched in the edge of the shell using a metallic hole puncher. Several days after notching, to allow for oyster recovery after the notching procedure, hemolymph samples were collected from each oyster through the notch in the shell using a using a sterile 1.5'' 25 G needle and 1-ml syringe primed with 100 µl of ice cold, 0.45-µm filtered sterile seawater (FSSW). The hemolymph from each individual oyster was filtered using a 75-µm mesh screen prior to pooling to remove large debris and tissue that may interfere with flow cytometry analysis. Hemolymph cell concentrations in each pool were measured using neutral red staining on a hemacytometer using a light microscope, and volume of *P. marinus* required to achieve the desired 1:1 Multiplicity Of Infection (MOI) were calculated based on hemocyte concentrations in each pool. Hemolymph suspensions were stored on ice through all the procedures to avoid hemocyte aggregation and used within hours of extraction from the oysters.

Dose and temporal effects of GDC-0152 and Z-VAD-FMK on oyster hemocytes

The effect of IAP inhibitor GDC-0152 (ApexBio Technology, cat. no A4224) and pan-caspase inhibitor Z-VAD-FMK (BD, CAT# BDB550377) on eastern oyster hemocyte cell viability, apoptosis, and caspase 3/7 activity in the absence of *P. marinus* was determined using flow cytometry (see methods below). This experiment was performed prior to the main experiment and utilized oysters from a single family to minimize biological variability. Hemolymph pools (n = 2 pools per treatment, n=8 oysters per pool) were incubated at room temperature with different concentrations for each inhibitor (10, 50, or 100 µM) or control (FSSW) for either 3 or 4 hr. Each treatment was performed in duplicate.

***In vitro* challenge of oyster hemocytes with *P. marinus* for flow cytometry**

Live *P. marinus* cells used for oyster hemocyte challenge were incubated with 2 µL of a 1-mM stock solution of CellTrace Far Red live cell stain (ThermoFisher C34564) in DMSO per 1 mL of *P. marinus* culture (final concentration 2µM/mL). Cells were gently agitated following reagent addition and incubated for 30 min at room temperature in the dark. Following incubation, cells were centrifuged at 2,000 g for 10 min at 4C, supernatant was removed, and cells were resuspended in 1 mL FSW.

Hemolymph (100 µL for all but the caspase 3/7 activity assay, 200 µL for the caspase 3/7 activity assay) was aliquoted into sterile 5-mL polystyrene, round-bottom tubes for flow cytometry to achieve a final concentration of $5 \times 10^3 - 9 \times 10^3$ cells per tube, depending on the initial hemocyte concentration of each pool. Treatments, each performed in triplicate, included: 1) Negative Control: hemocytes and FSW; 2) Positive Control:

hemolymph plus fluorescent beads (~6 µM Flow Check Ruby Red microspheres, Polysciences, CAT # 24288-5) coated with the pathogen-associated molecular pattern LPS (ThermoFisher, CAT #00-4976-93) (1:1 hemocyte to beads ratio based on starting hemolymph concentration); 3) *P. marinus*: hemolymph incubated with live-stained *P. marinus* at a 1:1 multiplicity of infection (MOI); 4) IAP inhibitor assay: hemolymph preincubated for 3 hr with 1-mM 50-µM of the IAP inhibitor GDC-0152 plus live-stained *P. marinus* at a 1:1 MOI; 5) Caspase inhibitor assay: hemolymph preincubated for 1 hr with 100-µM Z-VAD-FMK plus live-stained *P. marinus* at a 1:1 MOI. Hemocytes were incubated with *P. marinus,* beads, or FSW for 1 hr at room temperature, and flow cytometry was performed as described below.

Flow cytometry

Four assays were performed, each sample was assayed in triplicate: a) viability assay (4 µL 10X SYBR Green – SYBR- or 4 µL of 1 mg/ml propidium iodide – PI - in 100 µL hemolymph and 300 µL FSW) to measure the proportion of live (SYBR Green) and dead (PI) hemocytes in each sample (Croxton et al., 2012); b) apoptosis Assay (FITC Annexin-V, BD Pharmingen, catalog # 556419; final concentration of 25 µL/ml in 100 µL hemolymph and 100 µL FSW) to measure the proportion of apoptotic hemocytes in each sample (Hughes et al., 2010); c) caspase 3/7 activity (caspase) assay (CellEvent Caspase 3/7 Green Detection Reagent, Thermo Fisher, Cat #C10427; final concentration of 1.25 µL/ml in 200 µL hemolymph and 200 µL FSW) to measure the proportion of caspase 3/7 active hemocytes in each sample; and d) mitochondrial outer membrane permeabilization (MOMP) assay to measure the proportion of hemocytes with permeabilized outer

mitochondrial membranes, a critical morphological feature of intrinsic apoptosis (MitoProbe JC-1 Assay kit for Flow Cytometry, ThermoFisher Cat # M34152; 2 µM final concentration in 100 µL hemolymph and 100 uL FSW (Rodriguez et al., 2020)). Following reagent addition, tubes in the caspase and viability assays were incubated for 1 hr at room temperature in the dark, while apoptosis and MOMP assays incubated at room temperature in the dark for 15 min following kit manufacturer's instructions.

Additional control assays were performed (in triplicate) for particular assays listed above: 1) MOMP assay positive control, to confirm proper detection of MOMP in treated samples: hemolymph plus mitochondrial membrane disruptor CCCP (MitoProbe JC-1 Assay kit for Flow Cytometry, ThermoFisher Cat # M34152; 50 µM final concentration); 2) Unstained *P. marinus* control (all assays), to determine basal parameters in *P. marinus* in absence of oysters hemocytes; 3) Fluorescent probe single stained compensation controls, in order to assist with proper gating during flow cytometry results analysis: SYBR Green plus hemolymph, PI plus hemolymph, CellTrace Far Red live cell stain plus *P. marinus*, fluorescent beads plus hemolymph; 4) Hemolymph phagocytosis assay to compare hemocyte rates of phagocytosis between beads vs. *P. marinus*: hemolymph plus LPS-coated beads, or hemolymph plus *P. marinus*.

Flow cytometry assays were run on a BD Accuri C6+ flow cytometer (BD) (NOAA NEFSC Milford Laboratory) for 1 min 30 sec using a fast flow rate (66 µL/min) with a threshold of 100,000 on FSC-H. Instrument QC was checked prior to use using the BD CS&T RUO beads (Becton Dickinson, CAT # 661414). All flow cytometry plots were compensated using manufacturers recommendations for the BD Accuri C6+ in the BD Accuri C6 Plus flow Software (V 1.0.23.1). Populations of granulocytes, the main

phagocytic cell in the oyster, and agranulocytes, the non-phagocytic *C. virginica* hemocyte were gated using custom FSC-H vs SSC-H gates on scatterplots (Wikfors and Alix, 2014). Subpopulations of granular hemocytes with and without engulfed *P. marinus* were determined based on custom quadrant gates. Gating single stained controls for each fluorescent probe and samples plotted as count histograms for each stain were utilized to properly adjust gating positions for all assays.

Flow cytometry statistical analysis

Results are expressed as average ± sd of percent cells showing a particular phenotype (i.e. viability, apoptosis, etc.). Significant differences between treatment groups for apoptosis, viability, MOMP, and caspase 3/7 activity were measured using one-way and two-way ANOVA with arcsine transformed cell percentage data to ensure normal distribution. Post-hoc testing was performed for ANOVA tests with the Tukey Honestly Significant Difference (HSD) test. For comparison of granular and agranular cell composition and viability between cell types, differences were assessed using a Student's T-test (*t.test*). All statistical analyses were performed in R Studio (V 3.6.1) (Team., 2020). Plots were generated in R Studio using ggplot2 and compiled with egg (V 0.4.5) and cowplot (V 1.0.0) (Claus O. Wilke) (see code on github https://github.com/erinroberts/Dermo_apoptosis_analysis).

Hemocyte *in vitro* challenge with *P. marinus* for transcriptome sequencing

Assays for transcriptome analysis were performed in parallel with the flow cytometry assays, using cells from the same hemolymph pools and the same experimental conditions,

except for volume and in the absence of fluorescent stains. Hemolymph pools were aliquoted into three sterile 50 mL falcon tubes for each treatment (10 mL hemolymph each sample with 4.5-9 x 10^5 total hemocytes in each sample, 12 samples total, n = 3 for each treatment;). The following treatments were performed: 1) Hemolymph only; 2) Hemolymph plus unstained *P. marinus* (MOI 1:1); 3) Hemolymph pretreated for 3 hr with the IAP inhibitor GDC-0152 plus *P. marinus* (MOI 1:1); 4) Hemolymph pretreated for 1 hr with the pan-caspase inhibitor Z-VAD-FMK plus *P. marinus* (MOI 1:1). All treatments were incubated for 1 hr after *P. marinus* addition, at which point samples were centrifuged at 1,500 x g, 4 C for 15 min, supernatant was removed, cell pellets were flash frozen in liquid nitrogen, and samples were stored at -80C prior to RNA extraction.

RNA extraction, cDNA synthesis, sequencing

Cell pellets (from 10 mL hemolymph) were lysed by incubation with 750 µL of Trizol reagent (Invitrogen, CAT# 15596018) for 15 min on ice (ThermoFisher CAT #15596026). Cellular debris was removed by centrifugation at 12,000 g for 10 min at 4C. RNA was extracted with 200 µL of chloroform, shaken vigorously, and incubated at room temperature for 15 min. Following centrifugation at 12,000 x g at 4C for 15 min, the aqueous layer was removed. An additional chloroform extraction was performed with 500 µL of chloroform, shaken vigorously, and incubated at room temperature for 15 min. Following centrifugation at 12,000 x g at 4C for 15 min, the aqueous layer was removed. RNase-free glycogen (5 µg; ThermoFisher, CAT #AM9510) was added to all samples as a carrier to the aqueous phase. Room temperature 500 µL of isopropanol was added and incubated for 10 min at room temperature, followed by centrifugation at 12,000 x g for 10

min at 4 C. Three sequential washes were performed with ice-cold, molecular grade 75% ethanol. Samples were air-dried for 5 min and resuspended in 15 µL of DEPC-treated water. Samples were DNase treated using the DNA-free DNA Removal Kit (Invitrogen, CAT #AM1906) using manufacturer recommendations. Quality and quantity of extracted RNA was assessed using the Nanodrop 8000 Spectrophotometer (ThermoFisher). cDNA library preparation was performed by GENEWIZ using in-house protocols, including rRNA removal. Paired-end transcriptomes were sequenced on Illumina Hi-Seq 2 x150bp at a depth of 15-20 million reads per sample by GENEWIZ.

Mapping and Assembly of RNAseq data

BBTools BBMap (V 37.36) was used to trim adapters, quality trim the left and right sides of reads with Phred quality scores of less than 20 and removed entire reads with an average *Phred* score of less than 10 (Bushnell, n.d.). Transcriptomes were first aligned to the *C. virginica* reference genome sequence (GCF_002022765.2) using HISAT2 (V 2.1.0) with default parameters and without use of a reference annotation to allow for novel transcript discovery (Kim et al., 2016; Pertea et al., 2016). HISAT2 output files were sorted and converted to BAM format using SAMtools (V 1.9.0) (Li et al., 2009). Transcripts were assembled and quantified using the *C. virginica* reference genome annotation (GCF_002022765.2_C_virginica-3.0_genomic.gff) using Stringtie (V 2.1.0) (Pertea et al., 2016). Comparison of transcriptome annotation to the reference for each sample was conducted using *gffcompare* (V 0.11.5) (Pertea et al., 2016). Stringtie output was formatted into matrices of transcript count data and uploaded into R Studio (V 3.6.1) (Team., 2020). The same process for alignment, assembly, and quantification was repeated with

transcriptome files using the *P. marinus* reference genome sequence and reference annotation (GCA_000006405.1). Scripts used for analysis are available on github.

Differential Expression Analysis

Differential transcript expression for *C. virginica* hemocyte and *P. marinus* genes was calculated using DESeq2 (V 1.24.0) in R Studio (V 3.6.1) (Love et al., 2014; Team., 2020). To analyze hemocyte differential gene expression, the formula "~condition" was used to compare each individual treatment to the control non-treated hemocytes (control hemocyte alone compared to *P. marinus* treated hemocytes, GDC-0152 pretreated and *P. marinus* treated hemocytes, or Z-VAD-FMK pretreated and *P. marinus* treated hemocytes). To analyze the effect of inhibitor treatment on *P. marinus* differential gene expression, the formula "~condition" was used to compare *P. marinus* expression in *P. marinus* exposed to hemocytes pretreated with either GDC-0152 or ZVAD-FMK to expression in *P. marinus* exposed to untreated hemocytes. Transcript counts were log-scale transformed and normalized to the library size using the *rlog* formula (Love et al., 2014). Transcripts with < 10 counts were removed from analysis. Log fold changes (LFC) in expression between genes within experiments were considered significant when *p*-values adjusted (*Padj*) using the Benjamini–Hochberg to control for the False Discovery rate (FDR) were ≤ 0.05. LFC shrinkage was performed using "*apeglm*" to improve ranking genes by effect size and to enable comparison of LFC between experiments (Zhu et al., 2018). LFC heatmaps were generated with *ComplexHeatmap* (V 2.0.0) (Gu et al., 2016), transcript count heatmaps were produced with *pheatmap* (V) and volcano plots were generated with *ggplot2*. Gene Ontology enrichment was conducted with the list of

significantly correlated genes in each module using the package *topGO* (V 2.36.0) (Alexa A, 2019) in R (V 3.6.1). GO terms for each protein were obtained by running the full protein sequences for the eastern oyster genome assembly (GCA_002022765.4) and the *P. marinus* assembly (GCA_000006405.1) through Interproscan (V 5.44). Bubble plots of GO enrichment data were created with *ggplot2*. Treemap plots were generated with REVIGO using default parameters and the *treemap* package (V 2.4-2) in R (Supek et al., 2011).

Weighted Gene Correlation Network Analysis (WGCNA) and GO Enrichment

WGCNA was performed for both the hemocyte and *P. marinus* expression datasets to assess highly correlated sets of genes significantly responding to treatment and apoptosis phenotype (i.e. percent apoptotic hemocytes with engulfed *P. marinus,* as determined by flow cytometry) using WGCNA (V 1.68) in R (V 3.6.1) (Langfelder and Horvath, 2008). Expression data was transformed as for the DESeq2 experiment using the *rlog* transformation prior to network construction. Networks were constructed as "*signed hybrid*" type with robust correlation performed using the bi-weight mid-correlation (corFunc= "*bicor*") (Langfelder and Horvath, 2008). A soft thresholding power of 7 produced the best fit to scale free topology and was selected to construct each network. Significant correlation of modules with challenge condition (Pearson's correlation, *cor* function) was first used to prune module lists (p-value ≤ 0.05). For the hemocyte gene expression analysis, module lists were additionally subset based on the following criteria: 1) contain apoptosis-related transcripts (Witkop et al., in preparation, Chapter II), 2) have a high ($r>0.4$) and significant ($p<0.05$) correlation between gene significance and module

membership, indicating that highly connected genes in the module were also significant for the effect of *P. marinus* challenge of hemocytes, 3) are significantly correlated with apoptosis phenotype (arcsine transformed percentages of hemocytes that had engulfed *P. marinus* cells and were apoptotic). For the *P. marinus* gene expression analysis, module lists were subset based on the same criteria, except that modules were not pruned based on whether they contained hemocyte apoptosis-related transcripts. For both analyses, intramodular hub genes were identified as genes in each module with an absolute value for gene significance (GS) > 0.6, and an absolute value for module membership (MM) (calculated with the *signedKME* function) > 0.8. Gene Ontology enrichment was conducted with the list of significantly correlated genes in each module using the package topGO (V 2.36.0) (Alexa A, 2019) in R (V 3.6.1).

Modules of interest (identified using criteria above) were exported from WGCNA using *exportNetworkToCytoscape* without prior subsetting for edge weight, and edge files were then uploaded to Cytoscape (V 3.8.0) along with corresponding product annotations and trait significance for visualization (Shannon et al., 2003). Selected modules were subset for apoptosis-related genes of interest (both hub genes and non-hub genes identified above in WGCNA based on GS for treatment and MM) and genes of interest with significant correlations with apoptosis phenotype. The network was drawn with the prefuse force directed layout using edge weight (Shannon et al., 2003). For *P. marinus* modules, nodes were filtered to keep intramodular hub genes for treatment and edges with weights greater than or equal to the 80th percentile of edge weights from the entire module were kept. *P. marinus* modules were drawn using the circular layout.

Results

Apoptosis in unstimulated granulocytes was affected by IAP inhibitor pretreatment, but not by caspase inhibitor pretreatment

Potential mechanisms of hemocyte apoptosis and optimal conditions for treatment with inhibitors were investigated in unstimulated hemolymph (*i.e.* not challenged with *P. marinus*). The mean percentage of agranular hemocytes in pooled hemolymph was significantly higher (55% vs. 45%) than granular hemocytes (One-way ANOVA, Tukey HSD $p<0.05$; Figure 1a). Cell viability (100% minus the percentage of PI-stained necrotic cells) in untreated hemocytes was high in both the granular (92% viability, Figure 1b) and agranular subpopulations (99% viability, not shown). Treatment with the pan-caspase inhibitor Z-VAD-FMK did not significantly affect the viability of granular hemocytes at any of the tested concentrations (91-94%), suggesting no cytotoxic effects of inhibitor treatment (Figure 1b). Treatment with the IAP inhibitor GDC-0152 for 3 or 4 hr significantly increased granular hemocyte cell death at the 100 µM dose (One-way ANOVA, Tukey HSD, $p < 0.02$), indicating potential cytotoxicity of GDC-0152 at this concentration. To avoid potential cytotoxicity of GDC-0152, subsequent *in vitro* assays were performed with a 3 hr pre-incubation of GDC-0152 at a final concentration of 50 µM.

Levels of apoptosis in unstimulated granular and agranular hemocytes were low overall (Figure 1b, Supplementary Figure 1), but granular hemocyte apoptosis significantly differed in response to inhibitor treatment, while agranular cell apoptosis did not (Figure 1b, Supplementary Figure 1). Focus was placed on granular hemocytes in subsequent analyses based on these results and the known importance of these cells in oyster immune responses to *P. marinus* (La Peyre et al., 1995; Soudant et al., 2013; Vasta et al., 2020;

Wikfors and Alix, 2014). As predicted by the known action of GDC-0152 in other organisms (Hu et al., 2015), IAP inhibition significantly increased granular hemocyte apoptosis as compared to control in a dose-dependent manner (One-Way ANOVA, p = 0.001; Figure 1c, 1d), revealing some or all of granular hemocyte apoptosis is likely IAP-dependent. Caspase 3/7 activation was not significantly affected by IAP inhibition in granular hemocytes (Figure 1e), suggesting apoptosis triggered by IAP inhibition is likely caspase-independent.

As expected, treatment with the pan-caspase inhibitor Z-VAD-FMK led to a dose-dependent decrease in caspase 3/7 activation in granular hemocytes at 3 hr after treatment (Figure 1f). No significant differences were observed in caspase 3/7 inhibition between the two time points (3 vs. 4 hr incubation; p>0.05; Figure 1f). Treatment with the caspase inhibitor Z-VAD-FMK significantly increased apoptosis when the data from all concentrations were combined (One Way ANOVA, Tukey HSD p = 0.006), although no individual treatments were significantly different from control, possibly a consequence of lack of power in individual treatments (Figure 1c, d). This result is the opposite of expectations if unstimulated hemocyte apoptosis was caspase-dependent, because in this case caspase inhibition would be predicted to suppress apoptosis. A hemocyte pretreatment of 1 hr with the 100 µM concentration was used in subsequent experiments to streamline the assays (*i.e.* stagger the two inhibitor treatments).

Pretreatment with an IAP inhibitor affected *P. marinus* inhibition of apoptosis downstream of membrane permeabilization, while a caspase inhibitor had no effect

P. marinus cells used for hemocyte challenges had high levels of viability (SYBR green stained viable *P. marinus,* 95.0% ± 1.9%, not shown). Incubation of hemolymph with live *P. marinus* trophozoites for 1 hr led to a significantly higher phagocytosis rate in granulocytes compared to incubation with LPS-activated beads (13.2% vs 2.3%; One Way ANOVA, Tukey HSD $p = 0.0006$, not shown). Treatment with *P. marinus* led to a significant decrease in granular hemocyte apoptosis as compared to controls, an effect seen in both subsets of hemocytes (containing and not containing engulfed *P. marinus*; $p < 0.02$; Figure 2a, Supplementary Figure 2a). These results confirm previous research showing that *P. marinus* is able to suppress hemocyte apoptosis (Michael Goedken et al., 2005; Hughes et al., 2010). Treatment with LPS-activated beads did not trigger a significant change in apoptosis levels in granular hemocytes (Figure 2a).

To further investigate mechanisms of apoptosis inhibition by *P. marinus*, hemocyte apoptosis was modulated through pretreatment with the IAP inhibitor GDC-0152, which can affect both the intrinsic and extrinsic apoptosis pathways (Erickson et al., 2013; Hu et al., 2015; Tchoghandjian et al., 2016). While pretreatment of hemocytes with the IAP inhibitor GDC-0152 led to an increase in apoptosis in granular hemocytes as compared to non-treated controls (Figure 1a), pretreatment of hemocytes with the IAP inhibitor, followed by challenge with *P. marinus,* led to a significant decrease in levels of apoptosis in total granular hemocytes (both with and without engulfed *P. marinus;* Figure 2a, left panel) and the subset of hemocytes without engulfed *P. marinus*, as compared to control hemocytes (FSW treatment) (Figure 2a, middle panel). Apoptosis in the subset of granular hemocytes with engulfed *P. marinus* was also significantly lower in the dual GDC-0152 and *P. marinus* treatment than in the treatment with *P. marinus* alone ($p = 0.03$, Figure 2a).

These results suggest that *P. marinus* was able to overcome the increase in apoptosis allowed by release of the control that endogenous oyster apoptosis inhibitors (IAPs) exert on hemocyte apoptosis, being able to inhibit apoptosis even in absence of several functional oyster IAPs.

Despite the lack of increase in apoptosis observed in granular hemocytes pretreated with GDC-0152 and then exposed to *P. marinus* (Figure 2a), an overall significant increase in mitochondrial permeabilization was observed in these cells as compared to control granular hemocytes (p = 0.0005; Figure 2b, right panel, Supplementary Figure 2b). Furthermore, although pretreatment with GDC-0152 led to a significant suppression of granular hemocyte apoptosis in the subset of granular hemocytes with engulfed *P. marinus* (as compared to non-pretreated hemocytes; Figure 2a, right panel), mitochondrial permeabilization was not significantly affected by pretreatment with the IAP inhibitor (Figure 2b, right panel, Supplementary Figure 2a, b). These results imply that *P. marinus* suppressed apoptosis downstream of MOMP.

Finally, dual treatment of hemocytes with Z-VAD-FMK and *P. marinus* did not significantly affect granulocyte apoptosis as compared to *P. marinus* alone (Figure 2a). *P. marinus* treatment, as well as treatment with either Z-VAD-FMK or GDC-0152 and *P. marinus,* also had no significant effect on caspase 3/7 activity (Figure 2c, Supplementary Figure 2c), suggesting apoptotic processes suppressed by *P. marinus* do not rely on caspase 3/7 activation.

***P. marinus* triggered expression of oyster genes involved in catalytic and proteolytic activity, RNA binding, and metabolic processes in hemocytes, but few genes in apoptosis pathways were differentially expressed**

To further investigate mechanisms of oyster hemocyte apoptosis inhibition by *P. marinus*, the effect of incubation of *P. marinus* with oyster hemocytes on both *P. marinus* and oyster hemocyte gene expression was evaluated. Transcriptome sequencing produced 10-30 M reads per sample (not shown) and *rlog* transformed read counts clustered by hemocyte pool and treatment (Figure 3a).

P. marinus-treated hemocytes differentially expressed 518 total transcripts compared to control untreated hemocytes, most of which were upregulated in response to *P. marinus* (Figure 3b). Few apoptosis-related transcripts, 15 total and 3 with LFC > 1, all of which were IAP transcripts (Figure 3b), were differentially expressed in hemocytes challenged with *P. marinus*. Of the 3 differentially expressed IAP transcripts, two transcripts were upregulated (LFC >2), one with BIRC2/3-like architecture and another with TY-BIR-RING structure, and one BIRC was strongly downregulated (BIRC5-like, LFC = -5) (Witkop et al., in preparation, Chapter II). Differentially expressed apoptosis-related transcripts with low LFC (<1) included some involved in the TLR pathway (TLR13, MyD88, TRAF4), the TNFR pathway (BIRC2/3-like, caspase 8), and the ER and calcium signaling pathway (IP3R, PDCD6, calpain 9). These results show that *P. marinus* exposure triggered hemocyte expression of IAP proteins, but little change overall in apoptosis pathway gene expression.

Gene Ontology (GO) enrichment analysis was performed with the 581 differentially expressed genes from hemocytes exposed to *P. marinus* for 1 hr. This identified 18

molecular function (MF) and 14 biological process (BP) significantly enriched GO terms (Fisher's Exact test, $p \leq 0.05$) (Figure 3c). The top five significant MF terms were protein binding (GO:0005515), motor activity (GO:0003774), GTPase activator activity (GO:0005096), and ATP binding (GO:0005524), and the top five significant BP terms were anion transport (GO:0006820), protein phosphorylation (GO:0006468), signal transduction (GO:0007165) and transcription initiation from RNA polymerase (GO:0006367). Additional enriched terms were associated with key enzymes involved in responses to parasitic infection (Chakraborti et al., 2019; Dean et al., 2014; Siqueira-Neto et al., 2018; Xue, 2019), including serine-type endopeptidase inhibitor activity (GO:0004867), protein kinase activity (GO:0004672), peptidase activity (GO:0008233), and metallopeptidase activity (GO:0008237). REVIGO analysis revealed RNA binding, catalytic activity, motor activity, protein binding, GTPase activator activity, and cation transmembrane transporter activity to be the most representative enriched GO molecular functions, and anion transport, glycosaminoglycan metabolic processes and regulation of small GTPase mediated signal transduction to be the most representative biological processes (Supplementary Figure 3a, b).

Hemocyte transcripts differentially expressed to *P. marinus* challenge that were annotated with enriched GO terms were investigated to determine whether they overlapped with known enzymes or proteins previously implicated as important in *P. marinus* infection. Of greatest interest were 3 significantly differentially expressed transcripts that had GO terms for enriched serine-type endopeptidase activity, because serine protease inhibitors are important *C. virginica* secreted enzymes in defense against *P. marinus* and other pathogens (Xue, 2019). These transcripts included two inter-alpha-trypsin inhibitor

heavy chain H3-like proteins (XP_022300431.1, XP_022300432.1) possessing inter-alpha-trypsin domains (IPR013694) and one spondin-1-like transcript (XP_022294477.1) which possessed basic protease (Kunitz-type) inhibitor family signatures (IPR002223).

Pretreatment of hemocytes with IAP inhibitor GDC-0152 followed by exposure to *P. marinus* led to upregulation of oxidation-reduction processes and modulation of hemocyte TNFR and NF-kB pathway signaling

Results from the Z-VAD-FMK gene expression analysis are not presented here because apoptosis phenotypes following dual treatment with *P. marinus* and Z-VAD-FMK were not significantly different from apoptosis phenotypes following treatment with *P. marinus* alone. To better understand mechanisms that led to further suppression of apoptosis in the dual GDC-0152 and *P. marinus* treatment (Figure 2), hemocyte differential gene expression in this challenge was analyzed. Hemocyte *in vitro* pre-treatment with GDC-0152 followed by *P. marinus* challenge stimulated three times as many differentially expressed transcripts compared to challenge with *P. marinus* alone (1577 versus 518). This included a higher number of transcripts associated with apoptosis-related pathways, with 62 differentially expressed transcripts (17 with LFC >=1 or <= -1) compared to 15 (Figure 3b right panel, d, e). Similarly, many more GO terms were significantly enriched (44 MF, 37 BP) in the GDC-0152 and *P. marinus* treatment compared to *P. marinus* treatment alone (Figure 3c). The top five significant MF GO terms included protein binding (GO:0005515), ATP binding (GO:0005524), DNA-binding transcription factor activity (GO:0003700), unfolded protein binding (GO:0051082), and oxidoreductase activity, acting on diphenols and related substances as donors (GO:0016679). The top five BP enriched GO terms

included protein folding (GO:0006457), oxidation-reduction process (GO:0055114), regulation of transcription, DNA-template (GO:0006355), tRNA aminoacylation for protein translation (GO:0006418), and tissue regeneration (GO:0042246). REVIGO analysis of BP terms highlighted regulation of metal ion transport, metabolic processes, oxidation-reduction process, superoxide metabolic process and protein folding, among others, as key representative terms in the set of enriched BP terms (Supplementary Figure 3d).

Additional enriched GO terms previously implicated in intracellular parasite infections (Chakraborti et al., 2019; Dean et al., 2014; Siqueira-Neto et al., 2018; Xue, 2019) were regulation of metal ion transport (GO:0010959), superoxide metabolic processes (GO:0006801), and several endopeptidase related terms, including peptidase activity, endopeptidase activity (GO:0004175, DEGs proteasome subunit alpha type-4-like, proteasome subunit alpha type-3-like), threonine-type endopeptidase activity (GO:0004298, DEGs proteasome subunit beta type-6-like, proteasome subunit alpha type-2-like) and aspartic-type endopeptidase activity (GO:0004190, DEGs beta-secretase 1-like, signal peptide peptidase-like 2B, oxysterol-binding protein-related protein 1-like) (Figure 3e). Although serine-type endopeptidase inhibitor activity (GO:0004867) was not enriched in the treatment with GDC-0152 and *P. marinus*, the same inter-alpha-trypsin inhibitor heavy chain H3-like transcripts from the *P. marinus* challenge alone were differentially expressed in the GDC-0152 and *P. marinus* treatment.

One large difference between hemocyte response to *P. marinus* alone and dual treatment with GDC-0152 and *P. marinus* was the enrichment of oxidation-reduction processes in response to the combined treatment, which has previously been identified as

key in oyster response to *P. marinus* and intracellular parasites in general (Fernández-Robledo et al., 2008; Lau et al., 2018b; Proestou and Sullivan, 2020; Schott et al., 2003; Sullivan and Proestou, 2021; Xue, 2019). DEGs representing enriched superoxide metabolic processes included superoxide dismutase [Cu-Zn], chloroplastic-like (XP_022304796.1) and glutenin, high molecular weight subunit DX5-like (XP_022314583.1) which contains a Cu-Zn-superoxide dismutase family signature. DEGs also contained oxidoreductase activity related transcripts, which included a conditioned medium factor receptor 1-like (XP_022336529.1) with a GG-red-SF: geranylgeranyl reductase family domain, and 7-dehydrocholesterol reductase-like transcripts (XP_022318313.1, XP_022318314.1).

Further investigation of significantly differentially expressed apoptosis-related transcripts in the GDC-0152 and *P. marinus* treatment revealed complex responses of multiple apoptotic pathways, including strong upregulation of intrinsic (mitochondrial apoptosis, oxidative stress, ER stress, DNA damage response) and extrinsic apoptosis pathways (TNFR pathway, NF-kB pathway), strong upregulation of multiple IAPs, and downregulation of the TLR pathway (Figure 3c, d). Inflammatory pathways and extrinsic apoptosis were the most responsive apoptosis related pathways, including receptors (TNRSF5, TLR3,4,6,13), receptor adapter proteins (TRAF3,4,6, BIRC2/3-like), signal transduction molecules (MyD88), inhibitory molecules (hsp70, BAG3, hsp90), transcription factors (LITAF, AP-1, IRF1), and effector molecules (caspase 8, IRF1), although NF-kB specifically was not identified as differentially expressed. A total of 8 IAP transcripts were differentially expressed, 7 of those upregulated with LFC > 1, including 2 BIRC2/3 (TI-TII-DD-RING), 1 BIRC7 (TII-RING), 1 novel BIRC11 (TII-DD-RING), 1

novel BIRC12 (TII-TII-RING), and two BIRCs in un-supported groups with one containing a novel Type Y BIR domain (LOC111100402) and the other with TII-DD-RING structure (LOC111100400). These results indicate that GDC-0152 and *P. marinus* treatment stimulated complex oxidation-reduction processes which may trigger or work alongside TNFR and NF-kB inflammatory pathways involved in regulating apoptosis, potentially leading to the increased suppression of apoptosis in this treatment.

TNFR pathway and oxidoreductase transcripts were significantly associated with apoptosis inhibition following *P. marinus* and GDC-0152 treatment

To further explore the relationship between the apoptosis suppression phenotype and treatment with GDC-0152 and *P. marinus*, WGCNA was performed. WGCNA analysis identified 121 total modules of hemocyte transcripts, and 41 were significantly correlated with GDC-0152 and *P. marinus* treatment (Supplementary Figure 4). Modules for further analysis were prioritized based on the criteria outlined in Materials and Methods. Next, modules significant for *P. marinus* and GDC-0152 treatment and apoptosis phenotype, but with opposing directions of correlation were isolated (Figure 4a). Opposing directions of trait correlation were selected because transcripts potentially involved in apoptosis suppression in the GDC-0152 and *P. marinus* treatment group were hypothesized to be positively correlated with treatment (treatment leads to increased expression) and negatively correlated with apoptosis (treatment leads to decreased apoptosis).

Through this process, the navajowhite2 module was identified as the most interesting to investigate (Figure 4b, c, d). This module was perfectly correlated (r = 1, p = 7e-12) with the control *vs*. GDC-0152 and *P. marinus* treatment, was highly negatively correlated

with apoptosis phenotype (r = -0.86, p=3e-04), and had a strong correlation between GS for apoptosis phenotype and MM (*cor* = 0.63), indicating genes strongly associated with apoptosis were also highly connected in this module (Figure 4a, b). GO terms enriched in this module overlapped with terms enriched in the differentially expressed transcripts from the dual GDC-0152 and *P. marinus* treatment, including protein binding, ion transport, and oxidoreductase activity (Figure 4c). Two oxidoreductase-related transcripts were significantly associated with apoptosis phenotype; they coded for 7-dehydrocholesterol reductase-like, transcript variant X2 (which was an intramodular hub gene), and cytochrome P450 2D27-like. Genes coding for cytochrome P450 enzymes, which play critical roles in ROS production (Zangar et al., 2004) were also differentially expressed in this treatment (13 cytochrome-related DEGs). This module also contained 79 intramodular hub genes strongly associated with apoptosis phenotype, 5 of which were apoptosis-related and differentially expressed in the DEG analysis: caspase-2-like, heat shock protein 27-like, transcription factor AP-1-like, tumor necrosis factor receptor superfamily member 5-like, and the IAP uncharacterized LOC111100400, transcript variant X1 (a BIRC7-like protein; Witkop et al. in prep, Chapter II) (Figure 4d). The module also contained a caspase-8-like and a cdc42 homolog transcript which were significant for apoptosis phenotype but not hub genes.

Overall, oxidoreductase and apoptosis-related transcripts in the module presented complex connection patterns (Figure 4d). TNFR pathway transcripts (caspase 8-like, hsp-27-like, TNFRSF5-like) and inflammatory modulators (transcription factor AP-1, hsp-27) were directly connected with ROS production enzymes (cytochrome P450 2D27-like), suggesting they may work in similar pathways and/or may be co-regulated by GDC-0152

and *P. marinus* treatment. These results suggest GDC-0152 and *P. marinus* affect the NF-kB and TNFR pathways and oxidation-reduction processes in ways that are correlated with enhanced apoptosis suppression, providing further support that IAPs and NF-kB and TNFR pathways are important for apoptosis regulation in response to *P. marinus*.

P. marinus **WGCNA identifies candidate proteases, hydrolases, and kinases for future study as potential NF-kB pathway or TNFR pathway modulators**

To assess the role of *P. marinus* on suppression of apoptosis in hemocytes challenged with both GDC-0152 and *P. marinus* and identify genes from the parasite that may be modulating oyster hemocyte immune responses, including apoptosis, differential expression analysis and WGCNA of *P. marinus* genes was conducted. Because no control *P. marinus* alone samples without hemocyte exposure were sequenced, DEG analysis allowed only for identification of effects of IAP inhibitor GDC-0152 treatment on *P. marinus* gene expression. Overall, *P. marinus* transformed expression data clustered by biological replicate and then by treatment (Figure 5a), showing that pool identity (hemocyte context) had a stronger effect on *P. marinus* gene expression than the inhibitor treatment. Challenge of *P. marinus* with GDC-0152 pre-treated hemocytes led to significant differential gene expression of 39 transcripts as compared to *P. marinus* expression treated with hemocytes alone. Most *P. marinus* DEGs were upregulated in response to the inhibitor, although only 24 had LFCs > 1 or < -1 (Figure 5b,c). *P. marinus* DEG's did not include previously studied enzymes with known roles in *P. marinus* virulence and parasite apoptosis, such as superoxide dismutases and serine proteases (Joseph et al., 2010; Lau et al., 2018b; Xue, 2019), suggesting that inclusion of IAP

inhibitor pre-treatment does not affect expression of these virulence factors in *P. marinus* challenged with hemocytes (Supplementary Figure 4). Transmembrane transporter activity and methyltransferase activity were among the few enriched GO terms in *P. marinus* in response to hemocytes pre-treated with the IAP inhibitor (Figure 5d). This result is consistent with general drug treatment response since increased expression of transporters, particularly ABC transporters, plays critical roles in drug resistance of protozoan parasites (Pramanik et al., 2019; Sauvage et al., 2009).

WGCNA was performed to identify genes and pathways in *P. marinus* potentially contributing to inhibition of apoptosis by identifying gene modules positively correlated with exposure to oyster hemocytes. Data from both challenge with GDC-0152 pre-treated hemocytes or Z-VAD-FMK pre-treated hemocytes were included in this WGCNA analysis because the larger sample size improves WGCNA module assignment and allows for identification of common modules significant in *P. marinus* to both challenges that may be due to hemocyte exposure regardless of inhibitor treatment. Thus, modules of interest were those that were positively correlated in *P-marinus* exposed to hemocytes after pretreatment with either inhibitor, and had high GS and MM for exposure to hemocytes (Figure 6a, Supplementary Figure 4b,d). Using these criteria, the *P. marinus* blue4 module was isolated for further study (Figure 6a,b). This module contained 45 transcripts and was significantly enriched for protein processing, cell redox homeostasis, transferase activity, and cysteine-type endopeptidase activity (Figure 6c). Of those enriched GO term-related transcripts, only one (CAAX prenyl protease, putative (XM_002772524.1, associated with cysteine-type endopeptidase activity) was a highly interconnected intramodular hub gene. The module also contained several other hub gene enzymes: 1) Carboxypeptidase Y

precursor, putative, containing serine carboxypeptidase domains (IPR001563), 2) epoxide hydrolase, putative, containing hydrolytic enzyme domains (IPR000639, IPR000073), and 3) serine/threonine protein kinase 2, putative, containing protein kinase domain profile (IPR000719) (Figure 6d).

Discussion

Dermo disease caused by the intracellular parasite *P. marinus* is highly prevalent along the east coast of the US and is responsible for significant mortalities in both wild and farmed populations of eastern oysters, *Crassostrea virginica* (Smolowitz, 2013). Apoptosis of hemocytes infected intracellularly with *P. marinus* is an important host strategy to help limit parasite proliferation. However, *P. marinus* can evade and suppress this pathway through expression of unique enzymes and virulence factors, such as SOD and serine proteases (Brown and Reece, 2003; Lodoen and Lima, 2019; Smolowitz, 2013). Here we further elucidated the mechanisms and underlying pathways of hemocyte apoptotic response to *P. marinus* to improve our understanding of host-parasite interactions to Dermo disease.

In vitro challenge of *C. virginica* hemocytes with *P. marinus* first revealed that *P. marinus* significantly suppressed granular hemocyte apoptosis, confirming previous studies (Michael Goedken et al., 2005; Hughes et al., 2010; Lau et al., 2018b). Despite the apoptosis suppression observed following hemocyte *P. marinus* challenge, few apoptosis pathway transcripts were significantly differentially expressed, which has been noted in previous studies in Dermo susceptible oysters (Proestou and Sullivan, 2020). *P. marinus* challenge, on the other hand, did trigger expression of genes involved in catalytic activity,

RNA binding, metabolic processes and serine-type endopeptidase inhibitor activity, which have been recognized as a key component of eastern oyster defense against *P. marinus* (He et al., 2012; La Peyre et al., 2010; Xue, 2019; Xue et al., 2009). The very limited apoptosis pathway differential expression response observed in hemocytes challenged with *P. marinus* (which notably involved a relatively higher proportion of IAPs as compared to other apoptosis molecules) indicates that interference of apoptosis pathways by *P. marinus* virulence factors may be an important mechanism of apoptosis suppression in hemocytes. Despite limitations in the experimental design in this research, in which lack of a *P. marinus* only control group prevented disentangling the effect of inhibitor pre-treatment of hemocytes on *P. marinus* gene expression from the effect of the hemocytes alone, several genes and pathways were expressed in *P. marinus* when incubated with hemocytes that may contribute to hemocyte apoptosis inhibition. These included transcripts involved in parasite cell-redox homeostasis, as well as proteases, hydrolases, and kinases. Further investigation would be required to confirm the potential role of these processes on hemocyte apoptosis.

Treatment with the inhibitor GDC-0152 alone caused a significant increase in granular hemocyte apoptosis, revealing that basal (unstimulated) hemocyte apoptosis in granulocytes may be IAP-dependent. This strong increase in apoptosis following GDC-0152 treatment has been observed in other vertebrate and invertebrate species, and GDC-0152 is recognized as a potent apoptosis stimulator (Derakhshan et al., 2017; Erickson et al., 2013; Flygare et al., 2012; Hu et al., 2015; Rosner et al., 2019). Although treatment with GDC-0152 has been previously tested in urochordates (Rosner et al., 2019), this paper represents the first use of this novel, potent IAP inhibitor as an apoptosis modulator in

molluscs. This research also provides the first functional evidence that IAPs are involved in apoptosis in oysters and supports that future work should be done to investigate their specific roles in apoptosis regulation.

Challenge with *P. marinus* following pre-treatment with the pan-caspase inhibitor Z-VAD-FMK suggested *P. marinus* suppresses apoptosis in hemocytes through inhibition of a caspase-independent pathway. Z-VAD-FMK has been used in a previous *P. marinus* hemocyte challenge to inhibit caspases (Hughes et al., 2010). Both this study and the previous study (Hughes et al., 2010) support that *P. marinus* mediated apoptosis is caspase-independent *in vitro*, because levels of apoptosis following *P. marinus* challenge were not affected by pre-treatment with Z-VAD-FMK. Caspase-independent apoptosis is typically triggered in physiological and pathological conditions in response to intrinsic stimuli following MOMP (Tait and Green, 2008). Triggering or modulation of caspase-independent apoptosis following intracellular infection has been observed in previous bacterial and parasite infections. For example, intracellular infection with *Mycobacterium bovis* triggers caspase-independent apoptosis by AIF and endoG (Benítez-Guzmán et al., 2018), host apoptosis following intracellular *Chlamydia* infection is caspase-independent (Perfettini et al., 2002), and *T. gondii* can block caspase-independent apoptosis in hemocytes through interference with granzyme B (Yamada et al., 2011). It is important to note, however, that although apoptosis observed here was caspase-independent, oyster hemocyte apoptosis in other situations may be caspase-dependent (Romero et al., 2015). Overall, this finding is important for the study of hemocyte apoptotic response to *P. marinus* because it supports that other apoptosis enzymes, such as AIF which is a critical caspase-independent apoptosis enzyme, may be involved in *P. marinus* apoptosis

suppression and eliminates caspases as future targets for apoptosis manipulation during *in vitro P. marinus* infection.

Challenge with *P. marinus* following GDC-0152 pre-treatment revealed *P. marinus* was able to overcome the effects of GDC-0152 on apoptosis stimulation, further suppressing apoptosis in hemocytes that had engulfed *P. marinus.* Interestingly, apoptosis suppression in the dual treatment of hemocytes with GDC-0152 and *P. marinus* was not accompanied with a decrease in mitochondrial membrane permeabilization. These results suggest that *P. marinus* inhibits apoptosis downstream of MOMP, potentially through interference with an IAP-involved pathway or mechanism, such as interference with mitochondria released apoptotic proteins like AIF, which can be targeted for ubiquitination by BIRC4/XIAP -- a target of GDC-0152 (Wilkinson et al., 2008). Intracellular parasite suppression of AIF is a known mechanism of apoptosis modulation, and *Toxoplasma gondii* is able to prevent the release of AIF following mitochondrial permeabilization (Mammari et al., 2019). Previous research in eastern oysters has shown that hemocyte apoptosis suppression 24 h post-*P. marinus* infection also led to significant upregulation of AIF gene expression (Lau et al., 2018b). In the flat oyster, intracellular hemocyte infection with the parasite *Bonamia ostreae* induces early activation of hemocytes and upregulation of AIF expression, suggesting the involvement of AIF in oyster intracellular infection (Gervais et al., 2018; Martín-Gómez et al., 2014). The differential gene expression analysis done in our research did not support, however, modulation of AIF or BIRC4 (XIAP), a key modulator of AIF, by *P. marinus*. This may be attributable to the short time frame of our challenge (1 hr), and *P. marinus* modulation of AIF at longer time frames may be worth investigating. Future inhibition or knockout assays should also be

done to determine the role of AIF and BIRC4-like or other IAPs in hemocytes exposed to *P. marinus*. These studies should additionally couple assays measuring MOMP with measurement of other intrinsic apoptosis markers, such as cytochrome c and AIF release from the mitochondria to help assess the full extent of MOMP, as MOMP can affect only a portion of a cell's mitochondria or be reversed (Ichim et al., 2015; Sun et al., 2017; Tang and Tang, 2018).

Alternatively, *P. marinus* may be targeting an IAP-involved pathway not directly involved with MOMP such as the TNFR pathway, or NF-kB pathway where BIRC2/3 (cIAP1/2), another GDC-0152 target, are critical for signal transduction following extracellular ligand binding (Estornes and Bertrand, 2015). Although *P. marinus* challenge alone stimulated little apoptotic gene expression response in hemocytes, dual challenge with GDC-0152 and *P. marinus* stimulated TNFR and NF-kB pathways and a much stronger oxidation-reduction response than *P. marinus* alone. GDC-0152 treatment in model systems induces NF-kB and TNF-α signaling (Erickson et al., 2013; Vasilikos et al., 2017). Likewise, ROS, which are important in oyster responses to *P. marinus* infection, have been shown to trigger the TNF-α and NF-kB pathway (Blaser et al., 2016; Morgan and Liu, 2011; Vazquez-Medina, 2017; Yang et al., 2020), and NF-kB and TNFR have been shown to be upregulated following *P. marinus* challenge in previous literature (Lau et al., 2018). The correlation between TNFR pathway and oxidoreductase transcripts and further apoptosis suppression following GDC-0152 and *P. marinus* treatment, suggests there may be crosstalk between oxidation-reduction processes and the TNFR pathway, as observed in other studies (Blaser et al., 2016; Morgan and Liu, 2011; Yang et al., 2020). These results are also consistent with findings in other systems. For example, modulation

of host cell survival through parasite secreted enzymes, such as proteases and kinases, is key to host infection by the *Toxoplasma gondii* and *Leishmania* spp. These parasite-secreted enzymes directly interfere with host NF-kB signaling pathways (Hodgson and Wan, 2016; Ihara and Nishikawa, 2021; Mammari et al., 2019; Sangaré et al., 2019). The intracellular parasite *Cryptosporidium parvum* can also inhibit host cell apoptosis through activation of NF-kB (Di Genova and Tonelli, 2016; Mccole et al., 2000), and *T. gondii* dense granule protein GRA15 can activate the NF-kB pathway by interaction with TRAFs (Sangaré et al., 2019). Similarly, flat oyster intracellular infection with the parasite *Bonamia ostreae* triggers TNF upregulation following challenge (Martín-Gómez et al., 2014). Future research should investigate the role of *P. marinus* proteases and enzymes identified here, as well as previously recognized proteases such as perkinsin (Faisal et al., 1999; Xue et al., 2006), in NF-kB and TNFR pathway modulation in hemocytes.

Conclusion

Through a combination of phenotypic assays, treatment with chemical inhibitors of apoptosis pathway proteins (caspases and IAPs), and dual transcriptomic analysis of *C. virginica* and *P. marinus*, we conclude that basal hemocyte apoptosis in *C. virginica* may be IAP-dependent, *P. marinus* apoptosis suppression may involve caspase-independent apoptosis pathways and likely occurs downstream of mitochondrial permeabilization. The discovery that hemocyte apoptosis may be IAP-dependent is a novel finding that highlights the need for future work to determine the functions of members of this expanded and diverse gene family (Witkop et al., in preparation, Chapter II). This research also indicates that the mechanism of *P. marinus* apoptosis suppression in hemocytes involves oxidation-

reduction processes and TNFR and NF-kB pathway modulation in hemocytes. Synthesis of the phenotype and gene expression evidence presented here, combined with knowledge from previous research (Fernández-Robledo et al., 2008; Lau et al., 2018b; Smolowitz, 2013; Soudant et al., 2013), suggests a new, hypothetical model for mechanisms of apoptosis suppression in eastern oyster hemocytes following *P. marinus* intracellular infection (Figure 7). Following engulfment of *P. marinus*, hemocytes generate ROS and express serine protease inhibitors, while *P. marinus* secretes enzymes such as proteases, hydrolases, and kinases that activate the TNFR and NF-kB pathways, promoting cell survival, and/or interfere with mitochondrial secreted caspase-independent apoptosis enzymes such as AIF, resulting in suppression of apoptosis downstream of mitochondrial membrane permeabilization in a caspase-independent manner. These pathways may also involve crosstalk between ROS and the NF-kB and TNFR pathways (Morgan and Liu, 2011; Vazquez-Medina, 2017). Overall, this study informs future research of *P. marinus* apoptosis suppression mechanisms in the eastern oyster, advancing our general understanding of apoptosis in invertebrate host-parasite interactions.

Funding

This work was supported by a USDA NIFA Pre-Doctoral Fellowship Award# 2019-67011-29553 to EMR, Department of Commerce/NOAA Saltonstall-Kennedy Award #NA18NMF4270193 to MGC, David R. Nelson, and David C. Rowley, USDA NIFA AFRI Award #2015-67016-22942 to DCR, DRN and MGC, USDA ARS Collaborative Project 58-8030-5-009 to MGC, a USDA NRSP-8 award to MGC and DAP, and the Blount Family Foundation.

Acknowledgements

The authors thank the NOAA Northeast Fisheries Science Center Milford Laboratory for authorized use of their BD Accuri C6+ flow cytometer. The authors thank Stan Allen and Jessica Small at VIMS ABC for supplying lines of selectively bred oysters. The authors also like acknowledge Shannan Meseck at NOAA for assistance with flow cytometer troubleshooting. The authors also acknowledge Margaret Schedl for assistance performing the flow cytometry and transcriptome experiment.

References

Alavi, M.R., Fernández-Robledo, J., Vasta, G.R., 2009. Development of an in Vitro Assay to Examine Intracellular Survival of Perkinsus marinus Trophozoites upon Phagocytosis by Oyster (Crassostrea virginica and Crassostrea ariakensis) Hemocytes. J. Parasitol. 95, 900–907. https://doi.org/10.1645/GE-1864.1

Alexa A, R.J., 2019. topGO: Enrichment Analysis for Gene Ontology.

Allam, B., Carden, W.E., Ward, J.E., Ralph, G., Winnicki, S., Pales Espinosa, E., 2013. Early host-pathogen interactions in marine bivalves: Evidence that the alveolate parasite Perkinsus marinus infects through the oyster mantle during rejection of pseudofeces. J. Invertebr. Pathol. 113, 26–34. https://doi.org/10.1016/j.jip.2012.12.011

Benítez-Guzmán, A., Arriaga-Pizano, L., Morán, J., Gutiérrez-Pabello, J.A., 2018. Endonuclease G takes part in AIF-mediated caspase-independent apoptosis in Mycobacterium bovis-infected bovine macrophages. Vet. Res. 49, 1–9. https://doi.org/10.1186/s13567-018-0567-1

Blaser, H., Dostert, C., Mak, T.W., Brenner, D., 2016. TNF and ROS Crosstalk in Inflammation. Trends Cell Biol. 26, 249–261. https://doi.org/10.1016/j.tcb.2015.12.002

Bushek, D., Allen, S.K., 1996. Host-parasite interactions among broadly distributed populations of the eastern oyster Crassostrea virginica and the protozoan Perkinsus marinus. Mar. Ecol. Prog. Ser. 139, 127–141. https://doi.org/10.3354/meps139127

Bushek, D., Ford, S.E., Allen, S.K., 1994. Evaluation of methods using ray's fluid thioglycollate medium for diagnosis of Perkinsus marinus infection in the eastern

oyster, Crassostrea virginica. Annu. Rev. Fish Dis. 4, 201–217. https://doi.org/https://doi.org/10.1016/0959-8030(94)90029-9

Bushnell, B., n.d. BBMap. sourceforge.net/projects/bbmap/.

Chakraborti, S., Chakraborti, T., Chattopadhyay, D., Shaha, C., 2019. Oxidative stress in microbial diseases, Oxidative Stress in Microbial Diseases. https://doi.org/10.1007/978-981-13-8763-0

Croxton, A.N., Wikfors, G.H., Schulterbrandt-Gragg, R.D., 2012. Immunomodulation in eastern oysters, Crassostrea virginica, exposed to a PAH-contaminated, microphytobenthic diatom. Aquat. Toxicol. 118–119, 27–36. https://doi.org/10.1016/j.aquatox.2012.02.023

Dean, P., Major, P., Nakjang, S., Hirt, R.P., Martin Embley, T., 2014. Transport proteins of parasitic protists and their role in nutrient salvage. Front. Plant Sci. 5. https://doi.org/10.3389/fpls.2014.00153

Derakhshan, A., Chen, Z., Van Waes, C., 2017. Therapeutic small molecules target inhibitor of apoptosis proteins in cancers with deregulation of extrinsic and intrinsic cell death pathways. Clin. Cancer Res. 23, 1379–1387. https://doi.org/10.1158/1078-0432.CCR-16-2172

Di Genova, B.M., Tonelli, R.R., 2016. Infection strategies of intestinal parasite pathogens and host cell responses. Front. Microbiol. 7, 1–16. https://doi.org/10.3389/fmicb.2016.00256

Ekert, P.G., Silke, J., Vaux, D.L., 1999. Caspase inhibitors. Cell Death Differ. 6, 1081–1086. https://doi.org/10.1038/sj.cdd.4400594

Erickson, R.I., Tarrant, J., Cain, G., Lewin-Koh, S.C., Dybdal, N., Wong, H., Blackwood,

E., West, K., Steigerwalt, R., Mamounas, M., Flygare, J.A., Amemiya, K., Dambach, D., Fairbrother, W.J., Diaz, D., 2013. Toxicity profile of small-molecule IAP antagonist GDC-0152 is linked to TNF-α pharmacology. Toxicol. Sci. 131, 247–258. https://doi.org/10.1093/toxsci/kfs265

Estornes, Y., Bertrand, M.J.M., 2015. IAPs, regulators of innate immunity and inflammation. Semin. Cell Dev. Biol. 39, 106–114. https://doi.org/10.1016/j.semcdb.2014.03.035

Faisal, M., Schafhauser, D.Y., Garreis, K.A., Elsayed, E., La Peyre, J.F., 1999. Isolation and characterization of Perkinsus marinus proteases using bacitracin-sepharose affinity chromatography. Comp. Biochem. Physiol. - B Biochem. Mol. Biol. 123, 417–426. https://doi.org/10.1016/S0305-0491(99)00088-7

Fernández-Robledo, J.A., Schott, E.J., Vasta, G.R., 2008. Perkinsus marinus superoxide dismutase 2 (PmSOD2) localizes to single-membrane subcellular compartments. Biochem. Biophys. Res. Commun. 375, 215–219. https://doi.org/10.1016/j.bbrc.2008.07.162

Flygare, J.A., Beresini, M., Budha, N., Chan, H., Chan, I.T., Cheeti, S., Cohen, F., Deshayes, K., Doerner, K., Eckhardt, S.G., Elliott, L.O., Feng, B., Franklin, M.C., Reisner, S.F., Gazzard, L., Halladay, J., Hymowitz, S.G., La, H., LoRusso, P., Maurer, B., Murray, L., Plise, E., Quan, C., Stephan, J.-P., Young, S.G., Tom, J., Tsui, V., Um, J., Varfolomeev, E., Vucic, D., Wagner, A.J., Wallweber, H.J.A., Wang, L., Ware, J., Wen, Z., Wong, H., Wong, J.M., Wong, M., Wong, S., Yu, R., Zobel, K., Fairbrother, W.J., 2012. Discovery of a potent small-molecule antagonist of inhibitor of apoptosis (IAP) proteins and clinical candidate for the treatment of cancer (GDC-0152). J. Med.

Chem. 55, 4101–4113. https://doi.org/10.1021/jm300060k

Ford, S.E., Chintala, M.M., Bushek, D., 2002. Comparison of in vitro-cultured and wild-type Perkinsus marinus. I. pathogen virulence. Dis. Aquat. Organ. 51, 187–201. https://doi.org/10.3354/dao051187

Galluzzi, L., López-Soto, A., Kumar, S., Kroemer, G., 2016. Caspases Connect Cell-Death Signaling to Organismal Homeostasis. Immunity 44, 221–231. https://doi.org/10.1016/j.immuni.2016.01.020

Gerdol, M. et al., 2018. Immunity in Molluscs: Recognition and Effector Mechanisms, with a Focus on Bivalvia, in: Advances in Comparative Immunology. pp. 225–341.

Gervais, O., Renault, T., Arzul, I., 2018. Molecular and cellular characterization of apoptosis in flat oyster a key mechanisms at the heart of host-parasite interactions. Sci. Rep. 8, 1–12. https://doi.org/10.1038/s41598-018-29776-x

Goedken, Michael, Morsey, B., Sunila, I., De Guise, S., 2005. Immunomodulation of Crassostrea gigas and Crassostrea virginica cellular defense mechanism by Perkinsus marinus. J. Shellfish Res. 24, 487–496. https://doi.org/10.2983/0730-8000(2005)24

Goedken, Micheal, Morsey, B., Sunila, I., Dungan, C., De Guise, S., 2005. The effects of temperature and salinity on apoptosis of Crassostrea virginica hemocytes and Perkinsus marinus. J. Shellfish Res. 24, 177–183. https://doi.org/10.2983/0730-8000(2005)24[177:TEOTAS]2.0.CO;2

Gu, Z., Eils, R., Schlesner, M., 2016. Complex heatmaps reveal patterns and correlations in multidimensional genomic data. Bioinformatics 32, 2847–2849. https://doi.org/10.1093/bioinformatics/btw313

He, Y., Yu, H., Bao, Z., Zhang, Q., Guo, X., 2012. Mutation in promoter region of a serine

protease inhibitor confers Perkinsus marinus resistance in the eastern oyster (Crassostrea virginica). Fish Shellfish Immunol. 33, 411–417. https://doi.org/10.1016/j.fsi.2012.05.028

Hodgson, A., Wan, F., 2016. Interference with nuclear factor kappaB signaling pathway by pathogen-encoded proteases: global and selective inhibition. Mol. Microbiol. 99, 439–452. https://doi.org/10.1111/mmi.13245

Hu, R., Li, J., Liu, Z., Miao, M., Yao, K., 2015. GDC-0152 induces apoptosis through down-regulation of IAPs in human leukemia cells and inhibition of PI3K/Akt signaling pathway. Tumor Biol. 36, 577–584. https://doi.org/10.1007/s13277-014-2648-8

Hughes, F.M., Foster, B., Grewal, S., Sokolova, I.M., 2010. Apoptosis as a host defense mechanism in Crassostrea virginica and its modulation by Perkinsus marinus. Fish Shellfish Immunol. 29, 247–257. https://doi.org/10.1016/j.fsi.2010.03.003

Ichim, G., Lopez, J., Ahmed, S.U., Muthalagu, N., Giampazolias, E., Delgado, M.E., Haller, M., Riley, J.S., Mason, S.M., Athineos, D., Parsons, M.J., vandeKooij, B., Bouchier-Hayes, L., Chalmers, A.J., Rooswinkel, R.W., Oberst, A., Blyth, K., Rehm, M., Murphy, D.J., Tait, S.W.G., 2015. Limited Mitochondrial Permeabilization Causes DNA Damage and Genomic Instability in the Absence of Cell Death. Mol. Cell 57, 860–872. https://doi.org/10.1016/j.molcel.2015.01.018

Ihara, F., Nishikawa, Y., 2021. Toxoplasma gondii manipulates host cell signaling pathways via its secreted effector molecules. Parasitol. Int. 83, 102368. https://doi.org/10.1016/j.parint.2021.102368

Joseph, S.J., Fernández-Robledo, J.A., Gardner, M.J., El-Sayed, N.M., Kuo, C.H., Schott,

E.J., Wang, H., Kissinger, J.C., Vasta, G.R., 2010. The Alveolate Perkinsus marinus: Biological Insights from EST Gene Discovery. BMC Genomics 11. https://doi.org/10.1186/1471-2164-11-228

Kim, D., Langmead, B., Salzberg, S.L., 2016. HISAT: a fast spliced aligner with low memory requirements Daehwan 12, 357–360. https://doi.org/10.1038/nmeth.3317.HISAT

Kiss, T., 2010. Apoptosis and its functional significance in molluscs. Apoptosis 15, 313–321. https://doi.org/10.1007/s10495-009-0446-3

La Peyre, J.F., Chu, F. lin E., Vogelbein, W.K., 1995. In vitro interaction of Perkinsus marinus merozoites with eastern and pacific oyster hemocytes. Dev. Comp. Immunol. 19, 291–304. https://doi.org/10.1016/0145-305X(95)00017-N

La Peyre, J.F., Xue, Q.G., Itoh, N., Li, Y., Cooper, R.K., 2010. Serine protease inhibitor cvSI-1 potential role in the eastern oyster host defense against the protozoan parasite Perkinsus marinus. Dev. Comp. Immunol. 34, 84–92. https://doi.org/10.1016/j.dci.2009.08.007

Langfelder, P., Horvath, S., 2008. WGCNA: An R package for weighted correlation network analysis. BMC Bioinformatics 9. https://doi.org/10.1186/1471-2105-9-559

Lau, Y.T., Gambino, L., Santos, B., Pales Espinosa, E., Allam, B., 2018a. Transepithelial migration of mucosal hemocytes in Crassostrea virginica and potential role in Perkinsus marinus pathogenesis. J. Invertebr. Pathol. 153, 122–129. https://doi.org/10.1016/j.jip.2018.03.004

Lau, Y.T., Santos, B., Barbosa, M., Pales Espinosa, E., Allam, B., 2018b. Regulation of apoptosis-related genes during interactions between oyster hemocytes and the

alveolate parasite Perkinsus marinus. Fish Shellfish Immunol. 83, 180–189. https://doi.org/10.1016/j.fsi.2018.09.006

Li, H., Handsaker, B., Wysoker, A., Fennell, T., Ruan, J., Homer, N., Marth, G., Abecasis, G., Durbin, R., 2009. The Sequence Alignment/Map format and SAMtools. Bioinformatics 25, 2078–2079. https://doi.org/10.1093/bioinformatics/btp352

Lodoen, M.B., Lima, T.S., 2019. Mechanisms of Human Innate Immune Evasion by Toxoplasma gondii 9, 1–8. https://doi.org/10.3389/fcimb.2019.00103

Love, M.I., Huber, W., Anders, S., 2014. Moderated estimation of fold change and dispersion for RNA-seq data with DESeq2. Genome Biol. 15, 1–21. https://doi.org/10.1186/s13059-014-0550-8

Mammari, N., Halabi, M.A., Yaacoub, S., Chlala, H., Dardé, M.-L., Courtioux, B., 2019. Toxoplasma gondii Modulates the Host Cell Responses: An Overview of Apoptosis Pathways. Biomed Res. Int. 2019. https://doi.org/10.1155/2019/6152489

Martín-Gómez, L., Villalba, A., Carballal, M.J., Abollo, E., 2014. Molecular characterisation of TNF, AIF, dermatopontin and VAMP genes of the flat oyster Ostrea edulis and analysis of their modulation by diseases. Gene 533, 208–217. https://doi.org/10.1016/j.gene.2013.09.085

Mccole, D.F., Eckmann, L., Laurent, F., Kagnoff, M.F., 2000. Intestinal epithelial cell apoptosis following Cryptosporidium parrum infection. Infect. Immun. 68, 1710–1713. https://doi.org/10.1128/IAI.68.3.1710-1713.2000

Morgan, M.J., Liu, Z.G., 2011. Crosstalk of reactive oxygen species and NF-κB signaling. Cell Res. 21, 103–115. https://doi.org/10.1038/cr.2010.178

Perfettini, J.L., Reed, J.C., Israël, N., Martinou, J.C., Dautry-Varsat, A., Ojcius, D.M.,

2002. Role of Bcl-2 family members in caspase-independent apoptosis during Chlamydia infection. Infect. Immun. 70, 55–61. https://doi.org/10.1128/IAI.70.1.55-61.2002

Pertea, M., Kim, D., Pertea, G.M., Leek, J.T., Salzberg, S.L., 2016. Transcript-level expression analysis of RNA- seq experiments with HISAT , StringTie and Transcript-level expression analysis of RNA-seq experiments with HISAT , StringTie and Ballgown. Nat. Protoc. 11, 1650–1667. https://doi.org/10.1038/nprot.2016-095

Pramanik, P.K., Alam, M.N., Roy Chowdhury, D., Chakraborti, T., 2019. Drug Resistance in Protozoan Parasites: An Incessant Wrestle for Survival. J. Glob. Antimicrob. Resist. 18, 1–11. https://doi.org/10.1016/j.jgar.2019.01.023

Proestou, D.A., Jr, S.K.A., Corbett, R.J., Horin, T. Ben, Small, J.M., 2019. Defining Dermo resistance phenotypes in an eastern oyster breeding population 2142–2154. https://doi.org/10.1111/are.14095

Proestou, D.A., Sullivan, M.E., 2020. Variation in global transcriptomic response to Perkinsus marinus infection among eastern oyster families highlights potential mechanisms of disease resistance. Fish Shellfish Immunol. 96, 141–151. https://doi.org/10.1016/j.fsi.2019.12.001

Rodriguez, C., Simon, V., Conget, P., Vega, I.A., 2020. Both quiescent and proliferating cells circulate in the blood of the invasive apple snail Pomacea canaliculata. Fish Shellfish Immunol. 107, 95–103. https://doi.org/10.1016/j.fsi.2020.09.026

Romero, A., Novoa, B., Figueras, A., 2015. The complexity of apoptotic cell death in mollusks: An update. Fish Shellfish Immunol. 46, 79–87. https://doi.org/10.1016/j.fsi.2015.03.038

Rosner, A., Kravchenko, O., Rinkevich, B., 2019. IAP genes partake weighty roles in the astogeny and whole body regeneration in the colonial urochordate Botryllus schlosseri. Dev. Biol. 448, 320–341. https://doi.org/10.1016/j.ydbio.2018.10.015

Sangaré, L.O., Yang, N., Konstantinou, E.K., Lu, D., Mukhopadhyay, D., Young, L.H., Saeij, J.P.J., 2019. Toxoplasma GRA15 activates the NF-Kb pathway through interactions with TNF receptor-associated factors. MBio 10, 1–13. https://doi.org/10.1128/mbio.00808-19

Sauvage, V., Aubert, D., Escotte-Binet, S., Villena, I., 2009. The role of ATP-binding cassette (ABC) proteins in protozoan parasites. Mol. Biochem. Parasitol. 167, 81–94. https://doi.org/10.1016/j.molbiopara.2009.05.005

Schott, E.J., Pecher, W.T., Okafor, F., Vasta, G.R., 2003. The protistan parasite Perkinsus marinus is resistant to selected reactive oxygen species 105, 232–240. https://doi.org/10.1016/j.exppara.2003.12.012

Shannon, P., Markiel, A., Ozier, O., Baliga, N.S., Wang, J.T., Ramage, D., Amin, N., Schwikowski, B., Ideker, T., 2003. Cytoscape: a software environment for integrated models of biomolecular interaction networks. Genome Res. 13, 2498–2504.

Siqueira-Neto, J.L., Debnath, A., McCall, L.I., Bernatchez, J.A., Ndao, M., Reed, S.L., Rosenthal, P.J., 2018. Cysteine proteases in protozoan parasites. PLoS Negl. Trop. Dis. 12, 1–20. https://doi.org/10.1371/journal.pntd.0006512

Smolowitz, R., 2013. A Review of Current State of Knowledge Concerning Perkinsus marinus Effects on Crassostrea virginica (Gmelin) (the Eastern Oyster) 50, 404–411. https://doi.org/10.1177/0300985813480806

Soudant, P., Chu, F.E., Volety, A., 2013. Host – parasite interactions : Marine bivalve

molluscs and protozoan parasites , Perkinsus species. J. Invertebr. Pathol. 114, 196–216. https://doi.org/10.1016/j.jip.2013.06.001

Sullivan, M.E., Proestou, D.A., 2021. Survival and transcriptomic responses to different Perkinsus marinus exposure methods in an Eastern oyster family. Aquaculture 542, 736831. https://doi.org/10.1016/j.aquaculture.2021.736831

Sun, G., Guzman, E., Zhou, H.R., Kosik, K.S., Montell, D.J., 2017. A molecular signature for anastasis, recovery from the brink of apoptotic cell death. bioRxiv 216, 3355–3368. https://doi.org/10.1101/102640

Supek, F., Bošnjak, M., Škunca, N., Šmuc, T., 2011. Revigo summarizes and visualizes long lists of gene ontology terms. PLoS One 6. https://doi.org/10.1371/journal.pone.0021800

Tait, S.W.G., Green, D.R., 2008. Caspase-independent cell death: Leaving the set without the final cut. Oncogene 27, 6452–6461. https://doi.org/10.1038/onc.2008.311

Tang, H.M., Tang, H.L., 2018. Anastasis: Recovery from the brink of cell death. R. Soc. Open Sci. 5. https://doi.org/10.1098/rsos.180442

Tasumi, S., Vasta, G.R., 2007. A Galectin of Unique Domain Organization from Hemocytes of the Eastern Oyster (Crassostrea virginica) Is a Receptor for the Protistan Parasite Perkinsus marinus. J. Immunol. 179, 3086–3098. https://doi.org/10.4049/jimmunol.179.5.3086

Tchoghandjian, A., Soubéran, A., Tabouret, E., Colin, C., Denicolaï, E., Jiguet-Jiglaire, C., El-Battari, A., Villard, C., Baeza-Kallee, N., Figarella-Branger, D., 2016. Inhibitor of apoptosis protein expression in glioblastomas and their in vitro and in vivo targeting by SMAC mimetic GDC-0152. Cell Death Dis. 7, 1–10.

https://doi.org/10.1038/cddis.2016.214

Team., Rs., 2020. RStudio: Integrated Development for R. http://www.rstudio.com/.

Vasta, G.R., Feng, C., Tasumi, S., Abernathy, K., Bianchet, M.A., Wilson, I.B.H., Paschinger, K., Wang, L.X., Iqbal, M., Ghosh, A., Amin, M.N., Smith, B., Brown, S., Vista, A., 2020. Biochemical Characterization of Oyster and Clam Galectins: Selective Recognition of Carbohydrate Ligands on Host Hemocytes and Perkinsus Parasites. Front. Chem. 8, 1–15. https://doi.org/10.3389/fchem.2020.00098

Vazquez-Medina, J.P., 2017. Redox signaling and the onset of the inflammatory cascade, Immunity and Inflammation in Health and Disease: Emerging Roles of Nutraceuticals and Functional Foods in Immune Support. Elsevier Inc. https://doi.org/10.1016/B978-0-12-805417-8.00003-2

Wikfors, G.H., Alix, J.H., 2014. Granular hemocytes are phagocytic, but agranular hemocytes are not, in the Eastern Oyster Crassostrea virginica. Invertebr. Immun. 1, 15–21. https://doi.org/10.2478/invim-2014-0001

Wilkinson, J.C., Wilkinson, A.S., Galbán, S., Csomos, R.A., Duckett, C.S., 2008. Apoptosis-Inducing Factor Is a Target for Ubiquitination through Interaction with XIAP. Mol. Cell. Biol. 28, 237–247. https://doi.org/10.1128/mcb.01065-07

Witkop, E.M., Proestou, D.A., Gómez-Chiarri, M., n.d. The expanded Inhibitor of Apoptosis gene family in oysters possesses novel domain architectures and may play diverse roles in apoptosis following immune challenge. Prep. Chapter II.

Xue, Q., 2019. Pathogen proteases and host protease inhibitors in molluscan infectious diseases. J. Invertebr. Pathol. 166, 107214. https://doi.org/10.1016/j.jip.2019.107214

Xue, Q., Itoh, N., Schey, K.L., Cooper, R.K., La Peyre, J.F., 2009. Evidence indicating the

existence of a novel family of serine protease inhibitors that may be involved in marine invertebrate immunity. Fish Shellfish Immunol. 27, 250–259. https://doi.org/10.1016/j.fsi.2009.05.006

Xue, Q.G., Waldrop, G.L., Schey, K.L., Itoh, N., Ogawa, M., Cooper, R.K., Losso, J.N., La Peyre, J.F., 2006. A novel slow-tight binding serine protease inhibitor from eastern oyster (Crassostrea virginica) plasma inhibits perkinsin, the major extracellular protease of the oyster protozoan parasite Perkinsus marinus. Comp. Biochem. Physiol. - B Biochem. Mol. Biol. 145, 16–26. https://doi.org/10.1016/j.cbpb.2006.05.010

Yamada, T., Tomita, T., Weiss, L.M., Orlofsky, A., 2011. Toxoplasma gondii inhibits granzyme B-mediated apoptosis by the inhibition of granzyme B function in host cells. Int. J. Parasitol. 41, 595–607. https://doi.org/10.1016/j.ijpara.2010.11.012

Yang, Z., Min, Z., Yu, B., 2020. Reactive oxygen species and immune regulation. Int. Rev. Immunol. 39, 292–298. https://doi.org/10.1080/08830185.2020.1768251

Yee, A., Dungan, C., Hamilton, R., Goedken, M., Guise, S.D.E., Sunila, I., 2005. Apoptosis of the protozoan oyster pathogen Perkinsus marinus in vivo and in vitro in the Chesapeake Bay and the Long Island Sound. J. Shellfish Res. 24, 1035–1042. https://doi.org/10.2983/0730-8000(2005)24[1035:aotpop]2.0.co;2

Zangar, R.C., Davydov, D.R., Verma, S., 2004. Mechanisms that regulate production of reactive oxygen species by cytochrome P450. Toxicol. Appl. Pharmacol. 199, 316–331. https://doi.org/10.1016/j.taap.2004.01.018

Zhu, A., Ibrahim, J.G., Love, M.I., 2018. Heavy-tailed prior distributions for sequence count data: removing the noise and preserving large differences. Bioinformatics 35, 2084–2092. https://doi.org/10.1093/bioinformatics/bty895

Figures

Figure III-1. Basal apoptosis in unstimulated granular hemocytes may be IAP-dependent and involve caspase-independent pathways.
Percent (average +/- standard deviation) of hemocyte viability (A, B), apoptosis (C, D), and caspase 3/7 activity (E, F) following treatment with either GDC-0152 or Z-VAD-FMK was measured by flow cytometry. A) Percent of granular and agranular hemocytes in each pooled hemolymph sample (n=3). B) Percent live granular hemocytes measured as 100% minus the percent PI stained. C) Percent apoptotic granular hemocytes with all samples from each individual treatment analyzed together. D) Dose and time effect of inhibitor treatment on percent apoptotic granular hemocytes. E) Percent caspase 3/7 active granular hemocytes with all samples from each individual treatment analyzed together. F) Dose and time effect of inhibitor treatment on percent caspase 3/7 active granular hemocytes. Statistical tests were performed with arcsine transformed percentages (* *p<=0.05;* ** *p<=0.01;* *** *p<=0.001*).

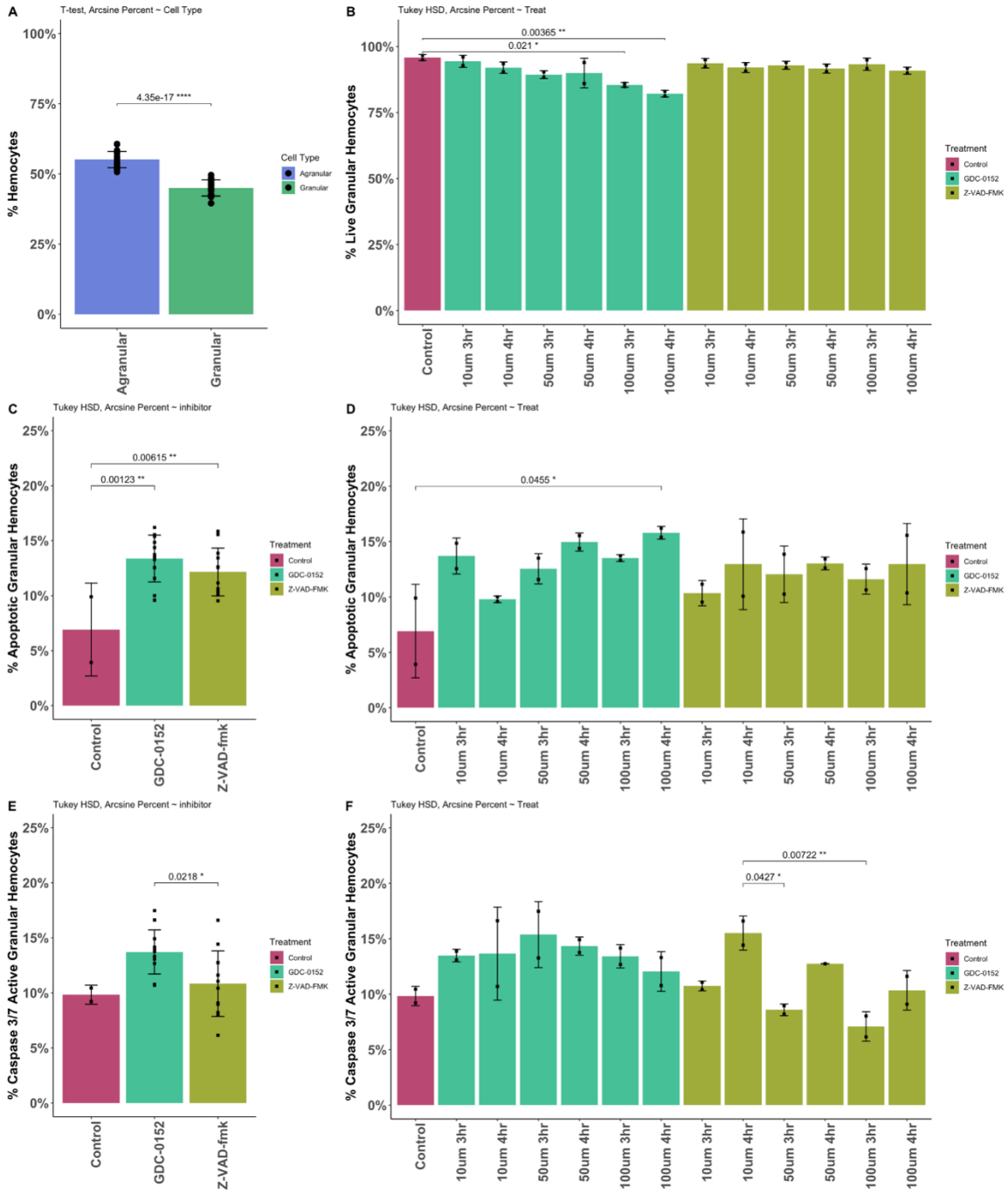
A
T-test, Arcsine Percent ~ Cell Type
% Hemocytes
4.35e-17 ****
Cell Type
Agranular
Granular
B
Tukey HSD, Arcsine Percent ~ Treat
% Live Granular Hemocytes
0.00365 **
0.021 *
Treatment
Control
GDC-0152
Z-VAD-FMK
C
Tukey HSD, Arcsine Percent ~ inhibitor
% Apoptotic Granular Hemocytes
0.00615 **
0.00123 **
D
Tukey HSD, Arcsine Percent ~ Treat
0.0455 *
E
Tukey HSD, Arcsine Percent ~ inhibitor
% Caspase 3/7 Active Granular Hemocytes
0.0218 *
F
Tukey HSD, Arcsine Percent ~ Treat
0.00722 **
0.0427 *

Figure III-2. Pretreatment with an IAP inhibitor affected *P. marinus* inhibition of apoptosis downstream of membrane permeabilization, while caspase inhibitors had no effect.

Control and inhibitor-pretreated (IAP inhibitor GDC-0152 for 3 hr or caspase inhibitor Z-VAD-FMK for 1 hr) hemolymph was incubated for 1 hr with activated beads or *P. marinus* at an MOI of 1:1, and the average +/- sd percent granular cell apoptosis (A, annexin-V assay), membrane permeabilization (B, JC-1 assay), and caspase 3/7 activation (C) was determined by flow cytometry. Percent of cells in different cellular portions (different gates) are presented: total granular hemocytes (left panel); granular hemocytes without engulfed *P. marinus* (middle panel), and granular hemocytes with engulfed *P. marinus* (right panel). Black lines represent the standard deviation. Statistical tests were performed with arcsine transformed percentages (* $p<=0.05$; ** $p<=0.01$; *** $p<=0.001$).

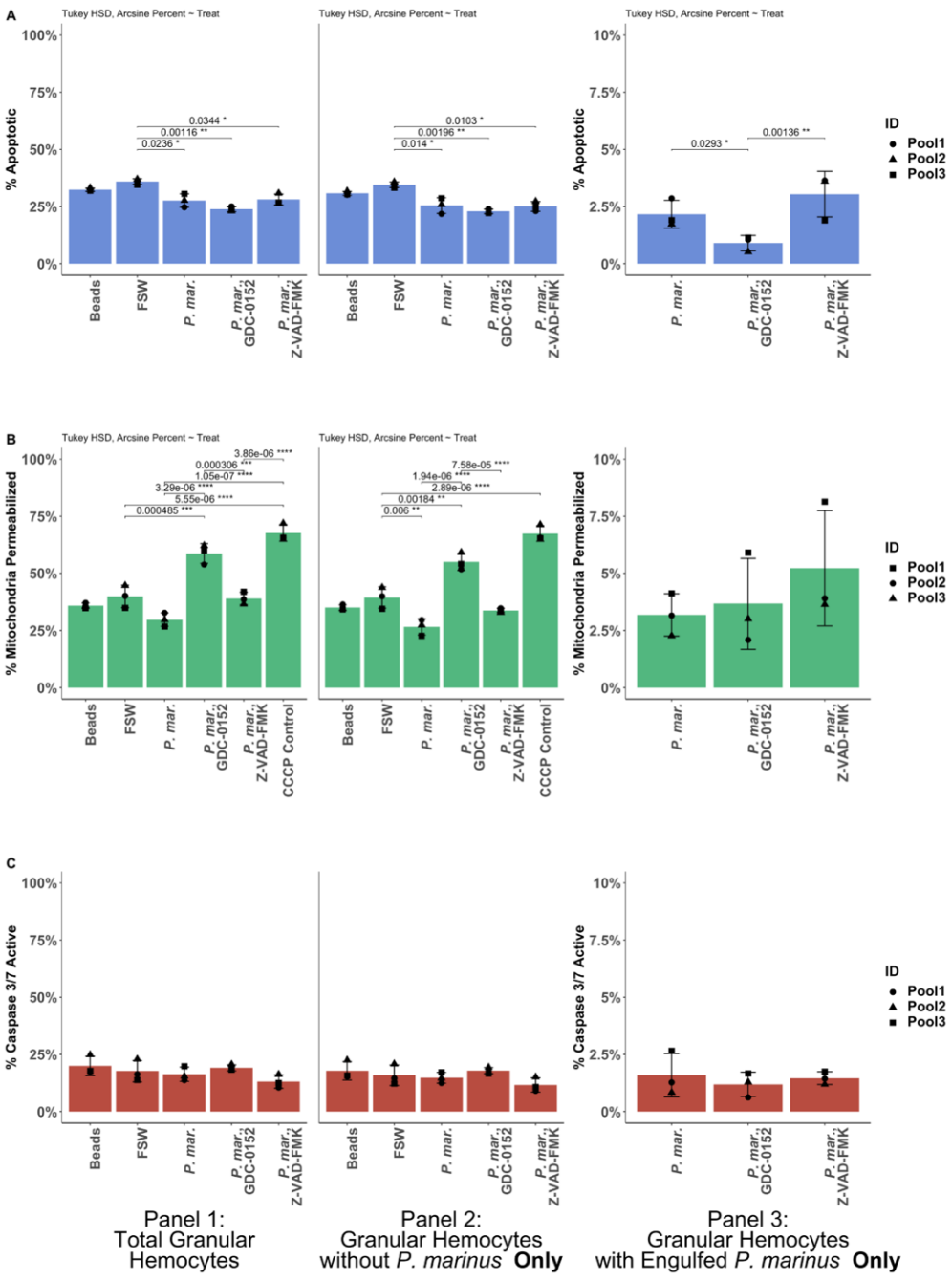
A
Tukey HSD, Arcsine Percent ~ Treat
% Apoptotic
100%
75%
50%
25%
0%
0.0344 *
0.00116 **
0.0236 *
0.0103 *
0.00196 **
0.014 *
10%
7.5%
5%
2.5%
0.0293 *
0.00136 **
Beads
FSW
P. mar.
P. mar.; GDC-0152
P. mar.; Z-VAD-FMK
ID
Pool1
Pool2
Pool3
B
Tukey HSD, Arcsine Percent ~ Treat
% Mitochondria Permeabilized
3.86e-06 ****
0.000306 ***
1.05e-07 ****
3.29e-06 ****
5.55e-06 ****
0.000485 ***
7.58e-05 ****
1.94e-06 ****
2.89e-06 ****
0.00184 **
0.006 **
CCCP Control
C
% Caspase 3/7 Active
Panel 1:
Total Granular
Hemocytes
Panel 2:
Granular Hemocytes
without P. marinus Only
Panel 3:
Granular Hemocytes
with Engulfed P. marinus Only

Figure III-3. Dual *P. marinus* and IAP inhibitor treatment triggered differential gene expression in oyster hemocytes of TNFR and NF-kB pathways and upregulation of oxidation-reduction processes compared to control.
Hemocytes were pretreated with control (FSSW) or 50 μM of GDC-0152 for 3 hr prior to incubation with *P. marinus* (1:1 MOI) for 1 hr before processing for RNA extraction. Gene expression in each treatment was compared to control non-exposed hemocytes. A) PCA plot of *rlog* transformed counts for each sample. B) Volcano plots of DEGs, with those transcripts involved in apoptosis plotted with red triangles. C) Bubble plot showing significantly enriched BP and MF GO terms identified by topGO in each set of DEGs. D) LFC plots of hemocyte apoptosis DEGs compared between both treatments. E) *rlog* transformed counts comparing significant DEGs for apoptosis transcripts between all samples.


A
PC2 (13.3%)
PC1 (15.96%)
Condition
P. marinus
P. marinus and GDC-0152
Control
Pool
1
2
3
B
Control vs P. marinus Treated Hemocyte DEGs
Control vs P. marinus and GDC-0152 Treated Hemocyte DEGs
-log10(adj. p-value)
log2 Fold Change
apop
Apoptosis-related transcripts
Non apoptosis-related transcripts
C
GO Enrichment of Significant Hemocyte DEGs
transmembrane transport
transcription initiation from RNA polyme...
superoxide metabolic process
sulfur compound biosynthetic process
sulfate transport
spliceosomal snRNP assembly
signaling
signal transduction
serine family amino acid biosynthetic pr...
rRNA metabolic process
regulation of small GTPase mediated sign...
regulation of phosphoprotein phosphatase...
regulation of microtubule-based process
regulation of metal ion transport
proteolysis involved in cellular protein...
protein-DNA complex assembly
protein targeting
protein phosphorylation
protein localization to organelle
protein import
protein ADP-ribosylation
phosphate ion transport
negative regulation of transcription by ...
ncRNA processing
mRNA splicing, via spliceosome
L-serine metabolic process
glycosaminoglycan metabolic process
G protein-coupled receptor signaling pat...
establishment of protein localization to...
DNA replication initiation
DNA catabolic process
deoxyribonucleotide biosynthetic process
chromosome organization
cell adhesion
cation transport
carboxylic acid metabolic process
carbohydrate metabolic process
biosynthetic process
ATP metabolic process
asparagine biosynthetic process
anion transport
ubiquitin-like protein-specific protease...
transmembrane transporter activity
transferase activity, transferring pento...
transferase activity, transferring acyl ...
transcription regulatory region DNA bind...
transaminase activity
threonine-type endopeptidase activity
sulfotransferase activity
serine-type endopeptidase inhibitor acti...
sequence-specific DNA binding
secondary active sulfate transmembrane t...
RNA binding
Rho GDP-dissociation inhibitor activity
protein kinase activity
peptidase activity
oxidoreductase activity, acting on the C...
omega peptidase activity
nucleic acid binding
nicotinate-nucleotide diphosphorylase (c...
NADH dehydrogenase (ubiquinone) activity
N-acetyltransferase activity
motor activity
molecular_function
metallopeptidase activity
lipid binding
L-ascorbic acid binding
inorganic phosphate transmembrane transp...
inorganic anion exchanger activity
GTPase activity
GTPase activator activity
GTP binding
gamma-tubulin binding
G protein-coupled receptor activity
endopeptidase activity
deoxyribonuclease II activity
cyclin-dependent protein serine/threonin...
cation transmembrane transporter activit...
catalytic activity
ATP binding
aspartic-type endopeptidase activity
asparagine synthase (glutamine-hydrolyzi...
anion transmembrane transporter activity
adenyl nucleotide binding
actin binding
BP
MF
GO Term
p-value
Significant
P.marinus
P. marinus and GDC-0152
Treatment
D
Apoptosis Transcript and Product Name
Log2 Fold Change
P. mar vs Control
P. mar GDC-0152 vs Control
E
Condition
Control
P. mar
P. mar. and GDC
2-control
1-control
3-control
2-Dermo-GDC
1-Dermo-GDC
3-Dermo-GDC
2-Dermo
1-Dermo
3-Dermo

Figure III-4. TNFR pathway and oxidoreductase transcript expression in oyster hemocytes were significantly correlated with apoptosis transcripts and apoptosis phenotype following dual *P. marinus* and IAP inhibitor treatment.
Hemocytes were pretreated with control (FSSW) or 50 μM of GDC-0152 for 3 hr and then incubated with *P. marinus* (1:1 MOI) for 1 hr before analysis of hemocyte gene expression. Associations between hemocyte gene expression and apoptosis phenotype (percent granular cell apoptosis in response to treatment) were investigated using WGCNA. A) Heatmap of modules selected based on the following criteria: significantly correlated with either *P. marinus* challenge alone or GDC-0152 and *P. marinus* treatment, showing high Gene Significance (GS) and Module Membership (MM) relationship, and containing apoptosis intramodular hub genes. Modules are plotted along with their correlation with apoptosis phenotype. X-axis indicates modules of correlated transcripts and the y-axis plots each trait for which module significance was calculated. Correlation values (-1 – 1), followed by and significance values (*p* between 0-1) in parentheses, are listed in each cell. Color indicates strength and direction of correlation. B) Relationship between GS and MM for the navajowhite2 module, where each point is a transcript in the module. C) GO enrichment for Biological Process (BP) and Molecular Function (MF) for the navajowhite2 module. D) Hemocyte navajowhite2 module network (Cytoscape, V 3.8.0) showing apoptosis-related and oxidoreductase genes of interest significantly correlated with apoptosis phenotype. Nodes colored by significance for apoptosis phenotype (yellow = high significance, blue = low significance), edge width and color were scaled to edge weight (thicker = higher weight, darker = higher weight), and node shape indicated hub gene status (triangle = hub gene, circle = non-hub gene). The network was drawn with the prefuse force directed layout using edge weight (Shannon et al., 2003).

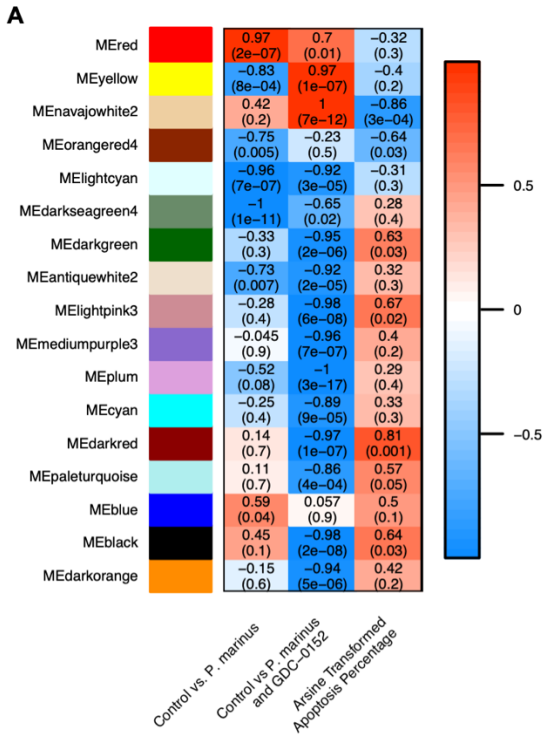
A
MEred
MEyellow
MEnavajowhite2
MEorangered4
MElightcyan
MEdarkseagreen4
MEdarkgreen
MEantiquewhite2
MElightpink3
MEmediumpurple3
MEplum
MEcyan
MEdarkred
MEpaleturquoise
MEblue
MEblack
MEdarkorange
0.97 (2e−07) 0.7 (0.01) −0.32 (0.3)
−0.83 (8e−04) 0.97 (1e−07) −0.4 (0.2)
0.42 (0.2) 1 (7e−12) −0.86 (3e−04)
−0.75 (0.005) −0.23 (0.5) −0.64 (0.03)
−0.96 (7e−07) −0.92 (3e−05) −0.31 (0.3)
−1 (1e−11) −0.65 (0.02) 0.28 (0.4)
−0.33 (0.3) −0.95 (2e−06) 0.63 (0.03)
−0.73 (0.007) −0.92 (2e−05) 0.32 (0.3)
−0.28 (0.4) −0.98 (6e−08) 0.67 (0.02)
−0.045 (0.9) −0.96 (7e−07) 0.4 (0.2)
−0.52 (0.08) −1 (3e−17) 0.29 (0.4)
−0.25 (0.4) −0.89 (9e−05) 0.33 (0.3)
0.14 (0.7) −0.97 (1e−07) 0.81 (0.001)
0.11 (0.7) −0.86 (4e−04) 0.57 (0.05)
0.59 (0.04) 0.057 (0.9) 0.5 (0.1)
0.45 (0.1) −0.98 (2e−08) 0.64 (0.03)
−0.15 (0.6) −0.94 (5e−06) 0.42 (0.2)
0.5
0
−0.5
Control vs. P. marinus
Control vs P. marinus and GDC−0152
Arsine Transformed Apoptosis Percentage

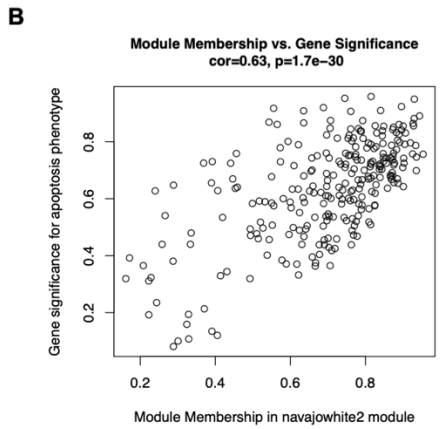
B
Module Membership vs. Gene Significance
cor=0.63, p=1.7e−30
Gene significance for apoptosis phenotype
0.2
0.4
0.6
0.8
Module Membership in navajowhite2 module

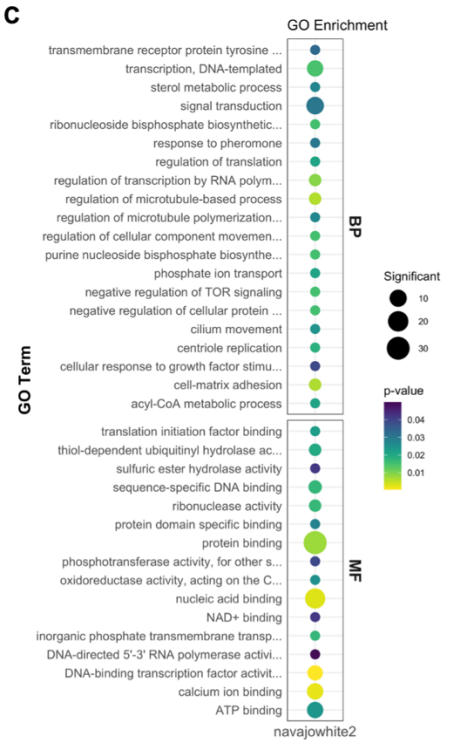
C
GO Enrichment
transmembrane receptor protein tyrosine ...
transcription, DNA-templated
sterol metabolic process
signal transduction
ribonucleoside bisphosphate biosynthetic...
response to pheromone
regulation of translation
regulation of transcription by RNA polym...
regulation of microtubule-based process
regulation of microtubule polymerization...
regulation of cellular component movemen...
purine nucleoside bisphosphate biosynthe...
phosphate ion transport
negative regulation of TOR signaling
negative regulation of cellular protein ...
cilium movement
centriole replication
cellular response to growth factor stimu...
cell-matrix adhesion
acyl-CoA metabolic process
BP
translation initiation factor binding
thiol-dependent ubiquitinyl hydrolase ac...
sulfuric ester hydrolase activity
sequence-specific DNA binding
ribonuclease activity
protein domain specific binding
protein binding
phosphotransferase activity, for other s...
oxidoreductase activity, acting on the C...
nucleic acid binding
NAD+ binding
inorganic phosphate transmembrane transp...
DNA-directed 5'-3' RNA polymerase activi...
DNA-binding transcription factor activit...
calcium ion binding
ATP binding
MF
GO Term
Significant
10
20
30
p-value
0.04
0.03
0.02
0.01
navajowhite2

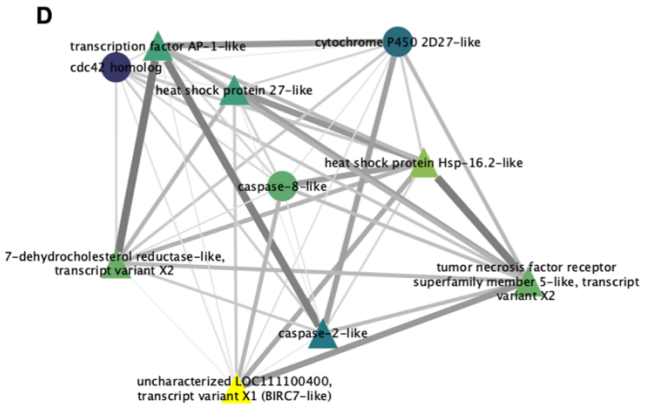
D
transcription factor AP−1−like
cytochrome P450 2D27−like
cdc42 homolog
heat shock protein 27−like
heat shock protein Hsp−16.2−like
caspase−8−like
7−dehydrocholesterol reductase−like, transcript variant X2
tumor necrosis factor receptor superfamily member 5−like, transcript variant X2
caspase−2−like
uncharacterized LOC111100400, transcript variant X1 (BIRC7−like)

Figure III-5. Pre-exposure of hemocytes with GDC-0152 before treatment with *P. marinus* induced differential expression of transporter genes in *P. marinus*.

Hemocytes were pretreated with control (FSSW) or 50 μM of GDC-0152 for 3 hr and then incubated with *P. marinus* (1:1 MOI) for 1 hr before analysis of *P. marinus* gene expression. *P. marinus* DEGs were analyzed in comparison to *P. marinus* expression in control (non-GDC treated) hemocytes. A) PCA plot of *rlog* transformed counts for each sample. B) Volcano plots of differentially expressed genes (DEGs) in *P. marinus* in response to GDC-0152 pretreatment of hemocytes. C) LFC heatmap plot of all identified *P. marinus* DEGs in response to GDC-0152 pretreatment of hemocytes. D) Bubble plot showing significantly enriched Biological Process and Molecular Function Gene Ontology terms identified by topGO in the DEGs.

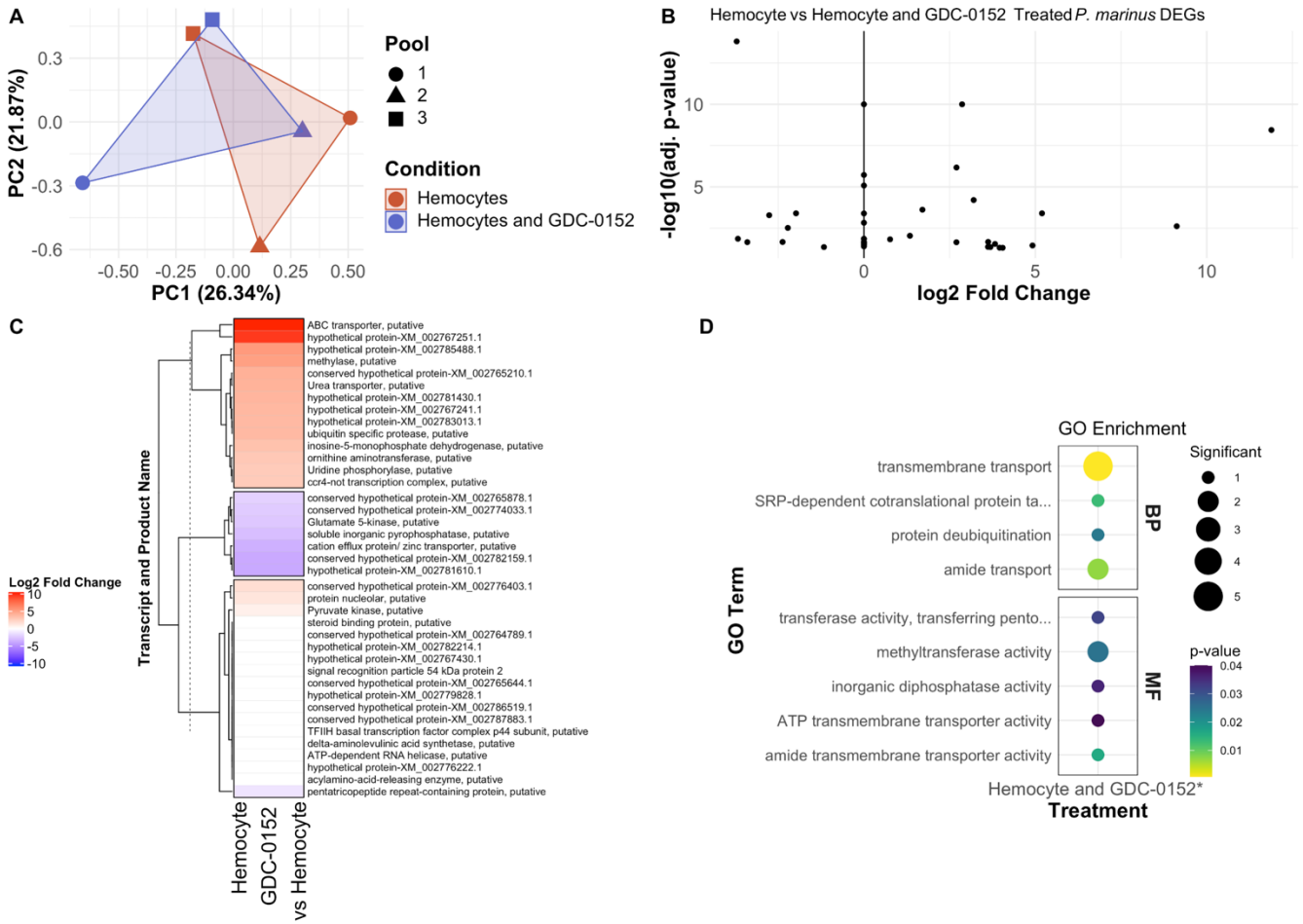
A
PC2 (21.87%)
PC1 (26.34%)
Pool
1
2
3
Condition
Hemocytes
Hemocytes and GDC-0152
B
Hemocyte vs Hemocyte and GDC-0152 Treated P. marinus DEGs
-log10(adj. p-value)
log2 Fold Change
C
Log2 Fold Change
Transcript and Product Name
ABC transporter, putative
hypothetical protein-XM_002767251.1
hypothetical protein-XM_002785488.1
methylase, putative
conserved hypothetical protein-XM_002765210.1
Urea transporter, putative
hypothetical protein-XM_002781430.1
hypothetical protein-XM_002767241.1
hypothetical protein-XM_002783013.1
ubiquitin specific protease, putative
inosine-5-monophosphate dehydrogenase, putative
ornithine aminotransferase, putative
Uridine phosphorylase, putative
ccr4-not transcription complex, putative
conserved hypothetical protein-XM_002765878.1
conserved hypothetical protein-XM_002774033.1
Glutamate 5-kinase, putative
soluble inorganic pyrophosphatase, putative
cation efflux protein/ zinc transporter, putative
conserved hypothetical protein-XM_002782159.1
hypothetical protein-XM_002781610.1
conserved hypothetical protein-XM_002776403.1
protein nucleolar, putative
Pyruvate kinase, putative
steroid binding protein, putative
conserved hypothetical protein-XM_002764789.1
hypothetical protein-XM_002782214.1
hypothetical protein-XM_002767430.1
signal recognition particle 54 kDa protein 2
conserved hypothetical protein-XM_002765644.1
hypothetical protein-XM_002779828.1
conserved hypothetical protein-XM_002786519.1
conserved hypothetical protein-XM_002787883.1
TFIIH basal transcription factor complex p44 subunit, putative
delta-aminolevulinic acid synthetase, putative
ATP-dependent RNA helicase, putative
hypothetical protein-XM_002776222.1
acylamino-acid-releasing enzyme, putative
pentatricopeptide repeat-containing protein, putative
Hemocyte
GDC-0152
vs Hemocyte
D
GO Enrichment
GO Term
transmembrane transport
SRP-dependent cotranslational protein ta...
protein deubiquitination
amide transport
BP
transferase activity, transferring pento...
methyltransferase activity
inorganic diphosphatase activity
ATP transmembrane transporter activity
amide transmembrane transporter activity
MF
Significant
p-value
Hemocyte and GDC-0152*
Treatment

Figure III-6. WGCNA reveals correlation of *P. marinus* proteases, hydrolases, and kinases in response to hemocyte exposure. Hemocytes were pretreated with control (FSSW), 50 μM of GDC-0152 for 3 hr, or 100 μM of Z-VAD-FMK for 1 hr and then incubated with P. marinus (1:1 MOI) for 1 hr before analysis of P. marinus gene expression. A) Heatmap of modules significantly correlated with hemocyte and either GDC-0152 or Z-VAD-FMK treatment and high Gene Significance and Module Membership relationship in both treatments are plotted along with their correlation with apoptosis phenotype (percent of apoptosis in granular hemocytes). X-axis indicates modules of correlated transcripts and the y-axis plots each trait for which module significance was calculated. Correlation values (-1 – 1), followed by significance values (p between 0-1) in parentheses, are listed in each cell. Color indicates strength and direction of correlation. B) Relationship between Gene Significance and Module Membership for the blue4 module, where each point is a transcript in the module. C) Gene Ontology enrichment for Biological Process and Molecular Function for the blue4 module. D) P. marinus blue4 module network (Cytoscape,V 3.8.0) showing highly connected intramodular hub genes. P. marinus modules were drawn using the circular layout.

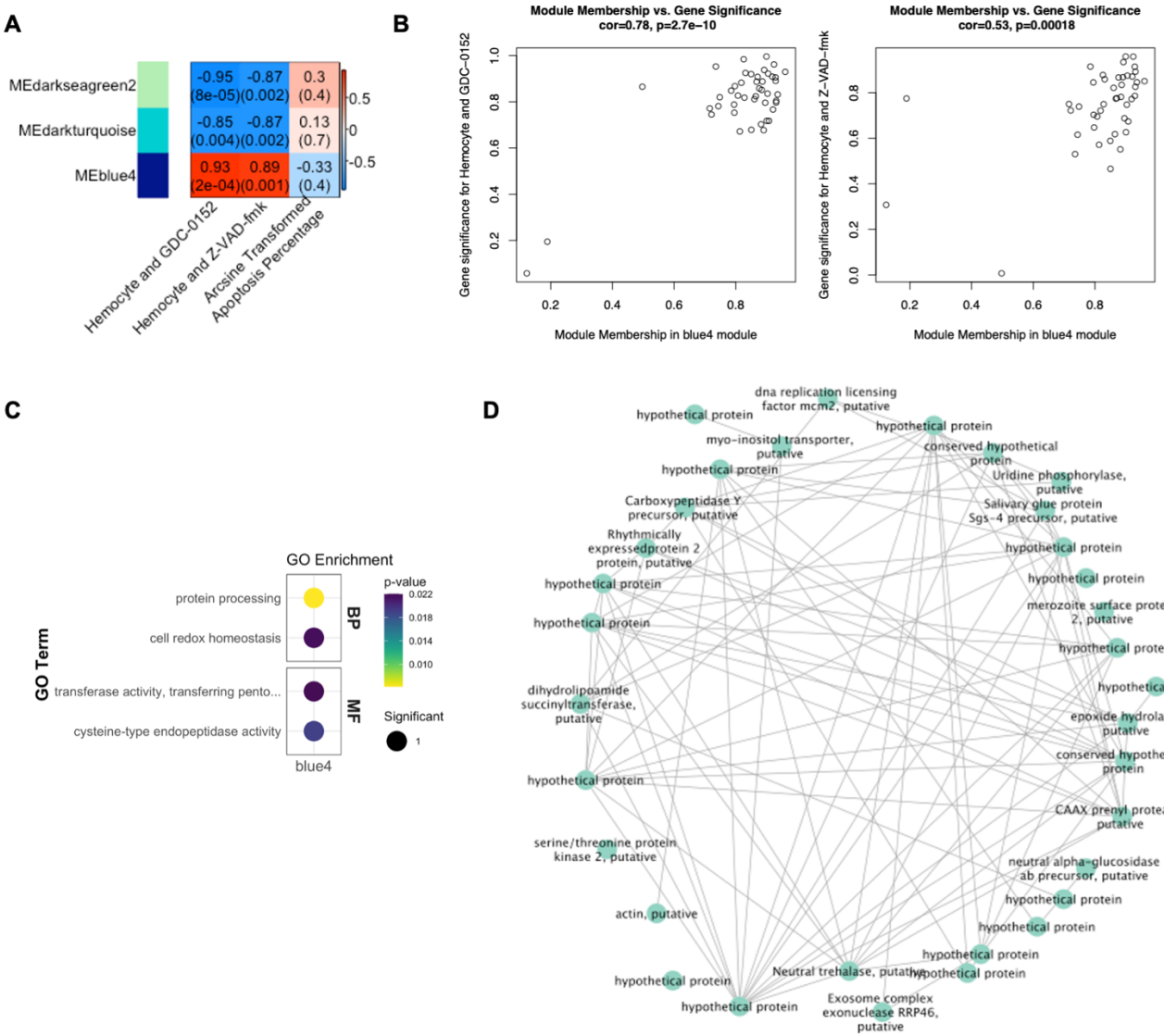
A
MEdarkseagreen2
MEdarkturquoise
MEblue4
-0.95 (8e-05)
-0.87 (0.002)
0.3 (0.4)
-0.85 (0.004)
-0.87 (0.002)
0.13 (0.7)
0.93 (2e-04)
0.89 (0.001)
-0.33 (0.4)
0.5
0
-0.5
Hemocyte and GDC-0152
Hemocyte and Z-VAD-fmk
Arcsine Transformed Apoptosis Percentage
B
Module Membership vs. Gene Significance
cor=0.78, p=2.7e−10
Gene significance for Hemocyte and GDC−0152
Module Membership in blue4 module
Module Membership vs. Gene Significance
cor=0.53, p=0.00018
Gene significance for Hemocyte and Z−VAD−fmk
Module Membership in blue4 module
C
GO Enrichment
GO Term
protein processing
cell redox homeostasis
transferase activity, transferring pento...
cysteine-type endopeptidase activity
BP
MF
blue4
p-value
0.022
0.018
0.014
0.010
Significant
1
D
dna replication licensing factor mcm2, putative
hypothetical protein
myo-inositol transporter, putative
conserved hypothetical protein
Uridine phosphorylase, putative
Carboxypeptidase Y precursor, putative
Salivary glue protein Sgs-4 precursor, putative
Rhythmically expressedprotein 2 protein, putative
merozoite surface protein 2, putative
dihydrolipoamide succinyltransferase, putative
epoxide hydrolase, putative
CAAX prenyl protease putative
serine/threonine protein kinase 2, putative
neutral alpha-glucosidase ab precursor, putative
actin, putative
Neutral trehalase, putative
Exosome complex exonuclease RRP46, putative

Figure III-7. *P. marinus*-induced hemocyte apoptosis suppression may involve interference with the TNFR or NF-kB pathways by *P. marinus* secreted enzymes and potential crosstalk with oxidation-reduction processes.
A) Model of *P. marinus* infection informed by work in previous studies (Soudant et al., 2013; Tasumi and Vasta, 2007; Vasta et al., 2020). B) Significantly differentially expressed genes and transcripts in eastern oyster hemocytes and *P. marinus* highlighted in this study were used to draw a hypothetical model of mechanism of action of *P. marinus* inhibition of eastern oyster hemocyte apoptosis. Critical molecules involved in implicated pathways but not significantly differentially expressed are outline in gray. Molecules involved in apoptosis pathways that have not identified in eastern oysters (based on (Witkop et al., in preparation, Chapter II) are outlined in black.

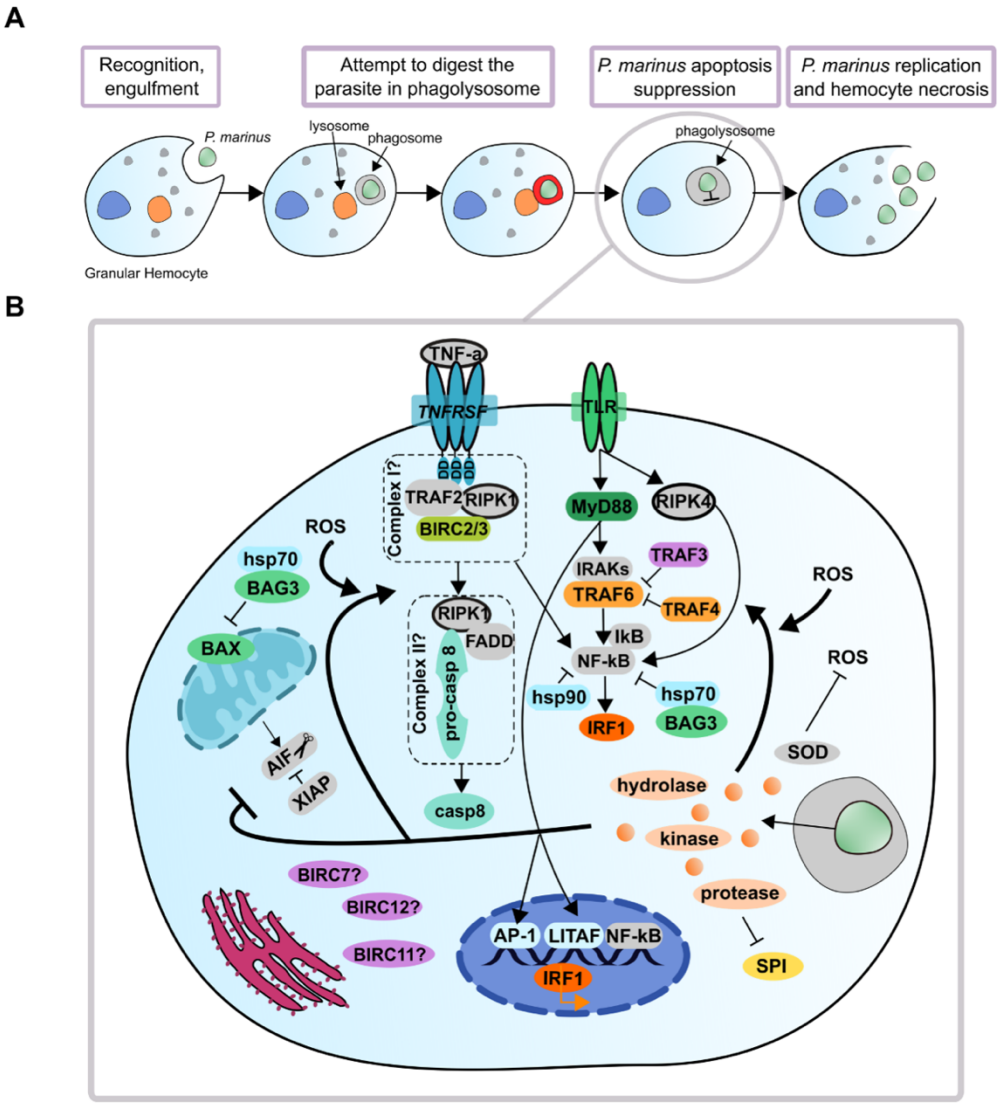
A
Recognition, engulfment
Attempt to digest the parasite in phagolysosome
P. marinus apoptosis suppression
P. marinus replication and hemocyte necrosis
P. marinus
lysosome
phagosome
phagolysosome
Granular Hemocyte
B
TNF-a
TNFRSF
TLR
Complex i?
TRAF2
RIPK1
BIRC2/3
MyD88
RIPK4
IRAKs
TRAF3
TRAF6
TRAF4
IkB
NF-kB
hsp90
hsp70
BAG3
IRF1
ROS
hsp70
BAG3
BAX
AIF
XIAP
Complex ii?
RIPK1
FADD
pro-casp 8
casp8
ROS
ROS
SOD
hydrolase
kinase
protease
SPI
BIRC7?
BIRC12?
BIRC11?
AP-1
LITAF
NF-kB
IRF1

Supplementary Material

Supplementary Figure 1: Apoptosis of unstimulated agranular hemocytes following GDC-0152 and Z-VAD-FMK treatment. Percent apoptotic agranular hemocytes in the unstimulated hemocyte experiment testing the effects of GDC-0152 and Z-VAD-FMK treatment. No statistical comparisons were significantly different.

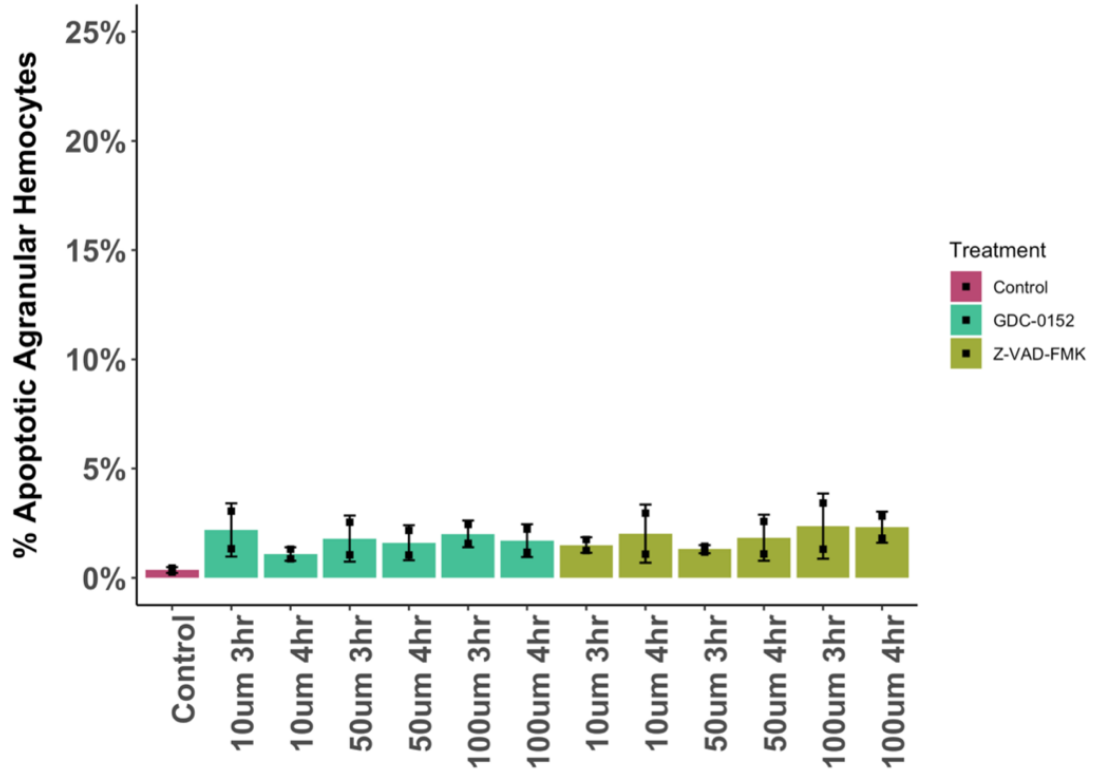

Supplementary Figure 2: Representative bubble plots of hemocyte and *P. marinus in vitro* cell phenotypes measured by flow cytometry. Plots were generated with the BD Accuri C6 Plus flow Software (V 1.0.23.1)**.** Red lines indicate gating used to delineate cells with each phenotype. A) Apoptosis assay (Annexin-V). B) Mitochondrial permeabilization (JC-1) assay. C) Caspase 3/7 activity assay.

A

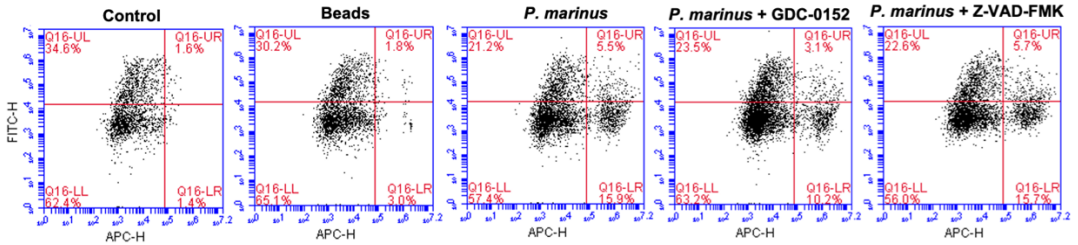

Q16-LL – Non-apoptotic hemocytes
Q16-UL – Apoptotic hemocytes – no *P. marinus*
Q16-LR – Non-apoptotic *P. marinus* or beads
Q16-UR – Apoptotic Hemocytes with beads or *P. marinus*

B

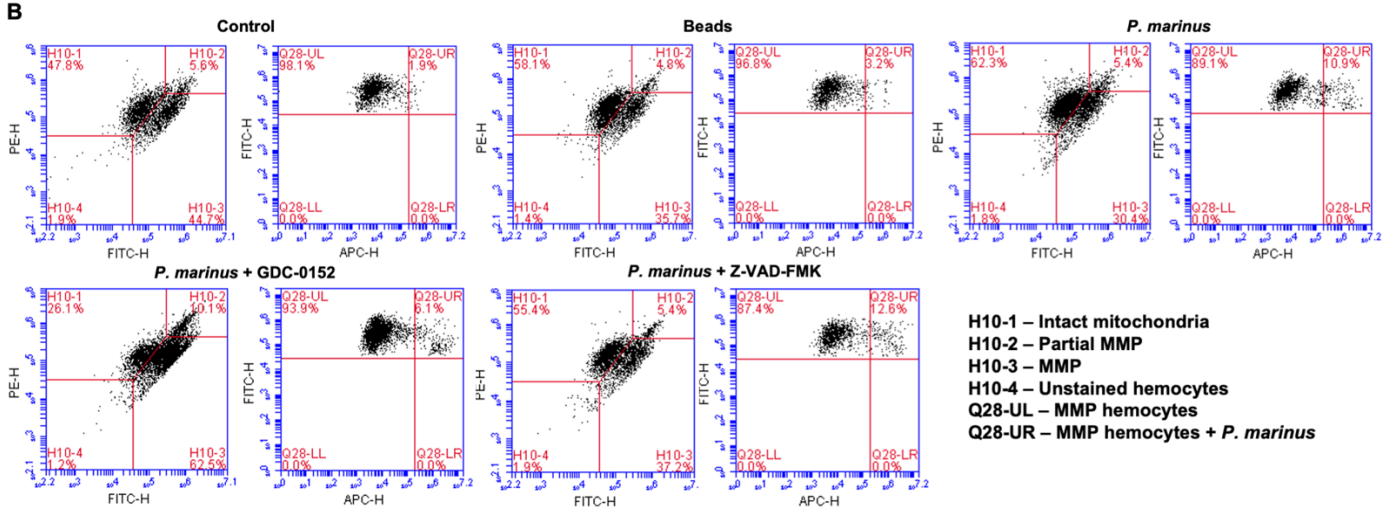

H10-1 – Intact mitochondria
H10-2 – Partial MMP
H10-3 – MMP
H10-4 – Unstained hemocytes
Q28-UL – MMP hemocytes
Q28-UR – MMP hemocytes + *P. marinus*

C

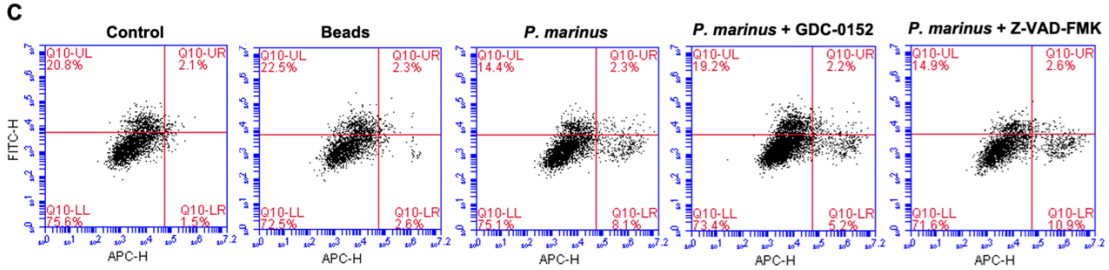

Q10-LL – Non-Caspase 3/7 active hemocytes
Q10-UL – Caspase 3/7 active hemocytes – no *P. marinus*
Q10-LR – Non-Caspase 3/7 active *P. marinus* or beads
Q10-UR – Caspase 3/7 active Hemocytes with beads or *P. marinus*

Supplementary Figure 3: Treemaps of hemocyte GO enrichment for biological process (BP) and molecular function (MF). REVIGO plots generated in R with treemap that show reduced representation lists of the most representative GO terms and groups them based on semantic similarity (Supek et al., 2011)**.** A) Control vs. *P. marinus* enriched MF terms. B) Control vs. *P. marinus* enriched BP terms. C) Control vs. *P. marinus* and GDC-0152 enriched MF terms. D) Control vs. *P. marinus* and GDC-0152 enriched BP terms.

A

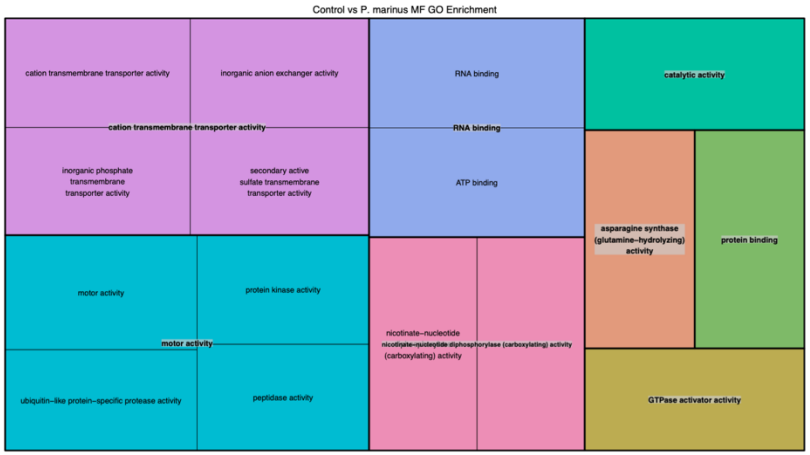
Control vs P. marinus MF GO Enrichment
cation transmembrane transporter activity
inorganic anion exchanger activity
RNA binding
catalytic activity
cation transmembrane transporter activity
RNA binding
inorganic phosphate transmembrane transporter activity
secondary active sulfate transmembrane transporter activity
ATP binding
asparagine synthase (glutamine-hydrolyzing) activity
protein binding
motor activity
protein kinase activity
nicotinate-nucleotide diphosphorylase (carboxylating) activity
motor activity
nicotinate-nucleotide (carboxylating) activity
ubiquitin-like protein-specific protease activity
peptidase activity
GTPase activator activity

B


Control vs P. marinus BP GO Enrichment
glycosaminoglycan metabolic process
DNA catabolic process
regulation of phosphoprotein phosphatase activity
regulation of small GTPase mediated signal transduction
signal transduction
glycosaminoglycan metabolic process
protein phosphorylation
transcription initiation from RNA polymerase II promoter
transmembrane transport
anion transport
anion transport
carboxylic acid metabolic process
asparagine biosynthetic process

C

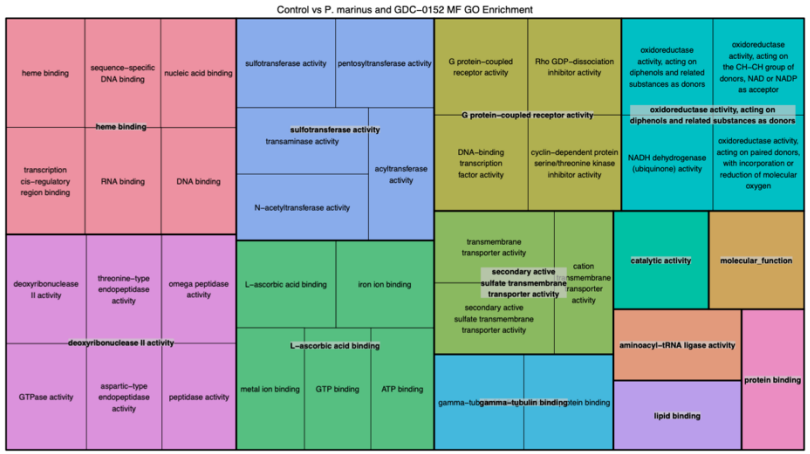
Control vs P. marinus and GDC-0152 MF GO Enrichment
heme binding
sequence-specific DNA binding
nucleic acid binding
sulfotransferase activity
pentosyltransferase activity
G protein-coupled receptor activity
Rho GDP-dissociation inhibitor activity
oxidoreductase activity, acting on diphenols and related substances as donors
oxidoreductase activity, acting on the CH-CH group of donors, NAD or NADP as acceptor
heme binding
sulfotransferase activity
G protein-coupled receptor activity
oxidoreductase activity, acting on diphenols and related substances as donors
transcription cis-regulatory region binding
RNA binding
DNA binding
transaminase activity
acyltransferase activity
DNA-binding transcription factor activity
cyclin-dependent protein serine/threonine kinase inhibitor activity
NADH dehydrogenase (ubiquinone) activity
oxidoreductase activity, acting on paired donors, with incorporation or reduction of molecular oxygen
N-acetyltransferase activity
transmembrane transporter activity
catalytic activity
molecular_function
deoxyribonuclease II activity
threonine-type endopeptidase activity
omega peptidase activity
L-ascorbic acid binding
iron ion binding
secondary active sulfate transmembrane transporter activity
cation transmembrane transporter activity
secondary active sulfate transmembrane transporter activity
aminoacyl-tRNA ligase activity
protein binding
deoxyribonuclease II activity
L-ascorbic acid binding
GTPase activity
aspartic-type endopeptidase activity
peptidase activity
metal ion binding
GTP binding
ATP binding
gamma-tubulin binding
gamma-tubulin binding
lipid binding

D

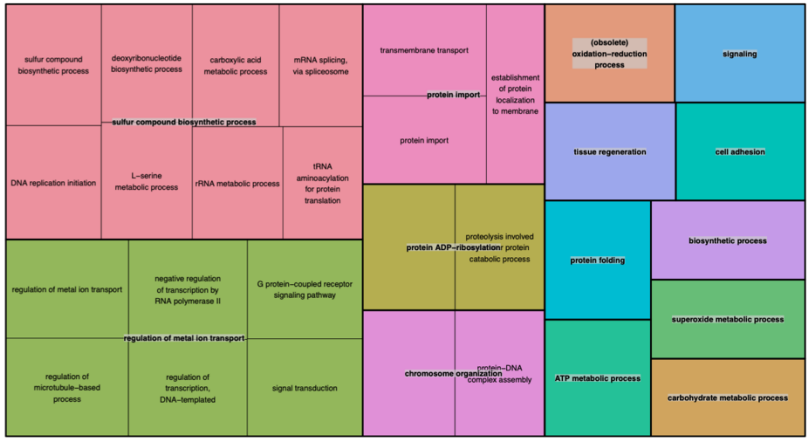
Control vs P. marinus and GDC-0152 BP GO Enrichment
sulfur compound biosynthetic process
deoxyribonucleotide biosynthetic process
carboxylic acid metabolic process
mRNA splicing, via spliceosome
transmembrane transport
protein import
establishment of protein localization to membrane
(obsolete) oxidation-reduction process
signaling
sulfur compound biosynthetic process
protein import
tissue regeneration
cell adhesion
DNA replication initiation
L-serine metabolic process
rRNA metabolic process
tRNA aminoacylation for protein translation
protein ADP-ribosylation
proteolysis involved in protein catabolic process
protein folding
biosynthetic process
regulation of metal ion transport
negative regulation of transcription by RNA polymerase II
G protein-coupled receptor signaling pathway
regulation of metal ion transport
superoxide metabolic process
regulation of microtubule-based process
regulation of transcription, DNA-templated
signal transduction
chromosome organization
protein-DNA complex assembly
ATP metabolic process
carbohydrate metabolic process

Supplementary Figure 4: WGCNA power selection and dendogram results. A) Hemocyte scale-free topology fit index plotted as a function of soft-thresholding power, calculated with *pickSoftThreshold*, and mean connectivity plotted as a function of the soft-thresholding power. B) *P. marinus* scale-free topology fit index plotted as a function of soft-thresholding power, calculated with *pickSoftThreshold*, and mean connectivity plotted as a function of the soft-thresholding power. C) Hemocyte dendrogram showing hierarchical clustering tree of genes, with dissimilarity based on topological overlap. D) *P. marinus* dendrogram showing hierarchical clustering tree of genes, with dissimilarity based on topological overlap.

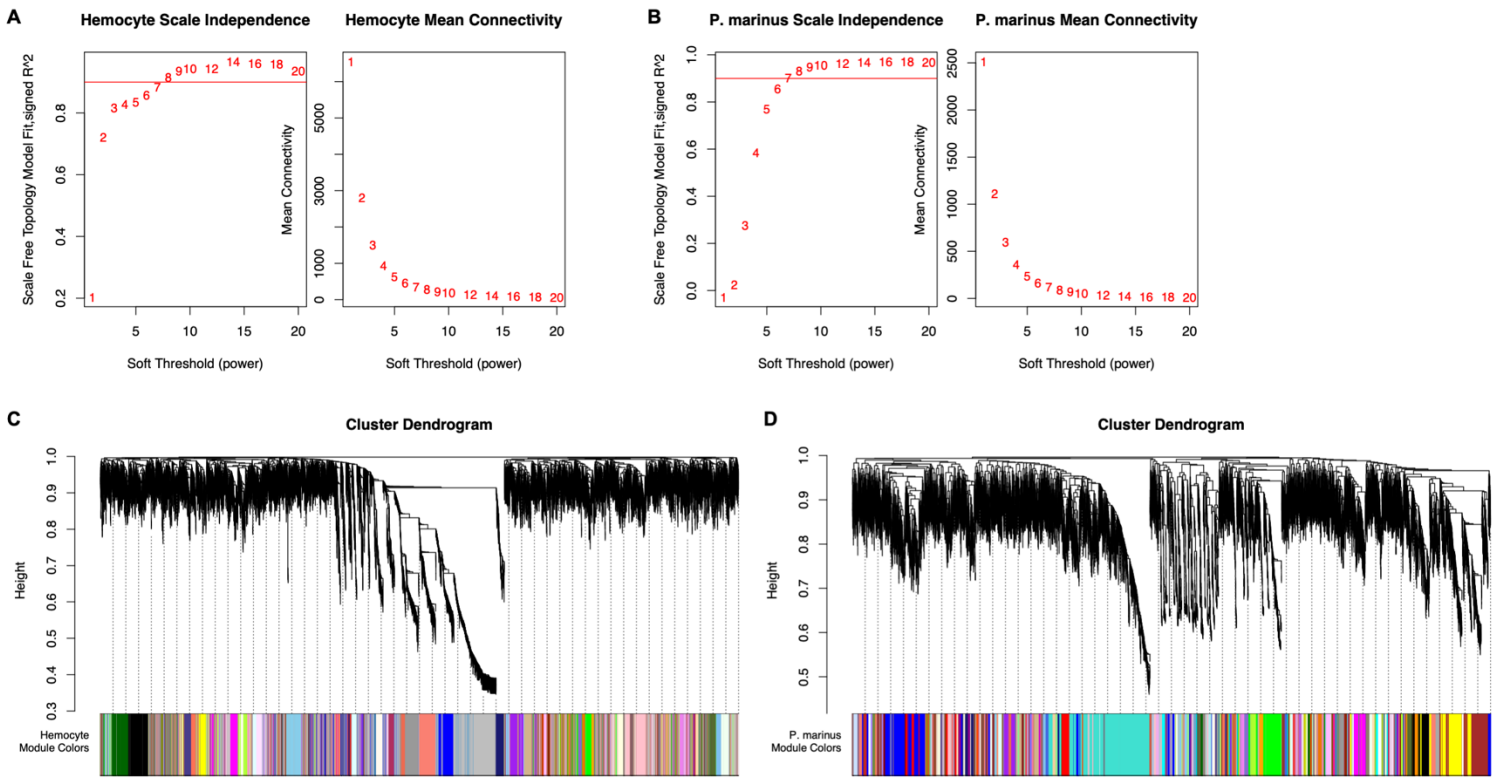

Supplementary Figure 5: *P. marinus* superoxide dismutase expression across treatments. Heatmap plotting *rlog* transformed read counts of 4 superoxide dismutase transcripts previously studied in *P. marinus* and recognized as important in *P. marinus* virulence and mechanisms of apoptosis suppression (Fernández-Robledo et al., 2008; Lau et al., 2018). No expression patterns with treatment were observed and transcripts were not significantly differentially expressed when comparing *P. marinus* samples challenged with hemocytes vs. *P. marinus* samples challenged with IAP inhibitor pre-treated hemocytes.

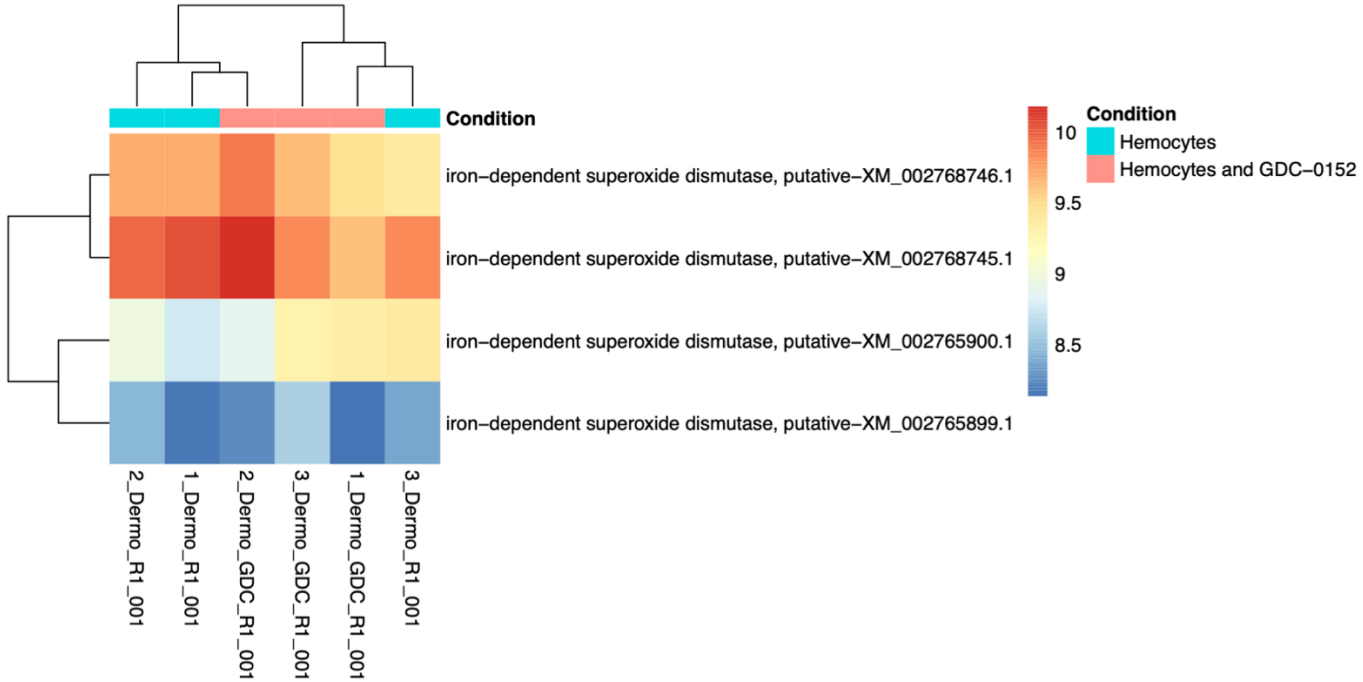

CHAPTER IV: Multifamily eastern oyster challenge with *Perkinsus marinus* reveals a correlation between hemocyte apoptosis and parasite resistance

Erin M. Roberts[1], Dina A. Proestou[2], Gary H. Wikfors[3], Kathryn Markey Lundgren[2], Mary Sullivan[2], Marta Gomez-Chiarri[1]

[1]University of Rhode Island, Department of Fisheries, Animal and Veterinary Science, 120 Flagg Rd. Kingston, RI, USA

[2]USDA ARS NEA NCWMAC Shellfish Genetics Program, 120 Flagg Rd. Kingston, RI, USA

[3]NOAA Northeast Fisheries Science Center Milford Laboratory, 212 Rogers Ave. Milford, CT, USA

Correspondence:

Marta Gomez-Chiarri

gomezchi@uri.edu

Prepared for ***Fish and Shellfish Immunology***

Keywords: oyster, apoptosis, selective breeding, resistance, caspase, IAP, Dermo disease

Highlights

- Eastern oyster *P. marinus* resistance differs between selectively bred families
- Hemocyte apoptotic response 7 d after *P. marinus* challenge differed between families
- *In vivo* hemocyte apoptotic response to *P. marinus* may be caspase-independent
- Hemocyte apoptosis 7 d after challenge and *P. marinus* resistance were correlated in the most resistant family

Abstract

Dermo disease, caused by the parasite *Perkinsus marinus*, is a widespread cause of mortality in wild and cultured eastern oysters, *Crassostrea virginica*, in the United States. Selective breeding for increased survival in Dermo prevalent areas has improved disease resistance, but the molecular mechanisms underlying resistance remain incompletely understood. Apoptosis of infected oyster hemocytes may limit *P. marinus* spread in tissues but high variability in apoptotic responses has been seen in oysters. This study challenged oysters from six selectively-bred families with *P. marinus* and assessed relationships between apoptosis phenotype and *P. marinus* resistance at 7 and 50 d post-challenge. Families significantly differed in *P. marinus* resistance, measured as change in parasite load over time after challenge. Mean acute (7 d after challenge) hemocyte apoptotic response to *P. marinus* differed between families and was highly variable within families. Hemocyte apoptosis and parasite load at 7 d post-challenge were negatively correlated in the most resistant family, suggesting that the acute apoptotic response may be indicative of *P. marinus* resistance. This challenge, however, should be repeated with families with

higher levels of resistance because of high-interindividual variation driving lack of power to detect significant differences between control and treated apoptotic response. This study informs breeding programs by revealing that hemocyte apoptosis phenotype may have some utility as a measure of Dermo disease resistance, and further elucidates mechanisms of apoptosis in response to *P. marinus*.

Introduction

The eastern oyster, *Crassostrea virginica*, is a filter-feeding bivalve mollusc that performs critical ecosystem services in its estuarine habitats (Coen et al., 2007). Eastern oyster populations have experienced significant declines along the east coast of the United States since the 1890's because of physical (storms, dredging) and biological damage (disease, predation) to oyster beds (Mackenzie, 2007). Dermo disease, caused by the alveolate parasite *Perkinsus marinus*, emerged in the 1950's in the Gulf of Mexico and has become a major cause of eastern oyster mortality (Smolowitz, 2013). Following hemocyte engulfment of infective *P. marinus* trophozoites by granular hemocytes (the other main hemocyte type in oysters, agranular hemocytes, are not phagocytic), *P. marinus* proliferates and causes tissue necrosis and inflammation that progresses to severe infection over a period of months and eventually leads to oyster death (Smolowitz, 2013; Wikfors and Alix, 2014).

Response to Dermo disease is affected by a variety of factors, including parasite strain pathogenicity, salinity, and temperature (Brown et al., 2005; Smolowitz, 2013). Traditional selective breeding methods, relying on differential survival at field sites where *P. marinus* is historically abundant, have enabled the development of oyster lines with resistance and/or tolerance to Dermo disease. This demonstrates a genetic basis for Dermo disease resistance and reveals selective breeding is an important Dermo mitigation strategy (Brown et al., 2005; Encomio et al., 2005; Frank-Lawale et al., 2014; Proestou et al., 2016). Fluctuating environmental conditions and inconsistent parasite exposure make the selective gains for Dermo resistance obtained during field exposures highly variable, however, prompting the recent development of laboratory challenge methods to evaluate

selectively-bred eastern oyster lines for Dermo resistance (Proestou et al., 2019, 2016; Proestou and Sullivan, 2020).

Several oyster immune mechanisms contribute to *P. marinus* resistance, including apoptosis of infected hemocytes (Goedken et al., 2005) and deployment of key defense molecules such as serine protease inhibitors (cvSI-1, cvSI-2) and reactive oxygen species (ROS) to combat intracellular infection (He et al., 2012; La Peyre et al., 2010; Y.-T. Lau et al., 2018; Xue et al., 2006). Apoptosis, or type 1 programmed cell death, is an important immune defense against *P. marinus* infection, and early induction of apoptosis following phagocytic engulfment by granular hemocytes may limit *P. marinus* replication (Hughes et al., 2010). Apoptosis involves two tightly controlled molecular pathways, the intrinsic (mitochondrial) pathway and the extrinsic (death receptor-mediated) pathway (Romero et al., 2015). Both pathways typically involve activation of multiple members of the caspase (cysteine-aspartic protease) family of enzymes. In caspase-dependent apoptosis pathways, activation of upstream caspases triggers activation of executioner caspase 3/7, which initiates the final steps of apoptosis (Sokolova, 2009). *P. marinus* is able to interfere with host apoptotic mechanisms and lead to significant apoptosis suppression in hemocytes of *P. marinus* susceptible oysters, possibly through the action of secreted enzymes such as superoxide dismutases (SOD) and serine proteases such as perkinsin (Faisal et al., 1999; Y. T. Lau et al., 2018; Witkop et al., n.d.; Xue et al., 2009). Mechanisms of apoptosis in response to *P. marinus* have mainly been assessed *in vitro* (Hughes et al., 2010), and not during large scale *in vivo* challenges.

Controlled laboratory challenges with eastern oysters from families selectively bred for high survival in *P. marinus* prevalent areas present an opportunity to evaluate the

connection between apoptosis and overall Dermo resistance. Focus is placed on granulocytes for analysis because these are the predominant cell type phagocytosing *P. marinus* (La Peyre et al., 1995; Soudant et al., 2013; Wikfors and Alix, 2014). Moreover, agranulocytes in oysters may be a premature developmental stage of granulocytes (Li et al., 2021; Rebelo et al., 2013). Although previous studies have assessed the connection between apoptosis and *P. marinus* resistance by comparing apoptotic responses to *P. marinus* in susceptible eastern oysters and naturally *P. marinus* resistant Pacific oysters, *Crassostrea gigas* (Goedken et al., 2005), it has not been studied across multiple eastern oyster families with differing levels of *P. marinus* susceptibility. If granular apoptosis phenotype is strongly associated with *P. marinus* resistance in eastern oysters, it could be used as an additional parameter of resistance evaluation during selective breeding for Dermo disease resistance.

Here we performed a large-scale multifamily eastern oyster *in vivo P. marinus* challenge to measure *P. marinus* resistance in terms of parasite load change over time. Apoptosis phenotype, specifically the percent of apoptotic and caspase 3/7 active hemocytes, was also quantified to determine the relationship between apoptosis and resistance. This work informs our knowledge of hemocyte apoptosis mechanisms in response to *P. marinus*, furthers our understanding of the connection between hemocyte apoptosis phenotype and resistance phenotype, and evaluates hemocyte apoptosis phenotype as a family-level diagnostic tool for evaluating disease resistance.

Materials and Methods

Oyster source and maintenance

One year old seed oysters from six full-sibling, selectively-bred families (A, B, D, E, J, L) exhibiting a range of survival were obtained from the family-based breeding program at the Aquaculture Genetics and Breeding Technology Center (ABC) at the Virginia Institute of Marine Science (VIMS). Oysters were acclimated and maintained according to previous protocols outlined in detail (Proestou et al., 2019). Briefly, seed was delivered to the USDA ARS Shellfish Genetics Laboratory, Kingston, RI, in early June and subjected to a state-required disinfection protocol. Following a two-week acclimation period, oysters from each family were maintained in a flow-through seawater system with six raceways, filtered (1 μm), UV-sterilized flowing seawater (23 - 25˚C, 28 - 30 PSU), and an ozone decontamination system for the effluent for six weeks, and monitored daily for survival. Oysters were fed daily with Shellfish Diet 1800® instant algae (Reed Mariculture).

Perkinsus marinus culture and *in vivo* challenge

Perkinsus marinus from ATCC® strain 50509, 'DBNJ' (American Type Culture Collection), was cultured using guidelines from Bushek (Bushek et al., 1994). This strain, originally isolated from diseased oysters from Delaware Bay, is comparable in virulence to *P. marinus* strains present in the Chesapeake Bay (Bushek and Allen, 1996). Cultures were used during the more virulent log phase growth stage (Ford et al., 2002). *P. marinus* cells were concentrated in 50 ml falcon tubes by centrifugation at 1,500g for 5 min at 4°C and washed using 0.45-μm filtered sterile seawater at 28 PSU (FSW) three times. Cell preparation was performed according to previous protocols (Proestou and Sullivan, 2020). Briefly, cells were counted using neutral red staining with a hemacytometer and light microscope, and cell concentration was adjusted to that desired for treatment.

Following acclimation, 30 oysters from each of the six families were either challenged with 5×10^7 *P. marinus* cells g^{-1} wet tissue weight (injected treatment, N =10 per family) or artificial seawater (control treatment, N =5 per family) by injection through a notch in the shell adjacent to the adductor muscle (Proestou and Sullivan, 2020). At 7 d and 50 d post-challenge, samples of tissue (for determination of family parasite elimination rate and transcriptome sequencing) and hemolymph from individual oysters (for flow cytometry, see details below) were collected. Mantle tissue from each oyster was preserved separately in RNAlater (Invitrogen, Waltham, MA, United States), and parasite load in censored oysters, expressed as log parasites g−1 wet tissue weight, was quantified using previously detailed protocols (DeFaveri et al., 2009; Proestou et al., 2019). Parasite load at 50 d post-challenge, percent survival at 50 d post-challenge, and *P. marinus* resistance in terms of change in parasite load over time were measured following previously established protocols (Proestou et al., 2019).

Prior to tissue sampling, at least 400 µL of hemolymph (or as much hemolymph as possible) was extracted from the adductor muscle tissue of each oyster through the notch site using a sterile 1.5'' 25 G needle and 1 mL syringe primed with 100 µl of ice cold, 0.45-µm filtered sterile seawater (FSSW). Hemolymph samples were assessed for the presence of tissue or gut debris on a microscope slide. If debris was present, samples were filtered using a separate 75-µm mesh screen for each family. Hemolymph samples from each individual oyster were aliquoted into separate sterile, 5 mL polystyrene round bottom tubes for each flow cytometry assay. Hemocytes were stored on ice prior to experimentation and used within hours of extraction from oysters.

Flow cytometry

For each treatment group three assays were performed. Cell viability (viability assay), measured as the percent of live, SYBR green stained hemocytes, was first assessed to get a general measure of oyster health and potential pathology in response to *P. marinus* challenge (4 µL 10X SYBR Green – SYBR- or 4 µL of 1 mg/mL propidium iodide – PI - in 100 µL hemolymph and 300 µL FSW) (Croxton et al., 2012). Next, the percent of apoptotic hemocytes (apoptosis assay) in each sample was measured in order to compare apoptotic responses to *P. marinus* within and between families (FITC Annexin-V, BD Pharmingen, catalog # 556419; final concentration of 25 µl/ml in 100 µl hemolymph and 100 µl FSW) (Hughes et al., 2010). Finally, the percent of caspase 3/7 active hemocytes (caspase assay) was measured since caspase 3/7 is the key apoptosis executioner enzyme in caspase-dependent apoptosis and it must be activated to perform its function (CellEvent Caspase 3/7 Green Detection Reagent, Thermo Fisher, Cat #C10427; final concentration of 1.25 µl/ml in 200 µl hemolymph and 200 µl FSW). Following reagent addition, tubes in the caspase and viability assays incubated for 1 hr at room temperature in the dark, while the apoptosis assay incubated at room temperature in the dark for 15 min.

Flow cytometry assays were run on a BD Accuri C6+ flow cytometer (BD) (NOAA NEFSC Milford Laboratory) for 1 min 30 sec using a fast flow rate (66 µl/min) with a threshold of 100,000 on FSC-H. Instrument QC was checked prior to use using the BD CS&T RUO beads (Becton Dickinson, CAT #661414). All flow cytometry plots were compensated using manufacturer recommendations for the BD Accuri C6+ in the BD Accuri C6 Plus flow Software (V 1.0.23.1). The two hemocyte cell types, granulocytes and agranulocytes, were gated using custom FSC-H vs SSC-H gates on scatterplots. Gating

single stained controls for each fluorescent probe and samples plotted as count histograms for each stain were utilized to properly adjust gating positions for all assays.

Statistical analysis

Significant differences between treatment groups for hemocyte viability, apoptosis, and caspase 3/7 activity were measured using one-way ANOVA with arcsine transformed percentage data to ensure normal distribution. Post-hoc testing was performed for ANOVA tests with the Tukey Honestly Significant Difference (HSD) test. For comparison of granular and agranular cell composition and viability between cell types, differences were assessed using a Student's T-test (*t.test*). Statistical analysis assessing the changes in apoptosis phenotype through time and the correlation between apoptosis phenotype and *P. marinus* resistance were performed using linear regressions (*lm*). All statistical analyses were performed in R Studio (V 3.6.1) (Team., 2020) and all P-values ≤ 0.05 were considered significant. Plots were generated in R Studio using ggplot2 (V 3.3.2) and compiled with egg (V 0.4.5) and cowplot (V 1.0.0) (Claus O. Wilke).

Results

P. marinus resistance differed in selectively bred families

Percent survival in *P. marinus* challenged oysters did not significantly differ between families over the course of the experiment (Figure 1a). Average parasite load through time significantly decreased in family J and this family was deemed the most *P. marinus* resistant (ANOVA p=0.001) (Figure 1b). Average parasite load significantly increased in family E and this family was deemed the least *P. marinus*-resistant (ANOVA p= 0.01).

Average parasite load in family A changed very little through time, while parasite levels slightly decreased in families B, D, and L, although not significantly. Levels of variation in parasite load between oysters within families was high and likely limited detection of further statistical differences. Overall parasite load at day 50 significantly differed between families overall (One-Way ANOVA p=0.04), and family E had higher parasite load than family J (Tukey HSD p= 0.07) (Figure 1c). Together these results show that *P. marinus* resistance, measured as change in parasite load over time, did differ between families, and families E and J were the most *P. marinus* susceptible and resistant, respectively.

Hemocyte viability in *P. marinus* challenged oysters differed between families, indicating differences in *P. marinus* induced pathology

A significant decrease in granular cell viability in response to challenge can be an indication of pathological changes induced by *P. marinus*. The viability of granular hemocytes in each hemocyte sample after *P. marinus* challenge was more variable within and between families (Figure 2) than the viability of agranular cells (98.7%-100%) at both day 7 and day 50 (Supplementary Figure 1a,b). Granular hemocyte viability at 7 and 50 d post-challenge, was not significantly different between control and challenged oysters in any of the families (Two Way ANOVA; Figure 2a,b). Granulocyte viability in *P. marinus*-challenged samples significantly differed between families at 7 d (One-way ANOVA, p = 0.03) and 50 d post-challenge (One-way ANOVA, p = 0.03). At 7 d post-challenge, specific family differences in granulocyte viability in challenged oysters were not identified in pairwise comparisons (Tukey HSD); however, at 50 d post-challenge, significantly more

granulocytes were viable in challenged oysters from family B compared to families E and L (Figure 2).

Acute hemocyte apoptotic response to *P. marinus* significantly differed between families but not between treatments

Next, hemocyte apoptotic response was assessed to understand the effect of treatment on apoptotic response between and within families. Levels of granulocyte apoptosis following challenge with *P. marinus* did not significantly change in any family compared to control at day 7 or 50 post-challenge (Figure 3a,b). However, granular hemocyte apoptosis in *P. marinus* injected oysters was significantly different between families 7 d post-challenge, but not at 50 d (Figure 3, Supplementary Figure 2). At 7 d post-challenge, mean granular hemocyte apoptosis in family A injected oysters was significantly lower than in family B (Tukey HSD $p = 0.004$) and D (Tukey HSD $p = 0.03$) injected oysters. Agranular cell apoptotic response differed between families at day 7 and day 50 (Supplementary Figure 2a,b). Significant differences in apoptotic response between families suggest differences in host genetics may affect apoptotic response to *P. marinus*. Significant differences in granular hemocyte apoptosis observed between families at day 7 and not day 50 suggest the apoptotic response to *P. marinus* may be more pronounced during the acute stage of infection.

Granular hemocyte apoptosis in response to *P. marinus in vivo* may be caspase 3/7 independent

Caspase 3/7 activation was measured in hemocytes to investigate *in vivo* apoptosis mechanisms in response to *P. marinus* as well as to compare *in vivo* responses to those observed in previous *in vitro* assays suggesting the apoptotic response of eastern oyster hemocytes to *P. marinus* is caspase-independent (Hughes et al., 2010; Witkop et al., in preparation; Chapter III). Due to overlap in fluorescent probes used to measure apoptosis and caspase 3/7 activity, assays could not be run together and the level of apoptotic cells that were also caspase 3/7 active was not measured. Granular hemocyte caspase 3/7 activation in *P. marinus* injected oysters was higher across families, on average, at day 7 (30-50%) than day 50 (15-36%). Caspase 3/7 activation in either granulocytes or agranulocytes did not differ between control and *P. marinus* treated oysters within families at either time point (Figure 4), although statistical comparison was only possible for all families at 50 d and family B 7 d post-challenge because of limited hemolymph in the small seed oysters early during challenge and prioritization of available hemolymph for viability and apoptosis measurements at day 7.

Granulocyte and agranulocyte caspase 3/7 activation was not significantly different in challenged oysters between families 7 d post-challenge (Figure 4, Supplementary Figure 3), despite significant differences in apoptosis levels in those oysters (Figure 3, Supplementary Figure 2). Notably, 50 d post-challenge, granular (and agranular) caspase 3/7 activation did differ between families while apoptosis levels did not, and family E had significantly greater caspase 3/7 activation than families A (Two Way ANOVA; Tukey HSD $p = 0.03$) and B (Tukey HSD $p = 0.02$) (Figure 4b). The median proportion of granular cells showing caspase 3/7 activation was typically lower within families than levels of apoptosis at both time points (*i.e.* day 7 median apoptosis in Family B 76.9% vs 53.5 %

caspase 3/7 activity), except for family A at day 7 and family E at day 50 wherein median caspase 3/7 activation was higher than median apoptosis. These results together reveal an inconsistent relationship between changes in apoptosis phenotype and caspase 3/7 activation during *P. marinus* challenge, and support previous *in vitro* results (Hughes et al., 2010; Witkop et al., in preparation, Chapter III) that apoptosis in response to *P. marinus* may not be dependent on caspase 3/7 activation.

Granular hemocyte apoptosis phenotype during acute infection was correlated with parasite load in the most resistant family

Significant differences observed in both granular apoptotic response and overall family-level *P. marinus* resistance enabled assessment of the relationship between these two parameters. The change in granular hemocyte apoptosis between 7 d and 50 d post-challenge in injected oysters was first assessed in order to compare this result to patterns of change in parasite load over time (a decrease in parasite load through time after challenge indicating resistance; Proestou et al., 2019) (Figure 5). Consistent with the hypothesis that granular apoptosis prevents parasite replication (Witkop et al., in prep, Chapter III), families showing a decrease in *P. marinus* load through time (family J) were expected to also show a decrease in granular apoptosis in that same period of time (*i.e.* a significant correlation would be observed between apoptosis and parasite load). Granular hemocyte apoptosis significantly decreased in families B, D, E and J between day 7 and day 50 post-challenge (T-test $p < 0.05$ for each family; Figure 5a), a pattern that was not consistent with changes in parasite load observed through time in each of these families (Figure 1b).

The relationship between granular hemocyte apoptosis and tissue parasite load in each individual oyster was next assessed at 7 d and 50 d post-challenge (Figure 5c). *P. marinus* tissue load was significantly negatively correlated with apoptosis phenotype in the most resistant family J at 7 d post-challenge (T-test $p = 0.05$), and significantly positively correlated with family A (which did not show strong resistance or susceptibility based on change in parasite load through time) at 50 d post-challenge (T-test $p = 0.04$) (Figure 5b). There was no correlation between granulocyte apoptosis levels and parasite load at day 7 or day 50 post-challenge when data from all families was combined (Figure 5c), indicating that the relationship between apoptosis at day 7 and resistance may be limited to only families with the strongest resistance during acute, early-stage infection.

Discussion

Numerous field trials have established that oyster ability to survive Dermo disease is heritable and selective breeding is an appropriate strategy for Dermo disease management (Brown et al., 2005; Calvo et al., 2003; Proestou et al., 2016). Conducting *P. marinus* challenge in a controlled laboratory environment reduces variability in challenge conditions and allows for more consistent disease pressure and direct measurement of resistance phenotypes (Proestou et al., 2019). Controlled lab challenges also provide an opportunity to compare changes in hemocyte apoptosis phenotype in response to *P. marinus*, which has previously been associated with *P. marinus* resistance (Goedken et al., 2005), across multiple selectively-bred families. Including apoptosis phenotype among resistance traits could improve breeding accuracy for Dermo resistance. Furthermore, the mechanism(s) of apoptosis in response to *P. marinus* are not completely understood and

additional research into these mechanisms will improve our understanding of host-parasite interactions in oysters.

Families did not differ in their percent survival to *P. marinus* challenge over the course of the experiment, perhaps as a consequence of the short time scale of the experiment, as *P. marinus* typically causes a chronic infection that takes several months to progress to mortality (Smolowitz, 2013). Measurement of apoptosis phenotype revealed granular hemocyte apoptosis during acute (7 d post-challenge) *P. marinus* response significantly differed between families in challenged oysters, but not between control and treated oysters within-family, indicating that factors other than *P. marinus* challenge (*e.g.* pre-existing family differences in physiological or disease status) could be driving variability in hemocytic apoptotic responses (Wang et al., 2017). Lack of differences in percent apoptotic granulocytes between control and treated oysters within families observed in our study may also be attributable to high within-family variation, insufficient sample size, or pre-existing infections at the start of the experiment. A previous comparison of susceptible and resistant oyster species revealed variation in apoptosis response between species, treatment groups (control vs. injected), and over time (Goedken et al., 2005). This previous study highlighted that choice of sampling timepoint is particularly important (Goedken et al., 2005). The need for time-series data to account for a sequence of responses, as well as a high degree of replication to account for inter-individual variability, and impact of other factors (*i.e.* environmental stress) on hemocyte apoptosis indicates that determination of hemocyte apoptosis phenotype by flow cytometry may not be an efficient screening tool for resistance.

Virulence of the *P. marinus* strain used in the lab challenge may also contribute to lack of significant differences observed in percent apoptotic granulocytes between control and *P. marinus* challenged oysters within families (Hughes et al., 2010). Strain differences in *P. marinus* virulence have been noted in several studies (Bushek and Allen, 1996; Ford et al., 2002; Hughes et al., 2010; Yee et al., 2005). The effect of *P. marinus* strain on hemocyte apoptosis was investigated by Hughes et al. (2010), which revealed that exposure to more virulent strains led to greater apoptosis suppression followed by return to basal apoptosis; whereas, less virulent strains led to initial apoptosis suppression followed by sustained apoptosis elevation. There could also be an interaction between *P. marinus* strain and oyster disease resistance, with some families showing higher resistance to some *P. marinus* strains than others. Future experiments across selectively-bred families should sample at additional time points, assess virulence levels of the lab cultured *P. marinus*, and potentially test multiple *P. marinus* strains.

This study also assessed involvement of the executioner caspase 3/7 enzyme in hemocyte apoptotic response to *P. marinus in vivo*. Apoptosis can take place with or without the action of executioner caspase 3/7 (Sokolova, 2009). Caspase-independent apoptosis takes place following mitochondrial outer membrane permeabilization (MOMP) and typically involves translocation of AIF and endoG from the mitochondria to the nucleus where they trigger the final steps of apoptosis (Tait and Green, 2008). The involvement of caspase-independent apoptosis in response to *P. marinus* infection in oysters has been studied *in vitro* previously (Hughes et al., 2010; Witkop et al., in preparation, Chapter III). This *in vivo* challenge found that caspase 3/7 activation levels were not significantly different during the acute phase of infection in granular or agranular

hemocytes, despite differences in granular hemocyte apoptosis levels between families. This suggests apoptosis *in vivo* following *P. marinus* infection may not rely entirely on caspase 3/7 activation, supporting previous *in vitro* studies (Hughes et al., 2010; Witkop et al., in preparation, Chapter III).

It is important to recognize, however, that caspase 3/7 activation does not always lead to apoptosis, caspase 3/7 can be transiently activated during cell fate determination, and caspase 3/7 activation is important in non-apoptotic processes such as cytoskeletal reorganization (Nakajima and Kuranaga, 2017). Recent research has also shown reversal of morphological signs of apoptosis following caspase 3/7 activation and cytochrome c release in a process called anastasis, including reversal of MOMP, chromatin condensation, and plasma membrane blebbing (Tang and Tang, 2018). Future assays should select more divergent fluorescent probes during apoptosis and caspase 3/7 activity assays so dual assays can be performed that measure the number of hemocytes that are both apoptotic and show caspase 3/7 activation.

Finally, significant differences observed in both resistance and apoptosis phenotype between selectively-bred families enabled exploration of possible relationships between apoptosis phenotype and resistance between families. This study revealed that while the change in apoptosis levels over time did not show patterns consistent with change in parasite load over time, apoptosis phenotype and parasite load were negatively correlated in individual oysters in the most *P. marinus*-resistant family J during the acute, 7 d post-challenge, infection response. To confirm the relationship between hemocyte apoptosis and oyster resistance to *P. marinus* infection and further assess the utility of this phenotype or the underlying genotype as a measurement of resistance during selective breeding, future

experiments should assess apoptosis at both earlier (1 d, 3 d post-challenge) and intermediate (28 d post-challenge) timepoints to better observe changes in apoptosis levels through time, and repeat with a range of families showing a clearer differentiation in the levels of *P. marinus* resistance, from highly susceptible to highly resistant.

Differences between families observed in apoptotic response to *P. marinus* and correlation between apoptosis phenotype with resistance during acute infection in the most resistant family suggest that genetic differences may be involved in apoptosis pathway regulation. To assess these potential differences, transcriptome sequencing and differential expression analysis should be performed to compare overall apoptosis pathway expression between families and control and treated oysters within families. Based on previous studies, we hypothesize that challenge with *P. marinus* will induce differential expression of oxidation-reduction process, NF-kB and TNFR related pathways (Y. T. Lau et al., 2018; Proestou and Sullivan, 2020; Witkop et al., in preparation; Chapter III)

This is the first study to systematically analyze apoptosis phenotype and its relationship with resistance across several selectively-bred families in eastern oysters and presents important results showing apoptosis may be related to resistance. However, this study needs to be expanded with increased sampling timepoints and potentially altered *P. marinus* dosing or strains to fully evaluate the usage of apoptosis phenotype as an additional measure of resistance following *P. marinus* challenge. Results from future gene expression analysis will inform what apoptotic pathways are important contributors to apoptosis phenotype following *P. marinus* challenge. This study advances methods for selective breeding for Dermo disease resistance in oysters and improves our understanding of host-parasite interactions in oyster immunity.

Conclusion

This study revealed that in selectively bred families with differing levels of *P. marinus* resistance, acute apoptotic response and parasite load may be correlated in families with strong resistance phenotypes, although high interindividual variation in apoptosis phenotype and detection of correlation in only the most resistant families may make this measurement unreliable for screening in selective breeding programs, but useful in identifying mechanisms of resistance. Significant differences in acute (7 d) apoptotic response to *P. marinus* between families suggest that expression of the many genes that regulate apoptosis may influence observed apoptosis phenotype. This study is the first to analyze the correlation between apoptosis and *P. marinus* disease resistance across multiple selectively-bred eastern oyster families. Knowledge gained informs selective breeding practices and eastern oyster immunity and host-parasite interactions in general.

Funding

This work was supported by a USDA NIFA Pre-Doctoral Fellowship Award# 2019-67011-29553 to EMR, Department of Commerce/NOAA Saltonstall-Kennedy Award #NA18NMF4270193 to MGC, David R. Nelson, and David C. Rowley, USDA NIFA AFRI Award #2015-67016-22942 to DCR, DRN and MGC, USDA ARS Collaborative Project 58-8030-5-009 to MGC, a USDA NRSP-8 award to MGC and DAP, and the Shellfish Restoration Foundation.

Acknowledgments

The authors thank the NOAA Northeast Fisheries Science Center Milford Laboratory for authorized use of their BD Accuri C6+ flow cytometer. The authors thank Stan Allen and Jessica Small at VIMS ABC for supplying lines of selectively bred oysters. The authors thank Tal Ben Horin for his assistance with oyster rearing, tank set up and experimentation. The authors thank Dr. Rebecca Stevick, Kathryn Brooks, Steph Spada, Isabel Nunez, Dijiorre Perez, and Steven Pitchford for their additional assistance during the experiment.

References

Brown, B.L., Butt, A.J., Meritt, D., Paynter, K.T., 2005. Evaluation of resistance to Dermo in eastern oyster strains tested in Chesapeake Bay. Aquac. Res. 36, 1544–1554. https://doi.org/10.1111/j.1365-2109.2005.01377.x

Bushek, D., Allen, S.K., 1996. Host-parasite interactions among broadly distributed populations of the eastern oyster Crassostrea virginica and the protozoan Perkinsus marinus. Mar. Ecol. Prog. Ser. 139, 127–141. https://doi.org/10.3354/meps139127

Bushek, D., Ford, S.E., Allen, S.K., 1994. Evaluation of methods using ray's fluid thioglycollate medium for diagnosis of Perkinsus marinus infection in the eastern oyster, Crassostrea virginica. Annu. Rev. Fish Dis. 4, 201–217. https://doi.org/https://doi.org/10.1016/0959-8030(94)90029-9

Calvo, L.M.R., Calvo, G.W., Burreson, E.M., 2003. Dual disease resistance in a selectively bred eastern oyster , Crassostrea virginica , strain tested in Chesapeake Bay 220, 69–87. https://doi.org/10.1016/S0044-8486(02)00399-X

Coen, L.D., Brumbaugh, R.D., Bushek, D., Grizzle, R., Luckenbach, M.W., Posey, M.H., Powers, S.P., Tolley, S.G., 2007. Ecosystem services related to oyster restoration. Mar. Ecol. Prog. Ser. 341, 303–307. https://doi.org/10.3354/meps341299

Croxton, A.N., Wikfors, G.H., Schulterbrandt-Gragg, R.D., 2012. Immunomodulation in eastern oysters, Crassostrea virginica, exposed to a PAH-contaminated, microphytobenthic diatom. Aquat. Toxicol. 118–119, 27–36. https://doi.org/10.1016/j.aquatox.2012.02.023

DeFaveri, J., Smolowitz, R.M., Roberts, S.B., 2009. Development and validation of a real-time quantitative PCR assay for the detection and quantification of perkinsus marinus

in the eastern oyster, crassostrea virginica. J. Shellfish Res. 28, 459–464. https://doi.org/10.2983/035.028.0306

Encomio, A.V.G., Stickler, S.M., Jr, S.K.A., Chu, F., Encomio, V.G., Stickler, S.M., Allen, S.K., Chu, F., 2005. Performance of "Natural Dermo-Resistant" Oyster Stocks-Survival, Disease, Growth, Condition and Energy Reserves. J. Shellfish Res. 24, 143–155. https://doi.org/10.2983/0730-8000(2005)24[143:pondos]2.0.co;2

Faisal, M., Schafhauser, D.Y., Garreis, K.A., Elsayed, E., La Peyre, J.F., 1999. Isolation and characterization of Perkinsus marinus proteases using bacitracin-sepharose affinity chromatography. Comp. Biochem. Physiol. - B Biochem. Mol. Biol. 123, 417–426. https://doi.org/10.1016/S0305-0491(99)00088-7

Ford, S.E., Chintala, M.M., Bushek, D., 2002. Comparison of in vitro-cultured and wild-type Perkinsus marinus. I. pathogen virulence. Dis. Aquat. Organ. 51, 187–201. https://doi.org/10.3354/dao051187

Frank-Lawale, A., Allen, S.K., Dégremont, L., 2014. Breeding and Domestication of Eastern Oyster (Crassostrea virginica) Lines for Culture in the Mid-Atlantic, Usa: Line Development and Mass Selection for Disease Resistance . J. Shellfish Res. 33, 153–165. https://doi.org/10.2983/035.033.0115

Goedken, M., Morsey, B., Sunila, I., Guise, S.D.E., Goedken, M., Morsey, B., Sunila, I., Guise, S.D.E., 2005. IMMUNOMODULATION OF CRASSOSTREA GIGAS AND CRASSOSTREA VIRGINICA CELLULAR DEFENSE MECHANISMS BY PERKINSUS MARINUS 24, 487–496.

He, Y., Yu, H., Bao, Z., Zhang, Q., Guo, X., 2012. Mutation in promoter region of a serine protease inhibitor confers Perkinsus marinus resistance in the eastern oyster

(Crassostrea virginica). Fish Shellfish Immunol. 33, 411–417. https://doi.org/10.1016/j.fsi.2012.05.028

Hughes, F.M., Foster, B., Grewal, S., Sokolova, I.M., 2010. Apoptosis as a host defense mechanism in Crassostrea virginica and its modulation by Perkinsus marinus. Fish Shellfish Immunol. 29, 247–257. https://doi.org/10.1016/j.fsi.2010.03.003

La Peyre, J.F., Chu, F. lin E., Vogelbein, W.K., 1995. In vitro interaction of Perkinsus marinus merozoites with eastern and pacific oyster hemocytes. Dev. Comp. Immunol. 19, 291–304. https://doi.org/10.1016/0145-305X(95)00017-N

La Peyre, J.F., Xue, Q.G., Itoh, N., Li, Y., Cooper, R.K., 2010. Serine protease inhibitor cvSI-1 potential role in the eastern oyster host defense against the protozoan parasite Perkinsus marinus. Dev. Comp. Immunol. 34, 84–92. https://doi.org/10.1016/j.dci.2009.08.007

Lau, Y.-T., Gambino, L., Santos, B., Pales Espinosa, E., Allam, B., 2018. Regulation of oyster (Crassostrea virginica) hemocyte motility by the intracellular parasite Perkinsus marinus : A possible mechanism for host infection. Fish Shellfish Immunol. 78, 18–25. https://doi.org/10.1016/j.fsi.2018.04.019

Lau, Y.T., Santos, B., Barbosa, M., Pales Espinosa, E., Allam, B., 2018. Regulation of apoptosis-related genes during interactions between oyster hemocytes and the alveolate parasite Perkinsus marinus. Fish Shellfish Immunol. 83, 180–189. https://doi.org/10.1016/j.fsi.2018.09.006

Li, F., Zheng, Z., Li, H., Fu, R., Xu, L., Yang, F., 2021. Crayfish hemocytes develop along the granular cell lineage. Sci. Rep. 1–16. https://doi.org/10.1038/s41598-021-92473-9

Mackenzie, C.L., 2007. CAUSES UNDERLYING THE HISTORICAL DECLINE IN EASTERN OYSTER (CRASSOSTREA VIRGINICA GMELIN , 1791) LANDINGS 26, 927–938.

Nakajima, Y.I., Kuranaga, E., 2017. Caspase-dependent non-apoptotic processes in development. Cell Death Differ. 24, 1422–1430. https://doi.org/10.1038/cdd.2017.36

Proestou, D.A., Jr, S.K.A., Corbett, R.J., Horin, T. Ben, Small, J.M., 2019. Defining Dermo resistance phenotypes in an eastern oyster breeding population 2142–2154. https://doi.org/10.1111/are.14095

Proestou, D.A., Sullivan, M.E., 2020. Variation in global transcriptomic response to Perkinsus marinus infection among eastern oyster families highlights potential mechanisms of disease resistance. Fish Shellfish Immunol. 96, 141–151. https://doi.org/10.1016/j.fsi.2019.12.001

Proestou, D.A., Vinyard, B.T., Corbett, R.J., Piesz, J., Allen, S.K., Small, J.M., Li, C., Liu, M., DeBrosse, G., Guo, X., Rawson, P., Gómez-Chiarri, M., 2016. Performance of selectively-bred lines of eastern oyster, Crassostrea virginica, across eastern US estuaries. Aquaculture 464, 17–27. https://doi.org/10.1016/j.aquaculture.2016.06.012

Rebelo, M. de F., Figueiredo, E. de S., Mariante, R.M., Nóbrega, A., de Barros, C.M., Allodi, S., 2013. New Insights from the Oyster Crassostrea rhizophorae on Bivalve Circulating Hemocytes. PLoS One 8, 1–6. https://doi.org/10.1371/journal.pone.0057384

Romero, A., Novoa, B., Figueras, A., 2015. The complexity of apoptotic cell death in mollusks: An update. Fish Shellfish Immunol. 46, 79–87. https://doi.org/10.1016/j.fsi.2015.03.038

Smolowitz, R., 2013. A Review of Current State of Knowledge Concerning Perkinsus marinus Effects on Crassostrea virginica (Gmelin) (the Eastern Oyster) 50, 404–411. https://doi.org/10.1177/0300985813480806

Sokolova, I., 2009. Apoptosis in molluscan immune defense. Invertebr. Surviv. J. 6, 49–58. https://doi.org/10.1242/jcs.00210

Soudant, P., Chu, F.E., Volety, A., 2013. Host – parasite interactions : Marine bivalve molluscs and protozoan parasites , Perkinsus species. J. Invertebr. Pathol. 114, 196–216. https://doi.org/10.1016/j.jip.2013.06.001

Tait, S.W.G., Green, D.R., 2008. Caspase-independent cell death: Leaving the set without the final cut. Oncogene 27, 6452–6461. https://doi.org/10.1038/onc.2008.311

Tang, H.M., Tang, H.L., 2018. Anastasis: Recovery from the brink of cell death. R. Soc. Open Sci. 5. https://doi.org/10.1098/rsos.180442

Team., Rs., 2020. RStudio: Integrated Development for R. http://www.rstudio.com/.

Wang, L., Song, X., Song, L., 2017. The oyster immunity. Dev. Comp. Immunol. https://doi.org/10.1016/j.dci.2017.05.025

Wikfors, G.H., Alix, J.H., 2014. Granular hemocytes are phagocytic, but agranular hemocytes are not, in the Eastern Oyster Crassostrea virginica. Invertebr. Immun. 1, 15–21. https://doi.org/10.2478/invim-2014-0001

Witkop, E.M., Wikfors, G.H., Proestou, D.A., Lundgren, K.M., Sullivan, M.E., Gomez-Chiarri, M., n.d. Perkinsus marinus suppresses in vitro eastern oyster apoptosis via IAP-dependent and caspase-independent pathways involving TNFR, NF-kB and oxidative pathway crosstalk. prep.

Xue, Q., Itoh, N., Schey, K.L., Cooper, R.K., La Peyre, J.F., 2009. Evidence indicating the

existence of a novel family of serine protease inhibitors that may be involved in marine invertebrate immunity. Fish Shellfish Immunol. 27, 250–259. https://doi.org/10.1016/j.fsi.2009.05.006

Xue, Q.G., Waldrop, G.L., Schey, K.L., Itoh, N., Ogawa, M., Cooper, R.K., Losso, J.N., La Peyre, J.F., 2006. A novel slow-tight binding serine protease inhibitor from eastern oyster (Crassostrea virginica) plasma inhibits perkinsin, the major extracellular protease of the oyster protozoan parasite Perkinsus marinus. Comp. Biochem. Physiol. - B Biochem. Mol. Biol. 145, 16–26. https://doi.org/10.1016/j.cbpb.2006.05.010

Yee, A., Dungan, C., Hamilton, R., Goedken, M., Guise, S.D.E., Sunila, I., 2005. Apoptosis of the protozoan oyster pathogen Perkinsus marinus in vivo and in vitro in the Chesapeake Bay and the Long Island Sound. J. Shellfish Res. 24, 1035–1042. https://doi.org/10.2983/0730-8000(2005)24[1035:aotpop]2.0.co;2

Figures

Figure IV-1. *P. marinus* resistance varied significantly across selectively bred families.
A) Percent survival calculated using the number of total individuals and number of deaths (not including censored oysters) over the experiment duration. Percent survival did not significantly differ between families. B) Log copies of *P. marinus* per 100 ng of DNA in injected oysters measured in each family at 7 d and 50 d post challenge, or from injected oysters that died during the experiment, with the rate of parasite load change through time plotted with a linear regression. Rate of parasite change over time differed significantly between families. Family J oysters had the greatest decrease in *P. marinus* load over time and was therefore the most resistant. Family E oysters had the greatest increase in *P. marinus* load over time and was the most susceptible. C) Log copies of *P. marinus* per 100 ng of DNA at 50 d post- challenge. Parasite load at the end of the experiment was significantly greater in family E than family J. For all plots significance levels are labeled with an asterisk (** p<=0.05; ** p<=0.01; ***p<=0.001*).

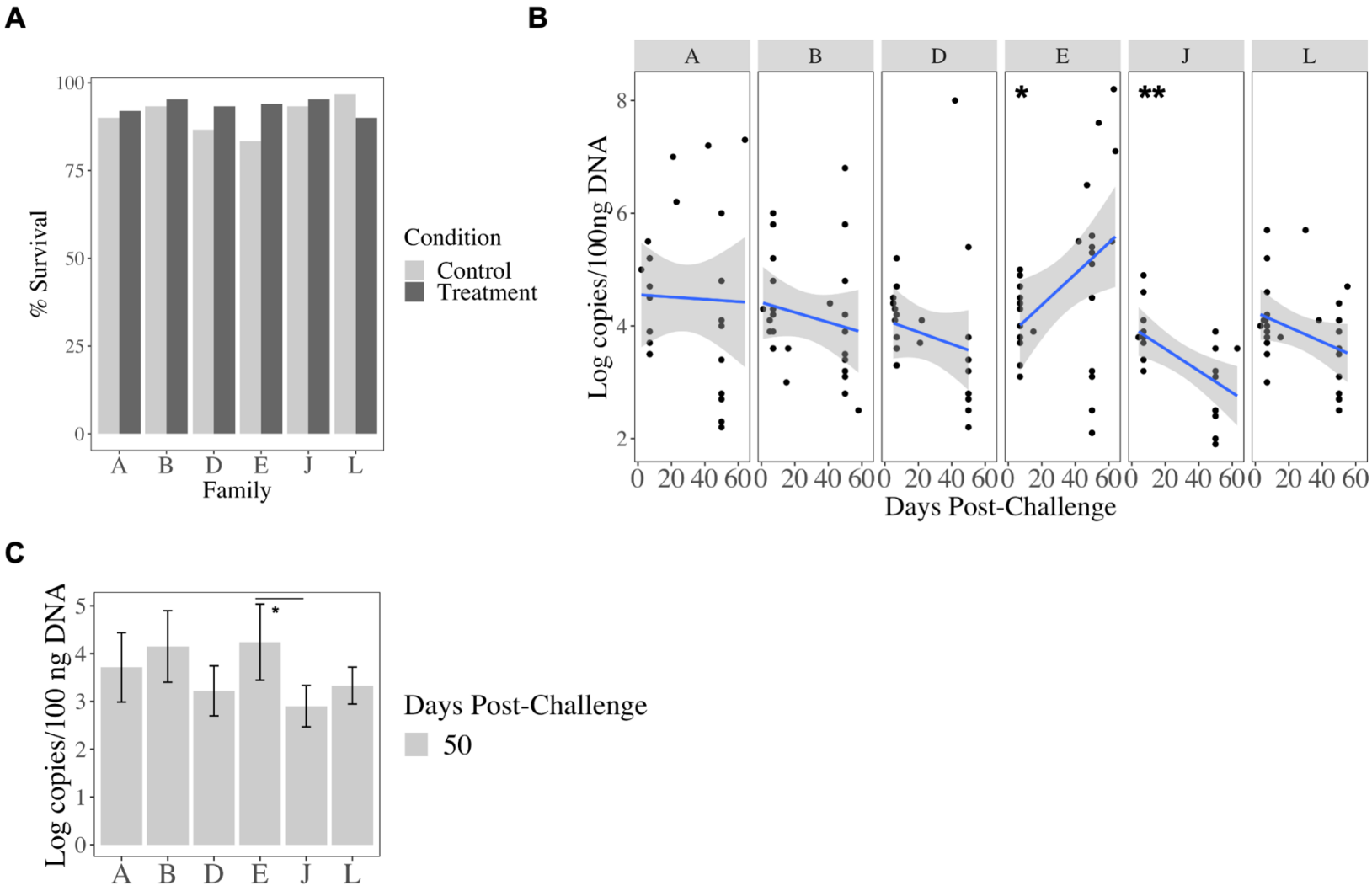
A
100
75
50
25
0
% Survival
A B D E J L
Family
Condition
Control
Treatment
B
A B D E J L
Log copies/100ng DNA
8
6
4
2
*
**
0 20 40 60
Days Post-Challenge
C
Log copies/100 ng DNA
5
4
3
2
1
0
*
A B D E J L
Days Post-Challenge
50

Figure IV-2. Granular hemocyte viability differed between families but not in response to challenge within family.
At both 7 d and 50 d post-challenge, granular hemocyte viability differed between families, but not between control and challenged oysters within families, indicating potential difference in pathological response. Statistical tests were performed with arcsine transformed percentages (* *p<=0.05; ** p<=0.01; ***p<=0.001*). A) Percent of live granular hemocytes 7 d post-challenge. B) Percent of live granular hemocytes 50 d post-challenge.

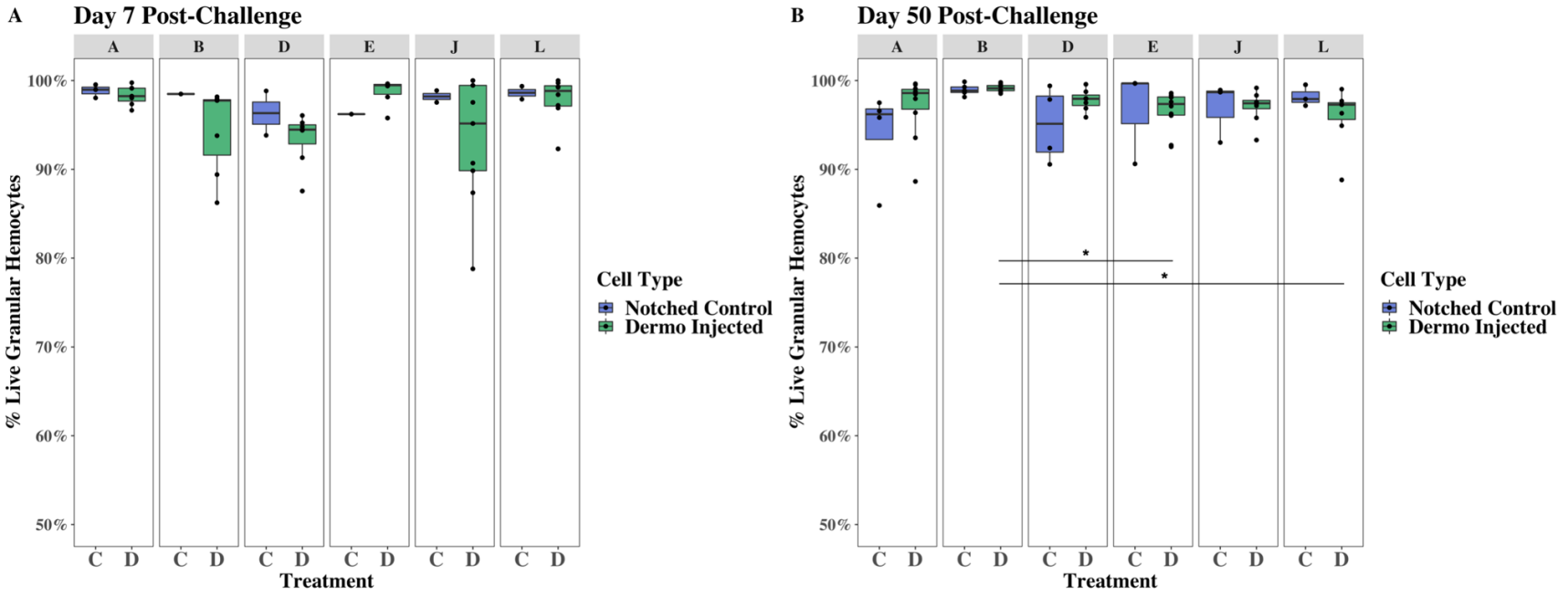

Figure IV-3. Granular hemocyte apoptosis significantly differed between families in challenged oysters 7 d post-challenge, but not between control and challenged oysters within families.
A) Percent of apoptotic granular hemocytes 7 d post-challenge. B) Percent of apoptotic granular hemocytes 50 d post-challenge. Statistical tests were performed with arcsine transformed percentages (* *p<=0.05; ** p<=0.01; ***p<=0.001*).

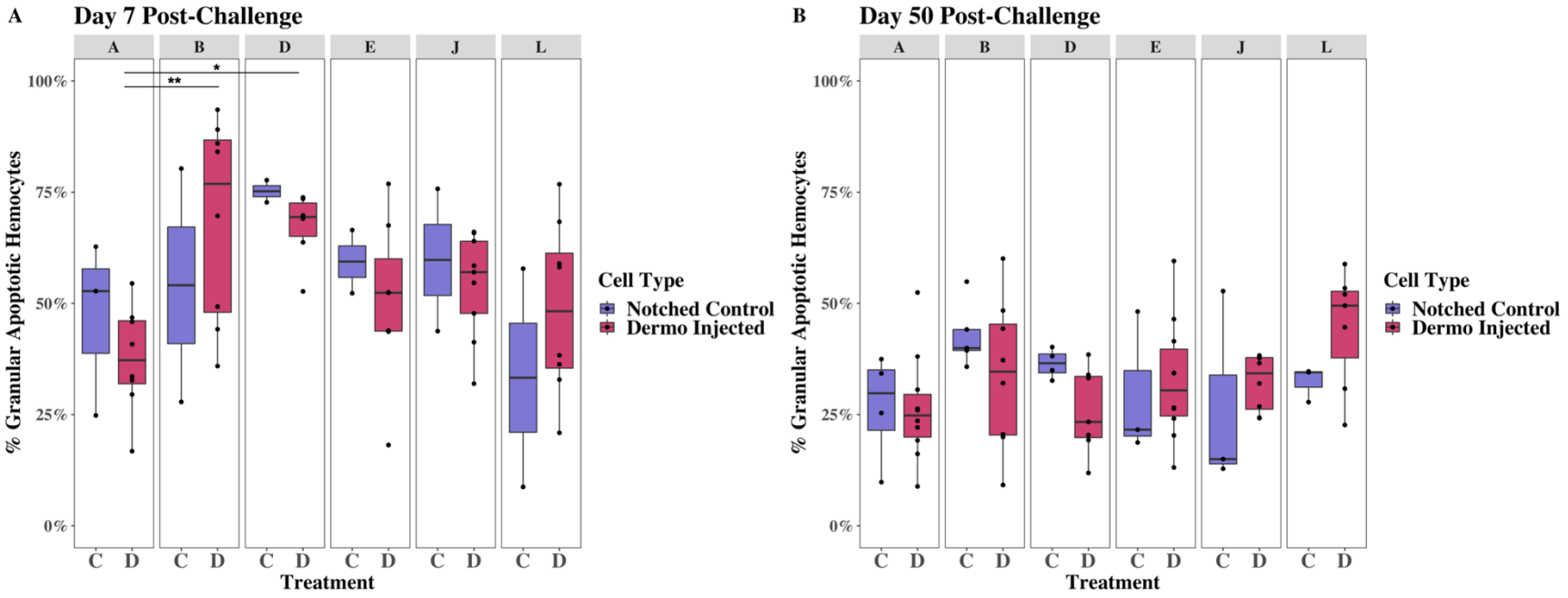

Figure IV-4. Caspase 3/7 activation in granulocytes significantly differed between families in challenged oysters 50 d post-challenge, but not between control and challenged oysters within families.
A) Percent of caspase 3/7 active granular hemocytes 7 d post-challenge. B) Percent of caspase 3/7 active granular hemocytes 50 d post-challenge. Statistical tests were performed with arcsine transformed percentages (* *p<=0.05;* ** *p<=0.01;* ***p<=0.001*).

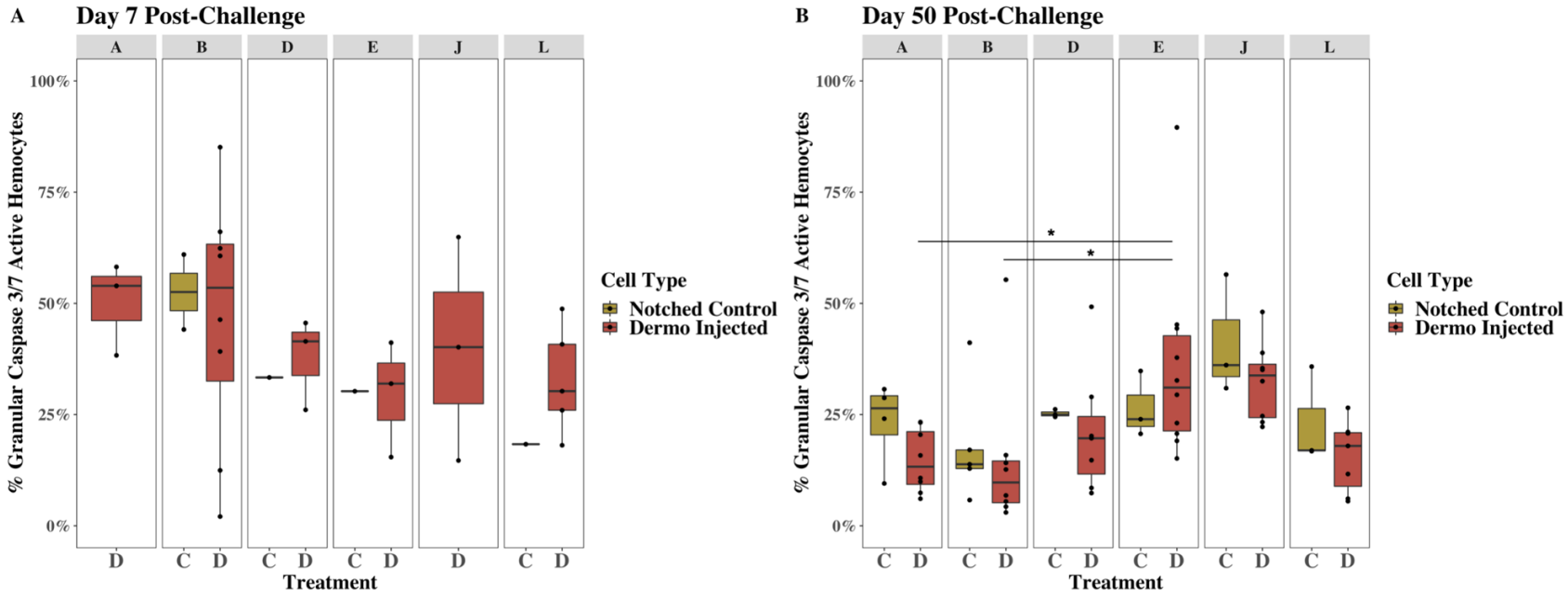

Figure IV-5. Granulocyte apoptosis phenotype was significantly correlated with *P. marinus* load only in the most resistant family at 7 days after *P. marinus* challenge.
Correlation between levels of granulocyte apoptosis and parasite load in each oyster were measured using linear regression and presented with T-test P-values for significant correlations (* *p<=0.05; ** p<=0.01; ***p<=0.001*). A) The change in percent granular hemocyte apoptosis between 7 d and 50 d post-challenge (*arcsine transformed apoptosis ~ Day*). B) The correlation between granular hemocyte apoptosis and *P. marinus* tissue load for each sample and family at each time point (*arcsine transformed apoptosis ~ avg. log copies P. marinus*). C) Overall correlation between granular hemocyte apoptosis and *P. marinus* tissue load in samples from all families at days 7 (top) and 50 (bottom) after challenge (*arcsine transformed apoptosis ~ avg. log copies P. marinus*).

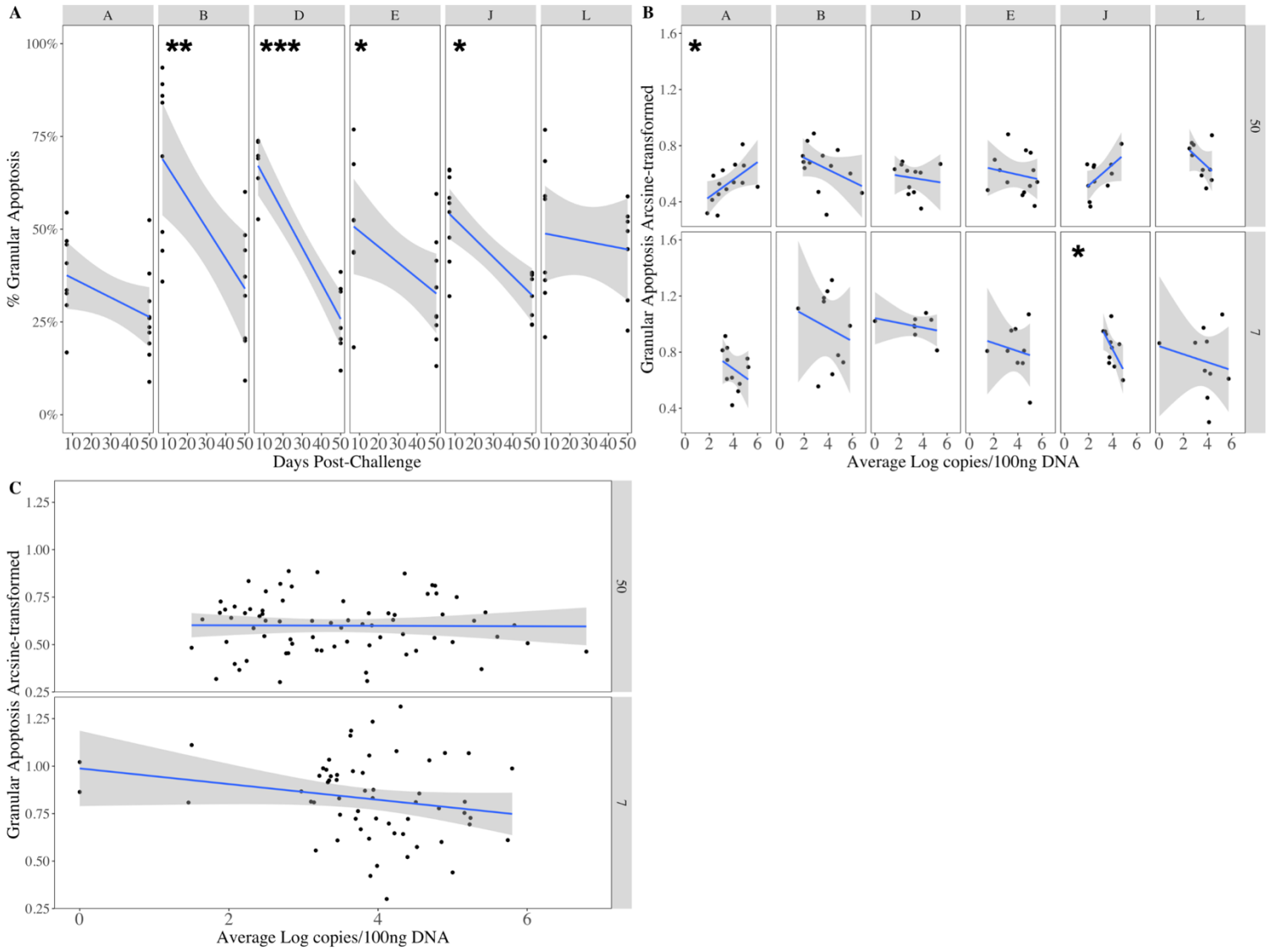
A
A
B
D
E
J
L
100%
75%
50%
25%
0%
% Granular Apoptosis
**
***
*
*
10 20 30 40 50
Days Post-Challenge
B
*
*
1.6
1.2
0.8
0.4
Granular Apoptosis Arcsine-transformed
50
7
0 2 4 6
Average Log copies/100ng DNA
C
1.25
1.00
0.75
0.50
0.25
Granular Apoptosis Arcsine-transformed
50
7
0
2
4
6
Average Log copies/100ng DNA

Supplementary Material

Supplementary Figure 1: Agranular hemocyte viability 7 d and 50 d post-challenge. Statistical tests were performed with arcsine transformed percentages (* *p<=0.05;* ** *p<=0.01;* ****p<=0.001*). A) Percent of live agranular hemocytes 7 d post-challenge. B) Percent of live agranular hemocytes 50 d post-challenge.

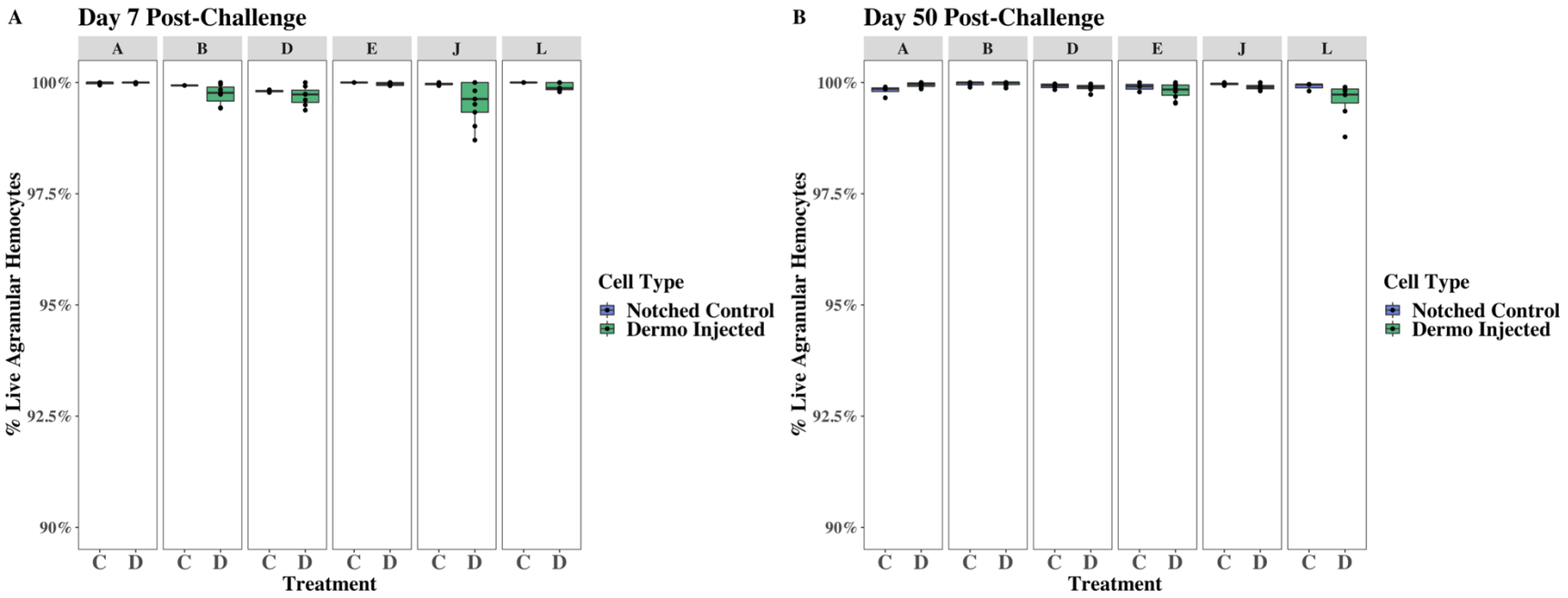

Supplementary Figure 2: Agranular hemocyte apoptosis 7 d and 50 d post-challenge. Statistical tests were performed with arcsine transformed percentages (* *p<=0.05; ** p<=0.01; ***p<=0.001*). A) Percent of apoptotic agranular hemocytes 7 d post-challenge. B) Percent of apoptotic agranular hemocytes 50 d post-challenge.

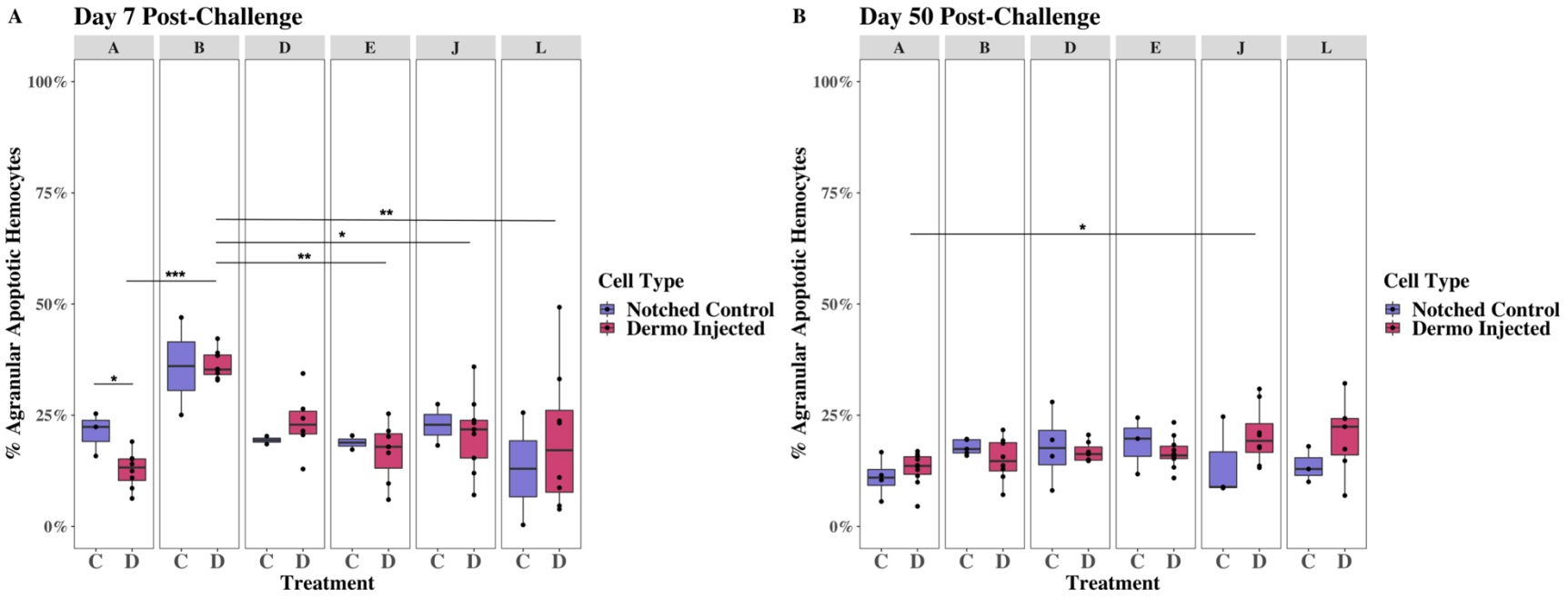

Supplementary Figure 3: Agranular hemocyte caspase 3/7 activation 7 d and 50 d post-challenge. Statistical tests were performed with arcsine transformed percentages (* *p<=0.05; ** p<=0.01; ***p<=0.001*). A) Percent of caspase 3/7 active agranular hemocytes 7 d post-challenge. B) Percent of caspase 3/7 active agranular hemocytes 50 d post-challenge.

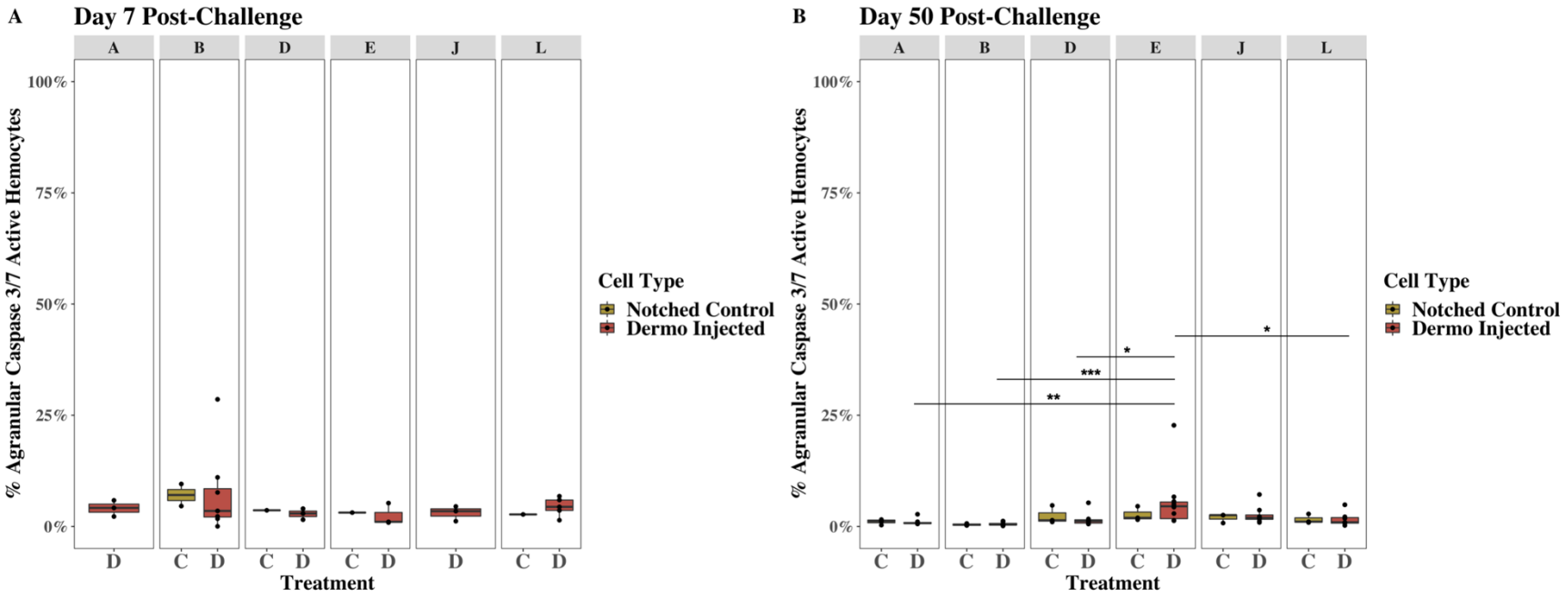

CHAPTER V: Conclusion

Eastern oysters are negatively affected by outbreaks of disease and rely on a highly complex innate immune system characterized by large expanded immune gene families to combat a diversity of pathogens in their environment (Dishaw and Litman, 2013; Zhang et al., 2015). Gene family expansion may enable oysters to better tailor their immune responses to a wide range of pathogens, but the connection between disease response and immune gene expansion has been explored relatively little (Song et al., 2021; Zhang et al., 2012, 2015). One critical immune pathway involving expanded gene families is apoptosis, or programmed cell death (Romero et al., 2015). Apoptosis pathway regulation is highly complex, involving specific and orchestrated expression of several expanded gene families, including the Inhibitor of Apoptosis (IAP) family which is critical in apoptosis regulation and whose diversity has not been fully characterized in oysters (Zhang et al., 2015). Apoptosis is a central immune response to Dermo disease caused by the parasite *Perkinsus marinus*, a leading cause of oyster mortality, and increased apoptosis following intracellular *P. marinus* infection may reduce parasite replication and contribute to increased disease resistance (Smolowitz, 2013). The complete molecular mechanisms of apoptosis in response to *P. marinus* and the relationship between apoptosis genotype, apoptosis phenotype, and Dermo disease resistance remain unknown. To fill these gaps in research, this dissertation coupled *in vivo* and *in vitro* challenge experiments with genomic and transcriptomic methods to 1) Determine the full repertoire of apoptosis genes in the eastern oyster, 2) Characterize oyster IAP gene family diversification, potential evolutionary mechanisms of expansion, and the role of this diversification in oyster disease response, 3) Investigate eastern oyster mechanisms of apoptosis response to *P. marinus*

challenge, and 4) Determine the connection between apoptosis phenotype and disease resistance to Dermo disease.

This dissertation first determined the full repertoire of apoptosis genes and alternative regulated cell death (RCD) pathway genes in the eastern oyster by mining the genome annotation and then repeating this process with the Pacific oyster genome for comparison. The following major questions were addressed: 1) Are the major extrinsic and intrinsic pathway members from model organisms annotated in the eastern oyster genome, 2) Are alternative RCD pathways annotated in the eastern oyster genome, and 3) Does the repertoire of apoptosis pathway genes differ between *C. virginica* and *C. gigas*? This research first revealed that the major intrinsic and extrinsic pathway genes from model organisms are annotated in eastern oysters, confirming previous studies (Kiss, 2010; Romero et al., 2015; Sokolova, 2009). In addition to apoptosis, this work next identified RCD pathway genes involved in necroptosis, lysosome-dependent cell death (LDCD), and parthanatos in *C. virginica*. This is the most extensive search of alternative RCD proteins in oysters to date, and identification of molecules present in these pathways informs future research to assess the function of these proteins and potential use of these pathways in eastern oyster disease response.

In both *C. gigas* and *C. virginica*, few Bcl-2 family members were annotated, confirming previous research in *C. gigas* (Li et al., 2017). Notably, p53, TNF- α and SMAC/diablo were annotated only in the Pacific oyster genome and have been identified in previous *C. gigas* studies (Lv et al., 2019; Plachetzki et al., 2020; Zhang et al., 2011). Lack of annotation for these proteins in *C. virginica* is more likely the result of standard annotation pipelines failing to detect distant homologs than true loss. The reliance of this

work on annotation pipeline annotations rather than manual annotation methods such as HMMER represents a limitation of this work. As a consequence of the scope of molecules investigated, manual annotation, however, would have been prohibitively labor intensive. Future research from the oyster genomics/immunology research community should use manual annotation approaches to assess the presence of key, missing proteins in the *C. virginica* annotation. Overall, this research is novel because it mined the eastern oyster genome for a broader range of apoptosis and RCD genes than previous studies (Dios et al., 2011; Li et al., 2017; Romero et al., 2015; Zhang et al., 2012, 2015) and presents the full list of identified genes and transcripts for use by future researchers.

Next this dissertation characterized IAP gene family diversification, potential evolutionary mechanisms of expansion, and the role of IAP diversification in oyster disease response. The following questions were investigated: 1) How many IAPs are present in the eastern and Pacific oysters and closely related molluscs, and what evolutionary mechanisms contributed to IAP expansion, 2) Do oyster IAPs contain conserved BIR domains and domain architecture, or novel domains and architectures, 3) Is the full diversity of expanded IAP genes expressed during challenge, and 4) Is IAP expression across diverse challenges characterized by usage of diverse genes and transcripts or expression of the same IAPs at different levels? First, IAP annotation across 10 mollusc genomes determined that *B. glabrata* has the greatest IAP expansion (88 genes), *Octopus* spp. have the least expansion (10, 11 in *O. vulgaris* and *O. bimaculoides*, respectively), and *C. virginica* is more greatly expanded than the closest relative with a genome, *C. gigas* (69 vs. 40 genes, respectively). Phylogenetic analysis revealed a complex history of IAP loss and gain in molluscs. Many *C. virginica* IAP genes were likely the result of tandem

duplications, and the presence of intronless genes and retroposition machinery in gene ORFs suggested retroposition may be responsible for the expansion of some IAPs. Levels of expansion across molluscs and expansion of IAPs by tandem duplication and retroposition have also recently been confirmed in *M. mercenaria* (Song et al., 2021), suggesting these may be general mechanisms of IAP gene family expansion in molluscs.

IAP analysis next discovered 3 novel Baculoviral IAP Repeat (BIR) domain types and 14 domain architecture types across gene clusters (including types not recognized by Song et al., (2021)), 4 of which are not present in model organisms (Estornes and Bertrand, 2015). Comparative analysis of IAP expression across 7 disease challenge experiments indicated that patterns of IAP and apoptosis-related differential gene expression differed between the two oyster species and *C. virginica* typically differentially expressed a unique set of IAP genes in each experiment, but *C. gigas* differentially expressed a more overlapping set of IAP genes across challenges. Finally, unique combinations of 1 to 12 IAP domain architectures, including novel types, were co-expressed with apoptosis pathways in response to different immune challenges, suggesting expansion of the IAP family might facilitate complex apoptosis pathway regulation during unique disease stressors.

Recently published work by Song et al., (2021) significantly overlaps with the study of IAPs in molluscs and oysters presented here, although several important differences exist. Our work compared IAP expression across a broader range of disease challenges with greater sample size, performed cross-species IAP expression analysis, and associated IAP and apoptosis pathway expression specifically using WGCNA. It additionally revealed considerable diversity in the BIR domain in oysters, as well as the presence of several

additional IAP domain architectures not seen on other organisms. This work also determined that oysters may possess a candidate BIRC2/3 protein with potential function analogous to mammalian IAPs. Prior publication of some similar results by Song et al., (2021) increases confidence in many fundamental findings and interpretations of this study; independent finding of similar results strengthens arguments presented in both papers and reinforces IAP gene family importance in molluscs.

Further work needs to be done addressing technical limitations that may affect the characterization of IAPs in oysters. First, functional analysis of IAPs with novel BIR domains and domain architecture is limited by lack of non-computational protein structure analyses, such as X-ray crystallography. Second, lack of common viral and parasitic challenge replicates between species limits the ability to assess specificity of particular domain architectures to certain challenge types. Third, the currently available eastern oyster annotation is likely bedeviled by assembly errors resulting in haplotigs (Puritz *personal communication*), or contigs of clones with the same haplotype (Makoff and Flomen, 2007). Although IAPs were analyzed for the presence of haplotigs, it is possible that future assembly versions with haplotigs resolved may have removed particular IAP genes.

IAP analysis presented in this dissertation also has several exciting implications and opportunities for future research. First, it highlights gene expansion mechanisms in oysters that can be studied in future gene families. Second, the novel, cross-species comparative approach across a broad array of disease challenges (bacterial, viral, parasitic) presents a framework for future research studying roles of expanded immune gene families in disease response. Third, this paper assists future researchers in IAP selection for targeted qPCR

during disease challenge. Previous papers analyzing IAP in oysters during immune challenges often hand selected one or two to study (Green et al., 2015; Lau et al., 2018). The great domain architecture diversity and varied IAP response across challenges found in this study indicate that functional or phenotypic hypotheses cannot be generated and tested by focusing on just one or two IAPs. IAP characterization presented here allows future researchers to select several IAPs to study with an array of domain architecture types. Targeting multiple IAP types may improve the ability to assess potential phenotypic outcomes of IAP expression. Finally, characterization of the potential homology of oyster IAPs to those characterized in model species provide more targeted hypothesis regarding potential functions (e.g. oyster candidate BIRC2/3 role in TLR and TNFR signal transduction) (Estornes and Bertrand, 2015).

Following IAP gene family analysis, this dissertation investigated eastern oyster apoptosis mechanisms in response to *P. marinus* challenge. The eastern oyster-Dermo challenge system presents a major opportunity to study the connection between apoptosis gene regulation and apoptosis phenotype and how this may affect disease resistance. Prior to this analysis however, apoptosis mechanisms in response to *P. marinus* must be better understood. Insights into Dermo-affected apoptosis mechanisms may also help develop phenotypic or genetic markers for resistance. Specifically, this dissertation addressed the following questions: 1) Is apoptosis in response to *P. marinus* caspase-dependent, 2) Does apoptosis in response to *P. marinus* involve mitochondrial permeabilization, 3) Are IAPs or IAP-involved pathways (intrinsic apoptosis, TLR and TNFR pathways) involved in the apoptotic response to *P. marinus*, 4) What apoptosis pathways are modulated by *P. marinus* and apoptosis inhibitor challenge, and what potential genes may *P. marinus*

express to influence the oyster apoptotic response, and 5) Is apoptosis gene expression correlated with changes in apoptosis phenotype? First, this study identified that *P. marinus* treatment caused significant apoptosis suppression *in vitro*, which has been observed by previous studies (Goedken et al., 2005; Hughes et al., 2010; Lau et al., 2018; Smolowitz, 2013). To investigate mechanisms of apoptosis in response to *P. marinus*, two novel apoptosis modulators were deployed; the pan-caspase inhibitor Z-VAD-FMK and the novel IAP inhibitor GDC-0152. Z-VAD-FMK has been used in previous study with *P. marinus* (Hughes et al., 2010), indicating that apoptosis in response to *P. marinus* changed little following Z-VAD-FMK treatment and suggesting that hemocyte apoptosis affected by *P. marinus* is caspase-independent. This result was supported by the present study, in which caspase inhibition did not change hemocyte apoptosis in response to *P. marinus*.

Next, challenge with the novel IAP inhibitor GDC-0152 revealed that hemocyte apoptosis in control hemocytes may be IAP dependent, as IAP inhibition caused a strong increased in apoptosis. This inhibitor has never been tested in a mollusc, although it has been used in a urochordate (Rosner et al., 2019), but IAP structural characterization in Chapter 2 revealed the BIR3 domain target of GDC-0152 is likely present in several oyster IAPs. Although key involvement of IAPs in oyster apoptosis was expected because of the critical roles of IAPs in model organism apoptosis (Estornes and Bertrand, 2015), this is an important finding not previously observed in oysters that helps researchers understand pathways of apoptosis in oysters. Future eastern oyster apoptosis research should identify IAPs inhibited by GDC-0152 to better characterize IAPs critical in oyster apoptosis regulation. Dual treatment with *P. marinus* and GDC-0152 allowed for normal apoptotic pathway perturbation prior to *P. marinus* challenge and helped reveal that *P. marinus* may

inhibit apoptosis downstream of mitochondrial apoptosis, possibly through inhibition of caspase-independent mitochondria-released enzymes such as AIF. Although the involvement of AIF in apoptosis induced by *P. marinus* has been proposed previously (Hughes et al., 2010), experimental evidence here suggesting mitochondrial permeabilization during *P. marinus* apoptotic response, which allows for AIF release, provides further characterization of this pathway.

Dual treatment of hemocytes with *P. marinus* and GDC-0152 next indicated that *P. marinus* was able to overcome the strong IAP induction triggered by GDC-0152 alone. This treatment also showed further apoptosis suppression in hemocytes with engulfed *P. marinus*, indicating a combined effect of GDC-0152 and *P. marinus* on overall apoptosis inhibition and suggesting *P. marinus* may normally affect IAP-involved pathways to suppress apoptosis. Although little transcriptional change was seen in hemocytes challenged with *P. marinus* alone, a result observed in susceptible oysters previously (Proestou and Sullivan, 2020), perturbation of the normal pathway with GDC-0152 treatment allowed for previously unseen responses to be observed. Future transcriptome analysis following treatment with GDC-152 alone should be conducted to compare patterns of gene expression with dual GDC-0152 and *P. marinus* treatment. Transcriptomic analysis from this dual *P. marinus* and GDC-0152 treatment overall revealed hemocyte apoptosis suppression likely involves oxidation-reduction processes, TNFR and NF-kB pathways, and suggests *P. marinus* secreted enzymes may inhibit these pathways.

WGCNA analysis finally identified apoptosis pathway genes highly correlated with one another and with the change in apoptosis phenotype in the dual GDC-0152 and *P. marinus* challenge. Although previous studies have implicated the NF-kB pathway as a

contributor to apoptosis suppression following *P. marinus* challenge (Lau et al., 2018), transcriptomics and WGCNA helped identify genes in these complex and diverse pathways that are involved in apoptosis and immunity. Although this study was limited by lack of sequencing of *P. marinus* parasite samples alone (not in the presence of hemocytes), and by sampling of only one time point post-challenge, this study advances research of eastern oyster immunity and host-parasite interactions and suggests that future research should attempt specific perturbations of the NF-kB and TNFR pathway during *P. marinus* infection to further investigate apoptosis mechanisms.

Finally, this dissertation investigated the connection between apoptosis phenotype and disease resistance to Dermo disease. The following questions were addressed: 1) Does *P. marinus* resistance differ across the selectively bred eastern oyster families selected with variable survival in the Chesapeake Bay, 2) Does *P. marinus* challenge significantly affect apoptosis phenotype and do families differ in their apoptotic response, 3) Is family level apoptosis phenotype correlated with family level resistance, and 4) Is the apoptotic response to *P. marinus* caspase-independent *in vivo? In vivo* challenge of six selectively-bred eastern oyster families first determined that families differed significantly in *P. marinus* resistance, when resistance was measured as the change in parasite load over time, underscoring a genetic component to Dermo disease resistance which is supported by previous studies (Proestou et al., 2019; Proestou and Sullivan, 2020). Apoptosis phenotype measured 7 d and 50 d post-challenge revealed that the acute apoptotic response to *P. marinus* differed between families. No studies have previously measured apoptosis across multiple-selectively bred families of eastern oysters. Differences in apoptosis regulation across families may be attributable to genetic differences or differences in gene expression.

This study is limited by the fact that challenge conditions did not generate significant differences between control and treated groups within family, although this has been seen previously at some timepoints (Goedken et al., 2005), suggesting that additional timepoints, *P. marinus* strains, *P. marinus* dosing levels, and additional lines with greater differences in resistance should be added in future experiments.

This study next compared the relationship between apoptosis phenotype and parasite load to determine correlation with resistance. Apoptosis phenotype and parasite load were significantly correlated in the most resistant family J at 7d post-challenge, suggesting apoptosis levels may be correlated with resistance during the acute infection stage. This correlation was not observed at day 50 after challenge, suggesting that the acute apoptosis response early during challenge may be a better indicator of Dermo resistance. This is consistent with previous studies in which apoptosis levels in challenged oysters remained relatively stable after the first week post challenge (Hughes et al., 2010). This study should be repeated with more families showing strong resistance to Dermo disease to confirm any potential relationship between acute apoptosis and resistance. If this relationship is found to be consistent in resistant families however, acute apoptosis phenotype could become an additional measure of family-level disease resistance during the selective breeding process. This would benefit hatcheries, farmers, and oyster restoration efforts.

Transcriptome sequencing followed by differential expression analysis and WGCNA should be undertaken next to explore the relationships between apoptosis phenotype, apoptosis genotype, and *P. marinus* resistance. Unforeseen delays in sequencing precluded the inclusion of this transcriptome analysis in this dissertation. When this data set is available, variation in apoptosis pathway transcription will be compared across families

and WGCNA analysis will allow for assessment of relationships between apoptosis gene expression, apoptosis phenotype, and Dermo resistance. IAP family expression will also be specifically assessed to determine if strong expression patterns within families may contribute to divergent phenotypes observed.

This dissertation addressed the role of immune gene family expansion in eastern oyster disease response, using apoptosis, expansion of the IAP gene family, and challenge with the economically relevant pathogen *P. marinus* as specific models to address these connections. Invertebrates have evolved incredibly diverse innate immune systems challenging the view that innate immunity is simple or less evolved (Dishaw and Litman, 2013; Loker et al., 2004). Maintenance of large, expanded gene families over time suggests their importance in immunity; studies continue to uncover the diverse and variable roles of expanded immune gene family members. Continued research into the role of gene family expansion in invertebrate immunity, and the highly economically important eastern oyster, will yield fundamental results that shape our understanding of immune system evolution and how invertebrates are able to thrive in diverse and challenging conditions. May the complexity and diversity of invertebrate immune systems explored in this research similarly captivate future scientists and inspire them to study an underappreciated aspect of these fascinating organisms.

References

Dios, S., Figueras, A., Novoa, B., Romero, A., Este, N., 2011. New Insights into the Apoptotic Process in Mollusks : Characterization of Caspase Genes in Mytilus galloprovincialis 6. https://doi.org/10.1371/journal.pone.0017003

Dishaw, L.J., Litman, G.W., 2013. Changing views of the evolution of immunity. Front. Immunol. 4, 2012–2014. https://doi.org/10.3389/fimmu.2013.00122

Estornes, Y., Bertrand, M.J.M., 2015. IAPs, regulators of innate immunity and inflammation. Semin. Cell Dev. Biol. 39, 106–114. https://doi.org/10.1016/j.semcdb.2014.03.035

Goedken, M., Morsey, B., Sunila, I., De Guise, S., 2005. Immunomodulation of Crassostrea gigas and Crassostrea virginica cellular defense mechanism by Perkinsus marinus. J. Shellfish Res. 24, 487–496. https://doi.org/10.2983/0730-8000(2005)24

Green, T.J., Rolland, J., Vergnes, A., Raftos, D., Montagnani, C., 2015. Fish & Shell fi sh Immunology OsHV-1 countermeasures to the Paci fi c oyster ' s anti-viral response. Fish Shellfish Immunol. 47, 435–443. https://doi.org/10.1016/j.fsi.2015.09.025

Hughes, F.M., Foster, B., Grewal, S., Sokolova, I.M., 2010. Apoptosis as a host defense mechanism in Crassostrea virginica and its modulation by Perkinsus marinus. Fish Shellfish Immunol. 29, 247–257. https://doi.org/10.1016/j.fsi.2010.03.003

Kiss, T., 2010. Apoptosis and its functional significance in molluscs. Apoptosis 15, 313–321. https://doi.org/10.1007/s10495-009-0446-3

Lau, Y.T., Santos, B., Barbosa, M., Pales Espinosa, E., Allam, B., 2018. Regulation of apoptosis-related genes during interactions between oyster hemocytes and the alveolate parasite Perkinsus marinus. Fish Shellfish Immunol. 83, 180–189.

https://doi.org/10.1016/j.fsi.2018.09.006

Li, Y., Zhang, L., Qu, T., Tang, X., Li, L., Zhang, G., 2017. Conservation and divergence of mitochondrial apoptosis pathway in the Pacific oyster , Crassostrea gigas 82898701, 1–13. https://doi.org/10.1038/cddis.2017.307

Loker, E.S., Adema, C.M., Zhang, S.M., Kepler, T.B., 2004. Invertebrate immune systems - Not homogeneous, not simple, not well understood. Immunol. Rev. 198, 10–24. https://doi.org/10.1111/j.0105-2896.2004.0117.x

Lv, Z., Song, X., Xu, J., Jia, Z., Yang, B., Jia, Y., Qiu, L., Wang, L., Song, L., 2019. The modulation of Smac/DIABLO on mitochondrial apoptosis induced by LPS in Crassostrea gigas. Fish Shellfish Immunol. 84, 587–598. https://doi.org/10.1016/j.fsi.2018.10.035

Makoff, A.J., Flomen, R.H., 2007. Detailed analysis of 15q11-q14 sequence corrects errors and gaps in the public access sequence to fully reveal large segmental duplications at breakpoints for Prader-Willi, Angelman, and inv dup(15) syndromes. Genome Biol. 8. https://doi.org/10.1186/gb-2007-8-6-r114

Plachetzki, D.C., Pankey, M.S., MacManes, M.D., Lesser, M.P., Walker, C.W., 2020. The Genome of the Softshell Clam Mya arenaria and the Evolution of Apoptosis. Genome Biol. Evol. 12, 1681–1693. https://doi.org/10.1093/gbe/evaa143

Proestou, D.A., Jr, S.K.A., Corbett, R.J., Horin, T. Ben, Small, J.M., 2019. Defining Dermo resistance phenotypes in an eastern oyster breeding population 2142–2154. https://doi.org/10.1111/are.14095

Proestou, D.A., Sullivan, M.E., 2020. Variation in global transcriptomic response to Perkinsus marinus infection among eastern oyster families highlights potential

mechanisms of disease resistance. Fish Shellfish Immunol. 96, 141–151. https://doi.org/10.1016/j.fsi.2019.12.001

Romero, A., Novoa, B., Figueras, A., 2015. The complexity of apoptotic cell death in mollusks: An update. Fish Shellfish Immunol. 46, 79–87. https://doi.org/10.1016/j.fsi.2015.03.038

Rosner, A., Kravchenko, O., Rinkevich, B., 2019. IAP genes partake weighty roles in the astogeny and whole body regeneration in the colonial urochordate Botryllus schlosseri. Dev. Biol. 448, 320–341. https://doi.org/10.1016/j.ydbio.2018.10.015

Smolowitz, R., 2013. A Review of Current State of Knowledge Concerning Perkinsus marinus Effects on Crassostrea virginica (Gmelin) (the Eastern Oyster) 50, 404–411. https://doi.org/10.1177/0300985813480806

Sokolova, I., 2009. Apoptosis in molluscan immune defense. Invertebr. Surviv. J. 6, 49–58. https://doi.org/10.1242/jcs.00210

Song, H., Guo, X., Sun, L., Wang, Qianghui, Han, F., Wang, H., Wray, G.A., Davidson, P., Wang, Qing, Hu, Z., Zhou, C., Yu, Z., Yang, M., 2021. The hard clam genome reveals massive expansion and diversification of inhibitors of apoptosis in Bivalvia 1–20.

Zhang, G., Fang, X., Guo, X., Li, L., Luo, R., Xu, F., Yang, P., Zhang, L., Wu, F., Chen, Y., Wang, J., Peng, C., Meng, J., Yang, L., Liu, J., Wen, B., Zhang, N., Huang, Z., 2012. The oyster genome reveals stress adaptation and complexity of shell formation. https://doi.org/10.1038/nature11413

Zhang, L., Li, L., Guo, X., Litman, G.W., Dishaw, L.J., Zhang, G., 2015. Massive expansion and functional divergence of innate immune genes in a protostome. Sci.

Rep. 5, 8693. https://doi.org/10.1038/srep08693

Zhang, L., Li, L., Zhang, G., 2011. Gene discovery, comparative analysis and expression profile reveal the complexity of the Crassostrea gigas apoptosis system. Dev. Comp. Immunol. 35, 603–610. https://doi.org/10.1016/j.dci.2011.01.005